UNIVERSITY OF CALIFORNIA, SAN DIEGO

SYSTEM AND DAMAGE IDENTIFICATION OF CIVIL STRUCTURES

A dissertation submitted in partial satisfaction of the requirements for the degree

Doctor of Philosophy

in

Structural Engineering

by

Babak Moaveni

Committee in charge:

Professor Joel P. Conte, Chair
Professor Raymond A. de Callafon
Professor Ahmed Elgamal
Dr. François M. Hemez
Professor Miroslav Krstic
Professor J. Enrique Luco

2007

The dissertation of Babak Moaveni is approved, and it is acceptable in quality and form for publication on microfilm:

_____

_____

_____

_____

_____

_____

Chair

University of California, San Diego

2007

To my wife, Sanaz,
my parents, Simin and Nasser,
and my sisters Ghazal and Sara.

TABLE OF CONTENTS

LIST OF TABLES

LIST OF FIGURES

ACKNOWLEDGEMENTS

The research for this dissertation was performed at the University of California at San Diego under the direction of Professor Joel P. Conte. I would like to express my deepest and most sincere gratitude to him. He has been for me a rigorous and insightful teacher, a reliable and enlightening guide in the research, and an inspiration in my decision to pursue a career in academia. His guidance and support have been the key to my academic growth over the past five and half years. I will forever be grateful to him.

Special thanks are given to all the members of my doctoral committee, Professors Raymond A. de Callafon, Ahmed Elgamal, J. Enrique Luco, Miroslav Krstic, and Dr. François M. Hemez, who have always been willing to dedicate their time to help me with my research.

I wish to thank my fellow students and friends. My research on system and damage identification has strongly benefited from my collaboration with Mr. Xianfei He. I also wish to thank Mr. Michele Barbato for helping me to organize my dissertation in the required format. The quality and joy of my work have been enhanced by my interactions with Maurizio Gobbato, Ozgur Ozcelik, Andrea Belleri, Houman Ghajari, Michele Barbato, Pablo Cicotti, Andre Barbosa, Kash Baghei, Mami Merati, Omid Kowsari, Pasha Misaghi, Giulio Cassarotti, Matteo Sabattini, Gabriel Acero, Fabio Matta, Carlo Piotti, Yuyi Zhang, Xianfei He, Salvatore Salamone, Ivan Bartoli, Marios Panagiotou, Manuel Dall'osto, Stefano Coccia, Andreas Stavridis, Giuseppe Canducci, Alessandro Zona, and many other dear friends who shared with me highs and lows in San Diego. Special thanks

go to my aunt Sussan, uncles Rahim and Sassan, and cousins Ellie, Pegah and Negar, and their husbands Shahriar and Babak who also helped me to feel at home in San Diego from my first day at UCSD.

Last but not least, I am most grateful to my wife and my family for their help, encouragement and support during all these years. I dedicate my work to them.

Chapter 3, with some modifications (extensions), is a reprint of the material submitted for possible publication in the Journal of Engineering Mechanics, ASCE (2007), De Callafon , R.A., Moaveni, B., Conte, J.P., He, X., and Udd, E. The dissertation author was second author of this paper. He strongly contributed to the development of the General Realization Algorithm presented and to the preparation of the manuscript.

Chapter 4 is an extended version of the material submitted for possible publication in the Journal of Structural Engineering, ASCE (2007), Moaveni, B., He, X., and Conte, J.P. The dissertation author is the first author and primary investigator of this paper.

Chapter 5, in full, is a reprint of the material accepted for publication in the Journal of Computer-Aided Civil and Infrastructure Engineering (2008), Moaveni, B., He, X., Conte, J.P., and De Callafon, R.A. The dissertation author was the first author and primary investigator of this paper.

Chapter 6 is an extended version of the manuscript in final stage of preparation for possible publication in the Journal of Structural Engineering, ASCE (2008), Moaveni, B., He, X., and Conte, J.P. The dissertation author is the first author and primary investigator of this paper.

Chapter 7, in full, is a reprint of the material published in the Proceedings of International Conference on Modal Analysis (IMAC-XXV) (2007), Moaveni, B., Barbosa, A.R., Conte, J.P., and Hemez, F.M. The dissertation author was the first author and primary investigator of this paper.

Chapter 8, in full, is a reprint of the material submitted for possible publication in the Journal of Computer-Aided Civil and Infrastructure Engineering (2008), Moaveni, B., Conte, J.P., and Hemez, F.M. The dissertation author was the first author and primary investigator of this paper.

Support of this research by (1) Lawrence Livermore National Laboratory with Dr. David McCallen as Program Leader, (2) the Englekirk Center Industry Advisory Board, (3) the National Science Foundation, Grant No. DMI-0131967, under a Blue Road Research STTR Project, and (4) the National Science Foundation, Grant No. 0205720, under an ITR Project, is gratefully acknowledged.

VITA

1999	Bachelor of Science, Sharif University of Technology
2001	Master of Science, Sharif University of Technology
2002-2007	Research Assistant, University of California, San Diego
2007	Doctor of Philosophy, University of California, San Diego

PUBLICATIONS

Moaveni, B., He, X., Conte J.P., and de Callafon, R.A. (2007). "Damage Identification of a Composite Beam Using Finite Element model Updating." *Journal of Computer Aided Civil and Infrastructure Engineering,* in press.

Conte, J.P., He, X., Moaveni, B., Masri, S.F., Caffrey, J.P., Wahbeh, M., Tasbihgoo, F., Whang, D.H., and Elgamal, A. (2007). "Dynamic Testing of Alfred Zampa Memorial Bridge." *Journal of Structural Engineering*, ASCE, in press.

He, X., Moaveni, B., Conte, J.P., Elgamal, A., and Masri, S.F. (2007). "Modal Identification of Vincent Thomas Bridge Using Simulated Wind Response Data." *Journal of Computer Aided Civil and Infrastructure*, tentatively accepted for publication.

De Callafon, R.A., Moaveni, B., Conte, J.P., He, X., and Udd, E. (2007). "General Realization Algorithm for Modal Identification of Linear Dynamic Systems." *Journal of Engineering Mechanics,* ASCE, under review.

He, X., Moaveni, B., Conte, J.P., Elgamal A., and Masri, S.F. (2007). "System Identification of Alfred Zampa Memorial Bridge Using Dynamic Field Test Data." *Journal of Structural Engineering,* ASCE, tentatively accepted for publication.

Moaveni, B., Conte, J.P., Hemez, F.M. (2008). "Uncertainty and Sensitivity Analysis of Damage Identification Results Obtained Using Finite Element Model Updating." *Journal of Computer Aided Civil and Infrastructure Engineering*, under review.

FIELDS OF STUDY

Major Field: Civil Engineering (Structural Engineering)

Studies in Structural Health Monitoring

Professors Joel P. Conte and Raymond A. De Callafon

Studies in Uncertainty Quantification

Dr. François M. Hemez

ABSTRACT OF THE DISSERTATION

System and Damage Identification of Civil Structures

by

Babak Moaveni

Doctor of Philosophy in Structural Engineering

University of California, San Diego, 2007

Professor Joel P. Conte, Chair

In recent years, structural health monitoring has received increasing attention in the civil engineering research community with the objective to identify structural damage at the earliest possible stage and evaluate the remaining useful life (damage prognosis) of structures. Vibration-based, non-destructive damage identification is based on changes in dynamic characteristics (e.g., modal parameters) of a structure for identifying structural damage. Experimental modal analysis (EMA) has been used as a technology for identifying modal parameters of a structure based on its measured vibration data. It should

be emphasized that the success of damage identification based on EMA depends strongly on the accuracy and completeness of the identified structural dynamic properties.

The objective of the research work presented in this thesis is to develop new, and improve/extend existing system identification and damage identification methods for vibration based structural health monitoring. In the first part of the thesis, a new system identification method is developed to identify modal parameters of linear dynamic systems subjected to measured (known) arbitrary dynamic loading from known initial conditions. In addition, a comparative study is performed to investigate the performance of several state-of-the-art input-output and output-only system identification methods when applied to actual large structural components and systems. In the second part of the thesis, a finite element model updating strategy, a sophisticated damage identification method, is formulated and computer implemented. This method is then successfully applied for damage identification of two large test structures, namely a full-scale sub-component composite beam and a full-scale seven-story R/C building slice, at various damage levels. The final part of the thesis investigates, based on numerical response simulation of the seven-story building slice, the effects of the variability/uncertainty of several input factors on the variability/uncertainty of system identification and damage identification results. The results of this investigation demonstrate that the level of confidence in the damage identification results obtained through FE model updating is a function of not only the level of uncertainty in the identified modal parameters, but also choices made in the design of experiments (e.g., spatial density of measurements) and modeling errors (e.g., mesh size).

CHAPTER 1

INTRODUCTION

1.1 Background and Motivation

The deterioration of the civil infrastructure in North America, Europe and Japan has been well documented. In the United States, 50% of all bridges were built before the 1940's and approximately 42% are structurally deficient (Stalling et al., 2000). In Canada, more than 40% of all bridges were built before the 1970's and a large number of these structures are in need of strengthening and rehabilitation (ISIS Canada, 2000a; 2000b). It has been estimated that the investments needed to enhance the performance of deficient infrastructures exceed 900 billion dollars worldwide (ISIS Canada, 2000a; 2000b). These statistics underline the importance of developing reliable and cost effective methods for the massive rehabilitation investments needed in the years ahead. In seismically active regions such as the West Coast of the United States and Japan, the problem of the gradual deterioration of civil structures over time is compounded by sudden damage events or the exacerbation of existing damage due to the occurrence of earthquakes. Furthermore, recent national attention has been focused on damage inflicted to the civil infrastructure by acts of terrorism.

Therefore, in recent years, structural health monitoring has received increased attention in the civil engineering research community with the objective to identify struc-

tural damage at the earliest possible stage and evaluate the remaining useful life (damage prognosis) of structures. Vibration-based, non-destructive damage identification is based on changes in dynamic characteristics (e.g., modal parameters) of a structure as a basis for identifying structural damage. Experimental modal analysis (EMA) has been used as a technology for identifying modal parameters of a structure based on its measured vibration data. It should be emphasized that the success of damage identification based on EMA depends strongly on the accuracy and completeness of the identified structural dynamic properties. An extensive literature review on vibration-based damage identification methods is provided in Chapter 2.

1.2 Objectives and Scope

The objective of the research work presented in this thesis is to develop or improve/extend the already existing system identification and damage identification methods for vibration based structural health monitoring. In the first part of this thesis, a new system identification method is developed to identify modal parameters of linear dynamic systems subjected to measured (known) arbitrary dynamic loading from known initial conditions. In addition, a comparative study is performed to investigate the performance of several state-of-the-art input-output and output-only system identification methods when applied to actual large structural components and systems.

In the second part of the thesis, the finite element model updating strategy, a sophisticated damage identification method, is extended and computer implemented. This method is then successfully applied for damage identification of two (large) test structures which underwent several levels of damage.

The final part of the thesis investigates, based on numerical simulation of structural response, the effects of the variability/uncertainty of several input factors on the variability/uncertainty of system identification and damage identification results. The input factors considered include: amplitude of excitation (and therefore of the response), measurement noise, length of response measurement data used for system identification, spatial density of sensors, estimation uncertainty of modal parameters, and finite element mesh size (for damage identification).

1.3 Organization of Thesis

The research presented in this thesis is partitioned into three topics, namely (1) system identification of structures considered as dynamic systems, (2) damage identification of structures, and (3) uncertainty analysis of system and damage identification results. A number of chapters is devoted to each of these topics.

Chapter 2 presents a comprehensive review of the existing literature on vibration based structural health monitoring. The first research topic is covered in Chapters 3 and 4. In Chapter 3, the General Realization Algorithm (GRA) is developed to identify modal parameters of linear multi-degree-of-freedom dynamic systems subjected to measured (known) arbitrary dynamic loading from known initial conditions. The GRA extends the well known Eigensystem Realization Algorithm (ERA) based on Hankel matrix decomposition by allowing an arbitrary input signal in the realization algorithm. In Chapter 4, six state-of-the-art system identification methods including three output-only and three input-output methods are used to estimate the modal parameters (natural frequencies, damping

ratios and mode shapes) of a full-scale seven-story reinforced concrete shear wall building slice which was tested on the UCSD-NEES shake table and underwent several levels of damage.

The second research topic damage identification of structures, is covered in Chapters 5 and 6. The study presented in Chapter 5, leveraged a full-scale sub-component experiment conducted in the Charles Lee Powell Structural Research Laboratories at the University of California, San Diego. In this chapter, the modal parameters of a full-scale composite beam are estimated at various damage levels, and are then used to identify the damage in the beam through a finite element model updating strategy. Chapter 6 uses the results obtained in Chapter 4 (system identification of shear wall test structure) as input to identify several levels of damage in the shear wall test structure.

The third research topic is the subject of Chapters 7 and 8. From the studies presented in the previous chapters, it was observed that the estimation uncertainty in the system and damage identification results is significant. This motivated the author to perform an uncertainty analysis of these system and damage identification results. Chapter 7 investigates the performance of three different output-only system identification methods, used for experimental modal analysis of the shear wall building slice, as a function of the uncertainty/variability in different input factors. Chapter 8 investigates the performance of the damage identification procedure based on FE model updating as a function of the variability/uncertainty in different input factors. Finally, Chapter 9 summarizes the work done, highlights important research findings and provides some suggestions for future research.

REFERENCES

Friswell, M.I., and Mottershead, J.E., (1995). *Finite element model updating in structural dynamics.* Kluwer Academic Publishers, Boston, USA.

ISIS Canada, (2000a). *Reinforcing concrete structures with fibre reinforced polymers.* ISIS Canada Design Manual, University of Manitoba, Winnipeg, Canada.

ISIS Canada, (2000b). *Strengthening reinforced concrete structures with externally bonded fibre reinforced polymers.* ISIS Canada Design Manual, University of Manitoba, Winnipeg, Canada.

Stallings, J. M., Tedesco, J. W., El-Mihilmy, M., and McCauley, M., (2000). "Field performance of FRP bridge repair." *Journal of Bridge Engineering,* ASCE, Vol. 5, No. 2, 107-113.

Teughels, A., and De Roeck, G. (2004). "Structural damage identification of the highway bridge Z24 by finite element model updating." *Journal of Sound and Vibration,* Vol. 274, 589-610.

CHAPTER 2

LITERATURE REVIEW ON STRUCTURAL HEALTH MONITORING

In the last decade, the subject of structural health monitoring has received growing interest from researchers in diverse fields of engineering who are interested in a wide spectrum of applications ranging from health monitoring of aerospace structures to damage identification in civil infrastructure systems. While there are many approaches and techniques involved in nondestructive evaluation (NDE) of structural systems, they can all be broadly categorized as local or global methods. The first category includes methods designed to provide information about a relatively small region of the system of interest by using local measurements (e.g., ultrasound, acoustic emission, infrared thermography). On the other hand, methods from the second category are based on measurements from a disperse array of sensors to obtain global information about the system condition. These two types of approaches are complementary to each other. The optimum choice of an NDE method depends on the scope of the problem at hand and the nature of the sensor network. Among the global NDE methods that have a strong appeal to researchers in the applied mechanics community are those based on signature analysis of vibration measurements in order to obtain global information about the condition or state of health of the test structure. A comprehensive literature review of global NDE methods has been performed and is presented in this chapter.

Mottershead and Frizwell (1993) present a literature survey related to finite element model updating, which has been used extensively for structural health monitoring. Another overview of NDE approaches for condition assessment is available in the work of Housner et al. (1997). Doebling et al. (1996, 1998) and Sohn et al. (2003) provide a comprehensive review of technical literature dealing with the detection, localization and quantification of structural damage using techniques that examine changes in dynamic signatures and/or properties inferred from dynamic measurement data. Zou et al. (2000) summarize the methods available for vibration-based damage identification in composite structures, with special emphasis on modeling techniques for delamination and methods for detecting delaminations.

The problem of damage identification is classified into four levels: (1) detection, (2) localization, (3) quantification, and (4) prediction of future damage (damage prognosis). At the level of damage detection (level 1), the existence of damage can be detected, while its location and severity are unknown. Information about location of the damage can be provided by localization techniques at level 2. At the damage quantification level (level 3), both the location and severity of damage are estimated. Finally, at the prediction level (level 4), the remaining life of the structure is estimated based on the (identified) current damage state and future loads and damage propagation. Most of the methods summarized in this review reach the second level of damage identification, which means they are able to detect and localize damage in structures, and a few methods are also able to estimate the severity of damage (level 3). As for the prediction level, it is still mainly an objective to pursue.

In this survey, damage identification methods are divided into 13 categories, namely methods based on: (1) Bayesian analysis, (2) control theory, (3) damage index, (4) empirical mode decomposition and Hilbert-Huang transformation, (5) changes in electrical impedance, (6) modal strain energy, (7) finite element model updating, (8) neural network, novelty detection, and genetic algorithms, (9) principal component analysis and singular value decomposition, (10) modal identification (these methods are themselves subdivided into six sub-categories), (11) residual forces, (12) time domain data, and (13) Wavelet transformation.

Although, a structure may experience various types of damage during its service life, most of the damage identification methods reviewed here are based on the assumption damage causes only a loss of stiffness in one or more regions of the structure but not a loss of mass. Another challenge in structural health monitoring consists of separating changes in the structural dynamic behavior due to damage from those caused by other sources such as varying environmental conditions (i.e., humidity, wind, and most importantly temperature) and changes in operating conditions (e.g., light vs. heavy traffic on a bridge). Most of the methods summarized in this review are based on the assumption that the changes in structural dynamic behavior are caused by damage only.

2.1 Methods Based on Bayesian Analysis

This section reviews Bayesian probabilistic approaches for damage identification. The basic idea is to search for the most probable damage state/scenario based on the computed posterior probabilities of the potential damage states/scenarios given the modal

identification/estimation results extracted from dynamic measurement data. Formulation of the posterior probabilities can be based on an output error, which is defined as the difference between the estimated modal parameters and their theoretical counterparts obtained from an analytical model of the structure. Generally, the structure stiffness matrix is represented as an assembly of substructure stiffness matrices and a dimensionless parameter is introduced to model the stiffness contribution of each substructure. Assuming a prior probability density function for the dimensionless parameter, the relative posterior probability of an assumed damage state/scenario is formulated and a branch-and-bound search scheme can be applied to identify the most likely damage states/scenarios.

Sohn and Law (1997) applied a Bayesian probabilistic approach to detect the most likely locations and extent of damage in a structure. In their work, the system stiffness matrix was represented as an assembly of substructure stiffness matrices and a dimensionless parameter was introduced to model the stiffness contribution of each substructure. To assess the performance of their proposed method, they applied it to three example structures simulated numerically, namely a six-story shear frame structure, a two-story and a five-story three-dimensional frame structures. As long as sufficient modal data sets are available, their method is able to identify the damage locations and extent in most cases where: (1) less than 10 percent noise levels are achieved in the estimated modal parameters (i.e., modal parameter estimation errors with less than 10% coefficient-of-variation), (2) 10-30 percent of all the degrees of freedom are recorded/measured, and (3) several fundamental modes of vibration are estimated.

Sohn and Law (2000) described the application of their Bayesian approach (Sohn and Law 1997) to predict the locations of plastic hinge deformation using experimental data obtained from vibration tests performed on a reinforced-concrete bridge column. Their damage identification method was able to locate the damaged regions (i.e., plastic hinges) using a simplified analytical model of the column and the modal parameters estimated from the vibration test data.

Sohn and Law (2001) discussed potential application of load-dependent Ritz vectors and their incorporation into the previously proposed Bayesian framework (Sohn and Law 1997) for damage diagnosis. They presented a procedure that extracts the Ritz vectors based on a flexibility matrix estimated from experimentally identified modal parameters. Damage diagnoses performed on a physical grid-type bridge model indicate that better damage location results are obtained when using Ritz vectors than when using modal vectors. For comparison purposes, they included the results obtained from the application of the Minimum Rank Perturbation Theory (MRPT) (Kaouk and Zimmerman 1993) and the Sensitivity-Based Element-By-Element (SB-EBE) method (Farhat and Hemez 1993) to the test data of the grid bridge structure considered. The results indicate that the use of load-dependent Ritz vectors produces better damage diagnosis results than the use of modal vectors. Also, the Bayesian probabilistic approach was shown to give better damage diagnosis results than commonly used deterministic methods.

Ching and Beck (2004) used a two-step probabilistic structural health monitoring approach to analyze the Phase II experimental benchmark studies sponsored by the IASC-ASCE Task Group on Structural Health Monitoring. The two-step approach involves

modal identification followed by damage assessment using the pre- and post-damage modal parameters based on the Bayesian updating methodology. An Expectation Maximization algorithm was proposed to find the most probable values of the updating parameters. It was shown that the brace damage was successfully detected and assessed from either the hammer or ambient vibration data. The connection damage was much more difficult to detect reliably and assess because the identified modal parameters were less sensitive to connection damage, allowing the modeling errors to have more influence on the results.

Yuen et al. (2004) applied Bayesian updating of dynamic models of structures to perform all four levels of structural damage identification and assessment: damage detection, finding its location and severity, and its impact on the structural reliability. The numerical integration that is required in Bayesian updating is known to be computationally prohibitive for problems of high dimensions. The proposed approach used the Markov chain Monte Carlo simulation based on the Metropolis-Hastings algorithm to tackle this problem in conjunction with an adaptive concept to obtain in an efficient manner information about the important regions of the updated probability distribution. The approach was applied to the ASCE-IASC benchmark structure, showing that it is capable of exhibiting the impact on structural reliability of low levels of damage in the two different damage identification cases.

2.2 Methods Based on Control Theory

This Section presents the work of researchers who employed different control theories for structural damage identification. Such control theories include feedback control, adaptive control, Linear Matrix Inequality, Regulation Theory, and Least Mean Square filtering. Housner et al. (1997) provided a point of departure for researchers to assess the state-of-the-art in control and monitoring of civil engineering structures and gave a link between structural control and other fields of control theory.

Lim and Kashangaki (1994) used the measured natural frequencies and mode shapes from a modal test to determine the location and magnitude of damage in a space truss structure. Damage was located by computing the Euclidean distances between the measured mode shapes and the best achievable eigenvectors. The latter are the projection of the measured mode shapes onto the subspace defined by the refined analytical model of the structure and the measured natural frequencies. Loss of both stiffness and mass properties can be detected, located and quantified. A laboratory eight-bay truss structure, instrumented with three accelerometers at each node was tested to examine the performance of the method. The method performed well to identify damage even though measurement errors inevitably make the damage localization more difficult.

Ge and Soong (1998 a) presented a procedure for damage identification through measured structural response. The cost function employed was based on the regulation method for inverse problems. An optimization procedure using the Euler-Lagrange equation was developed to reduce the minimization problem to a two-point boundary value problem. Compared to other existing techniques in solving the minimization problem, this

approach does not resolve to more advanced mathematical tool and is thus more easily accepted in the engineering application field. Another distinct advantage of this method is that the form of damage, be it stiffness losses, nonlinear functions, or hysteresis, do not need to be assumed a priori. Numerical studies of 2-DOF and 10-DOF shear beam type structures and experimental correlation with a three story model structure demonstrated the feasibility and accuracy of the proposed approach and were reported in the companion paper by Ge and Soong (1998 b).

Ray and Tian (1999) employed methods of enhancing sensitivity of modal frequencies to small changes in structure parameters and local geometry through use of feedback control. These methods were developed for smart structures, i.e., those capable of self-excitation, self-sensing, and closed-loop vibration control. Using state feedback, closed-loop modal frequencies are placed at locations in the complex plane that enhance sensitivity to particular types of damage. A simple example introduced the principle of sensitivity enhancing control for a single-degree-of-freedom structure. Then, the method was applied to finite element models of a cantilevered beam to demonstrate the magnitude of sensitivity enhancement achievable for modest local damage. Simulation results showed that significant enhancement in sensitivity of modal frequencies to damage can be achieved using a single actuator and multiple strain sensors along the beam.

Gangadharan et al. (1999) presented an antioptimization-based method for testing structural models and for identifying and detecting damage. This method used the maximum value of the ratio or the difference in the strain energies of two alternative models as a metric of their difference. The paper presented applications of antioptimization for com-

paring alternative finite element models using a real life complex automotive structure as illustrative example. The proposed approach relies on the hypothesis that the antioptimization load is located near the damage location.

Gattulli and Romeo (2000) proposed an integrated procedure based on a direct adaptive control algorithm to address a dual goal: (1) vibration suppression and (2) damage detection. This was accomplished in the former by tracking a reference output of an arbitrary model with desired damping characteristics and in the latter by detecting on-line mechanical parameters variations. Applications to shear-type models showed that an opportune selection of a reduced measure of the complete state variables guarantees exact output reference tracking.

Abdalla et al. (2000) employed linear matrix inequality (LMI) methods for computationally efficient solution of damage detection problems in structures. This problem was formulated as a convex optimization problem involving LMI constraints on the unknown structural stiffness parameters. The proposed techniques were applied to detect damage in simulation examples and in a cantilevered beam test-bed using experimental data obtained from modal tests. Both the LMI matrix update and the LMI parameter update resulted in accurate detection of the damage locations.

Nauerz and Fritzen (2001) presented a method for damage identification in structural models, which was particularly used for the localization and quantification of structural faults. Their proposed damage identification method is based on power spectral densities. This offers the possibility of working with ambient excitation and using output-only signals. The only assumption is that the input spectral density can be approximated

by ergodic white noise. The lack of measurement information was treated by means of dynamic condensation technique and the Kalman Bucy filter technique. The algorithm was applied to two examples. The first example tested the proposed damage identification method using the condensed model matrices and expanded displacements from a simulated beam structure. In the second example, the proposed method was applied to a real multistory frame. In both examples the location and the size of the deviation between the measured structure and the finite element model could be obtained.

Lin and Betti (2004) presented a robust on-line adaptive identification algorithm to identify the structural parameters in non-linear systems, based on a recursive least squares formulation. This approach used a variable forgetting factor technique to adaptively update the adaptation gain matrix at every time step.

Chase et al. (2005) presented methods for structural health monitoring (SHM) of civil structures using adaptive least mean square filtering theory. Damage that occurs in the structure can be identified by changes in the stiffness matrix. “One Step” and “Two Step” adaptive LMS based methods were developed and tested. The proposed methods were applied to both the 4 and 12 DOF cases of the SHM Task Group’s Benchmark problems, and the results showed that the adaptive LMS filtering is very effective for identifying damage in real-time.

2.3 Damage Index Methods

The damage index method was originally developed by Stubbs (1992) to identify the damage in structures using a ratio of strain energy in discrete structural elements

before and after the occurrence of damage. Mode shapes before and after damage are required in this method, but they do not need to be mass normalized. Cornwell et al. (1999) extended this method to plate-like structures that are characterized by two-dimensional curvature. Duffey et al. (2001) extended the damage index method to be applicable to structures undergoing vibrations predominantly in axial or torsional modes. In Duffey et al. (2001), the method was compared to the flexibility-change method presented by Pandey and Biswas (1994). The two methods were applied to both simulated and experimental spring-mass systems undergoing axial response. Both the flexibility-change method and the damage index method were successful in detecting damage and in locating damaged elements for 10-percent reduction in element stiffness in a simulated spring-mass system.

Kim and Stubbs (2002) presented an improved damage index algorithm to overcome the limits of the previous damage index algorithms, namely damage index algorithm A (Kim and Stubbs 1995) and damage index algorithm B (Stubbs and Kim 1996). The two existing algorithms and the new algorithm were evaluated by predicting damage location and severity estimation in a theoretical model of a two-span continuous beam. The following observations about the performance of the algorithms were made. First, the use of damage index A for damage identification resulted in (1) relatively small Type I error (inability to detect the true damage locations); (2) small localization error; (3) relatively high Type II error (prediction of locations that are not damaged); and (4) high severity estimation error. It consistently overestimated severities of damage by about 1.75 times the true damage. Second, the use of damage index B resulted in no error related to damage

localization but high severity estimation error. It consistently underestimated severities by about 0.15 times the true damage. Finally, the use of the improved damage index algorithm resulted in no error related to damage localization and very small severity estimation error. Compared to the other two algorithms, the new damage index algorithm enhanced significantly the accuracy of the damage localization and severity estimation results.

Barroso and Roddriguez (2004) proposed a new methodology based on ratios between stiffness and mass values from the eigenvalue problem to identify the undamaged state (baseline) of the structure. In this paper, the first generation benchmark problem on structural health monitoring developed by the ASCE Task Group on structural health monitoring was considered. This problem consists of a frame model of an existing four-story physical model at the University of British Columbia for which simulated data were used to perform system identification. Modal parameters were extracted using the frequency domain decomposition method (Brincker et al. 2000). The accuracy of the extracted baseline information depended on the level of damage in the structure, with better results obtained in the presence of small amounts of damage. Once the structural properties of both the baseline and damaged structure were determined, the damage index method was used to identify the location and severity of damage.

2.4 Methods Based on Empirical Mode Decomposition and Hilbert-Huang Transformation

The empirical mode decomposition (EMD) is a new signal processing method, which can decompose any data set into several intrinsic mode functions (IMFs) by a pro-

cedure called sifting process. The sifting process is conducted by first constructing the upper and lower envelopes of the signal through connecting its local maxima and local minima by a cubic spline. The mean of the two envelopes is then computed and subtracted from the original time history. The difference between the original time history and the mean value is called the first IMF. The difference between the original signal and the first IMF is then treated as a new time history and subjected to the same sifting process, giving the second IMF. The sifting procedure continues until the residue becomes so small that it is less than a predetermined value of consequence, or the residue becomes a monotonic function. By decomposing the vibration signal in the time domain using the EMD, the damage time instant and damage location can be identified using the signal feature of damage spike. The damage time instant can then be identified in terms of the occurrence time of the damage spike, and the damage location can be determined by the spatial distribution of the observed damage spikes. The Hilbert-Huang transform (HHT) consists of the empirical mode decomposition combined with Hilbert spectral analysis, with the EMD method representing the core of the HHT.

Xu and Chen (2004) presented an experimental investigation on the applicability of the EMD for identifying structural damage caused by a sudden change of structural stiffness. A three-story shear building model was constructed and installed on a shaking table with two horizontal springs connected to the first floor. Structural damage was simulated by suddenly releasing the two pretensioned springs either simultaneously or successively. A series of free vibration, random vibration, and earthquake simulation tests were performed on the building with sudden stiffness changes. The damage location was identi-

fied by analyzing the spatial distribution of the damage spikes along the building height. The EMD approach was found quite robust and not sensitive to the type of external excitation. Small damage severity and multiple damage events could be identified using this approach.

Yang et al. (2004) proposed two damage identification methods based on the measured data that contain damage events of the structure. The first method, based on the EMD, is capable of detecting the damage time instants and damage locations by identifying the damage spikes due to a sudden change in structural stiffness similar to the method of wavelet transform. The second method, based on EMD and Hilbert transform, is proposed to quantitatively (1) detect the damage time instants and (2) identify the natural frequencies and damping ratios of the structure before and after damage. The two proposed methods were applied to the ASCE benchmark problem (Johnson et al. 2000). Using simulated structural vibration response data, the first method was able to detect damage spikes if the measured data is free of noise pollution or the level of noise pollution is very small. For the second method proposed, the simulation results demonstrated that the method is capable of (1) accurately determining the time instant when the damage occurs regardless of the noise level and (2) identifying the natural frequencies and damping ratios of the structure before and after damage quite accurately.

Law and Zhu (2005) studied the signatures of non-linear characteristics in the vibration of damaged reinforced concrete beams using Hilbert-Huang transform with reference for possible use to detect damage in reinforced concrete structures. The measured vibration signal from several reinforced concrete beams in different cracked damage states

were decomposed into intrinsic mode functions (IMF) using the EMD, and the Hilbert-Huang spectrum was subsequently obtained for each of them. The time history of the instantaneous frequency of the beam, obtained from the IMFs, was found to correlate well with the opening and closure of the cracks and the elastic deformation of the beam.

2.5 Impedance Based Methods

Structural impedance is a function of the structural properties such as stiffness, damping, and mass. When damage occurs in a structure, it leads to variations in stiffness, damping, sometimes mass and, as a consequence, variations in the structural model and structural impedance response.

Fasel et al. (2005) used auto-regressive coefficients from a frequency domain ARX model as a powerful feature for non-linear damage diagnosis. The addition of Extreme Value Statistics (EVS) as a tool for establishing confidence limits greatly enhances this damage identification technique. The suitability of the ARX model, combined with EVS, for non-linear damage identification was demonstrated using vibration data obtained from a laboratory experiment of a three-story building model. The vibration-based method (used for comparative purposes) was not able to localize damage in the test structure, while the integration of the impedance-based active sensing method into the frequency domain ARX model, showed very promising results with regard to damage localization and data normalization.

Tseng et al. (2005) developed an impedance model to extract the structural impedance response from the electric admittance measurements of piezoelectric transducer

(PZT) patches bonded to the structure and to predict the dynamic output forces of PZT patches on the host structure. A structural damage identification technique was then presented using the structural impedance response and the analytical system matrices. The proposed damage identification technique is based on the assumption that there exists a finite element model of the structure well correlated to the structural impedance response in the frequency domain. The finite element model of the structure for the pre-damaged state is then updated to represent the real damaged state and used to identify the structural damage. A numerical example of a fixed-fixed beam was given to illustrate the effectiveness of the proposed algorithm.

2.6 Methods Based on Modal Strain Energy

A method based on changes of modal strain energy (MSE) in each structural element before and after the occurrence of damage to localize the damage was developed by Shi and Law (1998). The elemental MSE was defined as the product of the elemental stiffness matrix and the second power of the mode shape component. The measured mode shapes and elemental stiffness matrices are required in the identification algorithm. In practice, the measured mode shapes are usually incomplete due to the limited number of sensors. In order to apply this method for damage localization, the mode shape expansion technique was used to expand the measured mode shape to the full dimension of the finite element model. The modes expansion technique was discussed by Law et al. (1998), in which a three-staged damage detection method was described. The incomplete measured mode shapes were first expanded to the full dimension of the finite element model. The

modal strain energy of each element normalized with its potential energy was then used to locate the damage domain. The measured modal frequency changes were employed to determine the magnitude of damage through a sensitivity-based method. Instead of expanding measured mode shapes to the full dimension of the finite element model, Shi et al. (2000b and c) presented a sensitivity- and statistical-based method called the Multiple Damage Location Assurance Criterion (MDLAC) to locate structural damage using incomplete mode shapes directly. The damage sites were preliminarily located using incomplete measured mode shapes without reconstruction of the unmeasured information. The suspected damaged elements were assessed again using the more accurately measured modal frequency information, to determine the true sites and the extent of damage. The accuracy of damage localization using this method was closely related to the amount and quality of the measured data.

Shi et al. (2000a) discussed the method of using element modal strain energy change (MSEC) before and after damage to locate and quantify the damage. Results from a numerical example of a beam and an experiment on a single-bay, two-story portal steel frame structure were investigated. The obtained results indicate that the proposed method is effective in locating the damage, but is noise sensitive in the damage quantification. In order to reduce the truncation and modeling errors in the higher modes, Shi et al. (2002) presented the improved modal strain energy method for structural damage quantification. The improved algorithm used only a few lower analytical modes for damage quantification. The numerical example of a fixed-end beam and experimental results from a two-story steel portal frame demonstrated that the improved algorithm (1) reduces the trunca-

tion error in computation; (2) avoids the finite element modeling errors in higher modes; and (3) improves the rate of convergence in the computation.

Ren and De Roeck (2002a b) demonstrated that multiplying the damaged eigenvalue equations by the damaged modes or undamaged modes provides more equations than the strain energy-based method does, which will improve the damage localization. Several solution techniques were discussed and compared. The Moore-Penrose pseudo-inverse method and the non-negative least-squares (NNLS) method (Lawson and Hanson 1974) were used in the paper. The NNLS technique was found to be one of the suitable solution methods. The proposed method was verified by a simple beam and a continuous beam with a number of simulated damage scenarios. This damage identification technique was able to find the exact location and severity of the damaged elements. When simulated noise was added to the modal data, a fairly good agreement between the predicted and the assumed damage could still be achieved. The proposed method was also validated by an experimental program of a reinforced concrete beam in Ren and De Roeck (2002 b).

Li et al. (2006) developed the modal strain energy decomposition method as a new damage localization method, capable of identifying the damage of individual members for three-dimensional frame structures. This method is based on decomposing the modal strain energy of each structural member (or element) into two parts, one associated with the element's axial coordinates and the other with its transverse coordinates. Numerical studies were conducted for a three-dimensional five-story frame structure and a complicated offshore template platform, based on synthetic data generated from finite element

models. Although the method was able to locate the damage for three-dimensional frame structures, it did not perform well on estimating the corresponding severity of the damage.

2.7 Methods Based on Finite Element Model Updating

Another class of damage identification methods is based on the modification of structural model matrices such as mass, stiffness, and damping to reproduce as closely as possible the measured static and dynamic response from the data. These methods update the physical parameters of a FE model of the structure by minimizing an objective function expressing the discrepancy between FE predicted and experimentally identified structural dynamic properties that are sensitive to damage such as natural frequencies and mode shapes. Comparisons of the updated model parameters to the original ones provide an indication of damage and can be used to quantify the location and extent of damage. The difference between various algorithms can be found in objective functions to be minimized, constraints placed on the problem, and numerical scheme used to implement the optimization. A few of common model updating algorithms are optimal matrix update methods, sensitivity-based methods, eigenstructure assignment method and hybrid methods which use combination of two or more algorithms (Doebling et al. 1996). A thorough review and description of the state of the art in finite element model updating was also provided by Mottershead and Friswell (1993) and also in the book by Friswell and Mottershead (1995).

Zimmerman and Kaouk (1992) presented a damage identification methodology based on a pre-damage refined FE model of the structure and the results of post-damage

modal analysis. This algorithm determines perturbation matrices to the original FE model such that the updated FE model exhibits the measured modal characteristics of the damaged structure. The perturbation matrices were then examined to determine the location and extent of structural damage. The algorithm was tested on both simulated and actual experimental data. The algorithm performed well on the simulated test structure, and the accuracy of results depended on the measured degrees of freedom in the mode shapes. The algorithm was also tested using the results of an experimental modal test of a cantilever beam. A comparison of measured and analytical frequency response functions indicated the improvement made by the eigenstructure assignment algorithm used in this paper.

Zimmerman and Kaouk (1994) developed a computationally attractive algorithm to provide an insight to the location and extent of structural damage. The algorithm made use of an original finite element model and a subset of measured eigenvalues and eigenvectors. The developed theory approaches the damage localization and damage quantification in a decoupled fashion. First, a theory was developed to determine the location of structural damage. With the structural damage locations determined, an extent algorithm was then developed. The extent algorithm is a minimum rank update. The algorithms were demonstrated using both numerical and actual experimental data. The effects of eigenvector measurement and expansion errors were demonstrated and techniques to overcome the effects of noise were discussed.

Casas and Aparicio (1994) discussed a methodology for the use of dynamic response as an inspection and surveillance tool for concrete structures (mainly bridges). The method is based on FE model updating of stiffness characteristics (related to crack-

ing) starting from modal parameters obtained from dynamic tests (impact hammer test). Several damage-identification examples were performed on groups of reinforced concrete beams with different and well-defined cracking patterns. This experimental verification showed the effectiveness of the proposed method in the identification of location, extension, and amount of cracking.

Liu (1995) presented a methodology to identify damage in a truss structures. The measured natural frequencies and mode shapes of the truss were used in the identification process. The identification algorithm was formulated as an optimization problem in which the error norm of the eigenequation is minimized. The finite element analysis was adopted to derive the discretized eigenequation of the truss. The perturbation method was used to investigate the influence of the measurement errors on the identification results. A simply supported truss with 21 members and 10 nodes was used as a numerical example. This numerical example demonstrated the effectiveness of the proposed method in parametric identification of a truss.

Alvin (1997) presented a FE model updating method based on a minimization of dynamic residuals. The dynamic residual of interest was the force unbalance in the homogeneous equation of motion arising from errors in the model's mass and stiffness when evaluated with the identified modal parameters. The proposed algorithm is a modification and extension of a previously-developed Sensitivity-Based Element-By-Element (SB-EBE) method for damage detection and finite element model updating. In the proposed algorithm, SB-EBE was generalized to minimize a dynamic displacement residual quantity, which was shown to improve test-analysis mode correspondence. Furthermore, the

algorithm was modified to include Bayesian estimation concepts, and the underlying non-linear optimization problem was consistently linearized to improve the convergence properties. The resulting algorithm was demonstrated via numerical and experimental examples to be an efficient and robust method for both localizing model errors and estimating physical parameters. The numerical example was a planar truss with 44 translational DOF, 7 of which were measured. The experimental example was a tubular welded frame formed into a ladder and representative of an automotive engine support, measures by 96 accelerometers grouped in 16 locations and the excitation was hammer impact.

Cobb and Liebst (1997 a) used a FE model updating method to determine damaged structural elements from measured modal data. This study was focused on prioritizing sensor locations on a flexible structure. The proposed method is useful in applications where only a small subset of the total structural degrees of freedom can be instrumented. The prioritization was based on an eigenvector sensitivity analysis of a finite element model of the structure. An analytical example was presented that illustrates the relationship between the number of measured modes, the number of instrumented degrees of freedom, and the extent to which damage can be localized. Additionally, an analysis of an experimental cantilevered eight-bay truss assembly consisting of 104 elements instrumented with eight single-axis accelerometers was presented. The extent to which structural damage could be localized from the measurement data was limited by the number of measured modes.

Cobb and Liebst (1997 b) discussed a damage identification method using a newly developed Assigned Partial Eigenstructure (APE) method, which determines the required stiffness changes consistent with the FE formulation, to achieve the maximum correlation

with the measured eigendata. This method does not require the computation of the eigenstructure sensitivities and the corresponding eigenanalysis during the iteration process. This method was applied on both a fully instrumented and a sparsely instrumented experimental structure, and was able to correctly determine the location and amount of structure damage. The extent to which damage could be localized was limited by both model fidelity and accuracy of the measured modes.

Kim and Bartkowicz (1997) described a two-step damage identification approach for large and complex structures with limited number of measurements. The first step identifies a general area of structural damage using the optimal model updating method and a hybrid model reduction/eigenvector expansion technique. The second step will then locate a specific damaged structural component using a design sensitivity technique based on a priori information from the first step. Eigensystem Realization Algorithm (ERA) was used to extract the modal parameters. Performance of the proposed approach was demonstrated with testing and analysis of a ten-bay hexagonal truss structure. The specific damaged component was clearly located using sensitivity method together with initial damage identification results.

Fritzel et al. (1998) proposed a method to identify the location and extent of structural damage from measured vibration test data. The method is based on a mathematical model representing the undamaged vibrating structure and a local description of the damage (e.g., a finite element for a cracked beam). The concept of inverse sensitivity equations was used which can be based on any type of data such as modal data, FRFs, time series, or a combination of them. An orthogonalization strategy was also used to reduce

the parameter set. The method was validated through application to laboratory structures in the frequency domain using frequency response functions and also in the time domain.

Kiddy and Pines (1998) showed that, although it is impossible to simultaneously update both the full mass and stiffness matrices, it is possible to update both matrices simultaneously if a constraint is added to the problem. Furthermore, it was shown that this constraint does not drastically interfere with the capability of identifying damage as a change in the mass and stiffness matrices. A simple example of cantilever beam with 3 elements was considered under axial loading.

Lam et al. (1998) developed two techniques in their proposed method, namely the Approximate Parameter Change (APC) technique and the Damage Signature Matching (DSM) technique. The APC technique was able to locate the damage by calculating the approximate change of system parameters based on two sets of modal data, which were measured before and after the structure was damaged. The DSM technique was developed as a supplement to the APC technique for more complicated cases. Based on the same sets of modal data, measured damage signatures were determined. Predicted damage signatures for different possible damage locations were determined with reference to the mathematical model. The damage and its location on the structure were then identified from the pattern matching between the measured and predicted damage signatures. The proposed method was verified by numerical and experimental case studies with particular reference to steel-framed structures with damage at its connections.

Papadopoulos and Garcia (1998) presented a method to improve the robustness of current damage identification methodologies. Measured statistical changes in natural fre-

quencies and mode shapes along with a FE model were used to assess the integrity of a structure. The method was successful in identifying the probabilistic existence, location and extent of simulated structural damage in a one dimensional three-degree-of-freedom spring-mass system and on an Euler-Bernoulli cantilever aluminum beam.

Capecchi and Vestroni (1999) discussed a damage identification method based on the minimization of an objective function that accounts for the difference between analytical and experimental identified modal frequencies. The procedures developed are applied to sample cases: a supported beam, a clamped beam, a continuous beam and a shear-type frame, using experimental and simulated data. The identification procedure was carried out mainly by the computer code IDEFEM. When experimental data were used, the location of damage was accurate, though some discrepancies remained in its quantification, depending on which frequencies were selected from those available. The presence of modeling and experimental errors, however, considerably complicated the problem to reach the exact solution and more frequencies were required to reduce the effect of errors.

Zhang et al. (2000) presented a FE model updating procedure applied to complex structures using an eigenvalue sensitivity-based updating approach. The method is based on the first-order Taylor-series expansion of the eigenvalues with respect to some structural parameters selected to be adjusted. The changes in the updating parameters were found iteratively by solving a constrained optimization problem. The proposed method was applied to a 1/150 scaled suspension bridge model. Using 11 measured frequencies as reference, the FE model was updated by adjusting ten selected structural parameters. The

final updated FE model for the suspension bridge model was able to produce natural frequencies in close agreement with the measured ones.

Brownjohn et al. (2001) described a sensitivity-based FE model updating method and its application to structure condition assessment with particular reference to bridges. The accuracy analysis of damage assessment by model updating was investigated through a case study. A damaged steel portal frame was used to compare updated values of the geometrical parameters at damaged zones with their known real values.

Hemez and Doebling (2001) presented several numerical and experimental test beds that span a wide variety of applications (from non-linear vibrations to shock response) and difficulty (from a single-degree-of-freedom system with localized non-linearity to a three-dimensional multiple component assembly featuring non-linear material response and contact mechanics). These test beds were developed at Los Alamos National Laboratory. In the second part of this work, the state-of-the-art in the area of model updating for non-linear, transient dynamics was reviewed. The techniques identified as the most promising were assessed using data from the numerical or experimental test beds. This publication concluded with a brief description of current research directions in inverse problem solving for structural dynamics.

Abdel Wahab (2001) investigated the effect of using modal curvatures as modal parameters on the convergence of the updating algorithm for the purpose of damage identification. Simulated data of a simply supported beam were used to perform this study. A sensitivity-based updating algorithm was used. It was found that using modal curvatures in the model updating algorithm did not improve its convergence. Therefore, it was con-

cluded that modal curvatures are useful parameters for damage identification when using the response-based approach but not useful when using the model-based approach.

Cha and Switkes (2002) developed a new method to update the system mass, damping, and stiffness matrices in turn using frequency-response data. The method enforces the connectivity (or sparsity) information, therefore the size of the least-squares problem is drastically reduced. This new updating method was applied to a numerical example of 26 DOF shear building model. Numerical results verified the accuracy of the updating algorithm for calibrating the structural system parameters using frequency-response data.

Jang et al. (2002) considered a system identification method to identify structural parameters in a FE model by minimizing the error between measured and analytically computed responses. A regularization scheme was applied to alleviate the ill-posedness of an inverse problem by adding a regularization function to the primary error function. Two different algorithms were introduced depending on the type of measurements, static or modal response, but the essential idea behind them is identical. To consider noise in the measurements, a statistical evaluation scheme proposed by Yeo et al. (2000) was applied. Static displacements from static loading and vertical accelerations from impact vibration test were measured through laboratory experiments on a grid-type model bridge by accelerometers at 12 nodes. The baseline structural model and baseline properties were determined based on experimental data obtained from the tests on the undamaged model structure. The applicability of the proposed damage assessment algorithm was investigated through experimental examples.

Xia et al. (2002) proposed a method to identify structural damage based on comparing the measured frequencies and mode shapes before and after damage. The effects of uncertainties in both the measured vibration data and finite element model were considered as random variables in model updating. The statistics (mean and standard deviation) of the updated stiffness parameters in the damaged configurations were calculated with perturbation method and Monte Carlo simulation. The probability of damage existence was calculated to estimate the possibility of damage existence in the structural members. The proposed method was applied to a laboratory tested steel cantilever beam and frame structure. The results showed that the damage was identified correctly with high probabilities of damage existence. Discussions were also made on the applicability of the method when no measurement data of intact structure are available.

Pothisiri and Hjelmstad (2003) presented a global damage assessment algorithm based on a parameter estimation method using a FE model and the measured modal response of a structure. An optimization scheme was proposed to localize damaged regions in the structure. Damage probability functions were computed upon completion of the localization process for candidate elements. Monte Carlo methods were used to compute the required probabilities based on the statistical distributions of the parameters for the damaged and the associated baseline structure. The algorithm was tested in a numerical simulation environment using a planar bridge truss as a model problem. From the simulation results, it was concluded that the proposed algorithm can identify damage successfully in the presence of measurement noise provided that the noise level is low.

Xia and Hao (2003) developed a statistical damage identification algorithm based on changes in natural frequencies to account for the effects of random noise in the vibration data and finite element modeling error. The structural stiffness parameters in the intact state and damaged state were derived with a two-stage model updating process. The statistics of the parameters were estimated by the perturbation method and verified by Monte Carlo technique. The probability of damage existence was then estimated based on the probability density functions of the parameters in the two states. A higher probability implies a more likelihood of damage occurrence. The presented technique is applied to detect damage in a numerical cantilever beam and a laboratory tested steel cantilever plate.

Fanning and Carden (2003) presented a damage identification algorithm which relies on a single-input-single-output (SISO) measurement made at several frequencies and a correlated numerical model of the structure. The feasibility of the algorithm was based on a computationally efficient method of calculating a single FRF of the structure when it undergoes a stiffness change in a limited number of elements. Initially, the undamaged structure was tested and a calibrated finite element model was generated. The algorithm was shown to be successful numerically on a simple two-story frame structure when the maximum number potential damage locations has been limited to two.

Kim et al. (2004) discussed an iterative method to solve the inverse problem of dynamic structural systems. The structural modifications were sought for the characteristic changes assigned from the design goals or modal measurements. A finite element method was used for the system analysis and inverse problem. The method is based on the

equilibrium equations of a set of selected degrees of freedom and the energy equation associated with the frequency change. The mode shape change was expressed as a combination of the baseline mode shape and a complementary vector. A penalty function method was employed, along with an objective function of least structural change. Two numerical examples, a cantilever beam and a truss structure, were used to verify the proposed method. It was found that errors in the modal data had significant effects on the accuracy of the inverse solution.

Bassevillea et al. (2004) addressed the vibration-based structural health monitoring problem as the double task of detecting the damage, and localizing the detected damage within (a FEM of) the monitored structure. The proposed damage detection algorithm is based on a residual generated from a stochastic subspace-based covariance-driven identification method and on the statistical local approach to the design of detection algorithms. This algorithm basically computes a global test, which performs a sensitivity analysis of the residuals to the damage, relative to uncertainties and noises. Damage localization was stated as a detection problem.

Hwang and Kim (2004) discussed methods to identify the locations and severity of damage in structures using frequency response function (FRF) data. Basic methods identify the location and severity of structural damage by minimizing the difference between test and analytic FRFs, which is a type of model updating or optimization method; however, the method proposed in this paper used only a subset of vectors from the full set of FRFs for a few frequencies and calculates the stiffness matrix and reductions in explicit form. To verify the proposed method, examples of a simple cantilever and a helicopter

rotor blade were numerically demonstrated. The proposed method identified the location of damage in these objects, and characterized the damage to a satisfactory level of precision.

Lam et al. (2004) discussed a damage identification method based on a statistical model updating methodology which utilizes the measured vibration responses of the structure without any knowledge of the input excitation. The emphasis in this paper is on the application of the proposed methodology in Phase I of the benchmark study set up by the IASC-ASCE Task Group on structural health monitoring. The statistical model updating methodology adopted in this paper was based on the Bayesian modal identification approach presented in Katafygiotis and Yuen (2001). All six cases of the benchmark study were considered in this paper assuming unknown input. The methodology did not fail to identify damage in any of the cases considered, although the identified damage extent was slightly overestimated for cases with modeling error.

Teughels and De Roeck (2004) described an iterative sensitivity based FE model updating method in which the discrepancies in both the eigenfrequencies and unscaled mode shape data obtained from ambient tests were minimized. Additionally the optimization process was made more robust by using the trust region strategy in the implementation of the Gauss-Newton method, which was another original contribution of this work. The updating procedure was validated with a real application to a prestressed concrete bridge Z24 in Switzerland. The stochastic subspace technique was used to extract the modal data from the measured vibration data. The damage in the highway bridge was

identified by updating the Young's and the shear modulus, whose distribution over the FE model are approximated by piecewise linear functions.

2.8 Methods Based on Neural Network, Novelty Detection, and Genetic Algorithms

Artificial neural networks (ANNs) were developed as a methodology for emulating the biology of human brain, resulting in systems that learn by experience. Recently, the use of ANN has been extended to identify the structural damage. Masri et al. (2000) presented a nonparametric structural damage identification method based on neural network approach. The approach relied on the use of vibration measurements from a "healthy" system to train a neural network for identification purposes. Subsequently, the trained network was fed comparable vibration measurements from the same structure in order to monitor the health of the structure and thereby provide a relatively sensitive indicator of damage in the structure. Although the authors advocated the efficiency of nonparametric identification approaches such as the proposed neural networks, they also pointed out the limitations of such approaches in locating the damage unless a prior knowledge is available on states and their respective vibration signatures. Xu et al. (2003) presented a four-step procedure to identify damage using neural network method. A neural network emulator was first trained using the dynamic response from the healthy structure, then the damage was detected from the error between the dynamic response predicted by the emulator and their measured counterparts. A third step builds up a parametric neural

network for the proper selection of the evaluation index and eventually it was used in step four to quantify the damage.

A unifying framework for techniques from a wide range of disciplines was developed to identify damage based on novelty detection (Bishop 1994; Worden 1997; Worden et al. 2002). The philosophy of the approach is simply to establish a description of “normality” using features representing the undamaged condition of the structure and then test for “abnormality” or “novelty” when new data becomes available. There are numerous different methods of novelty detection including probability density estimation, artificial neural networks, outlier analysis (Worden et al. 2000). The validity of novelty methods were investigated by Worden et al. (2003) and Manson et al. (2003a, b). Worden et al. (2003) presented the experimental validation of novelty detection algorithms based on measured transmissibility FRFs from a simplified model of a metallic aircraft wing box. Three different novelty detection algorithms, namely outlier analysis, density estimation and an auto-associative neural network technique, were considered. All three methods were shown to be successful to an extent, although a critical comparison indicated reservations about the density estimation approach when used on sparse data sets. Manson et al. (2003 a) applied outlier analysis method on a more realistic structure, namely the wing of a Gnat aircraft, as opposed to the previously investigated laboratory structure, then Manson et al. (2003 b) extended the novelty detection method from damage detection to damage localization.

In the application of neural network methods, the optimization techniques are needed to find optimum values of the network weights such that the objective function is

minimized. There are a lot of optimization techniques available for this purpose such as the gradient-based methods, simulated annealing, genetic algorithms, and random perturbation methods. Hong and Xia (2002) applied a genetic algorithm (GA) with real number encoding to identify the structural damage by minimizing the objective function, which directly compares the changes in the measurements before and after damage. Three different criteria were considered, namely, the frequency changes, the mode shape changes, and a combination of the two. A laboratory tested cantilever beam and a frame were used to demonstrate the proposed technique. Numerical results showed that the damaged elements could be detected by genetic algorithm, even when the analytical model was not accurate. It is also demonstrated that the proposed method with a real-coded GA gives better damage detection results for the beam than the conventional optimization method.

Moslem and Nafaspour (2002) applied Steady-Sate Genetic Algorithms (SSGA) as an optimization tool to identify the extent of the damage in truss members. Two truss structures, one small and the other a relatively large truss were examined to validate the damage identification procedure proposed in this paper. Though the proposed algorithm has the advantage of being systematic, the inevitable errors such as measurement noise, model expansion, and especially model reduction errors presented difficulties in locating possible damaged areas.

2.9 Methods Based on Principal Component Analysis or Singular Value Decomposition

Bernal (2002) developed a damage localization method based on changes in measured flexibility through a singular value decomposition. This method identified the elements of the structure that were damaged as belonging to the set of elements whose internal forces under the action of a certain set of load vectors are zero. These vectors, which were designated as damage locating vectors (DLVs) define a basis for the null space of the change in flexibility and were computed from the measured data without reference to a model of the structure. The proposed method was demonstrated on two numerical examples of a truss having 44 bars and 9 sensors. In the first example the flexibility matrices for the truss were derived from state-space system identification of white noise excited responses and the localization was carried out for two different damage scenarios (reduction in element area). The second example used a truncated basis of analytically computed modes to assemble the flexibility matrices but examines 250 multiple damage cases to gain a statistical sense of performance.

Vanlanduit et al. (2005) proposed a system to identify damage in structures from measurements taken under different conditions (i.e. different operational excitation levels, geometrical uncertainties and surface treatments of the structure). This method is based on a robust singular value decomposition (RSVD). Using the RSVD the distance of an observation to the subspace spanned by the intact measurements can be computed. The proposed RSVD method was compared with an existing method based on the classical least-squares SVD. This damage identification method was validated on an aluminium beam

with different damage scenarios (a saw cut and a fatigue crack). In order to quantify the sensitivity of the proposed technique a simulation was performed in this paper. From the experimental results it was concluded that the classical least-squares SVD approach gives incorrect decomposition (and hence an incorrect classification between damaged and intact samples) when both damaged and intact measurements are used to compute the sub-space. It was shown that the iterative SVD slightly improved the classification results. However, in order to obtain reliable results, the introduced robust SVD should be used.

2.10 Modal Identification Based Methods

The modal identification based methods rely on the fact that modal parameters of the structure are functions of structural physical parameters, such as mass, stiffness, and damping. Changes to the material and/or geometric properties of systems, including changes to the boundary conditions and system connectivity, will produce changes in the modal parameters. Thus changes from modal properties and quantities derived from these properties such as mode shape curvature and dynamic flexibility matrix components can be utilized in the damage identification. Sensitivity of measured modal properties to potential damage in their practical application was studied by Alampalli et al. (1997), Palacz and Krawczuk (2002), and Zhu and Xu (2005). In Alampalli et al. (1997), modal tests were conducted through impact tests on a one-sixth scale multiple steel-girder model bridge and a fracture critical field bridge, including both intact and simulated damage states. Sensitivity of modal parameters to changes of the structural condition was studied using statistical methods. Results showed that even though modal frequencies and mode

shapes may be used to detect the existence of commonly observed bridge damage, it is difficult to identify their locations. The sensitivity coefficients of mode shapes, slopes and curvatures of mode shapes of a mono-coupled periodic structure with respect to damage was derived by Zhu and Xu (2005). The comparative study of a 10-element mono-coupled periodic spring-mass system showed that among natural frequencies, mode shapes, slopes and curvatures, the mode shape curvatures were the most sensitive dynamic features to damage, but the slopes of mode shapes were more indicative of damage location.

2.10.1 Methods Based on Changes in Natural Frequencies

Salawu (1997) presented a review on the use of changes in natural frequencies for damage detection only. It is in general difficult to localize damage (i.e., obtain spatial information on the detected structural damage) from changes in natural frequencies only. Bicanic and Chen (1997) developed a formulation for damage prediction using only the changes of natural frequencies. It was shown that the proposed method can predict the location of damage and also determine the amount of damage from a limited number of natural frequencies. Two computational procedures, the direct iteration (DI) technique and the Gauss-Newton least squares (GNLS) technique, were developed to solve for the element scalar damage indicators as primary unknowns. Different numerical examples were used to demonstrate the effectiveness of the proposed method.

Messina et al. (1998) extended the Multiple Damage Location Assurance Criterion (MDLAC) by introducing two methods of estimating the size of defects in a structure. The proposed methods only require information about the changes in a few of natural frequen-

cies between the undamaged and damaged state. Both algorithms for localizing and quantifying the damage are validated experimentally using a 3D beam test structure.

2.10.2 Methods Based on Changes in Flexibility

Usually, the dynamically measured flexibility matrix is estimated from the mass-normalized measured mode shapes and measured eigenvalue matrix. Damage is detected using flexibility matrices by comparing the flexibility matrix indices computed using the modes of the damaged structure to flexibility matrix indices computed using the undamaged structure. Pandey and Biswas (1994) presented changes in the flexibility matrix of the structure as a candidate method not only for damage detection but also for damage localization. It was shown that the flexibility matrix can be easily and accurately estimated from a few of lower vibration modes of the structure. The effect of structural damage on its flexibility was studied in simple analytical beam models. By using these analytical models, the effectiveness of using changes in flexibility matrix in detecting and locating damage was demonstrated. The procedure was then tested successfully with experimental data collected on a wide-flange steel beam.

Zhao and DeWolf (1999) presented a sensitivity study to determine which dynamic parameters are best for monitoring purposes for application to bridges. This study reviewed and investigated different diagnostic parameters, including the natural frequencies, the mode shapes, and the modal flexibility. A spring-mass system with five degrees of freedom was used to demonstrate the application of the sensitivity analysis. The minimum and maximum values based on using sensitivity coefficient for the natural frequen-

cies were 0.029 and 4.44, respectively. The minimum and maximum values for the mode shapes were 0.009 and 3.74, respectively. The minimum and maximum values for the modal flexibility were 3.70 and 524.6, respectively. The larger values for the modal flexibility indicate that modal flexibility will more readily indicate changes in stiffness than either the natural frequencies or mode shapes separately.

Catbas and Aktan (2000) carried out an extensive study for evaluation of different experimental and analytical techniques for damage identification of civil structures. A three span steel-stringer bridge (Seymoure Bridge) was subjected to a regime of deliberately induced damage to simulate many of the common deterioration and damage states that may affect these bridges. Multiple Reference Impact Testing (MRIT) was used as a testing procedure, for modal testing of the bridge. The damage was applied by removal of one bearing plate of a girder from one abutment. A number of different indices were employed for a comparative study on damage identification. A damage indicator (Bridge Girder Condition Indicator) based on the deflections computed using modal flexibility yielded very promising results for locating the damage and quantifying damaged response for certain loading patterns.

Duan et al. (2005) proposed an approach to assemble a proportional flexibility matrix (PFM) from arbitrarily scaled modes and modal frequencies with output only data. Instead of real flexibilities, the PFMs are incorporated into the damage locating vectors (DLV) method for damage localizations in ambient vibrations. PFMs for the pre- and post-damaged structure need to be comparable before being integrated into the DLV procedure. This requirements is guaranteed when there is at least one reference degree with

unchanged mass after damage. Two numerical examples showed that a small number of measured modes can produce PFMs with sufficient accuracy to correctly locate the damage by the DLV method from output-only data.

2.10.3 Methods Based on Changes in Frequency Response Functions

Lew (1995) presented a novel approach to locate the damage based on the comparison of the transfer function parameters of a system before and after occurrence of damage. A coherence approach was developed for locating the damage when the structural damage is observed. A nine-bay truss example was used to demonstrate and verify the approach developed.

Wang et al. (1997) formulated a new damage identification algorithm to utilize an original analytical model and frequency response function (FRF) obtained from measured data prior and posterior to damage. Based on nonlinear perturbation equations of FRF, an algorithm was derived which can be used to determine a damage vector indicating both location and magnitude of damage from perturbation equations of FRF. For extension of the proposed algorithm to cases of incomplete measurement in terms of coordinates, an iterative version of the proposed algorithm was introduced. The validity, accuracy and applicability of the proposed method was assessed by numerical and experimental studies using a practical plane 3-bay frame structure. In the numerical case study, the proposed algorithm accurately identified the location and extent of the damage even in presence of 5% measurement errors. In the experimental investigation, the identified damage slightly

mismatched the real damage, which could be attributed to inaccurate modeling of the joint elements and inaccurate representation of slot cut damage.

Sampaio et al. (1999) described the FRF curvature method theoretically and compared it with two of the most referenced methods on literature: mode shape curvature method and damage index method. The FRF curvature method is based on only the measured data without the need for any modal identification. This new damage identification method was demonstrated using a numerical 10 DOF lumped-mass system and the experimental data gathered from the I-40 Bridge. Results showed that the FRF curvature method perform well in detecting, locating and quantifying damage, although this last item (damage quantification) still has to be further developed and better characterized.

Ratcliffe (2000) presented a method for detecting and locating structural damage using experimental vibration data. The method used measured FRFs to obtain displacement as a function of frequency. The displacement functions were converted to curvature functions, which were further processed to yield a frequency dependent damage index using gapped-smoothing method. The location of the damage was revealed by showing the damage index as a contour plot of frequency versus position. The method was able to correctly locate the damage from the results of an experimental demonstration in which a steel beam was damaged with a narrow slot.

Reich and Park (2000) presented a method that utilizes an invariance property of transmission zeros of substructural frequency response functions. These functions were obtained by partitioning the global dynamic flexibility into a substructural form. It was shown that the transmission zeros of the frequency response functions of a damaged sub-

structure are invariant whereas those of healthy substructures are affected. The present method exploited this invariance property for the damage identification in a structure. Numerical examples were presented to demonstrate the utility of the proposed method.

2.10.4 Methods Based on Changes in Modal Curvature

Pandey et al. (1991) introduced the concept of using curvature mode shapes for damage localization. The difference in the modal curvature between the intact and the damaged case was utilized to locate the crack. It was demonstrated that the modal curvature is related to the stiffness of beam cross-sections and it was obtained numerically using the centre difference approximation algorithm. Both a cantilever and a simply supported beam models were used to demonstrate the modal curvature change as the damage indictor to identify the damage. It was shown that changes in the modal curvatures are sensitive to localized damage region, although the changes in mode shapes failed to localized the damage. Furthermore, it was also found that the Modal Assurance Criterion (MAC) and the Co-ordinate Modal Assurance Criterion (COMAC) are not sensitive enough to detect damage for the case investigated. An important remark in this study was that the difference in modal curvature between the intact and the damaged beam showed not only a high peak at the fault position but also some small peaks at different undamaged locations for the higher modes.This can cause confusion to the analyst in a practical application in which one does not know in advance the location of faults. In order to solve this problem, Abdel Wahab and De Roeck (1999) investigated the accuracy of using the central difference approximation to compute the modal curvature and determine the reason of the pres-

ence of misleading small peaks. In this paper, the authors introduced the concept of curvature damage factor (CDF), in which the difference in mode shape curvature was averaged over all modes. To establish the method, simply supported and continuous beams containing damaged parts at different locations were tested using simulated data. When the structure contains several damage locations, the CDF gave a clear identification of these locations. The technique was further applied to a real structure, namely Bridge Z24. It was found that the modal curvature of lower modes is in general more accurate than those of the higher ones and when more than one fault exist in the structure, and it is not possible to locate damage in all locations from the modal curvatures of only one mode.

Ratcliffe (1997) introduced a finite difference Laplacian function (which represents the curvature of mode shape) to identify the location of structural damage in a beam. When damage was less severe, further processing of the Laplacian was needed. The post-processing consisted of determining a cubic polynomial to fit the Laplacian locally at each spatial co-ordinate. A difference function between the cubic and Laplacian provided the information necessary to identify the location of damage. Mode shape data from the fundamental mode are most suited to the technique. However, data from the next three or four natural frequencies could be of use, particularly for verification of the results from the fundamental mode.

Oh and Jung (1998) proposed an improved damage identification algorithm based on system identification. In this approach, the complete sets of modes or displacements are not needed since the error function involved only the differences between components of those vectors. The proposed approach allowed the use of hybrid data, which consisted

of static displacements and eigenmodes. In the dynamic test, the curvature and slope of mode shapes were introduced to formulate the error responses. Using these techniques, a parametric study was conducted and the effectiveness of the method was discussed. A series of simulated tests for a predetermined damaged two-span continuous beam and a planar bowstring truss structure were performed. The damage identification results obtained using the proposed method were in good agreement with the simulated damage.

2.10.5 Methods Based on Changes in Stiffness

Koh et al. (1995) presented an improved condensation method for identification of local damage of multi-story frame buildings in terms of changes in story stiffness. Local here refers to story level rather than individual members. Static condensation was employed to reduce the system size. Identification was executed recursively on the remedial model in order to yield integrity indices for all stories. Numerical study of a 12-story building with various noise level showed the feasibility and computational efficiency of this method. The efficiency of the method was further validated through an experimental example of a 6-story laboratory model subjected to hammer impact tests.

Banks et al. (1996) discussed a theoretical, numerical and experimental investigation of the use of smart structures, parameterized partial differential equations and Galerkin approximation techniques to detect and locate damage. Smart structures refer to structures with embedded and/or surface mounted piezoceramic patches which may be used to sense and actuate vibrations of the host structure. Unlike many competing methods, this approach was independent of modal information from the structure. Changes in

damping, mass and stiffness properties of the structure were estimated using time histories of the input and vibration response of the structure, generated and measured by the piezo-ceramic patches internal to the structure. Using data from beam experiments, the feasibility of this approach was demonstrated in obtaining reliable, physically meaningful dynamic parameters such as stiffness, damping, and mass density, and hence identifying damage from the changes in those physical coefficients. Although results were obtained only for aluminum beams, the framework can be readily applied to plate, shell and beam like structures. However in the case of crack damage and delamination, the partial differential equation model developed here cannot be applied directly.

Caicedo et al. (2004) developed a least squares optimization method to estimate the stiffness parameters based on the measured modal parameters which were identified using Natural Excitation Technique combined with Eigensystem Realization Algorithm (NExT-ERA). The proposed method was applied to the simulated acceleration response data from an analytical model of an existing physical structure. Noise in the sensors was simulated in the benchmark problem by adding a stationary, broadband signal to the response. In order to identify the damage, the stiffness of each floor in the damaged case was compared to that of the undamaged case. The proposed method was applied using the structural response data generated with two different models, different excitations, and various damage patterns (12 DOF and 120 DOF model, wind and shaker excitations, six different damage cases by removing braces). The proposed method was shown to be effective for detecting, localizing and quantifying the damage.

Lus et al. (2004) briefly presented the theory for a system and damage identification algorithm for linear systems, and discussed the effectiveness of such a methodology in the context of a benchmark problem that was proposed by the ASCE Task Group in Health Monitoring. The proposed approach has two well-defined phases: (1) identification of a state space model using the Observer/Kalman filter identification algorithm, the eigensystem realization algorithm, and a nonlinear optimization approach based on sequential quadratic programming techniques, and (2) identification of the second-order dynamic model parameters from the realized state space model. The location and amount of the structural damage were determined by comparing the identified stiffness matrices for the undamaged and damaged cases. The numerical results for all the cases contained in the benchmark problem provided a good estimation of the location and amount of structural damage, even in the presence of substantial measurement noise and possible modeling errors.

2.10.6 Other Methods

This section reviews the system identification based methods which can not be categorized in any of above described groups. These methods use the same basic idea, employing the system identification methodology to identify the modal properties and track their changes to identify the damage.

Baruh and Ratan (1993) developed a method for detection and localization of structural damage. The detection is carried out in two parts. First, the eigensolution of system is computed using a modal parameter identification technique. Then the estimated

eigensolution is used together with the properties of the eigenvalue problem to identify the damaged components. The method was applied to a truss structure (with 12 elements, 20 nodes). A sensitivity analysis was performed, where the effects of modeling errors and inaccuracy in the identification procedure (estimation errors) were analyzed. It was observed that such errors, when relatively small, do not affect the damage identification results.

Soeiro and Hajela (1993) described a method to identify damage in composite structures that has its basis in methods of system identification. Two distinct analytical models, one using two-dimensional (2D) elements in conjunction with the classical lamination theory and another using three-dimensional (3D) elements were considered. The output error method for system identification was employed to determine changes in the analytical model necessary to minimize differences between the measured and predicted response. Numerical simulation of measurements such as static deflections, strains, and vibration modes were used in the identification procedure. The method has been implemented for a series of example problems with encouraging results.

Lim et al. (1996) employed a real-time modal parameter identification algorithm for structural damage detection. Because the modal parameter extraction process was conducted in real time, the algorithm is capable of identifying changes in structural properties attributable to structural damage as soon as they occur. Using the algorithm and a laboratory truss structure, it was demonstrated experimentally that continuous, real-time monitoring of anomalies attributable to structural damage is feasible. This monitoring capability will provide an early warning to an operator so that proper measures can be

taken before a catastrophic failure occurs. The results of this damage detection study using the truss were presented along with the description of the real-time modal parameter identification algorithm.

Hjelmstad and Shin (1997) developed a damage identification algorithm based on parameter estimation with an adaptive parameter grouping scheme. An adaptive parameter grouping scheme was proposed to localize damage in a structural system for which the measured data are sparse. A data perturbation scheme was proposed both for the baseline structure, to establish the damage threshold above which damage can be confidently discerned from noise, and for the damaged structure, to compute the damage indices. To examine and demonstrate the damage identification algorithm, a numerical simulation study on a planar bowstring truss structure was performed. The case studies showed that the developed algorithm can identify damage in structural systems even under sparse and noisy measured data.

Wong and Chen (2000) developed methods for the identification of structural damage in nonlinear structures. The damage was defined as either a reduction of stiffness or a change of restoring force characteristics from linear (undamaged state) to weak nonlinear (damaged state). The first method used for identifying both the location and type of damage is the location vector method (LVM). The LVM requires only the modal data from the first few fundamental modes. The second method, which was for quantifying the damage, is based on Fast Fourier Transform (FFT) and the least-squares method under the assumptions that the location of the damage can be identified. The methods were demonstrated by a five degree-of-freedom Duffing's nonlinear system. Measurement data were simulated

in the time domain and in the frequency domain by using the Runge-Kutta method and FFT, respectively. The robustness and effectiveness of the methods were examined by using a simulated output time history contaminated by a 5% white noise, which represented more realistic levels of measurement errors.

Di Paola and Bilello (2004) proposed a damage identification procedure for Euler-Bernoulli beams under static loads by using an integral formulation. This identification procedure is based on a least-square constrained nonlinear minimization problem. A proper objective function is defined as a function of theoretical and measured variations of a structural response characteristic in the presence of damage. If the experimental measurements are considered free from errors, the identification algorithm provides the exact estimation of damage parameters using the minimum number of information. The performance of the identification procedure was investigated in a rectangular cross-section beam with different damage scenarios. The results showed that, for an adequately small amplitude of noise, both mean errors and standard deviations of the estimated parameters are reduced with increasing amounts of information, so proving the consistency of the estimation.

Yoshimoto et al. (2005) presented a damage identification algorithm for structural health monitoring based on the subspace identification and the complex modal analysis. The proposed algorithm is applicable to any shear type structure. The algorithm is based on participation factors to identify the input-output relations for each mode obtained from the MIMO models. Introducing the substructure approach, the algorithm was tuned for base-isolated buildings so that the required number of sensors would be significantly

reduced. The effectiveness of the algorithm was examined through the simulations and the experiments. Furthermore, applying the algorithm to the existing 7-story base-isolated building that was equipped with an Internet-based monitoring system, the feasibility of the algorithm was verified.

2.11 Methods Based on Residual Forces

The residual force method was shown to be effective in damage localization using insufficient modal data as long as the modeling error is small for the undamaged structure (Ricles and Kosmatka 1992). This method is usually employed combined with another method. In Ricles and Kosmatka (1992), measured modal data along with a correlated analytical structural model were used first to localize potentially damaged regions using residual modal force vectors and then a weighted sensitivity analysis was conducted to assess the extent of damage. In Chiang and Lai (1999), the residual forces method was combined with the method of simulated evolution for damage identification. The damage localization algorithm based on the residual forces method was shown to successfully locate structural damage in the case that the analytical model used for damage identification can well represent the dynamic system of interest within the frequency range of measurement (eigenmodes) data.

The residual forces concept was employed to so called subspace rotation damage identification algorithm by Kahl and Sirkis (1996). The method was applied to identify the damage in beam element using the strain-based data instead of displacement data. It was found that the translational degrees of freedom are coupled to the rotational degrees of

freedom in a beam such that the subspace rotation algorithm does not work when the rotational degrees of freedom are condensed out. The relatively insensitivity of modal response of beams to certain types of damage leads to the conclusion that as many modes as possible must be used to locate damage event to add a degree of statistical confidence.

Kosmatka and Ricles (1999) presented a new methodology for the nondestructive evaluation of damage in flexible structures, the formulation and analytical studies of which were reported in an earlier publication by the authors (Ricles and Kosmatka 1992). The procedure was based on using experimentally measured natural frequencies and mode shapes in conjunction with vibratory residual forces and a weighted sensitivity analysis to estimate the extent of mass and/or stiffness variations in a structural system. Determination of the residual forces and weighted sensitivity analysis involved the use of an analytical model that is correlated to the experimental baseline data from a reference state. This reference state defines the undamaged structural configuration. The method was demonstrated by using a ten-bay space truss as an experimental test bed for various damage scenarios. The experimental results showed that the method can accurately predict the location and severity of stiffness change as well as any change in mass for different damage scenarios. The use of an analytical model that is correlated to the baseline test data was shown to improve the prediction; however, reasonable results were also obtained using an uncorrelated analytical model.

Zimmerman et al. (2001) presented an algorithm for damage detection and localization using expanded dynamic residuals. The methodology was shown to successfully detect and locate damage on the NASA 8- bay truss test-bed when limited sensor informa-

tion was utilized. The presented methodology, along with intelligent sensor placement, showed that damage localization can be achieved using limited instrumentation. However, it was observed that the success of this method is dependent on the number of sensors.

2.12 Methods Based on Time Domain Data

Although the widely used modal parameters based damage identification methodology appears intuitive, its actual application poses many significant technical challenges. One of the most fundamental challenges is that the experimental modal analysis will introduce additional uncertainties and measurement errors to damage identification process. To overcome this problem, another group of techniques are employed to detect identification using the raw measurement in time domain directly.

Majumder and Manohar (2003) developed a time-domain approach, within the framework of finite element modeling, to detect damage in bridge structures using data on vibration induced by a moving vehicle. The study reported in this paper accounted for several complicating features associated with response of bridge and vehicle system, including the effects due to dynamic interaction between vehicle and bridge, spatial incompleteness of measured data, deck unevenness and presence of measurement noise. The inclusion of vehicle inertia, stiffness and damping characteristics into the analysis made the system time variant which, in turn demands treatment of the damage identification problem in the time domain. The time-domain approach developed in this study leads to a set of over determined linear algebraic equations for the damage indicator variables

which were solved using pseudo-inverse theory. The performance of the procedures developed was demonstrated in a beam model using synthetically generated vibration data.

Choia and Stubbs (2004) presented the damage index algorithm using time-domain response data directly to identify the damage in the structure. The time-domain displacement response measurements were assumed to be measured at a finite number of locations in a structure and the mean strain energy over a specified time interval was obtained for each element of the structure. The mean strain energy for the elements was used to build an element damage index defined as the ratio of the stiffness parameter of the pre-damaged to the post-damaged elements. The standardized damage indices were then used as feature vectors in a classification scheme to identify damage. The classification scheme used here was based on the statistical decision technique of hypothesis testing. The feasibility of the methodology was demonstrated using simulated data from a continuous beam structure.

Lu and Gao (2005) proposed a novel time-domain auto-regressive model for damage identification, which stems from the linear dynamic system theory and it is formulated in the form of a prediction model of auto-regressive with exogenous input (ARX). The model coefficients correlate with the dynamic properties of the structure and they can be established from reference-state response signals. The residual error of the established model when applied on measured signals reflects the structural change, and the standard deviation of the residual error was found to be a damage sensitive feature. Numerical simulation studies of two structural models demonstrated that using the standard deviation of the residual errors as a feature, the occurrence of damage can be detected. It was observed

that the behavior of the proposed ARX model can be complicated when the location of the response point selected as the ARX model input is near the location of the damage. The standard deviation of the residual error of the ARX model, although sensitive to the occurrence of damage, did not give a precise indication of the extent of damage.

2.13 Wavelet Based Methods

Wavelet analysis may be viewed as an extension of the traditional Fourier transform with adjustable window location and size, therefore, transient behavior of data can be retained. Wavelet analysis has recently emerged as a promising tool for structural health monitoring and damage identification. The occurrence of damage and the moment when it happens can be identified by a spike or an impulse in the plots of higher resolution details from wavelet decomposition of response. Location of damage can also be identified by a pattern of spikes. The wavelet approach is less model dependent in the sense that only measurement data are required in the analysis. However, knowledge of structural details will be helpful to interpret the results from the wavelet analysis.

Hou and Noori (1999) presented a wavelet based approach for identification of damage locations. Occurrence of the damage was detected by a spike or an impulse in the acceleration response. Location of damage was identified by a pattern of spikes. This approach may be implemented both off-line and on-line, therefore, has a great promise for online health monitoring, integrated with structural control, and post-event damage assessment. The method successfully identified and located the damage in a numerical

example of a three degree-of-freedom spring-mass-dashpot system with multiple breakable springs.

Hou et al. (2000) discussed an extended version of their previous paper (Hou and Noori 1999). A wavelet-based approach was proposed for structural damage identification. The methodology was applied to simulation data generated from a simple structural model subjected to a harmonic excitation. The model consisted of multiple breakable springs, some of which could suffer irreversible damage when the response exceeds a threshold value or the number of cycles of motion is accumulated beyond their fatigue life. It was shown that structural damage or a change in system stiffness can be detected by spikes in the wavelet decomposition of the response data, and the locations of these spikes indicate the moments when the structural damage occurred.

Sun and Chang (2002) proposed a wavelet packet transform (WPT) based method for damage assessment of structures. One drawback of the Wavelet Transform (WT) is that its resolution is rather poor in the high-frequency region. Since structural damage is typically a local phenomenon captured most likely by high frequency modes, this potential drawback can affect the application of the wavelet-based damage assessment techniques. The WPT adopts redundant basis functions and hence can provide an arbitrary time-frequency resolution. In this paper, dynamic signals measured from a structure were first decomposed into wavelet packet components. Component energies are then calculated and used as inputs into neural network models for damage assessment. Numerical simulations were performed on a three-span continuous bridge under impact excitation. The

results showed that the WPT-based component energies are good candidate indices that are sensitive to structural damage.

Melhem and Kim (2003) studied two types of full-scale concrete structures subjected to fatigue loads: (1) Portland Cement Concrete Pavements (PCCP) on grade; and (2) a simply supported prestressed concrete beams. Fast Fourier Transform (FFT) and continuous wavelet transform (CWT) were used to analyze the dynamic impact response and evaluate the degradation of the slab and the simply supported beam after fatigue damage was gradually applied. Results from both procedures were compared. In the case of PCCP, the natural frequency was not consistently changing as more cracks were developed, and therefore damage could not be clearly identified. However, when analyzed by CWT, the results showed a clear difference between before and after damage, and were consistent with the damage progression. In case of the beam, both FFT and CWT produced satisfactory results. In general, both FFT and CWT can identify which frequency components exist in the signal. However, the advantage of the wavelet transform is that, in addition to the frequency components, it also shows when a particular frequency occurs.

Yuan et al. (2003) discussed an active monitoring method for damage identification applied to composite structures. Honeycomb sandwich and carbon fiber composite structures were studied. Two kinds of damage were considered: delamination and impact damage. Wavelet analysis methods were adopted to post-process the raw monitored signal. The proposed method was shown to be effective, reliable, and straightforward for the specimens considered in their study, which were composed of different materials and various levels of damage.

Hera and Hou (2004) presented an application of wavelet analysis for damage detection and locating damage region(s) for the ASCE structural health monitoring benchmark data. The response simulation data were generated basically by a FEM program provided by the ASCE Task Group and damage was introduced in the middle of response by breaking one or more structure elements such as inter-story braces. Wavelets were used to analyze the simulation data. It was found that structural damage due to sudden breakage of structural elements and the time when it occurred can be clearly detected by spikes in the wavelet details.

Law et al. (2006) analytically derived the sensitivity of wavelet coefficients from structural responses with respect to the system parameters. It was then used in a sensitivity-based inverse problem for structural damage detection with sinusoidal or impulsive excitation and acceleration and strain measurements. The sensitivity to the system parameters of wavelet coefficient was shown to be more significant than the response sensitivity with an example of a single story plane frame. Simulation results showed that the damage information was carried mostly in the higher vibration modes of the structure as diagnosed with the corresponding wavelet coefficients from its dynamic responses.

ACKNOWLEDGMENTS

The author wants to acknowledge Mr. Xianfei He for his significant contribution in performing the extensive literature review presented in this Chapter.

REFERENCES

Abdalla, M. O., Grigoriadis, K. M., and Zimmerman, D. C. (2000). "Structural damage detection using linear matrix inequality methods." *Journal of Vibration and Acoustics,* Vol. 122, No. 4, 448.

Abdel Wahab, M. M., and De Roeck, G. (1999). "Damage detection in bridges using modal curvatures: Application to a real damage scenario." *Journal of Sound and Vibration,* Vol. 226, No. 2, 217-235.

Abdel Wahab, M. M. (2001). "Effect of modal curvature on damage detection using model updating." *Mechanical Systems and Signal Processing,* Vol. 15, No. 2: 439-445.

Alampalli, S., Fu, G., and Dillon, E. W. (1997). "Signal versus noise in damage detection by experimental modal analysis." *Journal of Structural Engineering*, ASCE, Vol.123, No. 2, 237.

Alvin, K. F. (1997). "Finite element model update via Bayesian estimation and minimization of dynamic residuals." *AIAA Journal,* Vol. 35, No. 5, 879.

Banks, H. T., Inman, D. J., Leo, D. J. and Wang, Y. (1996). "An experimentally validated damage detection theory in smart structures." *Journal of Sound and Vibration*, Volume 191, Issue 5, 859-880.

Barroso, L. R., and Roddriguez, R. (2004). "Damage detection utilizing the damage index method to a benchmark structure." *J. Engrg. Mech.*, ASCE, Vol.130, 142.

Baruh, H., and Ratan, S. (1993). "Damage detection in flexible structures." *Journal of Sound and Vibration,* Vol. 166, Issue 1, 21-30.

Bassevillea, M., Mevelb, L., and Goursatc, M. (2004). "Statistical model-based damage detection and localization: subspace-based residuals and damage-to-noise sensitivity ratios." *Journal of Sound and Vibration,* Vol. 275, 769-794.

Bernal, D. (2002). “Load vectors for damage localization.” *Journal of Engineering Mechanics*, ASCE, Vol. 128, No. 1, 7-14.

Bicanic, N., and Chen, H. P. (1997). “Damage identification in framed structures using natural frequencies.” *International Journal for Numerical Methods in Engineering*, Vol. 40, 4451-4468.

Bishop, C. M. (1994). “Novelty detection and Neural Network validation.” *IEE Proc., Vision, Image and Signal Processing*, Vol. 141, No. 4, pp. 217-222, August.

Brincker, R., Andersen, P., Zhang, L. (2000) “Modal identification from ambient responses using frequency domain decomposition.” *Proc. of 18th International Modal Analysis Conference (IMAC)*, 625-630, San Antonio, Texas,.

Brownjohn, J. M. W., Xia, P. Q., Hao, H., and Xia, Y. (2001). “Civil structure condition assessment by finite element model updating: methodology and case studies.” *Finite Elements in Analysis and Design*, Vol. 37, 761-775.

Caicedo, J. M., Dyke, S. J., and Johnson, E. A. (2004). “Natural excitation technique and eigensystem realization algorithm for Phase I of the IASC-ASCE benchmark problem: simulated data.” *Journal of Engineering Mechanics*, ASCE, Vol. 130, No. 1, 49-60.

Capecchi, D., and Vestrini, F. (1999). “Monitoring of structural systems by using frequency data.” *Journal of Earthquake Engng. Struct. Dyn.*, Vol. 28, 447-461.

Casas, J. R., and Aparicio, A. C. (1994). “Structural damage identification from dynamic-test data.” *Journal of Structural Engineering*, ASCE, Vol. 120, No. 8, 2437.

Catbas, F. N., and Aktan, A. E. (2000). “Modal analysis as a bridge health monitoring tool.” *Proc. of 14th analysis and computational specialty conference.*

Cha, P. D., and Switkes, J. P. (2002). “Enforcing structural connectivity to update damped systems using frequency response.” *AIAA Journal*, Vol. 40, No. 6, 1197.

Chase, J. G., Hwang, K. L., Barroso, L. R., and Mander, J. B. (2005). “A simple LMS-based approach to the structural health monitoring benchmark problem.” *Earthquake Engng Struct. Dyn*., Volume 34, Issue 6, 575 - 594.

Chiang, D. Y., and Lai, W. Y. (1999). “Structural damage detection using the simulated evolution method.” *AIAA Journal*, Vol. 37, Issue 10, 1331.

Ching, J., and Beck, J. L. (2004). “Bayesian analysis of the Phase II IASC--ASCE structural health monitoring experimental benchmark data.” *J. Engrg. Mech.,* ASCE, 130, 1233.

Choia, S., and Stubbs, N. (2004). “Damage identification in structures using the time-domain response.” *Journal of Sound and Vibration*, 275, 77-590.

Cobb, R. G., and Liebst, B. S. (1997). “Sensor placement and structural damage identification from minimal sensor information.” *AIAA Journal*, v35 n2 p369(6).

Cobb, R. G., and Liebst, B. S. (1997). “Structural damage identification using assigned partial eigenstructure.” *AIAA Journal*, v35 n1 p152(7).

Cornwell, P., Doebling, S. W. and Farrar, C. R., (1999). “Application of the strain energy damage detection method to plate-like structures.” *Journal of Sound and Vibration*, 224 (2), 359-374.

Di Paola, M., and Bilello, C. (2004). “An integral equation for damage identification of Euler-Bernoulli beams under static loads.” *Journal of Engineering Mechanics*, ASCE, v130 i2 p225(10).

Doebling, S.W., Farrar, C.R., Prime, M.B., and Shevitz, D.W., (1996). *Damage identification in structures and mechanical systems based on changes in their vibration characteristics: A detailed literature survey.* Los Alamos National Laboratory, Rep. No. LA-13070-MS, Los Alamos, New Mexico, USA.

Doebling, S.W., Farrar, C.R., and Prime, M.B., (1998) “A summary review of vibration-based damage identification methods.” *The Shock and Vibration Digest*, Vol. 30, No. 2, 99-105.

Duan, Z., Yan, G., Ou, J., and Spencer, B. F. (2005). “Damage localization in ambient vibration by constructing proportional flexibility matrix.” *Journal of Sound and Vibration*, Vol. 284, No. 1-2, 455-466.

Duffey, T. A., Doebling, S. W., Farrar, C. R., Baker, W. E., and Rhee, W. H. (2001). “Vibration-based damage identification in structures exhibiting axial and torsional response.” *Journal of Vibration and Acoustics*, Vol. 123, No. 1, 84-91.

Fanning, P. J., Carden, E. P. (2003). “Damage detection based on single-input single-output Measurements.” *J. Engrg. Mech.*, ASCE, Vol. 129.

Farhat, C. and Hemez, F. (1993). “Updating finite element dynamic models using an element-by-element sensitivity methodology.” *AIAA Journal*, Vol. 31, No. 9, 1702-1711.

Fasel, T. R., Sohn, H., Park, G., and Farrar, C. R. (2005). “Active sensing using impedance-based ARX models and extreme value statistics for damage detection.” *Earthquake Engng Struct. Dyn.*, Vol. 34, No. 7, 763-785.

Friswell, M.I., and Mottershead, J.E., (1995). *Finite element model updating in structural dynamics.* Kluwer Academic Publishers, Boston, USA.

Fritzel, A. P., Jennewin, D., and Kiefer, T. (1998). “Damage detection based on model updating methods.” *Mechanical Systems and Signal Processing*, Vol. 12, No. 1, 163-186.

Gangadharan, S. N., Nikolaidis, E., Lee, K., Haftka, R. T., and Burdisso, R. (1999). “Anti-optimization for comparison of alternative structural models and damage detection.” *AIAA Journal*, Vol. 37, No. 7, 857.

Gattulli, V., and Romeo, F. (2000). “Integrated procedure for identification and control of MDOF structures.” *Journal of Engineering Mechanics*, ASCE, Vol. 126, No. 7, 730.

Ge, L., and Soong, T. T. (1998). “Theory: Damage identification through regularization method, part 1.” *Journal of Engineering Mechanics*, ASCE, Vol. 124, No. 1, 103.

Ge, L., and Soong, T. T. (1998). “Applications: Damage identification through regularization method, part 2).” *Journal of Engineering Mechanics*, ASCE, Vol. 124, No. 1, 109.

Hemez, F. M., and Doebling, S. W. (2001). “Review and assessment of model updating for non-linear, transient dynamics.” *Mechanical Systems and Signal Processing*, Vol. 15, No. 1, 45-74.

Hera, A., and Hou, Z. (2004). “Application of Wavelet approach for ASCE structural health monitoring benchmark studies.” *J. Engrg. Mech.*, ASCE, Vol. 130, 96.

Hjelmstad, K. D., and Shin, S. (1997). “Damage detection and assessment of structures from static response.” *J. Engrg. Mech.*, ASCE, Vol. 123, 568.

Hong, H., and Xia, Y. (2002). “Vibration-based damage detection of structures by genetic algorithm.” *Journal of Computing in Civil Engineering*, Vol. 16, No. 3, 222.

Hou, Z., and Noori, M. (1999). “Application of wavelet analysis for structural health monitoring.” *Proc., 2nd Int. Workshop on Struct. Health Monitoring,* Stanford University, Stanford, Calif., 946-955

Hou, Z., Noori, M., and Amand, R. St. (2000). “Wavelet-based approach for structural damage detection.” *J. Engrg. Mech.*, ASCE, Vol. 126, 677.

Housner, G. W., Bergman, L. A., Caughey, T. K., Chassiakos, A. G., Claus, R. O., Masri, S. F., Skelton, R. E., Soong, T. T., Spencer, Jr., B. F., and Yao, J. T. P. (1997). “Structural control: Past, present and future.” *Journal of Engineering Mechanics,* ASCE, 123(9), 897-971.

Hwang, H. Y., and Kim, C. (2004). “Damage detection in structures using a few frequency response measurements.” *Journal of Sound and Vibration*, Vol. 270, No. 1-2, 1-14.

Jang, J. H., Yeo, I., Shin, S., and Chang, S. P. (2002). “Experimental investigation of system-identification-based damage assessment on structures.” *Journal of Structural Engineering*, ASCE, Vol. 128, No. 5, 673.

Johnson, E. A., Lam, H. F., Katafygiotis, L. S., and Beck, J. L. (2000). "A benchmark problem for structural health monitoring and damage detection." *Proc. of the 14th ASCE Engineering Mechanics Conference*, Austin, Texas, May 21-24.

Kahl, K., and Sirkis, J. S. (1996). "Damage detection in beam structures using subspace rotation algorithm with strain data." *AIAA Journal*, Vol. 34, No. 12, 2609-2614.

Kaouk, M. and Zimmerman, D.C. (1994). "Structural damage assessment using a generalized minimum rank perturbation theory." *AIAA Journal*, 32(4), 836-842.

Katafygiotis, L. S., and Yuen, K.-V. (2001). "Bayesian spectral density approach for modal updating using ambient data." *Earthquake Eng. Struct. Dyn.*, 30(8), 1103-1123.

Kiddy, J., and Pines, D. (1998). "Constrained damage detection technique for simultaneously updating mass and stiffness matrices." *AIAA Journal*, Vol. 36, No. 7, 1332.

Kim, J. T., and Stubbs, N., (1995). "Model uncertainty impact and damage detection accuracy in plate girder." *Journal of Structural Engineering*, ASCE, Vol. 121, No. 10, 1409-1417.

Kim, J. T., and Stubbs, N., (2002). "Improved damage identification method based on modal information." *Journal of Sound and Vibration*, Vol. 252, No. 2, 223-238.

Kim, H. M., and Bartkowicz, T. J. (1997). "A two-step structural damage detection approach with limited instrumentation." *Journal of Vibration and Acoustics*, Vol. 119, No. 2, 258.

Kim, K. O., Cho, J. Y., and Choi, Y. J. (2004). "Direct approach in inverse problems for dynamic systems." *AIAA Journal*, Vol. 42, No. 8, 1698.

Koh, C. G., See, L. M., Balendra, T. (1995). "Damage detection of buildings: Numerical and experimental studies." *J. Struct. Engrg.*, ASCE, Vol. 121, 1155.

Kosmatka, J. B., and Ricles, J. M. (1999). “Damage detection in structures by modal vibration characterization.” *Journal of Structural Engineering*, ASCE, Vol. 125, No. 12, 1384.

Lam, H. F., Katafygiotis, L. S., and Mickleborough, N. C. (2004). “Application of a statistical model updating approach on Phase I of the IASC-ASCE structural health monitoring benchmark study.” *J. Engrg. Mech.*, ASCE, Vol. 130, No. 34.

Lam, H. F., Ko J. M., and Wong, C. W. (1998). “Localization of damaged structural connections based on experimental modal and sensitivity analysis.” *Journal of Sound and Vibration*, Vol. 210, No. 1, 91-115.

Law, S. S., Li, X. Y., and Lu, Z. R. (2006). “Structural damage detection from Wavelet coefficient sensitivity with model errors.” *J. Engrg. Mech.*, ASCE, Vol. 132, No. 10, 1077-1087.

Law, S. S., Shi, Z. Y., and Zhang, L. M. (1998). “Structural damage detection from incomplete and noisy modal test data.” *J. Engrg. Mech.*, ASCE, Vol. 124, 1280.

Law, S. S., and Zhu, X. Q. (2005). “Nonlinear characteristics of damage reinforced concrete beams from Hilbert-Huang transform.” *J. Struct. Engrg.*, ASCE, Vol. 133, No. 8, 1186-1191.

Lawson, C. L., and Hanson, R. J. (1974). *Solving least squares problems*, Prentice-Hall, Englewood Cliffs, New Jersey.

Lew, J. S. (1995). “Using transfer function parameter changes for damage detection of structures.” *AIAA Journal*, Vol. 33, No. 11, 2189.

Li, H., Yang, H., and Hu, S. L. J. (2006). “Modal strain energy decomposition method for damage localization.” *Journal of Engineering Mechanics*, ASCE, Vol. 132, No. 9, 941-951.

Lim, T. W., Bosse, A., and Fisher, S. (1996). “Structural damage detection using real-time modal parameter identification algorithm.” *AIAA Journal*, Vol. 34, No. 11, 2370.

Lim, T. W., and Kashangaki, T. A. L. (1994). “Structural damage detection of space truss structures using best achievable eigenvectors.” *AIAA Journal*, Vol. 32, No. 5, 1049.

Lin, J. W., and Betti, R. (2004). “On-line identification and damage detection in non-linear structural systems using a variable forgetting factor approach.” *Earthquake Engng Struct. Dyn.*, Vol. 33, 419-444.

Liu, P. L. (1995). “Identification and damage detection of trusses using modal data.” *J. Struct. Engrg.*, ASCE, Vol. 121, No. 599.

Lu, Y., and Gao, F. (2005). “A novel time-domain auto-regressive model for structural damage diagnosis.” *Journal of Sound and Vibration*, Volume 283, Issue 3-5, 031-1049.

Lus, H., Betti, R., Yu, J., and De Angelis, M. (2004). “Investigation of a system identification methodology in the context of the ASCE benchmark problem.” J. *Engrg. Mech.*, ASCE, Vol. 130, 71.

Majumder, L., and Manohar, C. S. (2003). “A time-domain approach for damage detection in beam structures using vibration data with a moving oscillator as an excitation source.” *Journal of Sound and Vibration*, Volume 268, Issue 4, Pages 699-716.

Manson, G., Worden, K., G. and Allman, D. (2003 a). “Experimental validation of a structural health monitoring methodology: Part II. Novelty detection on la gnat aircraft.” *Journal of Sound and Vibration*, Volume 259, Issue 2, 345-363.

Manson, G., Worden, K., and Allman, D. (2003 b). “Experimental validation of a structural health monitoring methodology: Part III. Damage location on an aircraft wing.” *Journal of Sound and Vibration*, 259 (2), pp. 365-385.

Masri, S. F., Smyth, A. W., Chassiakos, A. G., Caughey T. K., and Hunter, N. F. (2000). “Application of neural networks for detection of changes in nonlinear systems.” *Journal of Engineering Mechanics*, ASCE, Vol. 126, No. 7, 666.

Melhem, H., and Kim, H. (2003). “Damage detection in concrete by Fourier and wavelet

analyses.” *J. Engrg. Mech*., ASCE, Vol. 129, No. 5, 571.

Messina, A., Williams, E. J., and Contursi, T. (1998). “Structural damage detection by a sensitivity and statistical-based method.” *Journal of Sound and Vibration*, Volume 216, Issue 5, Pages 791-808.

Moslem, K., and Nafaspour, R. (2002). “Structural damage detection by genetic algorithms.” *AIAA Journal*, Vol. 40, No. 7, 1395.

Mottershead, J. E., and Friswell M. I. (1993). “Model updating in structural dynamics: A Survey.” *Journal of Sound and Vibration*, 167, 347-375.

Nauerz, A., and Fritzen, C. P. (2001). “Model based damage identification using output spectral densities.” *Journal of Dynamic Systems, Measurement, and Control*, Vol. 123, No. 4, 691.

Oh, H. B., Jung, B. S. (1998) “Structural damage assessment with combined data of static and modal tests.” *J. Struct. Engrg.*, ASCE, 124, 956.

Pandey, A. K., and Biswas, M. (1994). “Damage detection in structures using changes in flexibility.” *Journal of Sound and Vibration*, Volume 169, Issue 1, Pages 3-17.

Pandey, A. K., Biswas, M., and Samman, M. M. (1991). “Damage detection from changes in curvature mode shapes.” *Journal of Sound and Vibration*, Volume 145, Issue 2, Pages 321-332.

Pothisiri, T., and Hjelmstad, K. D. (2003). “Structural damage detection and assessment from modal response.” *J. Engrg. Mech.*, ASCE, 129, 135. 37

Papadopoulos, L., and Garcia, E. (1998). “Structural damage identification: a probabilistic approach.” *AIAA Journal*, Vol. 36, No. 11, 2137.

Ratcliffe, C. P. (1997). “Damage detection using a modified Laplacian operator on mode shape data.” *Journal of Sound and Vibration*, Volume 204, Issue 3, Pages 505-517.

Ratcliffe, C. P. (2000). “A frequency- and curvature-based experimental method for locating damage in structures.” *Journal of Vibration and Acoustics*, ASCE, Vol. 122, No. 3, 324.

Ray, L. R., and Tian, L. (1999). “Damage detection in smart structures through sensitivity enhancing feedback control.” *Journal of Sound and Vibration*, Volume 227, Issue 5, Pages 987-1002.

Ren, W. X., and De Roeck, G. (2002). “Structural damage identification using modal data. I: simulation verification.” *Journal of Structural Engineering*, ASCE, Vol. 128, No. 1, 87.

Ren, W. X., and De Roeck, G. (2002). “Structural damage identification using modal data. II: test verification.” *Journal of Structural Engineering*, ASCE, Vol. 128, No. 1, 96.

Reich, G. W., and Park, K. C. (2000). “Use of substructural transmission zeros for structural health monitoring.” *AIAA Journal*, Vol. 38, No. 6, 1040.

Ricles, J. M., and Kosmatka, J. B. (1992). “Damage detection in elastic structures using vibratory residual forces and weighted sensitivity.” *AIAA Journal*, Vol. 30, No. 9, 2310.

Salawu, O.S. (1997). “Detection of structural damage through changes in frequency: A review.” *Engineering Structures*, 19(9), 718-723.

Sampaio, R. P. C., Maia, N. M. M., and Silva, J. M. M. (1999). “Damage detection using the frequency-response-function curvature method.” *Journal of Sound and Vibration*, Volume 226, Issue 5, Pages 1029-1042.

Shi, Z. Y. and Law, S. S. (1998). “Structural damage localization from modal strain energy change.” *Journal of Sound and Vibration*, Vol. 218, No. 5, 825-844.

Shi, Z. Y., Law, S. S., and Zhang, L. M. (2000). “Damage localization by directly using incomplete mode shapes.” *Journal of Engineering Mechanics*, ASCE, Vol. 126: 656, No. 5.

Shi, Z. Y., Law, S. S., and Zhang, L. M. (2000). “Optimal sensor placement for structural damage detection.” *Journal of Engineering Mechanics,* ASCE, Vol. 126, 1173.

Shi, Z. Y., Law, S. S., and Zhang, L. M. (2000). “Structural damage detection from modal strain energy change.” *Journal of Engineering Mechanics,* ASCE, Vol. 126, 1216-122.

Shi, Z.Y., Law, S. S., and Zhang, L.M. (2002). “Improved damage quantification from elemental modal strain energy change.” *Journal of Engineering Mechanics,* ASCE, Vol. 128, 521.

Soeiro, F. J., and Hajela, P. (1993). “Damage detection in composite materials using identification techniques.” *Journal of Aerospace Engineering,* ASCE, Vol. 6, No. 4 363.

Sohn, H., Farrar, C.R., Hemez, F.M., Shunk, D.D., Stinemates, D.W., and Nadler, B.R., (2003). *A review of structural health monitoring literature: 1996-2001*. Los Alamos National Laboratory, Report No. LA-13976-MS, Los Alamos, New Mexico, USA.

Sohn, H., and Law, K. H. (1997). “A Bayesian probabilistic approach for structure damage detection.” *Earthquake Engng. Struct. Dyn.,* 26, 1259-1281.

Sohn, H., and Law, K. H. (2000). “Bayesian probabilistic damage detection of a reinforced-concrete bridge column.” *Earthquake Engng Struct. Dyn.,* 29, 1131-1152.

Sohn, H., and Law, K. H. (2001). “Damage diagnosis using experimental Ritz vectors.” *J. Engrg. Mech.,* ASCE, 127, 1184.

Stubbs, N., Kim, J. T., and Topole, K., 1992, “An efficient and robust algorithm for damage localization in offshore platforms”, *Proc. of the ASCE Tenth Structures Congress*, 543-546, San Antonio, Texas.

Stubbs, N. and Kim, J. T., (1996). “Damage localization in structures without baseline modal parameters.” *AIAA Journal,* Vol. 34, No. 8, 1644-1649.

Sun, Z., and Chang, C. C. (2002). “Structural damage assessment based on Wavelet Packet Transform.” *Journal of Structural Engineering,* ASCE, Vol. 128, 1354.

Teughels, A., and De Roeck, G. (2004). “Structural damage identification of the highway bridge Z24 by finite element model updating.” *Journal of Sound and Vibration*, Vol. 274, 589-610.

Tseng, K. K., and Wang, L. (2005). “Impedance-based method for nondestructive damage identification.” *Journal of Engineering Mechanics,* ASCE, Vol. 131, No. 1, 58.

Vanlanduit, S., Parloo, E., Cauberghe, B., Guillaume, P., and Verboven, P. (2005). “A robust singular value decomposition for damage detection under changing operating conditions and structural uncertainties.” *Journal of Sound and Vibration*, Volume 284, Issues 3-5, Pages 1033-1050

Wang, Z, Lin, R. M., and Lim, M. K. (1997). “Structural damage detection using measured FRF data.” *Computer Methods in Applied Mechanics and Engineering*, 147, 187-197.

Wong, L. A., and Chen, J. C. (2000). “Damage identification of nonlinear structural systems.” *AIAA Journal,* Vol. 38, No. 8, 1444.

Worden, K. (1997). “Structural fault detection using a novelty measure.” *Journal of Sound and Vibration*, 201, 85-101.

Worden, K., Manson, G., and Allman, D. (2003). “Experimental validation of a structural health monitoring methodology: Part I. Novelty detection on laboratory structure.” *Journal of Sound and Vibration,* Volume 259, Issue 2, Pages 323-343.

Worden, K., Manson, G., and Fieller, N. J. (2000). “Damage detection using outlier analysis.” *Journal of Sound and Vibration*, Vol. 229, 647-667.

Worden, K., Sohn, H., and Farrar, C. R. (2002). “Novelty detection in a changing environment: regression and interpolation approaches.” *Journal of Sound and Vibration,* Vol. 58, No. 4, 741-761.

Xia, Y., and Hao, H. (2003). “Statistical damage identification of structures with frequency changes.” *Journal of Sound and Vibration,* Volume 263, Issue 4, Pages 853-870.

Xia, Y., Hao, H., Brownjohn, J. M. W., and Xia, P. Q. (2002). “Damage identification of structures with uncertain frequency and mode shape data.” *Earthquake Engng Struct. Dyn.,* Vol. 31, 1053- 1066.

Xu, Y. L., and Chen, J. (2004). “Structural damage detection using empirical mode decomposition: experimental investigation.” *J. Engrg. Mech.,* ASCE, 130, 1279.

Xu, B, Wu, Z. S. and Yokoyama K. (2003). “Response time series based structural parametric assessment approach with neural networks.” *Structural Health Monitoring and Intelligent Infrastructures.* Vol. 1: 601-609.

Yang, J. N., Lei, Y., Lin, S., and Huang, N., (2004). “Hilbert-Huang based approach for structural damage detection.” *J. Engrg. Mech.,* ASCE, 130, 85.

Yeo, I. H., Shin, S., Lee, H. S., and Chang, S. P. (2000). “Statistical damage assessment of framed structures from static responses.” *J. Eng. Mech.,* ASCE, 126(4), 414-421.

Yoshimoto, R., Mita, A., and Okada, K. (2005). “Damage detection of base-isolated buildings using multi-input multi-output subspace identification.” *Earthquake Engng Struct. Dyn.,* Volume 34, Issue 3, Pages 307-324.

Yuan, S., Lei, W., and Shi, L. (2003). “Active monitoring for on-line damage detection in composite structures.” *Journal of Vibration and Acoustics,* Vol. 125, No. 2, 178.

Yuen, K. V., Beck, J. L., and Au, S. K. (2004). “Structural damage detection and assessment by adaptive Markov chain Monte Carlo simulation.” *Struct. Control Health Monit.,* Vol. 11, 327-347.

Zhang, Q. W., Chang, C. C., and Chang, T. Y. P. (2000). “Finite element model updating for structures with parametric constraints.” *Earthquake engineering and Structural Dynamics*, Vol. 29, 927-944.

Zhao, J., and DeWolf, J. T. (1999). “Sensitivity study for vibrational parameters used in damage detection.” *Journal of Structural Engineering*, ASCE, Vol. 125, No. 4, 410-416.

Zhu, H. P., and Xu, Y. L. (2005). “Damage detection of mono-coupled periodic structures based on sensitivity analysis of modal parameters.” *Journal of Sound and Vibration*, Volume 285, Issues 1-2, Pages 365-390

Zimmerman, D. C., and Kaouk, M. (1992). “Eigenstructure assignment approach for structural damage detection.” *AIAA Journal*, Vol. 30, No. 7, 1848.

Zimmerman, D. C., and Kaouk, M. (1994). “Structural damage detection using a minimum rank update theory.” *Journal of Vibration and Acoustics*, Vol. 116, No. 2, 222.

Zimmerman, D. C., Kim, H. M., Bartkowicz, T. J., and Kaouk, M. (2001). “Damage detection using expanded dynamic residuals.” *Journal of Dynamic Systems, Measurement, and Control*, Vol. 123, No. 4, 699.

Zou, Y., Tong, L., and Steven, G. P. (2000). “Vibration-based model dependent damage (delamination) identification and health monitoring for composite structures: A review.” *Journal of Sound and Vibration*, Volume 230, Issue 2, Pages 357-378.

CHAPTER 3

GENERAL REALIZATION ALGORITHM FOR MODAL IDENTIFICATION OF LINEAR DYNAMIC SYSTEMS

3.1 INTRODUCTION

As the performance of computational algorithms and computers have drastically increased, the problem of identifying the properties and conditions of structures from their measured response to an external excitation has received considerable attention. There has been a vast number of studies and algorithms concerning the construction of state-space representations of linear dynamic systems in the time domain, starting with the work of Gilbert (1963) and Kalman (1963). One of the first important results in this field is about minimal state-space realization, indicating a model with the smallest state-space dimension among realized systems that have the same input-output relations within a specified degree of accuracy (Juang and Pappa 1985). It was shown by Ho and Kalman (1965) that the minimum representation problem is equivalent to the problem of identifying the sequence of real matrices, known as the Markov parameters, which represent the impulse response of a linear dynamic system. Numerous studies (Silverman 1971, Phan et al. 1991) have been conducted on the subject of Markov parameters and their relations to different representations of linear dynamic systems.

Following a time-domain formulation and incorporating results from control theory, Juang and Pappa (1985) proposed the Eigensystem Realization Algorithm (ERA) for modal parameter identification and model reduction of linear dynamic systems. ERA extends the Ho-Kalman algorithm and creates a minimal realization that mimics the output history of the system when it is subjected to a unit pulse input. Later, this algorithm was refined to better handle the effects of noise and structural nonlinearities, and ERA with data correlations (ERA/DC) was proposed (Juang et al. 1988). The Natural Excitation Technique combined with ERA (NExT-ERA), first proposed by James et al. (1993), is based on the same idea as ERA/DC in order to identify the modal parameters of a system using ambient vibration data. Peeters and De Roeck (2001) reviewed several output-only system identification methods which are useful for operational modal analysis under the condition that the input excitation is broadband (ideally white noise). Although these methods are powerful in generating dynamic models from impulse response and/or ambient vibration data, realization algorithms similar to ERA that can handle arbitrary input signals are needed. For arbitrary input signal, identification methods based on prediction error minimization (Ljung 1999) or subspace methods (Van Overschee and De Moore 1996) can be used. Unfortunately, prediction error methods require an intricate model parametrization, specially for multivariable systems, along with a nonlinear optimization to identify model parameters. These issues have been resolved in subspace based identification, but the link with direct realization algorithms is not transparent. This paper establishes a straightforward extension of the well-known eigensystem realization algorithm, by development of the General Realization Algorithm (GRA) on the basis of an arbitrary input signal.

The proposed GRA allows for the realization of a state-space model on the basis of input-output measurement data using a Hankel matrix based realization algorithm similar to the well-known ERA. GRA allows for an explicit use of the input signal through construction of a so-called weighted Hankel matrix from the input-output measurements. In the special case where the input excitation is an impulse signal, GRA reduces down to ERA in which a Hankel matrix is formed on the basis of impulse (free vibration) response measurements. The explicit use of the input signal to construct the weighted Hankel matrix in GRA shows an advantage in comparison to the case where only Markov parameter estimates are used to initiate a standard Hankel matrix based realization as in ERA. This advantage is more significant when the input excitation is a short-duration and/or non-broadband (colored) signal such as earthquake ground motions.

In this paper, the GRA is presented to identify the dynamic characteristics of linear multi-degree-of-freedom dynamic systems subjected to arbitrary loading from zero (at rest) or known non-zero initial conditions. The identified state-space matrices are improved by a least squares algorithm, upon state reconstruction, to get the minimum prediction error for the response. Statistical properties (i.e., bias, variance, and robustness to added output noise) of the modal parameter estimators provided by the GRA are investigated through a numerical simulation study based on a benchmark problem with non-classical damping.

3.2 IDENTIFICATION VIA STATE-SPACE REALIZATION

3.2.1 State-Space Representation of Linear Dynamic Systems

Consider a *P* degree-of-freedom (DOF) linear dynamic system represented by the following second-order differential equation of motion and measurement equation:

$$\begin{aligned} \mathcal{M}\ddot{\mathbf{p}}(t) + \mathcal{D}\dot{\mathbf{p}}(t) + \mathcal{K}\mathbf{p}(t) &= \mathcal{B}\mathbf{u}(t) \\ \mathbf{y}(t) &= \mathcal{C}\left[\mathbf{p}(t)^{\mathrm{T}} \ \dot{\mathbf{p}}(t)^{\mathrm{T}} \ \ddot{\mathbf{p}}(t)^{\mathrm{T}}\right]^{\mathrm{T}} \end{aligned} \tag{3.1}$$

where $\mathbf{p}(t) \in \mathbb{R}^{P \times 1}$ denotes the displacement response vector of the system as a function of time *t*, the superimposed dot indicates a single differentiation with respect to time, and the superscript T indicates the matrix transpose operation. Matrices $\mathcal{M}$, $\mathcal{D}$ and $\mathcal{K}$ represent the $(P \times P)$ mass, damping and stiffness matrices of the system, respectively. The input matrix $\mathcal{B}$ defines the spatial distribution (among the system DOFs) of the (measurable) external forcing function $\mathbf{u}(t)$. The output vector $\mathbf{y}(t) \in \mathbb{R}^{m \times 1}$ represents the measured system response, and the output matrix $\mathcal{C}$ captures the possible linear combination of the acceleration, velocity and displacement vectors in the measured response.

A linear dynamic system can also be represented in state-space form, which is often more suitable for system identification purposes, as

$$\begin{aligned} \dot{\mathbf{x}}(t) &= \mathbf{F}\mathbf{x}(t) + \mathbf{G}\mathbf{u}(t) \\ \mathbf{y}(t) &= \mathbf{H}\mathbf{x}(t) + \mathbf{E}\mathbf{u}(t) \end{aligned} \tag{3.2}$$

in which $\mathbf{x}(t) \in \mathbb{R}^{n \times 1}$ ($n = 2P$) denotes an *n*-dimensional state vector consisting of an arbitrary linear combination of the displacement, $\mathbf{p}(t)$, and velocity, $\dot{\mathbf{p}}(t)$, response vectors

in Eq. (3.1). The state matrix $\mathbf{F} \in \mathbb{R}^{n \times n}$, input matrix $\mathbf{G} \in \mathbb{R}^{n \times r}$, output matrix $\mathbf{H} \in \mathbb{R}^{m \times n}$ and feed-through matrix $\mathbf{E} \in \mathbb{R}^{m \times r}$ in Eq. (3.2) completely define a linear dynamic system with an *r*-dimensional forcing function, $\mathbf{u}(t)$, and *m*-dimensional output measurement, $\mathbf{y}(t)$.

As an example, consider the measurement of $\ddot{\mathbf{p}}(t)$ (i.e., $m = P$) using accelerometers mounted on a structural system. By selecting $\bar{\mathbf{x}}(t) = \left[\mathbf{p}(t)^{\mathrm{T}}\ \dot{\mathbf{p}}(t)^{\mathrm{T}}\right]^{\mathrm{T}}$ as (physical) state vector and $\mathbf{y}(t) = \ddot{\mathbf{p}}(t)$ in Eq. (3.2), it can be seen that Eq. (3.1) with $\mathcal{C} = \left[\mathbf{0}_{(P \times P)}\ \mathbf{0}_{(P \times P)}\ \mathbf{I}_{(P \times P)}\right]$ can be re-written in the form of Eq. (3.2) with the following state-space matrices:

$$\bar{\mathbf{F}} = \begin{bmatrix} \mathbf{0}_{(P \times P)} & \mathbf{I}_{(P \times P)} \\ -\mathcal{M}^{-1}\mathcal{K} & -\mathcal{M}^{-1}\mathcal{D} \end{bmatrix}_{(2P \times 2P)}, \quad \bar{\mathbf{G}} = \begin{bmatrix} \mathbf{0}_{(P \times r)} \\ -\mathcal{M}^{-1}\mathcal{B} \end{bmatrix}_{(2P \times r)} \tag{3.3}$$

$$\bar{\mathbf{H}} = \left[-\mathcal{M}^{-1}\mathcal{K} \quad -\mathcal{M}^{-1}\mathcal{D}\right]_{(P \times 2P)}, \quad \bar{\mathbf{E}} = \left[-\mathcal{M}^{-1}\mathcal{B}\right]_{(P \times r)}$$

which are completely defined from the mass, damping, stiffness and input matrices of the second-order system in Eq. (3.1). When identifying a state-space model of a dynamic system, the identified state-space model correspond to a general state (different than physical state) as in Eq. (3.2). The identified state-space model can be converted to an equivalent model with physical state ($\bar{\mathbf{x}}(t)$) and state-space matrices defined in Eq. (3.3) through a state transformation (similarity transformation) $\bar{\mathbf{x}}(t) = \mathbf{T}\mathbf{x}(t)$ where $\mathbf{T} \in \mathbb{R}^{n \times n}$ is a non-singular matrix. The transformed state-space model takes the form

$$\begin{aligned} \dot{\bar{\mathbf{x}}}(t) &= \bar{\mathbf{F}}\bar{\mathbf{x}}(t) + \bar{\mathbf{G}}\mathbf{u}(t) \\ \mathbf{y}(t) &= \bar{\mathbf{H}}\bar{\mathbf{x}}(t) + \bar{\mathbf{E}}\mathbf{u}(t) \end{aligned} \tag{3.4}$$

where $\bar{\mathbf{F}} = \mathbf{T}\mathbf{F}\mathbf{T}^{-1}$, $\bar{\mathbf{G}} = \mathbf{T}\mathbf{G}$, $\bar{\mathbf{H}} = \mathbf{H}\mathbf{T}^{-1}$ and $\bar{\mathbf{E}} = \mathbf{E}$ have the form given in Eq. (3.3), from which the second-order differential equation model could be derived.

As a final step towards the representation of dynamic structural systems for identification purposes, the framework of discrete time domain systems is used in this paper. Typically, measurements of the output $\mathbf{y}(t)$ and/or the input $\mathbf{u}(t)$ are obtained at discrete times $t = k\,\Delta T$, $k = 0, 1, 2, ...$, with a constant sampling time ΔT. For a continuous time system sampled at ΔT, a discrete time state-space model

$$\begin{aligned} \mathbf{x}((k+1)\Delta T) &= \mathbf{A}\mathbf{x}(k\Delta T) + \mathbf{B}\mathbf{u}(k\Delta T) \\ \mathbf{y}(k\Delta T) &= \mathbf{C}\mathbf{x}(k\Delta T) + \mathbf{D}\mathbf{u}(k\Delta T) \end{aligned} \tag{3.5}$$

is needed to represent the dynamics of the structural system. Depending on the assumption of inter-sample behavior of the input signal $\mathbf{u}(t)$ or the approximation of the differentiation operator in discrete time, different equivalent discrete time models of the continuous time system can be found (see Appendix I). The inter-sample behavior of the input $\mathbf{u}(t)$ can be approximated by a constant value $\mathbf{u}(t) = \mathbf{u}(k\Delta T)$ for $k\Delta T \le t \le (k+1)\Delta T$, yielding a Zero Order Hold (ZOH) approximation. Such an approximation is viable in case of fast sampling (small ΔT) and slowly varying input signals. However, for fast changing input signals due to shock-type excitation (pulse-like input force), a ZOH approximation of the input yields an inaccurate discrete state-space model of the underlying continuous system. A more accurate inter-sample behavior is to extrapolate the sample $\mathbf{u}(k\Delta T)$ so as to

approximate linearly the continuous input signal $\mathbf{u}(t)$ in the time interval $k\Delta T \le t \le (k+1)\Delta T$, i.e.,

$$\mathbf{u}(t) \approx \frac{\mathbf{u}((k+1)\Delta T) - \mathbf{u}(k\Delta T)}{\Delta T} \cdot t + \mathbf{u}(k\Delta T)(k+1) - \mathbf{u}((k+1)\Delta T)k \tag{3.6}$$

Such an approximation is known as triangle-hold equivalent (or first-order hold) and leads to a causal discrete time system, although the impulse response of a triangular hold is non-causal in continuous time (Franklin et al. 1998). Using a triangle-hold (T-H) approximation, the discrete time state-space model in Eq. (3.5) is related to the continuous time state-space model in Eq. (3.2) via

$$\begin{aligned} \mathbf{A} &= \mathbf{\Phi}, & \mathbf{B} &= \mathbf{\Gamma}_1 + \mathbf{\Phi}\mathbf{\Gamma}_2 - \mathbf{\Gamma}_2 \\ \mathbf{C} &= \mathbf{H}, & \mathbf{D} &= \mathbf{E} + \mathbf{H}\mathbf{\Gamma}_2 \end{aligned} \tag{3.7}$$

where $\mathbf{\Phi}$, $\mathbf{\Gamma}_1$, and $\mathbf{\Gamma}_2$ are computed from the solution of (Franklin et al. 1998)

$$\exp\left(\begin{bmatrix} \mathbf{F}\Delta T & \mathbf{G}\Delta T & \mathbf{0} \\ \mathbf{0} & \mathbf{0} & \mathbf{I} \\ \mathbf{0} & \mathbf{0} & \mathbf{0} \end{bmatrix}\right) = \begin{bmatrix} \mathbf{\Phi} & \mathbf{\Gamma}_1 & \mathbf{\Gamma}_2 \\ \mathbf{0} & \mathbf{I} & \mathbf{I} \\ \mathbf{0} & \mathbf{0} & \mathbf{I} \end{bmatrix} \tag{3.8}$$

It can be seen from Eqs. (3.7) and (3.8) that the discrete time state matrix $\mathbf{A}$ for the T-H approximation is identical to that for the ZOH approximation $\mathbf{A} = \exp(\mathbf{F}\Delta T)$, yielding the same discrete time poles as for the ZOH approximation. However, the input matrix $\mathbf{B}$ and feed through matrix $\mathbf{D}$ for the T-H approximation differ from their ZOH counterparts and the corresponding discrete time state-space model yields a better approximation of the sampled output of the underlying continuous time model than its ZOH counterpart in the case of a shock-type (pulse-like) or fast varying input signal.

3.2.2 Eigensystem Realization Algorithm (ERA)

In order to better present the main concepts behind the General Realization Algorithm (GRA) for arbitrary input signals, first the Eigensystem Realization Algorithm (ERA) for pulse input signal is briefly reviewed in this section; more details can be found in Juang and Pappa (1985). In the next section, ERA is generalized for arbitrary input signals, which often characterize the input excitation of actual dynamic systems (e.g., seismic excitation of a bridge or building structure). To simplify notations, the discrete time impulse response measurements, $\mathbf{g}(k\Delta T)$, (also referred to as Markov parameters for unit pulse input), are assumed to be vector valued (i.e., single input, multiple output system). The formulation of ERA can be generalized to multiple input - multiple output systems (Juang and Pappa 1985) that is avoided here in order to focus on the main concepts.

Given the discrete time state-space model of a linear dynamic system, as in Eq. (3.5), the output $\mathbf{y}(k\Delta T)$ due to the arbitrary input signal $\mathrm{u}(k\Delta T)$ can be written explicitly as

$$\mathbf{y}(k) = \mathbf{D}\mathrm{u}(k) + \sum_{i=1}^{\infty} \mathbf{G}(i)\mathrm{u}(k-i), \quad \mathbf{G}(i) = \mathbf{C}\mathbf{A}^{i-1}\mathbf{B} \tag{3.9}$$

where $\mathbf{G}(i)$ denote the Markov parameters, ΔT has been normalized to $\Delta T = 1$ for the sake of notational brevity, and k indicates the input and output samples at discrete times $t = k$ ($k = 0, 1, ..., 2N$). Given the discrete output measurements $\mathbf{y}(k)$ and possibly the input measurements $\mathrm{u}(k)$ for $k = 0, 1, 2, ..., 2N$, the objective is to determine the appropriate size n (McMillan degree) of the state vector $\mathbf{x}(k)$ in Eq. (3.5) (i.e., order of the model to real-

ize), and to estimate a discrete time state-space realization (**A**, **B**, **C**, **D**) of the dynamic system considered.

For the special case of a unit pulse input defined as

$$u(k) = \begin{cases} 1, & k = 0 \\ 0, & k \neq 0 \end{cases}, \tag{3.10}$$

the output $\mathbf{y}(k)$ corresponds to the Markov parameters, $\mathbf{G}(k)$, of the discrete time system. To set up the realization algorithm on the basis of the impulse response measurements, $\mathbf{g}(k) = \mathbf{y}(k)$ ($k = 0, 1, 2, ..., 2N$), first an $(m \times N) \times N$ Hankel matrix **H** is constructed as

$$\mathbf{H} = \begin{bmatrix} \mathbf{g}(1) & \mathbf{g}(2) & \dots & \mathbf{g}(N) \\ \mathbf{g}(2) & \mathbf{g}(3) & \dots & \mathbf{g}(N+1) \\ \dots & \dots & \dots & \dots \\ \mathbf{g}(N) & \mathbf{g}(N+1) & \dots & \mathbf{g}(2N-1) \end{bmatrix}_{(m \times N) \times N} \tag{3.11}$$

and a corresponding shifted Hankel matrix $\overline{\mathbf{H}}$ of the same size is defined as

$$\overline{\mathbf{H}} = \begin{bmatrix} \mathbf{g}(2) & \mathbf{g}(3) & \dots & \mathbf{g}(N+1) \\ \mathbf{g}(3) & \mathbf{g}(4) & \dots & \mathbf{g}(N+2) \\ \dots & \dots & \dots & \dots \\ \mathbf{g}(N+1) & \mathbf{g}(N+2) & \dots & \mathbf{g}(2N) \end{bmatrix}_{(m \times N) \times N} \tag{3.12}$$

In case $\mathbf{g}(k)$ are noise free impulse response measurements generated by Eq. (3.5), it follows that

$$\mathbf{g}(k) = \mathbf{G}(k) = \begin{cases} \mathbf{D}, & \text{for } k = 0 \\ \mathbf{C}\mathbf{A}^{k-1}\mathbf{B}, & \text{for } k \geq 0 \end{cases} \tag{3.13}$$

where **B** is the input matrix of the state-space model in Eq. (3.5). The Hankel matrix **H** in Eq. (3.11) can be expressed as

$$\mathbf{H} = \mathbf{H}_1\mathbf{H}_2 \tag{3.14}$$

in which $\mathbf{H}_1$ and $\mathbf{H}_2$ are the observability and controllability matrices, respectively,

$$\mathbf{H}_1 = \begin{bmatrix} \mathbf{C} \\ \mathbf{CA} \\ \mathbf{CA}^2 \\ \cdots \\ \mathbf{CA}^{N-1} \end{bmatrix}_{(m \times N) \times n} \quad \text{and} \quad \mathbf{H}_2 = \begin{bmatrix} \mathbf{B} & \mathbf{AB} & \mathbf{A}^2\mathbf{B} & \cdots & \mathbf{A}^{N-1}\mathbf{B} \end{bmatrix}_{n \times N} \tag{3.15}$$

For a discrete time state-space model, Eq. (3.5), of order (or McMillan degree) *n*, it can be shown via the Cayley-Hamilton theorem that both $\mathbf{H}_1$ and $\mathbf{H}_2$ have full column rank *n* and full row rank *n*, respectively. As a result, the Hankel matrix $\mathbf{H}$ has rank *n*. Furthermore, from its definition, the shifted Hankel matrix $\overline{\mathbf{H}}$ can be shown to have the following shift property:

$$\overline{\mathbf{H}} = \mathbf{H}_1 \mathbf{A} \mathbf{H}_2 \tag{3.16}$$

where $\mathbf{H}_1$ and $\mathbf{H}_2$ are as defined as in Eq. (3.15). As both $\mathbf{H}_1$ and $\mathbf{H}_2$ have respectively full column and row rank *n*, there exists a left inverse $\mathbf{H}_1^{\dagger}$ and a right inverse $\mathbf{H}_2^{\dagger}$ such that

$$\mathbf{H}_1^{\dagger}\mathbf{H}_1 = \mathbf{I}_{n \times n} \quad \text{and} \quad \mathbf{H}_2\mathbf{H}_2^{\dagger} = \mathbf{I}_{n \times n} \tag{3.17}$$

so that, from Eq. (3.16),

$$\mathbf{A} = \mathbf{H}_1^{\dagger} \overline{\mathbf{H}} \mathbf{H}_2^{\dagger} \tag{3.18}$$

The above left and right inverses are obtained as

$$\begin{aligned} \mathbf{H}_1^{\dagger} &= [\mathbf{H}_1^{\mathrm{T}}\mathbf{H}_1]^{-1}\mathbf{H}_1^{\mathrm{T}} \\ \mathbf{H}_2^{\dagger} &= \mathbf{H}_2^{\mathrm{T}}[\mathbf{H}_2\mathbf{H}_2^{\mathrm{T}}]^{-1} \end{aligned} \tag{3.19}$$

During the identification process, the decomposition of $\mathbf{H}$ into $\mathbf{H}_1$ and $\mathbf{H}_2$ according to Eq. (3.14) can be performed through a singular value decomposition (SVD), $\mathbf{H} = \mathbf{U}\boldsymbol{\Sigma}\mathbf{V}^{\mathrm{T}}$, where both $\mathbf{U}$ and $\mathbf{V}$ are orthonormal matrices and $\boldsymbol{\Sigma}$ is a diagonal matrix with the (non-negative) singular values ordered in decreasing magnitude on the main diagonal. The SVD provides insight into the rank of $\mathbf{H}$ (Vandewalle and de Moor 1991), as the rank of $\mathbf{H}$ is given by the number of non-zero diagonal elements (singular values) in $\boldsymbol{\Sigma}$ for the case of noise free measurements. In the case where the rank of $\mathbf{H}$ is significantly larger than n (due to the presence of measurement noise), a decision can be made regarding the order n of the system (or effective rank of the Hankel matrix $\mathbf{H}$) on the basis of the plot of the singular values. In this case, the SVD allows to approximate the high rank Hankel matrix $\mathbf{H}$ into a lower rank (n) matrix via a separation of large and small singular values of matrix $\mathbf{H}$. The use of SVD to compute a low rank decomposition of the Hankel matrix is essential in the realization method and has been used in the classical Kung's realization algorithm (Kung 1978) as well as in ERA (Juang and Pappa 1985). The SVD of the Hankel matrix $\mathbf{H}$ can be expressed as

$$\mathbf{H} = \mathbf{U}\boldsymbol{\Sigma}\mathbf{V}^{\mathrm{T}} = \begin{bmatrix}\mathbf{U}_n & \mathbf{U}_s\end{bmatrix}\begin{bmatrix}\boldsymbol{\Sigma}_n & \mathbf{0} \\ \mathbf{0} & \boldsymbol{\Sigma}_s\end{bmatrix}\begin{bmatrix}\mathbf{V}_n^{\mathrm{T}} \\ \mathbf{V}_s^{\mathrm{T}}\end{bmatrix} \tag{3.20}$$

in which $\boldsymbol{\Sigma}$ is split up in the two diagonal matrices $\boldsymbol{\Sigma}_n$ and $\boldsymbol{\Sigma}_s$, where $\boldsymbol{\Sigma}_s$ and $\boldsymbol{\Sigma}_n$ denote the part of $\boldsymbol{\Sigma}$ with the s small (zero in the case of noise free measurements) singular values and the part of $\boldsymbol{\Sigma}$ with the n large (non-zero in the case of noise free measurements) singu-

lar values, respectively. As already mentioned above, a decision on an appropriate value of the rank *n* of the reduced-rank Hankel matrix can be made by plotting the singular values.

Using the partitioned SVD in Eq. (3.20), the high rank Hankel matrix **H** can be approximated by a reduced rank *n* matrix $\mathbf{H}_n$ of the same dimension as

$$\mathbf{H}_n = \mathbf{U}_n \Sigma_n \mathbf{V}_n^{\mathrm{T}} \tag{3.21}$$

which can be shown to minimize $\left\|\mathbf{H} - \mathbf{H}_n\right\|_2$ where $\| \ldots \|_2$ denotes the induced two-norm or maximum singular value of a matrix. On the basis of the above rank *n* decomposition, the matrices $\mathbf{H}_1$ and $\mathbf{H}_2$ in Eq. (3.14) can be estimated as

$$\begin{aligned} \mathbf{H}_1 &= \mathbf{U}_n \boldsymbol{\Sigma}_n^{1/2} \\ \mathbf{H}_2 &= \boldsymbol{\Sigma}_n^{1/2} \mathbf{V}_n^{\mathrm{T}} \end{aligned} \tag{3.22}$$

from which the expressions for the left inverse $\mathbf{H}_1^{\dagger}$ and right inverse $\mathbf{H}_2^{\dagger}$ simplify to

$$\begin{aligned} \mathbf{H}_1^{\dagger} &= \boldsymbol{\Sigma}_n^{-1/2} \mathbf{U}_n^{\mathrm{T}} \\ \mathbf{H}_2^{\dagger} &= \mathbf{V}_n \boldsymbol{\Sigma}_n^{-1/2} \end{aligned} \tag{3.23}$$

From the results in Eqs. (3.21) through (3.23) and using Eqs. (3.13), (3.15) and (3.18), it follows that the state-space matrices of the discrete time model in Eq. (3.5) are given by

$$\mathbf{D} = \mathbf{g}(0), \quad \mathbf{C} = \mathbf{H}_1(1{:}m, :), \quad \mathbf{B} = \mathbf{H}_2(:, 1) \quad \text{and} \quad \mathbf{A} = \mathbf{H}_1^{\dagger} \overline{\mathbf{H}} \mathbf{H}_2^{\dagger} \tag{3.24}$$

where the notations (1:*m* , :) and (: , 1) denote the first *m* rows and the first column of a matrix, respectively. It should be noted that ERA is also readily applicable to free vibration response data. In this case, the Hankel matrix is constructed using free vibration data (i.e., **y**(0) as first element of the Hankel matrix), and the identified input matrix **B** repre-

sents the non-zero initial state $\mathbf{x}_0$, which is related to the initial nodal displacements and velocities in the physical state $\bar{\mathbf{x}}_0$ through the linear transformation $\bar{\mathbf{x}}_0 = \mathbf{T}\mathbf{x}_0$.

3.2.3 General Realization Algorithm (GRA)

As discussed in the previous section, ERA assumes either a pulse input signal or free vibration response to construct the Hankel matrix. In many practical situations, the dynamic excitation acts over a finite-time or continually and the dynamic response of the structure during forced vibration contains valuable information on the system dynamics. Unfortunately, ERA cannot incorporate this information directly. The objective of this section is to extend ERA to accommodate arbitrary excitation signals.

Although ERA is not directly applicable to general excitation signals, estimates of the Markov parameters can be obtained separately and fed into ERA. Such an estimation can be achieved via (i) non-parametric estimation methods such as correlation analysis, e.g., NExT-ERA by James et al. (1993), (ii) estimation of a Finite Impulse Response (FIR) model, e.g., Oppenheim and Schafer (1989), (iii) inverse Fourier transformation of an empirical transfer function estimate, e.g., Ljung (1999), or (iv) wavelet transformation, e.g., Alvin et al. (2003). Unfortunately, for accurate estimation of the Markov parameters, these methods require a broadband excitation signal u(*k*). A narrow band excitation will lead to biased and noisy (large variance) estimation of the Markov parameters that will in turn pollute the results of the subsequent application of ERA. An alternative would be to reconstruct the Markov parameters from a Kalman filter or other state observer, as done in Phan et al. (1992). Although this is a powerful method, it requires relatively long input-

output data in the least squares procedure used to compute the Markov parameters (Lus et al. 2002). The method presented below aims at estimating the dynamic properties of the structure based on a (short-time) input-output data sequence available.

To illustrate the main idea behind GRA, consider the discrete time input-output relationship given in Eq. (3.9) that can be rewritten in the following Hankel matrix based representation

$$\mathbf{Y} = \mathbf{H}\mathbf{U} + \mathbf{E} \tag{3.25}$$

where **H** is the truncated (the first i block rows with $i < N$) Hankel matrix given in Eq. (3.11) and

$$\mathbf{Y} = \begin{bmatrix} \mathbf{y}(1) & \mathbf{y}(2) & \dots & \mathbf{y}(N) \\ \mathbf{y}(2) & \mathbf{y}(3) & \dots & \mathbf{y}(N+1) \\ \dots & \dots & \dots & \dots \\ \mathbf{y}(i) & \mathbf{y}(i+1) & \dots & \mathbf{y}(i+N-1) \end{bmatrix}_{(m\times i)\times N}, \quad \mathbf{U} = \begin{bmatrix} \mathrm{u}(0) & \mathrm{u}(1) & \dots & \mathrm{u}(N-1) \\ 0 & \mathrm{u}(0) & \dots & \mathrm{u}(N-2) \\ \dots & \dots & \dots & \dots \\ 0 & 0 & \dots & \mathrm{u}(0) \end{bmatrix}_{N\times N},$$

$$\mathbf{E} = \begin{bmatrix} \mathbf{g}(0)\mathrm{u}(1) & \mathbf{g}(0)\mathrm{u}(2) & \dots & \mathbf{g}(0)\mathrm{u}(N) \\ \mathbf{g}(0)\mathrm{u}(2)+\mathbf{g}(1)\mathrm{u}(1) & \mathbf{g}(0)\mathrm{u}(3)+\mathbf{g}(1)\mathrm{u}(2) & \dots & \mathbf{g}(0)\mathrm{u}(N+1)+\mathbf{g}(1)\mathrm{u}(N) \\ \dots & \dots & \dots & \dots \\ \sum_{l=0}^{i-1}\mathbf{g}(l)\mathrm{u}(i-l) & \sum_{l=0}^{i-1}\mathbf{g}(l)\mathrm{u}(i-l+1) & \dots & \sum_{l=0}^{i-1}\mathbf{g}(l)\mathrm{u}(i+N-l-1) \end{bmatrix}_{(m\times i)\times N} \tag{3.26}$$

In the above equation, **H** is the conventional Hankel matrix of impulse response coefficients **g**(k) and **Y** is a Hankel matrix consisting of the measured output data due to the (arbitrary) input u(k). The input data is stored in the $N \times N$ square matrix **U**, which is non-singular provided that $\mathrm{u}(0) \neq 0$. It is observed from Eqs. (3.25) and (3.26) that matrix **E** contains terms defined as the sum of input signals weighted by the corresponding Markov parameters, which can be estimated from input-output data. To show this, consider the

input measurement u(0), which corresponds to the start of the non-zero input signal during the experiment, to be normalized to u(0) = 1 without loss of generality[1]. This greatly simplifies the formulation and with u(k) = 0 for $k < 0$, $\mathbf{g}(l)$ can be computed recursively from the input-output data as

$$\mathbf{g}(l) = \mathbf{y}(l) - \sum_{k=0}^{l-1} \mathbf{g}(k)\mathrm{u}(l-k), \quad \mathbf{g}(0) = \mathbf{y}(0) \tag{3.27}$$

which is equivalent to

$$\mathbf{G}_N = \mathbf{Y}_N \cdot \mathbf{U}^{-1} \tag{3.28}$$

where $\mathbf{U}$ is given in Eq. (3.26) with u(0) = 1, and

$$\mathbf{Y}_N = \left[\mathbf{y}(0)\ \mathbf{y}(1)\ \ldots\ \mathbf{y}(N-1)\right]_{m \times N} \quad \text{and} \quad \mathbf{G}_N = \left[\mathbf{g}(0)\ \mathbf{g}(1)\ \ldots\ \mathbf{g}(N-1)\right]_{m \times N} \tag{3.29}$$

Although matrix $\mathbf{U}$ is an upper triangular matrix with a determinant of one, this matrix can be ill-conditioned, especially for a large number of data points N. Numerically, is it advantageous to replace Eq. (3.28) by

$$\mathbf{G}_N = \mathbf{Y}_N \cdot \mathbf{U}^{\dagger} \tag{3.30}$$

where $\mathbf{U}^{\dagger}$ is the Moore-Penrose pseudo-inverse (Noble and Daniel, 1988) of $\mathbf{U}$ with a tolerance on the singular values considered in computing this matrix. It should be noted that the impulse response estimate (or Markov parameter estimates) can also be obtained using different methods than the one shown in Eq. (3.30). Some of these methods such as Observer/Kalman filter identification (Phan et al. 1991) can be used to estimate Markov

1. Both the input u and the output $\mathbf{y}$ are scaled by the same factor, namely the original/unscaled value of u(0).

parameters without requiring knowledge of the initial conditions. The impulse response estimates are then used to compute the elements of matrix **E** which can be calculated as

$$\mathbf{E}(i,k) = \sum_{l=0}^{i-1} \mathbf{G}_N(l+1)\mathrm{u}(k+i-l-1) \tag{3.31}$$

where $\mathbf{E}(i,k)$ denotes the k^{th} column of i^{th} block row of matrix **E** and $\mathbf{G}_N(l+1)$ is the $(l+1)^{\text{th}}$ column of $\mathbf{G}_N$ matrix given in Eq. (3.30). In the case of noisy measurements $\mathbf{Y}_N$, the variance of $\mathbf{G}_N(l)$ increases with *l*. It can be observed from Eq. (3.31) that increasingly values of *l* in $\mathbf{G}_N(l)$ are needed to compute the successive block rows of the matrix **E**. To mitigate the effects of the increasing variance (as a function of *l*) of the impulse response estimates $\mathbf{G}_N(l)$, a limited number *i* $(n \le i < N)$ of block rows of matrix **E** of dimension $(m \times i) \times N$ is used such that $\mathbf{G}_N(i)$ has a reasonably small variance. In the previous statement, *N* denoted the total number of data points minus *i*, and *n* is the anticipated order of the model to be estimated. Defining $\mathbf{R} = \mathbf{Y} - \mathbf{E} = \mathbf{HU}$ as a weighted Hankel matrix, it follows from the full rank property of **U** that rank (**H**) = rank (**R**). In the case of noise free measurements, rank (**R**) is equal to the exact order of the system to be identified. GRA allows a state-space realization of the system directly on the basis of the weighted Hankel matrix **R**, from which the modal parameters of the system can be obtained. Alternatively to the above, matrix **H** could be computed via $\mathbf{H} = \mathbf{RU}^{-1}$ (or $\mathbf{H} = \mathbf{RU}^{\dagger}$), but that would require an additional inverse (or pseudo-inverse) of the possibly ill-conditioned matrix **U** which would result in large variances of the high column entries of the Hankel matrix **H**.

To continue the development of GRA, a lower rank decomposition via SVD is applied to **R** as

$$\mathbf{R} = \mathbf{U}\boldsymbol{\Sigma}\mathbf{V}^{\mathrm{T}} = \begin{bmatrix}\mathbf{U}_n & \mathbf{U}_s\end{bmatrix}\begin{bmatrix}\boldsymbol{\Sigma}_n & \mathbf{0} \\ \mathbf{0} & \boldsymbol{\Sigma}_s\end{bmatrix}\begin{bmatrix}\mathbf{V}_n^{\mathrm{T}} \\ \mathbf{V}_s^{\mathrm{T}}\end{bmatrix} \tag{3.32}$$

which is similar to Eq. (3.20) for Hankel matrix **H**. Using this SVD decomposition, matrix **R** can be approximated by a rank n matrix $\mathbf{R}_n$ of the same dimensions as

$$\mathbf{R}_n = \mathbf{U}_n\boldsymbol{\Sigma}_n\mathbf{V}_n^{\mathrm{T}} \tag{3.33}$$

which can be shown to minimize $\left\|\mathbf{R} - \mathbf{R}_n\right\|_2$. Therefore, $\mathbf{R}_n$ can be factorized as

$$\mathbf{R}_n = \mathbf{R}_1\mathbf{R}_2 \tag{3.34}$$

in which

$$\begin{aligned}\mathbf{R}_1 &= \mathbf{U}_n\boldsymbol{\Sigma}_n^{1/2} \\ \mathbf{R}_2 &= \boldsymbol{\Sigma}_n^{1/2}\mathbf{V}_n^{\mathrm{T}}\end{aligned} \tag{3.35}$$

Similar to Hankel matrix $\mathbf{H}$ in Eq. (3.16), matrix **R** has the shift property

$$\overline{\mathbf{R}} = \mathbf{R}_1\mathbf{A}\mathbf{R}_2 \tag{3.36}$$

where $\overline{\mathbf{R}} = \overline{\mathbf{Y}} - \overline{\mathbf{E}}$ in which shifted matrix $\overline{\mathbf{Y}}$ is defined similar to $\overline{\mathbf{H}}$ in Eq. (3.12) and $\overline{\mathbf{E}}$ is given by

$$\overline{\mathbf{E}} = \begin{bmatrix} \mathbf{g}(0)\mathrm{u}(2) + \mathbf{g}(1)\mathrm{u}(1) & \mathbf{g}(0)\mathrm{u}(3) + \mathbf{g}(1)\mathrm{u}(2) & \cdots & \mathbf{g}(0)\mathrm{u}(N+1) + \mathbf{g}(1)\mathrm{u}(N) \\ \cdots & \cdots & \cdots & \cdots \\ \sum_{l=0}^{i} \mathbf{g}(l)\mathrm{u}(i+1-l) & \sum_{l=0}^{i} \mathbf{g}(l)\mathrm{u}(i-l+2) & \cdots & \sum_{l=0}^{i} \mathbf{g}(l)\mathrm{u}(i+N-l-1) \end{bmatrix}_{(m\times i)\times N} \tag{3.37}$$

From the above properties of matrix $\mathbf{R}$, it follows that a realization based algorithm similar to ERA based on the input-output data matrices $\mathbf{R}$ and $\overline{\mathbf{R}}$ can be used to construct the discrete time state-space matrices in Eq. (3.5) for the case of arbitrary input u(k). This is achieved simply by replacing $\mathbf{H}$ by $\mathbf{R}$ in Eq. (3.24).

The main idea behind GRA is to use the information of the input signal to create a weighted Hankel matrix $\mathbf{R} = \mathbf{Y} - \mathbf{E} = \mathbf{HU}$, instead of creating a (unweighted) Hankel matrix **H** by first estimating a large number of Markov parameters on the basis of a short-time and/or non-white input sequence. In the application of GRA, the Markov parameter estimates are used to build up the error matrix **E**, which in turn is used to create the weighted Hankel matrix **R** on which a realization algorithm is performed to compute a state-space model. However, by carefully examining the formula and size of matrix **E**, it is observed that only a small number of Markov parameter estimates is needed to create a "large fat" (very high number of columns compared to the number of block-rows) matrix **E** and consequently matrix $\mathbf{R} = \mathbf{Y} - \mathbf{E}$. Therefore, the use of a "large fat" unweighted Hankel matrix **H** for which a large number of Markov parameters would be required, is avoided. In other words, as compared to ERA, the proposed GRA reduces the required length of the Markov parameter sequence to obtain accurate system identification results.

To show that GRA is a generalization of ERA, it can be seen that for a unit pulse input u(k) as defined in Eq. (3.10), matrix **U** becomes the $N \times N$ identity matrix, while matrix **E** becomes a $(m \times i) \times N$ zero matrix since u(k) = 0 for $k \neq 0$. In another special case where the input signal u(k) is the unit step defined as

$$\mathrm{u}(k) = \begin{cases} 1, k \geq 0 \\ 0, k < 0 \end{cases}, \tag{3.38}$$

which is typically applied to flexible mechanical (servo) systems in order to study their transient dynamic behavior, matrix **U** is an upper triangular matrix and matrix **E** is a row-wise listing of output signals as

$$\mathbf{U} = \begin{bmatrix} 1 & 1 & \dots & 1 \\ 0 & 1 & \dots & 1 \\ \dots & \dots & \dots & \dots \\ 0 & 0 & \dots & 1 \end{bmatrix}_{N \times N}, \qquad \mathbf{E} = \begin{bmatrix} \mathbf{y}(0) & \mathbf{y}(0) & \dots & \mathbf{y}(0) \\ \mathbf{y}(1) & \mathbf{y}(1) & \dots & \mathbf{y}(1) \\ \dots & \dots & \dots & \dots \\ \mathbf{y}(i-1) & \mathbf{y}(i-1) & \dots & \mathbf{y}(i-1) \end{bmatrix}_{(m \times i) \times N} \tag{3.39}$$

as previously shown by de Callafon (2003). In the latter case, applying GRA to matrix **R** which depends only on step response data yields significantly better results in terms of system realization than applying ERA based on impulse response data obtained through differentiating the step response measurements (de Callafon 2003).

3.2.4 Refinement of State-Space Realization through Least Squares Optimization

Although Eq. (3.24) allows to identify the state-space matrices **A**, **B** and **C** based on the SVD of a high-dimensional Hankel matrix both for ERA and GRA, the feed-through matrix **D** is estimated from the single, possibly noisy, measurement **g**(0). Using the estimates of the state matrix **A** and the input matrix **B** obtained through ERA or GRA, the state vector **x**(k) can be reconstructed as

$$\mathbf{x}(k+1) = \mathbf{A}\mathbf{x}(k) + \mathbf{B}\mathrm{u}(k), \qquad \mathbf{x}(0) = \mathbf{0} \tag{3.40}$$

for k = 0, 1, ..., 2N. With the reconstructed state vector **x**(k), the realization algorithm (ERA or GRA) that is used to compute matrices **A** and **B** can be followed by a standard

Least Squares (LS) optimization problem to improve the estimation of the state-space matrices. The LS problem can be stated by rewriting Eq. (3.5) and adding the zero mean noise vector $\mathbf{V}(k)$ as

$$\mathbf{Y}(k) = \mathbf{\Theta U}(k) + \mathbf{V}(k), \qquad k = 1, \ldots, 2N \tag{3.41}$$

where

$$\mathbf{Y}(k) = \begin{bmatrix} \mathbf{x}(k+1) \\ \mathbf{y}(k) \end{bmatrix}, \quad \mathbf{\Theta} = \begin{bmatrix} \mathbf{A} & \mathbf{B} \\ \mathbf{C} & \mathbf{D} \end{bmatrix}, \quad \mathbf{U}(k) = \begin{bmatrix} \mathbf{x}(k) \\ \mathrm{u}(k) \end{bmatrix} \quad \text{and} \quad \mathbf{V}(k) = \begin{bmatrix} \mathbf{w}(k) \\ \mathbf{v}(k) \end{bmatrix} \tag{3.42}$$

in which $\mathbf{w}(k)$ represents the possible noise on the reconstructed state vector $\mathbf{x}(k)$ and $\mathbf{v}(k)$ the noise on the measured output $\mathbf{y}(k)$ which includes measurement noise. Noise vector $\mathbf{V}(k)$ could also include the effects of parameter estimation errors and modeling error. Including all input-output data for $k = 1, \ldots, 2N$ in a single matrix representation, Eq. (3.41) can be rewritten as

$$\mathbf{Y} = \mathbf{\Theta U} + \mathbf{V}, \qquad \mathbf{Y} = \begin{bmatrix} \mathbf{Y}(0) & \mathbf{Y}(1) & \ldots & \mathbf{Y}(2N) \end{bmatrix}, \qquad \mathbf{U} = \begin{bmatrix} \mathbf{U}(0) & \mathbf{U}(1) & \ldots & \mathbf{U}(2N) \end{bmatrix} \tag{3.43}$$

Then the state-space matrices in $\mathbf{\Theta}$ can be updated via a standard least squares solution as

$$\hat{\mathbf{\Theta}}_{\mathrm{LS}}^{N} = \mathbf{Y}\mathbf{U}^{\mathrm{T}}[\mathbf{U}\mathbf{U}^{\mathrm{T}}]^{-1} \tag{3.44}$$

provided that matrix $\mathbf{U}$ has full row rank. The full row rank condition of matrix $\mathbf{U}$ is related to the input excitation $\mathrm{u}(k)$ and is trivially satisfied for broad-band forcing function (e.g., pulse/impact load, earthquake ground excitation). The least squares improvement renders the estimated state-space matrices less sensitive to noise. If the input $\mathrm{u}(k)$ and the reconstructed state $\mathbf{x}(k)$ are uncorrelated with the state noise $\mathbf{w}(k)$ and the measurement noise $\mathbf{v}(k)$, i.e., $\lim_{N \to \infty} (1/N) \times \mathbf{V}\mathbf{U}^{\mathrm{T}} = 0$, consistent estimates of the state-space

matrices are obtained. This condition is satisfied asymptotically as $N \to \infty$ provided that the experiments are conducted in such a way that the input excitation is uncorrelated with the measurement noise.

3.3 NUMERICAL VALIDATION

3.3.1 Definition of Benchmark Problem

In order to investigate the performance of the proposed GRA, the eight-story linear elastic shear building model shown in Figure 3.1 subjected to seismic base excitation is used as a case study. This shear building has a constant floor mass of 625 tons, a constant story stiffness of 10^6 [kN/m], and damping properties represented through the non-classical damping matrix **C** (Veletsos and Ventura 1986). The latter was generated from an assumed configuration of inter-multiple-story viscous dampers installed on the structure (between floors 1 and 4, 2 and 6, and 3 and 8) and is given by

$$\mathbf{C} = 400 \times \begin{bmatrix} 16 & -6 & 0 & -4 & 0 & 0 & 0 & 0 \\ -6 & 15 & -5 & 0 & 0 & -4 & 0 & 0 \\ 0 & -5 & 14 & -5 & 0 & 0 & 0 & -4 \\ -4 & 0 & -5 & 12 & -3 & 0 & 0 & 0 \\ 0 & 0 & 0 & -3 & 6 & -3 & 0 & 0 \\ 0 & -4 & 0 & 0 & -3 & 8 & -1 & 0 \\ 0 & 0 & 0 & 0 & 0 & -1 & 2 & -1 \\ 0 & 0 & -4 & 0 & 0 & 0 & -1 & 5 \end{bmatrix} \quad [\mathrm{kN \cdot sec/m}] \tag{3.45}$$

Viscously damped systems that do not satisfy the Caughey-O'Kelly condition (Caughey and O'Kelly 1965) generally have complex-valued natural modes of vibration. Such systems are said to be non-classically or non-proportionally damped. Foss (1958)

presented a generalization of the modal superposition method to evaluate the response of such systems. The modal parameters of the shear building model considered here are obtained through solving a complex eigenvalue problem in state-space. The computed natural frequencies and damping ratios are reported in Table 3.1. It is worth noting that the natural frequencies of a non-classically damped system extracted through eigen-analysis of the state matrix, referred to as pseudo-undamped natural frequencies (Veletsos and Ventura 1986), differ from the corresponding natural frequencies of the associated undamped system. This difference is due to the fact that the eigenvalues of the state matrix of a non-classically damped system are functions of the damping in the system. Figure 3.2 shows the complex-valued mode shapes of the shear building as rotating vectors in the complex plane called polar plots. The indices on the vectors in each polar plot indicate the DOF number (i.e., floor number). The polar plot representation of a mode shape displays the degree of non-classical damping characteristics of that mode. If the components (or DOFs) of a mode shape are collinear (i.e., in phase or out of phase) in the complex plane, then this mode is classically (or proportionally) damped. The more a mode shape's components are scattered in the complex plane, the more this mode is non-classically damped. Since the higher order mode shapes of the shear building considered here exhibit strong non-classical characteristics (Figure 3.2), the real parts of these mode shape components do not remain proportional as the complex vectors rotate, i.e., these (real-valued) mode shapes change continuously within one vibration period. In Figure 3.3, the real part of all eight complex mode shapes are plotted at four snapshots with 90 degree phase shifts during a vibration period.

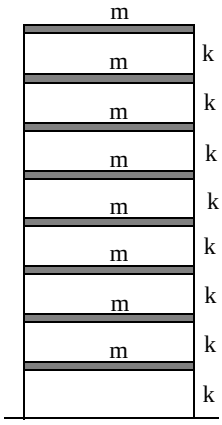

Fig. 3.1 Eight story shear building model

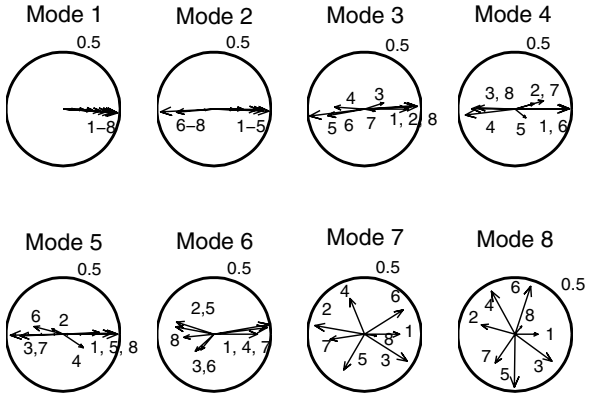

Fig. 3.2 Polar plot representation of complex mode shapes

3.3.2 Simulation of Measurement Data

The shear building model is subjected to a horizontal base excitation defined as the strong motion part (2-30 sec) of the Imperial Valley, 1940 earthquake ground motion recorded at the El Centro station (see Figure 3.4). The shear building output data used in this study consist of the floor absolute acceleration responses to this earthquake excitation. The differential equations of motion formulated in state-space are integrated via complex modal analysis (Peng and Conte 1998), assuming a piecewise linear forcing function, and using piecewise linear exact integration of the complex-valued first-order modal equations of motion. A constant time increment of $\Delta T = 0.02$ sec is used to integrate the equations of motion. To model measurement noise, zero-mean Gaussian white noise processes are added to the simulated output signals. The reason for considering up to high levels of measurement noise (4% in root-mean-square ratio) is to allow for the higher vibration modes to become more difficult to extract from the data due to decreasing signal-to-noise ratio at higher frequencies, a phenomenon typically seen in real-life applications.

Table 3.1 Modal parameters of shear building structure

	Mode 1	Mode 2	Mode 3	Mode 4	Mode 5	Mode 6	Mode 7	Mode 8
Undamped frequency [Hz]	1.175	3.484	5.675	7.673	9.409	10.825	11.873	12.516
Pseudo-undamped frequency [Hz]	1.176	3.486	5.687	7.674	9.406	10.871	12.012	12.278
Damped frequency [Hz]	1.175	3.473	5.675	7.662	9.388	10.859	11.977	12.251
Damping ratio [%]	3.77	8.54	6.5	5.65	6.12	4.71	7.68	6.65

The performance (e.g., statistical properties of estimated modal parameters) of the new system identification procedure presented above is investigated under increasing level of noise. For a given floor, the noise level is defined as the ratio (in percent) of the root mean square (RMS) of the added noise process to the RMS of the floor absolute acceleration response (computed over the time interval 2-30 sec). The added noise processes at the various floors are simulated as statistically independent. Figure 3.5 compares the added noise realizations of various amplitudes (1%, 2%, 3%, and 4%) to all eight modal components of the noise free roof absolute acceleration response obtained as explained in Appendix II. It is clearly observed that depending on the mode and noise level, the modal absolute acceleration response may be buried in the noise, which renders the corresponding modal parameters difficult to identify.

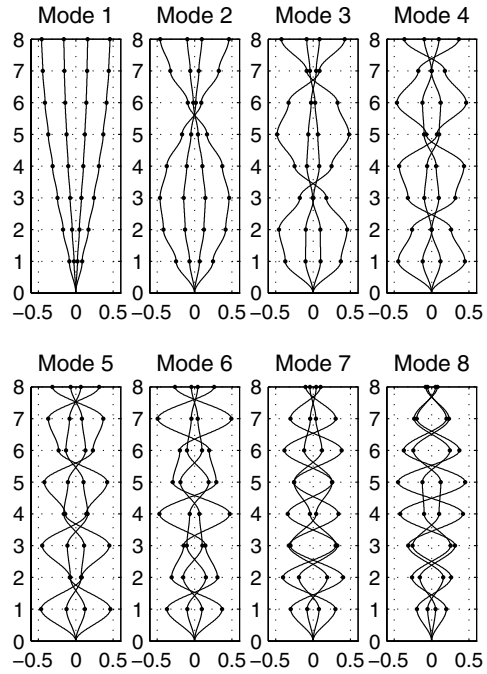

Fig. 3.3 Exact complex mode shapes of the non-classically damped shear building shown at different phases $(0, \pi/2, \pi, 3\pi/2)$

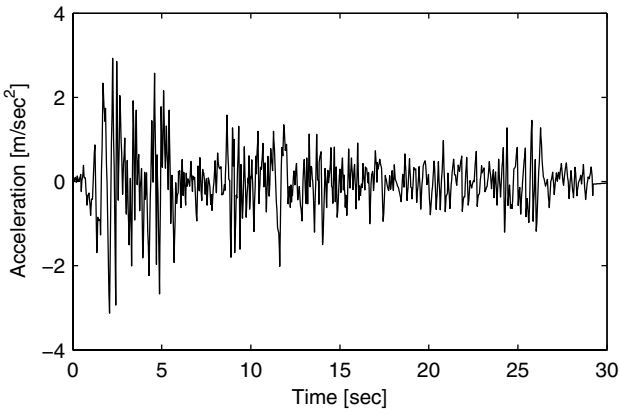

Fig. 3.4 Imperial Valley, El Centro 1940 earthquake ground motion record

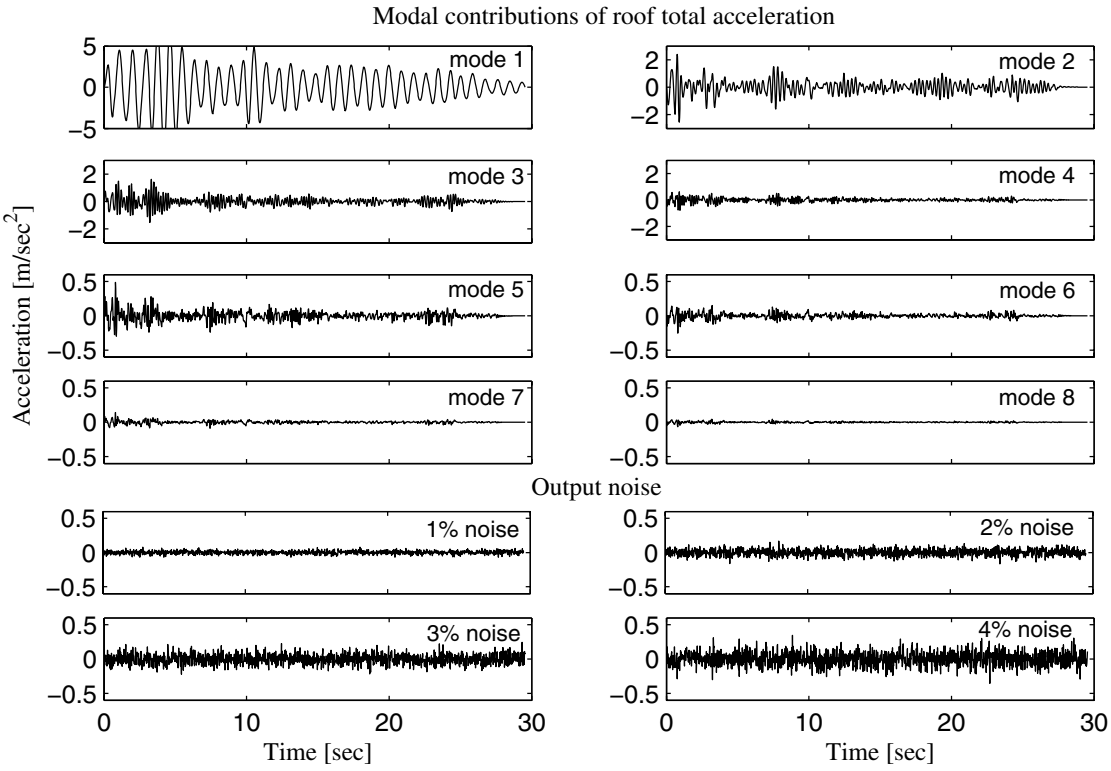

Fig. 3.5 Modal contributions of total acceleration response at roof level and different levels of added noise

3.3.3 Application of GRA and Discussion of Results

In order to apply GRA to the seismic input and simulated output data, matrices **E** and $\bar{\mathbf{E}}$ of size $(8 \times 40) \times 1400$ are formed based on the whole length of the simulated data (1440 data points) as described in Section 2.3. The identified modal natural frequencies and damping ratios are obtained through eigen-analysis of the estimated discrete time state matrix **A**, while the identified mode shapes are obtained as described in Appendix III. The modal parameters (natural frequencies, damping ratios, and mode shapes) of all eight modes of the shear building identified from noise free input-output data are in perfect agreement with the corresponding exact values given in Table 3.1 and Figure 3.3. The sta-

tistical properties (bias and variance) of the estimated modal parameters using GRA are investigated as a function of the noise level.

Table 3.2 Statistics of modal parameters identified using GRA based on 100 identification trials at 1% noise level

	Identified-to-exact natural frequency ratio				Identified-to-exact modal damping ratio			
	mean	cov [%]	min	max	mean	cov [%]	min	max
Mode 1	1.000	0.00	1.000	1.000	1.000	0.05	0.998	1.001
Mode 2	1.000	0.01	1.000	1.000	1.000	0.15	0.995	1.003
Mode 3	1.000	0.01	1.000	1.000	1.000	0.23	0.995	1.007
Mode 4	1.000	0.06	0.999	1.005	1.003	0.64	0.989	1.034
Mode 5	1.001	0.13	0.998	1.009	1.020	1.92	0.971	1.084
Mode 6	1.003	0.20	0.995	1.007	1.037	4.33	0.932	1.132

For this purpose, a set of 100 identifications was performed at each of nine different noise levels (0%, 0.5%, 1%, 1.5%, 2%, 2.5%, 3%, 3.5%, 4%) for the same noise free input-output data. The added vector (8-DOF) noise processes for the 100 identification trials are simulated as statistically independent. Statistics (mean and mean +/- one standard deviation) of the identified-to-exact natural frequency and damping ratios are shown in Figures 3.6 and 3.7, respectively, as a function of the noise level and for the first six vibration modes. Due to the low contribution of the seventh and eighth modes to the total building response (see Figure 3.5) and therefore the very weak signal-to-noise ratio, the modal parameters of these modes cannot be identified at and above the minimum level of added noise considered here (0.5%) as the modal responses are buried in the noise. From Figures 3.6 and 3.7, it is observed that (i) the identified modal frequencies and damping ratios are in very good agreement with their exact counterparts, and (ii) in general both bias and variance of the modal frequency and damping ratio estimators based on GRA increase as a

function of the noise level. However, in the particular application, the estimated natural frequencies of the first four modes appear to be quasi unbiased at the noise levels considered, which may be due to the significant contribution of these modes to the total response (see Figure 3.5).

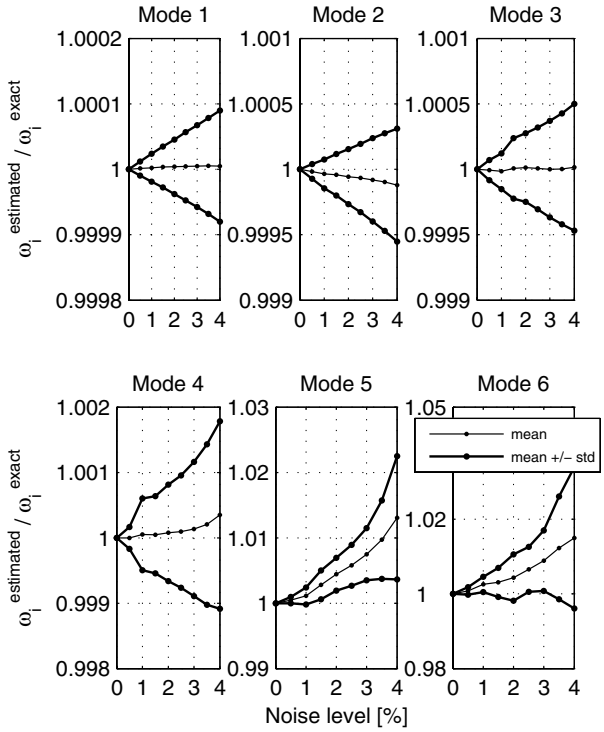

Fig. 3.6 Statistics of identified-to-exact frequency ratios as a function of measurement noise

Comparison of Figures 3.6 and 3.7 shows that both bias and standard deviation of the modal damping ratio estimates are significantly larger than those of the natural frequency estimates, as expected from the system identification literature. To complement Figures 3.6 and 3.7, the cumulative distribution functions of the identified-to-exact natural frequencies and damping ratios are plotted in Figures 3.8 and 3.9, respectively, for 1%, 2%, and 3% noise levels and for the first 6 vibration modes (modes 1, 2, and 3 in the left column and modes 4, 5, and 6 in the right column). Figures 3.6 through 3.9 show that (i) the

variance of the estimated modal frequencies and damping ratios is significantly larger for higher modes, and (ii) the estimated modal frequencies and damping ratios are generally more sensitive to the noise level for the higher modes. These two observed trends may be due to the fact that the higher modes contribute less to the total response as shown in Figure 3.5. Table 3.2 provides the statistics (mean, coefficient-of-variation, min, max) of the estimated modal frequencies and damping ratios based on 100 identification trials in the presence of 1% output noise.

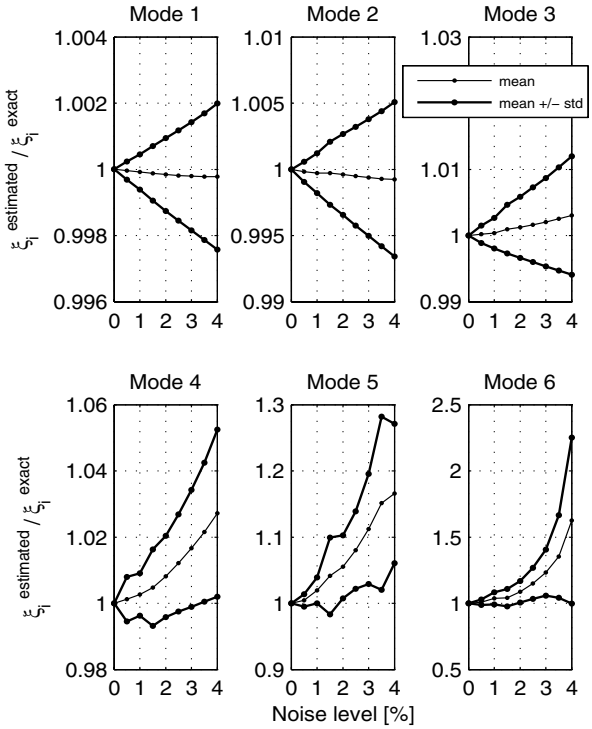

Fig. 3.7 Statistics of identified-to-exact modal damping ratios as a function of measurement noise

The modal assurance criterion (MAC) is used to compare the estimated mode shapes with their exact counterparts at different levels of noise. The MAC value is bounded between 0 and 1, measures the degree of correlation between an estimated mode

shape, $\psi_{estimated}$, and its exact counterpart, ψ_{exact}, (MAC value of 1 for exactly estimated mode shape), and is defined as

$$MAC(\psi_{estimated}, \psi_{exact}) = \frac{\left|\psi^{*}_{estimated} \cdot \psi_{exact}\right|^2}{\left|\psi_{estimated}\right|^2 \cdot \left|\psi_{exact}\right|^2} \tag{3.46}$$

where superscript * denotes the complex conjugate transpose. The mean and coefficient-of-variation (cov) of the MAC values between estimated and exact mode shapes based on 100 identification trials are reported in Table 3.3 for all noise levels considered herein and for the first six modes. From these results, it is observed that (i) the first four mode shapes are identified very accurately even in the presence of high amplitude output noise (4%), and (ii) estimates of the higher mode shapes become less accurate with increasing level of noise.

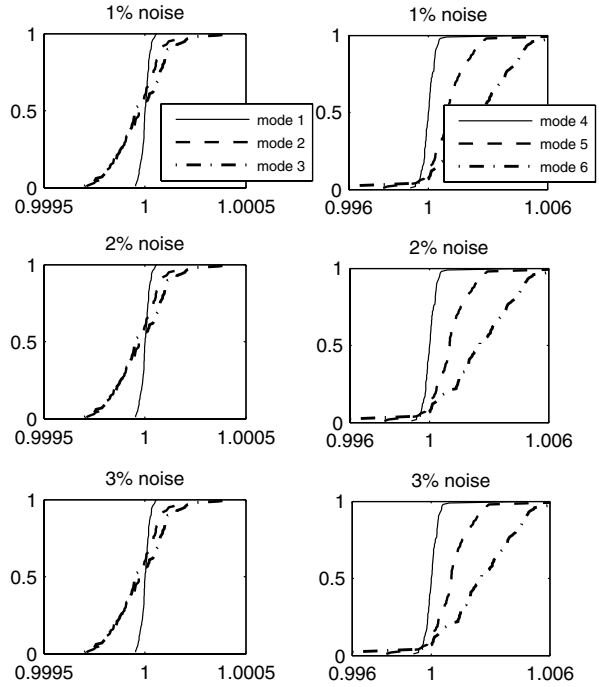

Fig. 3.8 Cumulative histogram of identified-to-exact modal frequency ratios based on 100 identification trials at noise levels of 1%, 2%, and 3%

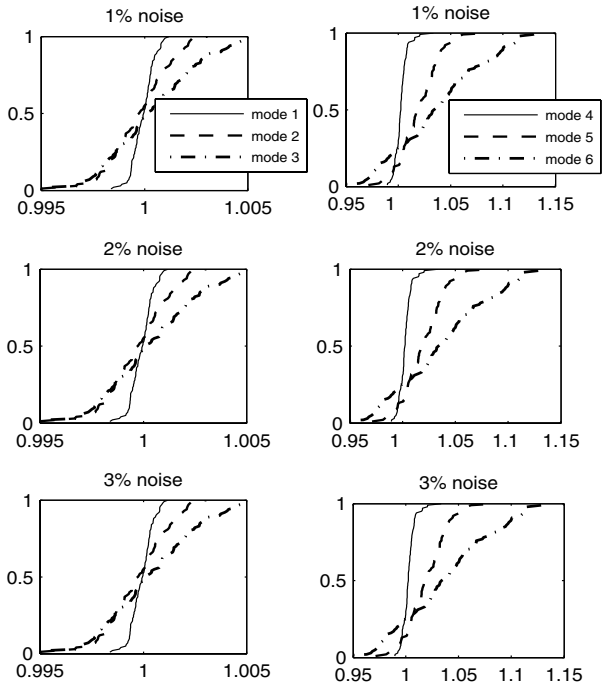

Fig. 3.9 Cumulative histogram of identified-to-exact modal damping ratios based on 100 identification trials at noise levels of 1%, 2%, and 3%

Table 3.3 Mean and coefficient-of-variation (COV) [%] of MAC values between identified and exact mode shapes based on 100 identification trials at different noise levels

	Mode 1		Mode 2		Mode 3		Mode 4		Mode 5		Mode 6	
	Mean	COV	Mean	COV	Mean	COV	Mean	COV	Mean	COV	Mean	COV
No noise	1.000	0.00	1.000	0.00	1.000	0.00	1.000	0.00	1.000	0.00	1.000	0.00
0.5% noise	1.000	0.03	0.997	0.39	0.991	1.25	0.978	2.96	0.966	4.20	0.903	10.80
1% noise	1.000	0.03	0.997	0.38	0.990	1.27	0.976	3.06	0.959	4.42	0.901	7.35
1.5% noise	1.000	0.03	0.997	0.38	0.990	1.28	0.976	2.99	0.948	4.36	0.860	4.43
2% noise	1.000	0.03	0.997	0.40	0.988	1.31	0.970	3.11	0.937	4.13	0.827	5.78
2.5% noise	1.000	0.03	0.997	0.40	0.988	1.31	0.969	3.14	0.929	4.13	0.818	5.02
3% noise	1.000	0.04	0.997	0.40	0.988	1.31	0.970	3.14	0.922	4.14	0.803	5.61
3.5% noise	1.000	0.04	0.997	0.40	0.988	1.31	0.968	3.15	0.908	4.35	0.780	6.54
4% noise	1.000	0.03	0.997	0.40	0.989	1.31	0.968	3.10	0.888	4.49	0.741	8.98

3.4 CONCLUSIONS

This paper presents the General Realization Algorithm (GRA), a new system realization algorithm to identify modal parameters of linear dynamic systems based on general input-output data. This algorithm is a generalization of the Eigensystem Realization Algorithm (ERA), which is based on singular value decomposition (SVD) of a Hankel matrix constructed from impulse response or free vibration response data. This generalization is obtained through SVD of a weighted Hankel matrix of input-output data, where the weighting is determined by the loading. Using GRA, the state-space matrices are estimated in a two-step process that includes a state reconstruction followed by a least squares optimization yielding a minimum prediction error for the response. An application example consisting of an 8-story shear building model subjected to earthquake base excitation is used for the multiple purposes of validating the new algorithm, evaluating its performance, and investigating the statistical properties (i.e., bias/unbias, variance, and robustness to added output noise introduced to model measurement noise and modeling errors) of the GRA modal parameter estimates. Based on the extensive simulation study performed, it is found that the proposed new algorithm yields very accurate estimates of the modal parameters (natural frequencies, damping ratios, and mode shapes) in the case of noise free input-output data or low output noise. The bias and variance of the modal parameter estimates increase with the level of output noise and with vibration mode order (due to the lower participation of higher modes to the total response and weak signal-to-noise ratio in the application example considered). Both bias and variance of the modal damping ratio estimates are significantly larger that those of the corresponding modal fre-

quency estimates as expected from the system identification literature. In summary, application of GRA is recommended for realization of linear dynamic systems subjected to short-duration and/or non-broadband excitations such as earthquake and shake table excitations when information about the input is available.

ACKNOWLEDGEMENTS

Chapter 3, with some modifications (extensions), is a reprint of the material submitted for possible publication in the Journal of Engineering Mechanics, ASCE (2007), De Callafon, R.A., Moaveni, B., Conte, J.P., He, X., and Udd, E. The dissertation author was second author of this paper. He strongly contributed to the development General Realization Algorithm presented and to the preparation of the manuscript.

Support of this research by the National Science Foundation, Grant No. DMI-0131967, under a Blue Road Research STTR Project on which UCSD was the principal subcontractor is gratefully acknowledged. Any opinions, findings, and conclusions or recommendations expressed in this material are those of the authors and do not necessarily reflect those of the National Science Foundation.

REFERENCES

Alvin, K. F., Robertson, A. N., Reich, G. W., and Park, K. C. (2003). “Structural system identification: from reality to models.” *Comput. Struct.*, 81(12), 1149–1176.

Caughey, T. H., and O'Kelly, M. E. J. (1965). “Classical normal modes in damped linear dynamic systems.” *J. Appl. Mech.*, ASME, 32, 583-588.

De Callafon, R. A. (2003). “Estimating parameters in a lumped parameter system with first principle modeling and dynamic experiments.” *Proc., 13th IFAC Symposium on System Identification,* Rotterdam, the Netherlands, 1613-1618.

Foss, K. A. (1958). “Coordinates which uncouple the equations of motion of damped linear dynamic systems.” *J. Appl. Mech.*, ASME, 25, 361-364.

Franklin, G. F., Powel, J. D., and Workman, M. (1998). *Digital control of dynamic systems*, 3rd Ed., Addison-Wesley, Boston, Massachusetts.

Gilbert, E. G. (1963). “Controllability and observability in multivariable control systems.” *SIAM J. Control*, 1(2), 128-151.

Ho, B. L., and Kalman R. E. (1966). “Effective construction of linear state-variable models from input-output functions.” *Regelungstechnik*, 14(12), 545-592.

James, G. H., Carne, T. G., and Lauffer, J. P. (1993). *The natural excitation technique for modal parameters extraction from operating wind turbines.* SAND92-1666, UC-261, Sandia National Laboratories, Sandia, New Mexico.

Juang, J. N., and Pappa, R. S. (1985). “An eigensystem realization algorithm for model parameter identification and model reduction.” *J. Guidance Control Dyn.,* 8(5), 620-627.

Juang, J. N., Cooper J. E. and Wright J. R. (1988). “An eigensystem realization algorithm using data correlations (ERA/DC) for model parameter identification.” *Control Theory Adv. Technol.,* 4(1), 5-14.

Kalman, R. E. (1963). “Mathematical description of linear dynamical systems.” *SIAM J. Control,* 1(2), 152-192.

Kung, S. Y. (1978). “A new identification and model reduction algorithm via singular value decomposition.” *Proc., 12th Asilomar Conference on Circuits, Systems and Computers,* Pacific Grove, USA, 705-714.

Ljung, L. (1999). *System identification: theory for the user,* 2nd Ed., Prentice-Hall, Englewood Cliffs, New Jersey.

Lus, H., Betti, R., and Longman, R. W. (1999). “Identification of linear structural systems using earthquake induced vibration data.” *Earthquake Eng. Struct. Dyn.*, 28(11), 1449-1467.

Lus, H., Betti, R., and Longman, R. W. (2002). “Obtaining refined first order predictive models of linear structural systems.” *Earthquake Eng. Struct. Dyn.,* 31(7), 1413-1440.

Noble, B., and Daniel, J. W. (1988). *Applied linear algebra,* 2nd Ed., Prentice Hall, Englewood Cliffs, New Jersey.

Oppenheim, A. V., and Schafer R. W. (1989). *Discrete-time signal processing,* Prentice Hall, Englewood Cliffs, New Jersey.

Peeters, B., and De Roeck, G. (2001). “Stochastic system identification for operational modal analysis: a review.” *Journal of Dynamic Systems, Measurements and Control*, 123(4), 659-667.

Peng, B. F., and Conte, J. P. (1998). “Closed-form solutions for the response of linear systems to fully nonstationary earthquake excitation.” *Journal of Engineering Mechanics*, ASCE, 124(6), 684-694.

Phan, M., Horta, L. G., Juang, J.-N., and Longman, R. W. (1992). *Identification of linear systems by an asymptotically stable Observer.* NASA Technical Paper TP-3164, Langley Research Center, Hampton, Virginia.

Phan, M., Juang, J. N., and Longman, R. W. (1991). *On Markov parameters in system identification.* NASA Technical Memorandum 104156, Langley Research Center, Hampton, Virginia.

Silverman, L. M. (1971). “Realization of linear dynamical systems.” *IEEE Trans. Automat. Control,* AC-16(6), 554-567.

Van Overschee, P., and de Moor, B. (1996). *Subspace identification for linear systems,* Kluwer Academic Publishers, Massachusetts, USA.

Vandewalle, J., and de Moor, B. (1988). “On the use of the singular value decomposition in identification and signal processing.” *Proc. of the workshop of the NATO Advanced Study Institute on Numerical Linear Algebra, Digital Signal Processing and Parallel Algorithms,* Leuven, Belgium, 321-360.

Veletsos, A. S., and Ventura, C. E. (1986). “Modal analysis of non-classically damped linear systems.” *Earthq. Engng. Struct. Dyn.*, 14(2), 217-243.

APPENDIX I: TIME DISCRETIZATION OF CONTINUOUS-TIME STATE-SPACE DYNAMIC MODEL

Consider the continuous-time state-space model presented in Eq. (3.2)

$$\begin{aligned} \dot{\mathbf{x}}(t) &= \mathbf{F}\mathbf{x}(t) + \mathbf{G}\mathbf{u}(t) \\ \mathbf{y}(t) &= \mathbf{H}\mathbf{x}(t) + \mathbf{E}\mathbf{u}(t) \end{aligned} \tag{3.47}$$

Performing a Laplace transformation on the state equation yields

$$\mathbf{X}(s) = (s\mathbf{I} - \mathbf{F})^{-1}\mathbf{G}\mathbf{U}(s) = \sum_{i=0}^{\infty} \frac{\mathbf{F}^i}{s^{i+1}} \mathbf{G}\mathbf{U}(s) \tag{3.48}$$

The solution of Eq. (3.48) in time domain is expressed as

$$\mathbf{x}(t) = \mathrm{e}^{\mathbf{F}\cdot(t-t_0)}\mathbf{x}(t_0) + \int_{t_0}^{t} \mathrm{e}^{\mathbf{F}\cdot(t-\sigma)}\mathbf{G}\cdot\mathbf{u}(\sigma)\mathrm{d}\sigma \tag{3.49}$$

or equivalently

$$\mathbf{x}(t_2) = \mathrm{e}^{\mathbf{F}\cdot(t_2-t_1)}\mathbf{x}(t_1) + \int_{t_1}^{t_2} \mathrm{e}^{\mathbf{F}\cdot(t_2-\sigma)}\mathbf{G}\cdot\mathbf{u}(\sigma)\mathrm{d}\sigma \tag{3.50}$$

By defining $\mathbf{A}(t_2, t_1) = \mathrm{e}^{\mathbf{F}\cdot(t_2-t_1)}$ and considering $t_2 = t_{\mathrm{k}+1} = (\mathrm{k}+1)\cdot\Delta\mathrm{T}$ and $t_1 = t_{\mathrm{k}} = \mathrm{k}\cdot\Delta\mathrm{T}$, Eq. (3.50) can be rewritten as

$$\mathbf{x}(t_{\mathrm{k}+1}) = \mathbf{A}(t_{\mathrm{k}+1}, t_{\mathrm{k}})\cdot\mathbf{x}(t_{\mathrm{k}}) + \int_{t_{\mathrm{k}}}^{t_{\mathrm{k}+1}} \mathbf{A}(t_{\mathrm{k}+1}, \sigma)\mathbf{G}\cdot\mathbf{u}(\sigma)\mathrm{d}\sigma \tag{3.51}$$

For a linear time-invariant system,

$$\mathbf{A}(t_{\mathrm{k}+1}, t_{\mathrm{k}}) = \mathbf{A} = \mathrm{e}^{\mathbf{F}\cdot\Delta\mathrm{T}}, \qquad \forall\mathrm{k} \tag{3.52}$$

and therefore the state equation at time $t_{k+1} = (k+1)\cdot\Delta T$ can be expressed as

$$\mathbf{x}(t_{k+1}) = \mathbf{A}\cdot\mathbf{x}(t_k) + \int_{t_k}^{t_{k+1}} \mathbf{A}(t_{k+1},\sigma)\mathbf{G}\cdot\mathbf{u}(\sigma)d\sigma \tag{3.53}$$

Depending on the assumption of inter-sample behavior of the input signal $\mathbf{u}(t)$, different equivalent discrete time models of the continuous time system can be obtained. The inter-sample behavior of the input $\mathbf{u}(t)$ can be approximated by a constant value $\mathbf{u}(t) = \mathbf{u}(k\Delta T) = \mathbf{u}(t_k)$ for $k\Delta T \le t \le (k+1)\Delta T$, yielding the following Zero Order Hold (ZOH) approximation

$$\mathbf{x}(t_{k+1}) = \mathbf{A}\cdot\mathbf{x}(t_k) + \int_{t_k}^{t_{k+1}} \mathbf{A}(t_{k+1},\sigma)\mathbf{G}d\sigma\cdot\mathbf{u}(t_k) \tag{3.54}$$

Defining $\mathbf{B} = \int_{t_k}^{t_{k+1}} \mathbf{A}(t_{k+1},\sigma)\mathbf{G}d\sigma$, the discrete-time state equation becomes

$$\mathbf{x}(t_{k+1}) = \mathbf{A}\cdot\mathbf{x}(t_k) + \mathbf{B}\cdot\mathbf{u}(t_k) \tag{3.55}$$

or $\mathbf{x}(k+1) = \mathbf{A}\mathbf{x}(k) + \mathbf{B}\mathbf{u}(k)$, yielding the discrete-time state-space model as in Eq. (3.5)

$$\begin{aligned}\mathbf{x}(k+1) &= \mathbf{A}\mathbf{x}(k) + \mathbf{B}\mathbf{u}(k)\\ \mathbf{y}(k) &= \mathbf{C}\mathbf{x}(k) + \mathbf{D}\mathbf{u}(k)\end{aligned} \tag{3.56}$$

The choice on inter-sample behavior of the input affects the derivation of the discrete input matrix **B** and feed-through matrix **D** only, and has no effect on the derivation of the discrete state matrix **A** and output matrix **C**. Therefore, the relationship between the poles of a continuous-time system (s) and their discrete-time counterparts (z) (i.e., eigenvalues of the continuous and discrete state matrices) is given by

$$z = e^{s \cdot \Delta T} \tag{3.57}$$

independently of the discretization scheme used for the input (see Eq. (3.52)).

In another class of time-discretization schemes, a discrete-time state-space model can be obtained by approximating the time differentiation operator in discrete time using finite difference methods such as the forward or backward Euler method. In this case, the relationship between poles of a continuous-time system and their discrete-time counter-parts do not follow Eq. (3.57).

APPENDIX II: MODAL CONTRIBUTIONS TO TOTAL RESPONSE FROM STATE-SPACE REALIZATION

To uncouple the state-space differential equations, we transform the identified continuous-time state-space matrices (**F**, **G**, **H**, and **E**) through a state transformation matrix $\mathbf{T}^{-1}$ to obtain a new state vector $\mathbf{z} = \mathbf{T}^{-1}\mathbf{x}$, where **T** is the matrix of eigenvectors of the identified state matrix **F**. The updated state-space formulation changes from its identified format as shown in Eq. (3.74) to

$$\begin{aligned} \dot{\mathbf{z}}(t) &= \mathbf{T}^{-1}\mathbf{F}\mathbf{T}\mathbf{z}(t) + \mathbf{T}^{-1}\mathbf{G}\mathbf{u}(t) \\ \mathbf{y}(t) &= \mathbf{H}\mathbf{T}\mathbf{z}(t) + \mathbf{E}\mathbf{u}(t) \end{aligned} \tag{3.58}$$

in which $\mathbf{T}^{-1}\mathbf{F}\mathbf{T} = \mathbf{\Lambda}$ is a diagonal matrix with eigenvalues λ_i of **F** on the diagonal so that Eq. (3.58) represents a set of uncoupled first-order differential equations in the modal coordinates/states z_i

$$\dot{z}_i(t) = \lambda_i z_i(t) + \Gamma_i u(t), \quad i = 1, 2, \ldots, n \tag{3.59}$$

where $\mathbf{\Gamma} = \mathbf{T}^{-1}\mathbf{G}$. Defining the normalized complex modal responses as $s_i = (1/\Gamma_i) \cdot z_i$, the above equations become

$$\dot{s}_i(t) = \lambda_i s_i(t) + u(t), \quad i = 1, 2, \ldots, n \tag{3.60}$$

Considering that the input u(t) is piece-wise linear in the time interval $m \cdot \Delta T \le t \le (m+1) \cdot \Delta T$ and is equal to $u(t) = c_1 + c_2 \cdot t$, solution of the above differential equation during this time period is given by

$$s_i(t) = \left(s_i(m \cdot \Delta T) + \frac{c_1}{\lambda_i} + \frac{c_2}{\lambda_i^2}\right)e^{\lambda_i t} - \frac{c_2}{\lambda_i} \cdot t - \left(\frac{c_1}{\lambda_i} + \frac{c_2}{\lambda_i^2}\right) \tag{3.61}$$

The k^{th} modal contribution of the identified state $\mathbf{x}$ is given by

$$\mathbf{x}^{(k)} = \mathbf{T}_{2k-1}z_{2k-1} + \mathbf{T}_{2k}z_{2k} \tag{3.62}$$

where $\mathbf{T}_i$ denotes the i^{th} column of eigen-matrix $\mathbf{T}$ and $\{\mathbf{T}_{2k-1}, \mathbf{T}_{2k}\}$ and $\{z_{2k-1}, z_{2k}\}$ are complex conjugate pairs so that $\mathbf{x}^{(k)}$ is real valued. Thus, the k^{th} modal contribution of the system output can be expressed as

$$\mathbf{y}^{(k)} = \mathbf{H}(\mathbf{T}_{2k-1}z_{2k-1} + \mathbf{T}_{2k}z_{2k}) \tag{3.63}$$

The corresponding transfer function (in Laplace domain) between the input $\mathbf{u}$ and the k^{th} mode contribution to the response $\mathbf{y}^{(k)}$ can be expressed as

$$\mathcal{H}^{(k)}(s) = \mathbf{H}\mathbf{T}(s\mathbf{I} - \mathbf{\Lambda})^{-1}\mathbf{I}_{2k}\mathbf{T}^{-1}\mathbf{G} \tag{3.64}$$

where $\mathbf{I}_{2k} = \begin{bmatrix} 0 & \cdots & 0 & 0 & \cdots & 0 \\ \cdots & \cdots & \cdots & \cdots & \cdots & \cdots \\ 0 & \cdots & 1 & 0 & \cdots & 0 \\ 0 & \cdots & 0 & 1 & \cdots & 0 \\ \cdots & \cdots & \cdots & \cdots & \cdots & \cdots \\ 0 & \cdots & 0 & 0 & \cdots & 0 \end{bmatrix}_{(n \times n)}$ (only the $(2k\text{-}1)^{\text{th}}$ and $2k^{\text{th}}$ diagonal terms are non-zero). It is interesting to note that the k^{th} complex mode shape of the system can be computed by inserting $s = j\omega_0$ in Eq. (3.64) where ω_0 is an arbitrary frequency, although the best choice for ω_0 is the k^{th} modal natural frequency where the amplitude of the transfer function is the largest. Figure 3.10 displays a block diagram of the modal decomposition for a linear dynamic system presented in state-space formulation as in Eq.

(3.58), where $\mathbf{\Gamma}_k$ and $\mathbf{h}_k$ refer to the k^{th} row of matrix $\mathbf{\Gamma}$ and k^{th} column of matrix $\mathbf{H} \cdot \mathbf{T}$, respectively.

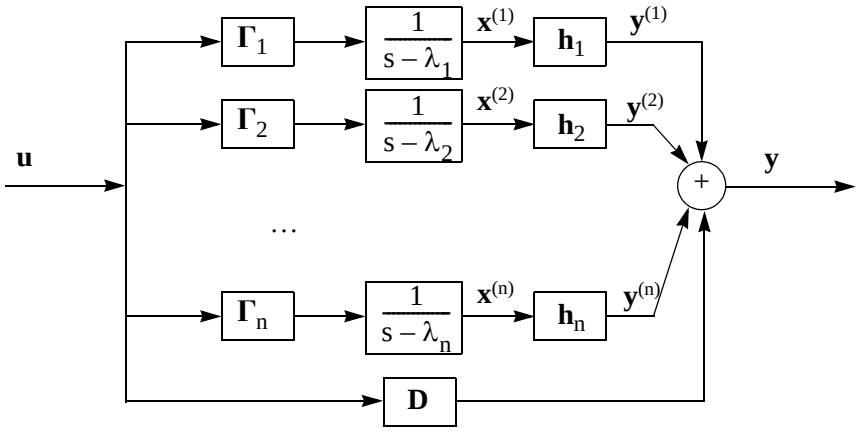

Fig. 3.10 Modal decomposition of a linear dynamic system in state-space representation

In the case that the input is an acceleration base excitation, the equation of motion is written as

$$\mathcal{M}\ddot{\mathbf{p}}(t) + \mathcal{D}\dot{\mathbf{p}}(t) + \mathcal{K}\mathbf{p}(t) = (-\mathcal{M}\mathcal{B})\ddot{p}_g(t) \tag{3.65}$$

where $\ddot{p}_g(t)$ refers to the base acceleration. With the choice of state vector $\bar{\mathbf{x}}(t) = \left[\mathbf{p}(t)^{\mathrm{T}}\ \dot{\mathbf{p}}(t)^{\mathrm{T}}\right]^{\mathrm{T}}$ and output vector $\mathbf{y}(t) = \ddot{\mathbf{p}}(t)$ (relative acceleration) the state-space matrices are given by

$$\bar{\mathbf{F}} = \begin{bmatrix} \mathbf{0} & \mathbf{I} \\ -\mathcal{M}^{-1}\mathcal{K} & -\mathcal{M}^{-1}\mathcal{D} \end{bmatrix}, \qquad \bar{\mathbf{G}} = \begin{bmatrix} \mathbf{0} \\ -\mathcal{B} \end{bmatrix}$$
$$\bar{\mathbf{H}} = \begin{bmatrix} -\mathcal{M}^{-1}\mathcal{K} & -\mathcal{M}^{-1}\mathcal{D} \end{bmatrix}, \qquad \bar{\mathbf{E}} = \begin{bmatrix} -\mathcal{B} \end{bmatrix} \tag{3.66}$$

With the choice of output vector $\mathbf{y}(t) = \ddot{\mathbf{p}}(t) + \boldsymbol{\mathcal{B}}\ddot{p}_g(t)$ (absolute or total acceleration) then the feed-through matrix $\bar{\mathbf{E}} = \mathbf{0}$, therefore the modal compositions of the response ($\mathbf{y}^{(k)}$) sum up exactly to the total absolute acceleration (see Figure 3.10). Thus, in the case of acceleration base excitation, the modal compositions of the output accelerations, computed as explained above, are the absolute acceleration decompositions rather than relative acceleration decompositions. It should be noted that the relative acceleration decompositions can also be computed by differentiating Eq. (3.61) as

$$\dot{s}_i(t) = \left(s_i(m \cdot \Delta T) + \frac{c_1}{\lambda_i} + \frac{c_2}{\lambda_i^2} \right) e^{\lambda_i t} \cdot \lambda_i - \frac{c_2}{\lambda_i} \tag{3.67}$$

and then the relative acceleration decompositions is given by

$$\mathbf{y}_{\text{relative}}^{(k)} = \begin{bmatrix} \mathbf{0} & \mathbf{I} \end{bmatrix} (\mathbf{T}_{2k-1} \Gamma_{2k-1} \dot{s}_{2k-1} + \mathbf{T}_{2k} \Gamma_{2k} \dot{s}_{2k}) \tag{3.68}$$

APPENDIX III: EXTRACTING MODE SHAPES FROM STATE-SPACE REALIZATION

Consider a *P*-degrees-of-freedom second-order linear dynamic system represented by Eq. (3.1) recalled below:

$$\begin{aligned} \boldsymbol{\mathcal{M}}\ddot{\mathbf{p}}(t) + \boldsymbol{\mathcal{D}}\dot{\mathbf{p}}(t) + \boldsymbol{\mathcal{K}}\mathbf{p}(t) &= \boldsymbol{\mathcal{B}}\mathbf{u}(t) \\ \mathbf{y}(t) &= \boldsymbol{\mathcal{C}}\left[\mathbf{p}(t)^{\mathrm{T}}\ \dot{\mathbf{p}}(t)^{\mathrm{T}}\ \ddot{\mathbf{p}}(t)^{\mathrm{T}}\right]^{\mathrm{T}} \end{aligned} \tag{3.69}$$

where $\mathbf{p}(0) = \mathbf{p}_0$ and $\dot{\mathbf{p}}(0) = \dot{\mathbf{p}}_0$ are the initial nodal displacement and nodal velocity response vectors, respectively; $\boldsymbol{\mathcal{M}}$, $\boldsymbol{\mathcal{D}}$, $\boldsymbol{\mathcal{K}}$ = mass, damping, and stiffness matrices, respectively; $\boldsymbol{\mathcal{B}}$ = input matrix; $\boldsymbol{\mathcal{C}}$ = output matrix as already defined in Section 2.1. The second-order matrix differential equation can be converted to the state-space formulation given in Eq. (3.2) recalled below:

$$\begin{aligned} \dot{\bar{\mathbf{x}}}(t) &= \bar{\mathbf{F}}\bar{\mathbf{x}}(t) + \bar{\mathbf{G}}\mathbf{u}(t) \\ \mathbf{y}(t) &= \bar{\mathbf{H}}\bar{\mathbf{x}}(t) + \bar{\mathbf{E}}\mathbf{u}(t) \end{aligned} \tag{3.70}$$

where $\bar{\mathbf{x}}(t) = \left[\mathbf{p}(t)^{\mathrm{T}}\ \dot{\mathbf{p}}(t)^{\mathrm{T}}\right]^{\mathrm{T}}$. Note that by choosing $\boldsymbol{\mathcal{C}} = [\mathbf{0}\ \mathbf{0}\ \mathbf{I}]$ in Eq. (3.69), the output (measured/observed response) vector $\mathbf{y}(t) = \ddot{\mathbf{p}}(t)$. With this choice of state vector $\mathbf{x}(t)$ and output vector $\mathbf{y}(t)$, the state-space matrices in the state-space realization are given by Eq. (3.3) recalled below for convenience:

$$\begin{aligned} \bar{\mathbf{F}} &= \begin{bmatrix} \mathbf{0} & \mathbf{I} \\ -\boldsymbol{\mathcal{M}}^{-1}\boldsymbol{\mathcal{K}} & -\boldsymbol{\mathcal{M}}^{-1}\boldsymbol{\mathcal{D}} \end{bmatrix}, \qquad \bar{\mathbf{G}} = \begin{bmatrix} \mathbf{0} \\ -\boldsymbol{\mathcal{M}}^{-1}\boldsymbol{\mathcal{B}} \end{bmatrix} \\ \bar{\mathbf{H}} &= \begin{bmatrix} -\boldsymbol{\mathcal{M}}^{-1}\boldsymbol{\mathcal{K}} & -\boldsymbol{\mathcal{M}}^{-1}\boldsymbol{\mathcal{D}} \end{bmatrix}, \qquad \bar{\mathbf{E}} = \begin{bmatrix} -\boldsymbol{\mathcal{M}}^{-1}\boldsymbol{\mathcal{B}} \end{bmatrix} \end{aligned} \tag{3.71}$$

Notice that we can omit the term $(+\bar{\mathbf{E}}\mathbf{u}(t))$ in the output equation simply because it is invariant under state transformation and does not get involved in the algorithm discussed in this study. Performing an eigenvalue decomposition of matrix $\bar{\mathbf{F}}$,

$$\bar{\mathbf{F}}\bar{\mathbf{T}} = \bar{\mathbf{T}}\bar{\mathbf{\Lambda}} \tag{3.72}$$

where $\bar{\mathbf{\Lambda}}$ is a diagonal matrix containing the eigenvalues of $\bar{\mathbf{F}}$, and $\bar{\mathbf{T}}$ is the matrix of eigenvectors, $\bar{\mathbf{T}} = \begin{bmatrix} \mathbf{\Psi}^{\mathrm{d}} \\ \mathbf{\Psi}^{\mathrm{d}}\bar{\mathbf{\Lambda}} \end{bmatrix}$, and $\mathbf{\Psi}^{\mathrm{d}}$ is the complex-valued displacement mode shape matrix of the system. In the case of acceleration outputs, $\mathbf{y}(t) = \ddot{\mathbf{p}}(t)$, $\bar{\mathbf{H}} = \begin{bmatrix} -\mathcal{M}^{-1}\mathcal{K} & -\mathcal{M}^{-1}\mathcal{D} \end{bmatrix} = \begin{bmatrix} \mathbf{0} & \mathbf{I} \end{bmatrix}\bar{\mathbf{F}}$ and then

$$\bar{\mathbf{H}}\bar{\mathbf{T}} = \begin{bmatrix} \mathbf{0} & \mathbf{I} \end{bmatrix}\bar{\mathbf{F}}\bar{\mathbf{T}} = \begin{bmatrix} \mathbf{0} & \mathbf{I} \end{bmatrix}\bar{\mathbf{T}}\bar{\mathbf{\Lambda}} = \mathbf{\Psi}^{\mathrm{d}}\bar{\mathbf{\Lambda}}^{2} \tag{3.73}$$

which is the complex-valued acceleration mode shape matrix. In the case of displacement outputs, $\mathbf{y}(t) = \mathbf{p}(t)$, $\bar{\mathbf{H}} = \begin{bmatrix} \mathbf{I} & \mathbf{0} \end{bmatrix}$ and $\bar{\mathbf{H}}\bar{\mathbf{T}} = \begin{bmatrix} \mathbf{I} & \mathbf{0} \end{bmatrix}\bar{\mathbf{T}} = \mathbf{\Psi}^{\mathrm{d}}$ is the complex-valued displacement mode shape matrix, while for the case of velocity outputs, $\mathbf{y}(t) = \dot{\mathbf{p}}(t)$, $\bar{\mathbf{H}} = \begin{bmatrix} \mathbf{0} & \mathbf{I} \end{bmatrix}$ and $\bar{\mathbf{H}}\bar{\mathbf{T}} = \begin{bmatrix} \mathbf{0} & \mathbf{I} \end{bmatrix}\bar{\mathbf{T}} = \mathbf{\Psi}^{\mathrm{d}}\bar{\mathbf{\Lambda}}$ is the complex-valued velocity mode shape matrix. Now to show that the matrix $\bar{\mathbf{H}}\bar{\mathbf{T}}$ is invariant under any transformation of state, consider a state transformation $\mathbf{x} = \mathbf{R}\bar{\mathbf{x}}$, with $\mathbf{R}$ a positive definite transformation matrix. With this choice of $\bar{\mathbf{x}} = \mathbf{R}^{-1}\mathbf{x}$, the state-space formulation in the transformed state is given by

$$\begin{aligned} \dot{\mathbf{x}}(t) &= \mathbf{F}\mathbf{x}(t) + \mathbf{G}\mathbf{u}(t) \\ \mathbf{y}(t) &= \mathbf{H}\mathbf{x}(t) + \mathbf{E}\mathbf{u}(t) \end{aligned} \tag{3.74}$$

in which $\mathbf{F} = \mathbf{R}\bar{\mathbf{F}}\mathbf{R}^{-1}$, $\mathbf{G} = \mathbf{R}\bar{\mathbf{G}}$, $\mathbf{H} = \bar{\mathbf{H}}\mathbf{R}^{-1}$ and $\mathbf{E} = \bar{\mathbf{E}}$ are the transformed state-space matrices (generally the identified state-space are in this form). An eigenvalue decomposition of $\mathbf{F}$ gives

$$\mathbf{FT} = \mathbf{T}\boldsymbol{\Lambda} \tag{3.75}$$

where $\boldsymbol{\Lambda}$ is a diagonal matrix containing the eigenvalues of $\mathbf{F}$ and $\mathbf{T}$ is the matrix of eigenvectors. From linear algebra, it follows that $\boldsymbol{\Lambda} = \bar{\boldsymbol{\Lambda}}$ and $\mathbf{T} = \mathbf{R}\bar{\mathbf{T}}$, so that

$$\mathbf{HT} = (\bar{\mathbf{H}}\mathbf{R}^{-1})(\mathbf{R}\bar{\mathbf{T}}) = \bar{\mathbf{H}}\bar{\mathbf{T}} = \boldsymbol{\Psi} \tag{3.76}$$

thus showing that $\mathbf{HT}$ is invariant under any state transformation $\mathbf{R}$ and always equal to (displacement, velocity, or acceleration) mode shape matrix $\boldsymbol{\Psi}$. This proof is also valid for the discrete time state-space representation of a dynamic system due to the fact that matrices $\mathbf{H}$ and $\mathbf{T}$ remain the same under any discretization method.

CHAPTER 4

SYSTEM IDENTIFICATION OF SEVEN-STORY REINFORCED CONCRETE BUILDING SLICE TESTED ON THE UCSD-NEES SHAKE TABLE

4.1 INTRODUCTION

In recent years, structural health monitoring has received increased attention from the civil engineering research community as a potential tool to develop methods through which structural damage can be identified at the earliest possible stage and the remaining useful life of structures evaluated (damage prognosis). Civil structures may be damaged due to natural and man-made hazards such as earthquakes, hurricanes, and explosions. Also under service load conditions, they undergo progressive damage in the form of aging and deterioration due to environmental conditions. Damage identification consists of detecting the occurrence of damage, localizing the damage area(s), and estimating the extent of damage. Standard damage identification procedures involve conducting repeated vibration surveys on the structure during its lifetime. Experimental modal analysis (EMA) has been explored as a technology for identifying dynamic characteristics as well as condition assessment and damage identification of structures. Extensive literature reviews were provided by Doebling et al. (1996 and 1998) and Sohn et al. (2003) on damage iden-

tification, based on changes in modal characteristics. It should be indicated that the success of damage identification based on EMA depends strongly on the accuracy and completeness of the identified structural dynamic properties.

The UCSD-NEES shake table is located at the Englekirk Structural Engineering Center, 15km east of the main campus of the University of California at San Diego (UCSD). This unique facility, commissioned in October 2004, allows to perform landmark seismic experiments on large- or full-scale structural and soil-foundation-structure interaction systems. A full-scale seven-story reinforced concrete shear wall building slice was tested on the UCSD-NEES shake table in the period October 2005 - January 2006. The objective of this test program was to verify the seismic performance of a mis-rise reinforced concrete shear wall building designed for lateral forces obtained from a displacement-based design methodology, which are significantly smaller than those dictated by current force-based seismic design provisions in United States. The shake table tests were designed so as to damage the building progressively through several historical seismic motions reproduced on the shake table. At various levels of damage, several low amplitude white noise base excitations were applied through the shake table to the building which responded as a quasi-linear system with dynamic parameters depending on the level of structural damage. In addition to white noise base excitation tests, ambient vibration tests were also performed on the building specimen at different damage levels. Six different state-of-the-art system identification methods, consisting of three input-output and three output-only methods, were applied to dynamic response measurements obtained using accelerometers and linear variable displacement transducers (LVDTs) in order to

estimate modal parameters (natural frequencies, damping ratios and mode shapes) of the building in its undamaged (baseline) and various damage states. The system identification methods used include: (1) Multiple-reference Natural Excitation Technique in conjunction with Eigensystem Realization Algorithm (MNExT-ERA); (2) Data-driven Stochastic Subspace Identification (SSI-DATA); (3) Enhanced Frequency Domain Decomposition (EFDD); (4) Deterministic-Stochastic Subspace Identification (DSI); (5) Observer/Kalman filter Identification combined with ERA (OKID-ERA); and (6) General Realization Algorithm (GRA). The first three algorithms are based on output-only data (from white noise and ambient vibration tests) while the latter three are based on input-output measured data (from white noise tests). Finally, the identified modal parameters of the structure in its undamaged state were compared to their counterparts computed from a three-dimensional finite element model of the building developed in structural analysis software SAP2000 (Computers and Structures, Inc. 2004).

4.2 TEST SPECIMEN, TEST SETUP AND DYNAMIC EXPERIMENTS

4.2.1 Seven-Story Reinforced Concrete Shear Wall Building Slice

The test structure which represents a slice of a full-scale reinforced concrete shear wall building consists of a main shear wall (web wall), a back wall perpendicular to the main wall (flange wall) for transversal stability, a concrete slab at each floor level, an auxiliary post-tensioned column to provide torsional stability, and four gravity columns to transfer the weight of the slabs to the shake table. Pin-pin slotted slab connections capable

of transferring in-plane diaphragm forces are placed between the web and flange walls at floor levels in order to minimize the moment transfer and coupling between the two walls. Figures 4.1 and 4.2 show the test structure mounted on the shake table and an elevation view with its general dimensions, respectively. Figure 4.3 displays a plan view of the structure with walls and slab dimensions at different levels. More details about the test structure can be found in Panagiotou et al. (2007).

Fig. 4.1 Test structure

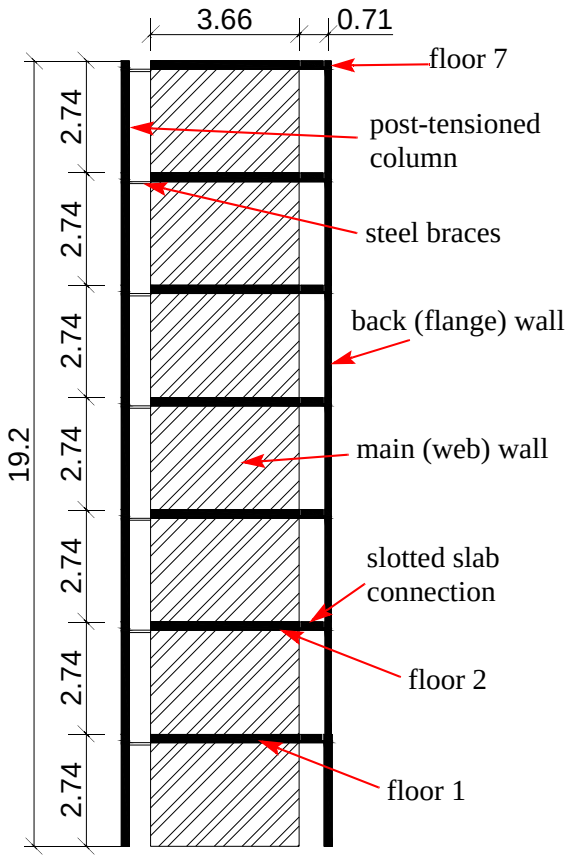

Fig. 4.2 Elevation of test structure (units: m)

4.2.2 Instrumentation Layout

The test structure was instrumented with an extensive array of accelerometers, strain gages, potentiometers, and Linear Variable Displacement Transducers (LVDTs), all sampling data simultaneously using a nine-node distributed data acquisition system. The accelerometer array consisted of 14 uni-axial accelerometers on the foundation/pedestal of the test structure, 106 uni-axial accelerometers on the floor slabs and the web wall, 8 uni-axial accelerometers on the platen of the shake table, 9 uni-axial accelerometers on the reaction block of the shake table and 1 tri-axial accelerometer on the surrounding ground (free field), resulting in a total of 140 channels of acceleration measurements. The 54 LVDTs were installed along both edges (east and west) of the web wall, while the 8 potentiometers were installed diagonally along only the first two stories of the web wall. A total of 231 strain gages were deployed on the test specimen consisting of 143 on the longitudinal and horizontal steel reinforcement of the web wall, 64 on the longitudinal and horizontal steel reinforcement of the flange wall, 16 on the gravity columns and 8 on the steel braces connecting the slabs to the post-tensioned column. In addition, the displacement response of selected points on the structure were measured in three dimensions using 6 global positioning system (GPS) sensors, 3 of them on the top floor slab, 2 on the flange wall and 1 on the platen of the shake table. Table 4.1 provides a summary of the heterogeneous sensor array installed on the test structure. The technical characteristics of the accelerometers are: MEMS-Piezoresistive MSI model 3140, amplitude range: +/-5g, frequency range (min): 0-300Hz, voltage sensitivity: 400mV/g. The technical characteristics of the LDVTs are: Penny & Giles model MLS130, resolution: virtually infinite, repeatability: <

0.01m, electrical stroke: 50/100mm depending on sensor location. The data acquisition system used had 16 bits of resolution.

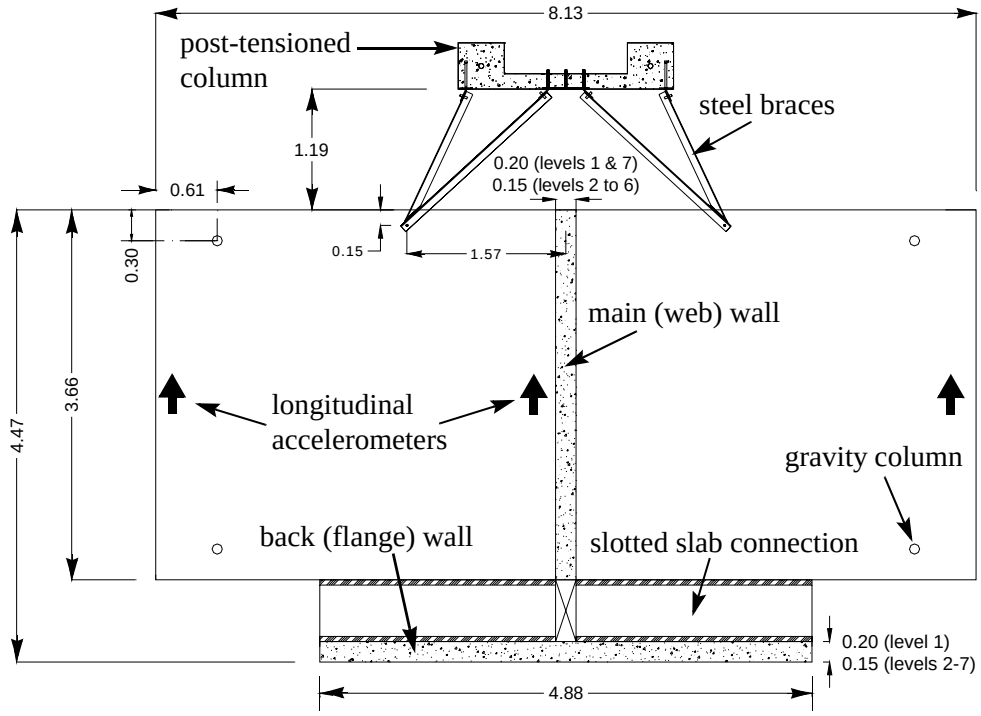

Fig. 4.3 Plan view of test structure (units: m)

In this study, measured response data from 28 longitudinal accelerometers (three on each floor slab as shown in Figure 4.3 and one on the web wall at mid-height of each story) as well as 28 LVDTs (six 0.41m-long LVDTs along each edge of the web wall for the first and second stories and two 1.27m-long LVDTs along each edge of the web wall for the third story) were used to identify the modal parameters of the test structure. Figure 4.4 shows six filtered (0.5-25Hz) absolute acceleration time histories recorded on the web wall at floor levels 1, 4 and 7 during white noise base excitation (left column) and ambient vibration (right column) tests performed on the test structure in its undamaged state. The corresponding Fourier Amplitude Spectra (FAS) are given in Figure 4.5. From Figure 4.5,

it is observed that: (1) the FAS plot is very jagged/noisy which can be due to some rattling behavior caused by loose connections, especially at both ends of the steel braces connecting the slabs to the post-tensioned column; (2) the first longitudinal vibration mode has a predominant contribution to the total response, especially at the higher floors, which renders the identification of higher (than the first longitudinal) vibration modes more difficult; and (3) the FAS of the acceleration response histories at the first floor have a drop in their amplitude around 11.5 Hz which is due to the application of a notch filter in the control loop of the shake table to reduce the effects of the oil column resonance. Figure 4.6 shows six strain time histories recorded by LVDTs attached to the web wall at the bottom of the first, second and third stories during white noise base excitation (left column) and ambient vibration (right column) tests with the structure in its undamaged state. Lack of symmetry in the time histories during white noise base excitation can be due to the fact that concrete cracks will open when a concrete section is in the tension therefore yielding larger LVDT measurements during tension than compression. The corresponding strain FAS are given in Figure 4.7. From Figures 4.6 and 4.7, it is observed that: (1) amplitude of strain data measured during ambient vibration tests is smaller than the resolution of LVDTs, therefore ambient vibration strain data are not used in this system identification study. (2) The contribution of higher (> 6Hz) vibration modes to the total strain measurements during white noise base excitation tests is very small, therefore these modes may only be identified with a very high level of uncertainty.

Table 4.1 Summary of instrumentation deployed on the test structure

Sensor Type	Location	Quantity
Accelerometer (138)	Foundation/pedestal	14
	Slabs and walls	106
	Shake table platen	8
	Reaction block	9
	Free field	1 (tri-axial)
LVDT (54)	Web wall (levels 1-2)	34
	Web wall (levels 3-7)	20
Potentiometer (8)	Web wall (levels 1-2)	8
GPS (6)	Top floor	3
	Flange wall	2
	Platen	1
Strain Gage (231)	Web wall	143
	Flange wall	64
	Gravity columns	16
	Braces connecting slabs to post-tensioned column	8

4.2.3 Dynamic Tests Performed

A sequence of dynamic tests (68 tests in total) was applied to the test structure during the period October 2005 - January 2006 including ambient vibration, free vibration, and forced vibration tests (white noise and seismic base excitations) using the UCSD-NEES shake table. The shear wall structure was damaged progressively through a sequence of four historical ground motion records used as table input motions and the modal parameters of the test structure were identified at various damage states using six different system identification methods based on different dynamic test data.

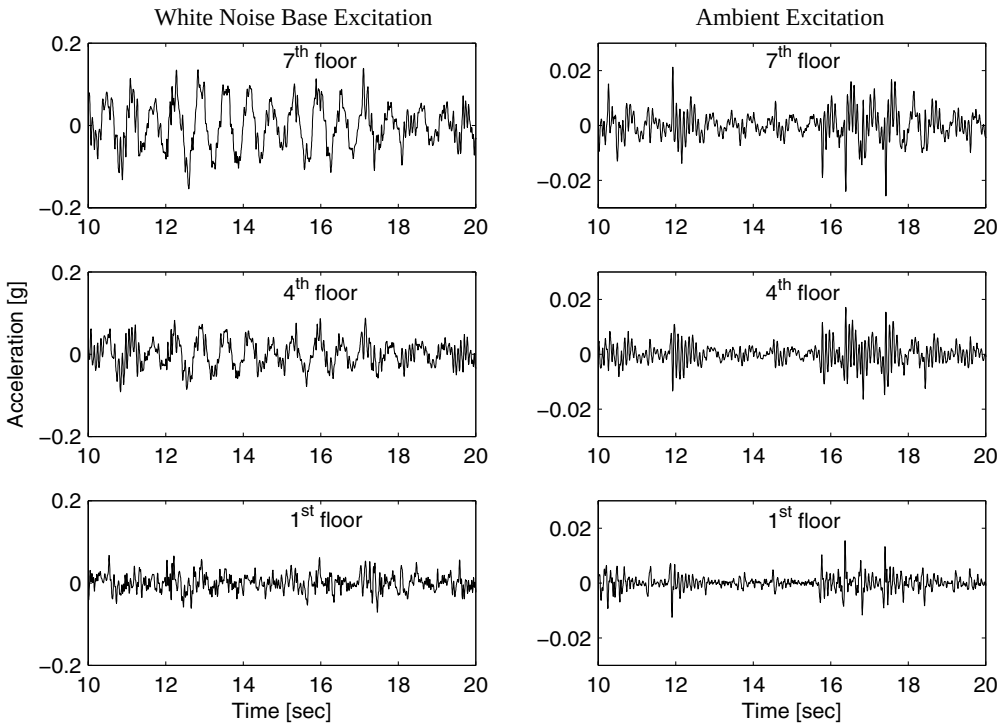

Fig. 4.4 Absolute acceleration time histories at floors 1, 4, and 7 due to white noise base excitation (left) and ambient excitation (right)

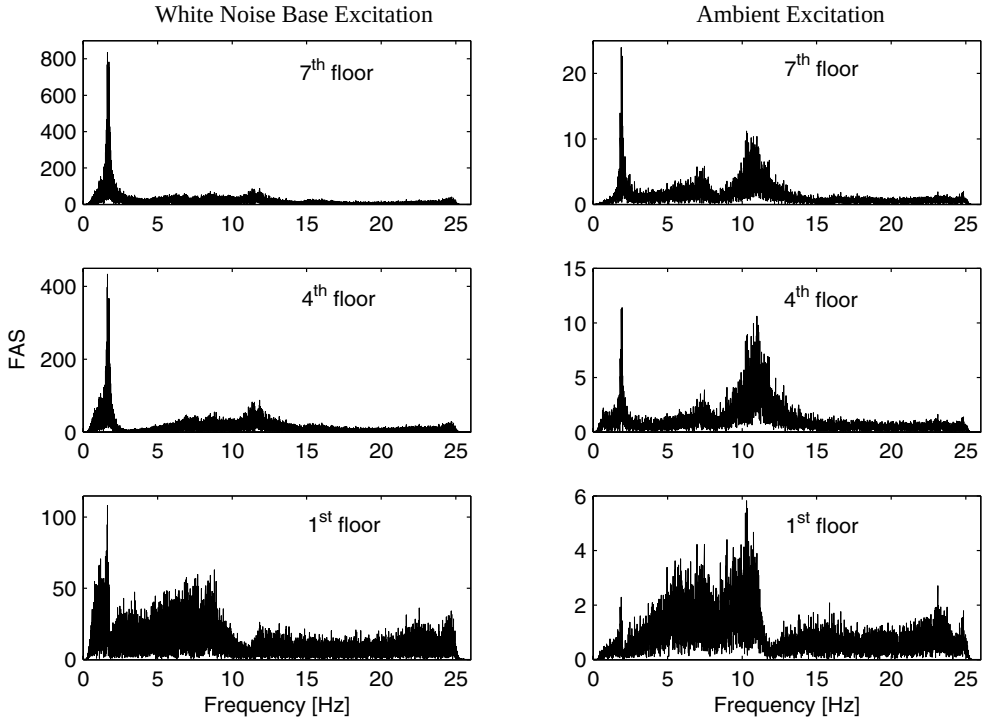

Fig. 4.5 Fourier Amplitude Spectra of acceleration data at floors 1, 4, and 7 due to white noise base excitation (left) and ambient excitation (right)

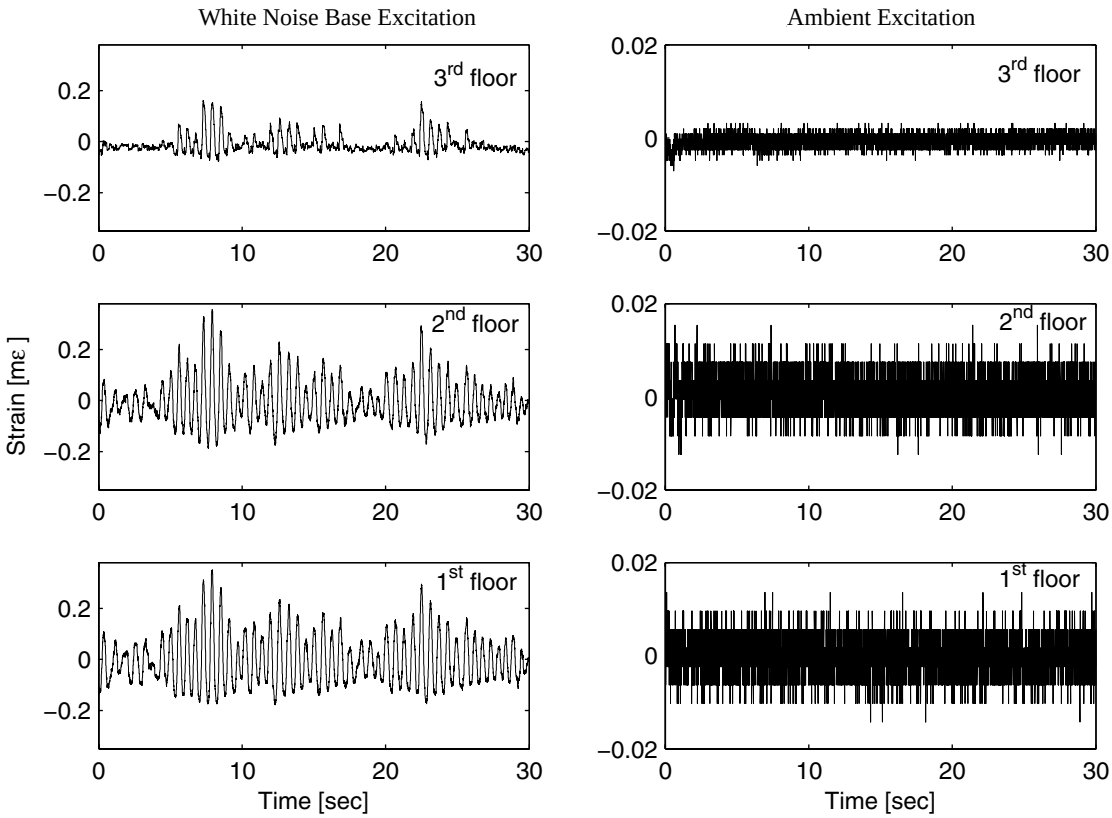

Fig. 4.6 Strain time histories from LVDTs on the web wall at bottom of first, second and third stories due to white noise base excitation (left) and ambient excitation (right)

The four historical earthquake records applied to the test structure consist of (http:// peer.berkeley.edu/smcat): (1) longitudinal component of the 1971 San Fernando earthquake (M = 6.6) recorded at the Van Nuys station (EQ1), (2) transversal component of the 1971 San Fernando earthquake recorded at the Van Nuys station (EQ2), (3) longitudinal component of the 1994 Northridge earthquake (M = 6.7) recorded at the Oxnard Boulevard station in Woodland Hill (EQ3), and (4) 360 degree component of the 1994 Northridge earthquake recorded at the Sylmar station (EQ4). The ground acceleration time histories of these four earthquake records are shown in Figure 4.8. The input white noise base excitation consisted of a realization of a banded white noise (0.25-25Hz) process with a root-mean-square (RMS) amplitude of 0.03g as shown in Figure 4.9. Table 4.2

describes the dynamic tests used in this study on system identification of the shear wall building at various damage states. Figure 4.10 shows the pseudo-acceleration elastic response spectra (Spa) of the four earthquake records and the input white noise base excitation (0.03g RMS) for 5% damping ratio and a natural period of vibration between 0.001 and 5 seconds. The dominant vibration mode of the shear wall structure during these dynamic tests is the first longitudinal mode with a natural period in the range between 0.5 and 1.0 second depending on the level of structural damage. From Figure 4.10, in can be observed that in the natural period range 0.5-1.0 seconds: (1) the Spa of each earthquake record is of higher amplitude than that of the previous earthquake record, except for EQ2 and EQ3 which are of similar magnitude, and (2) the Spa of the input white noise base excitation (0.03g RMS) is almost half the Spa of EQ1.

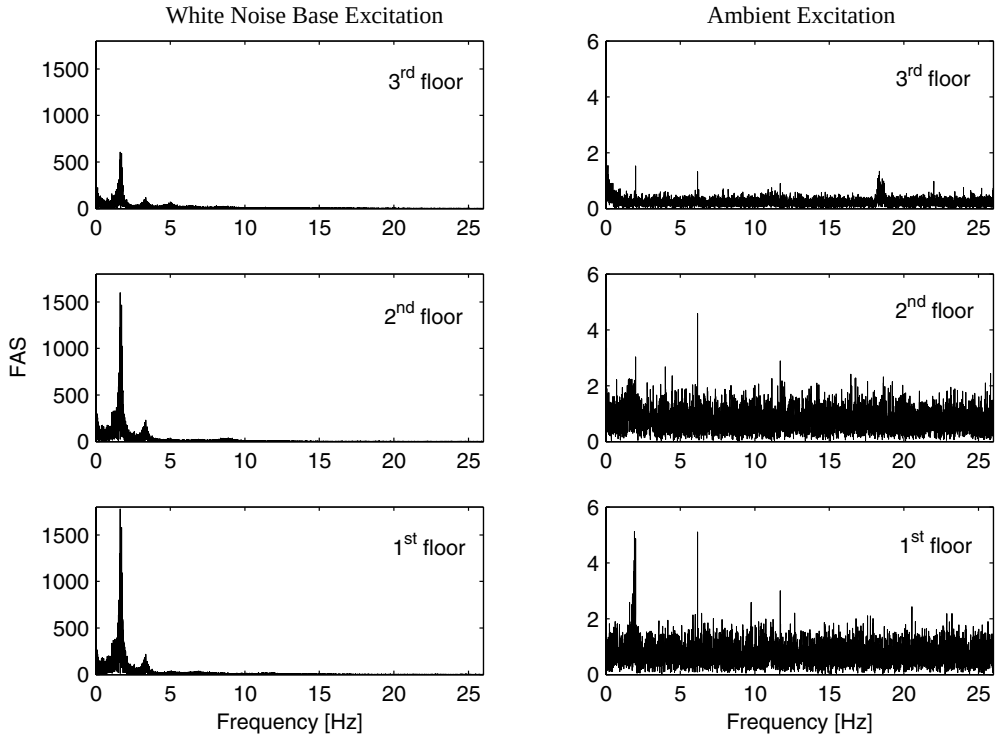

Fig. 4.7 Fourier Amplitude Spectra of LVDT strain data at bottom of first, second and third stories of the web wall due to white noise base excitation (left) and ambient excitation (right)

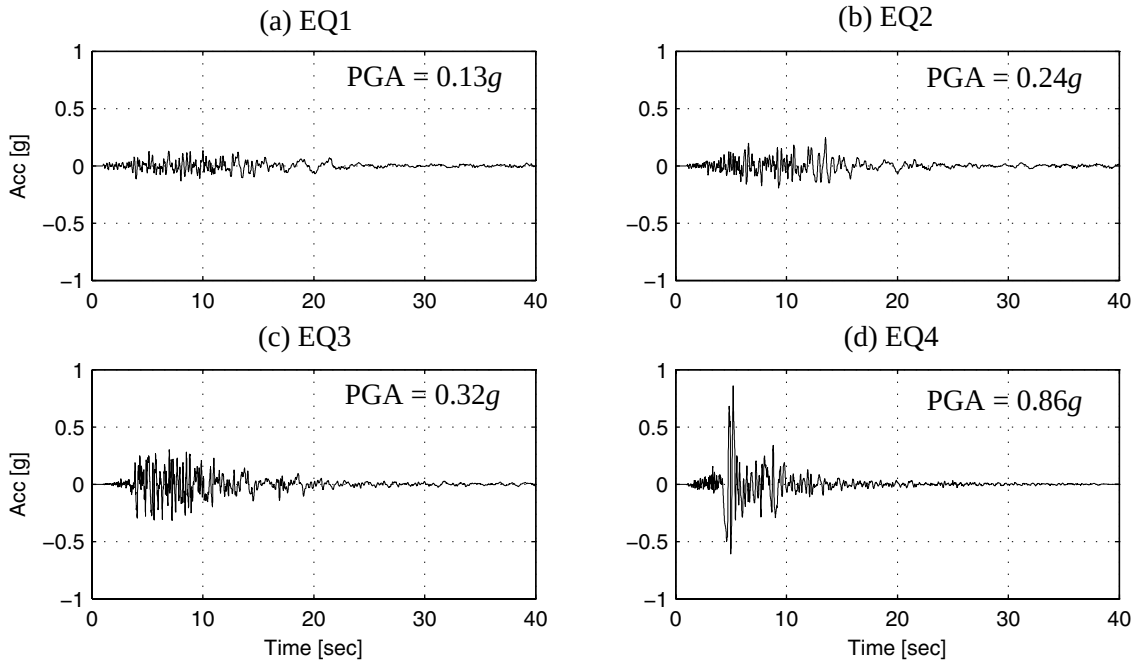

Fig. 4.8 Earthquake ground acceleration time histories applied to the test structure: (a) Long. and (b) transv. comp. of 1971 San Fernando earthquake recorded at the Van Nuys station, (c) long. comp. of 1994 Northridge earthquake recorded at the Oxnard Blvd. station, (d) 360 deg. comp. of 1994 Northridge earthquake recorded at the Sylmar station

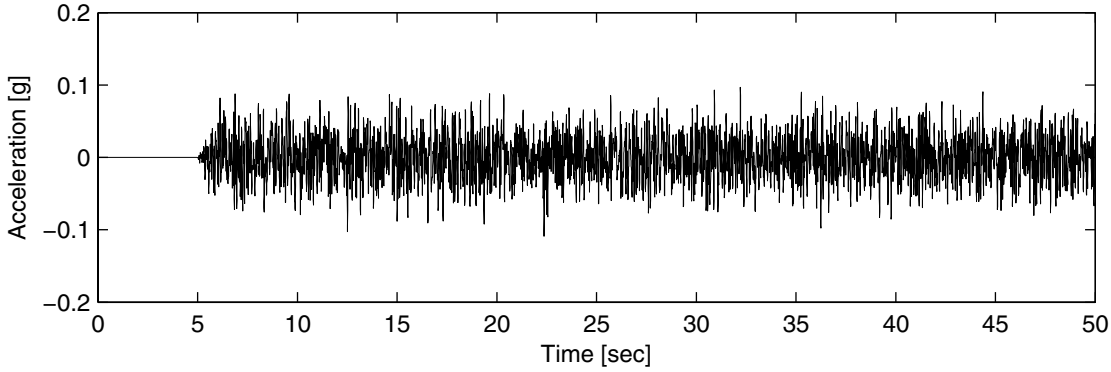

Fig. 4.9 The first 50 seconds of the banded white noise base acceleration time history applied to the test structure

Table 4.2 Dynamic tests used in this study
(WN: white noise base excitation test and AV: ambient vibration test)

Test No.	Date	Test Description	Damage State
37	11/18/05	8min WN (0.03*g*)	S0
39	11/21/05	8min WN (0.03*g*) + 3min AV	S0
40	“	EQ1	
41	“	8min WN (0.03*g*) + 3min AV	S1
43	“	EQ2	
45	11/22/05	2min WN (0.03*g*)	S2
46	“	8min WN (0.03*g*) + 3min AV	S2
48	“	EQ3	
49	“	8min WN (0.03*g*) + 3min AV	S3.1
56	12/5/05	8min WN (0.03*g*)	S3.1
61	1/14/06	8min WN (0.03*g*) + 3min AV	S3.2
62	“	EQ4	
64	1/14/06	8min WN (0.03*g*) + 3min AV	S4
67	“	8min WN (0.03*g*)	S4

4.3 REVIEW OF SYSTEM IDENTIFICATION METHODS USED

Six different state-of-the-art system identification methods were applied to estimate the modal parameters of the test structure at various damage states. These methods consist of: (1) Multiple-reference Natural Excitation Technique combined with the Eigensystem Realization Algorithm (MNExT-ERA), (2) Data-driven Stochastic Subspace Identification (SSI-DATA), (3) Enhanced Frequency Domain Decomposition (EFDD), (4) Deterministic-stochastic Subspace Identification (DSI), (5) Observer/Kalman filter Identification combined with ERA (OKID-ERA), and (6) General Realization Algorithm

(GRA). These six methods are briefly reviewed in this section. The measured acceleration and strain responses were sampled at a rate of 240Hz resulting in a Nyquist frequency of 120Hz, which is much higher than the modal frequencies of interest in this study (< 25Hz). Before applying the above mentioned system identification methods to the measured data, all the absolute acceleration and LVDT strain time histories were band-pass filtered between 0.5Hz and 25Hz using a high order (1024) FIR filter. The absolute horizontal acceleration measurements from white noise base excitation tests were also converted to relative accelerations by subtracting the base/table horizontal acceleration.

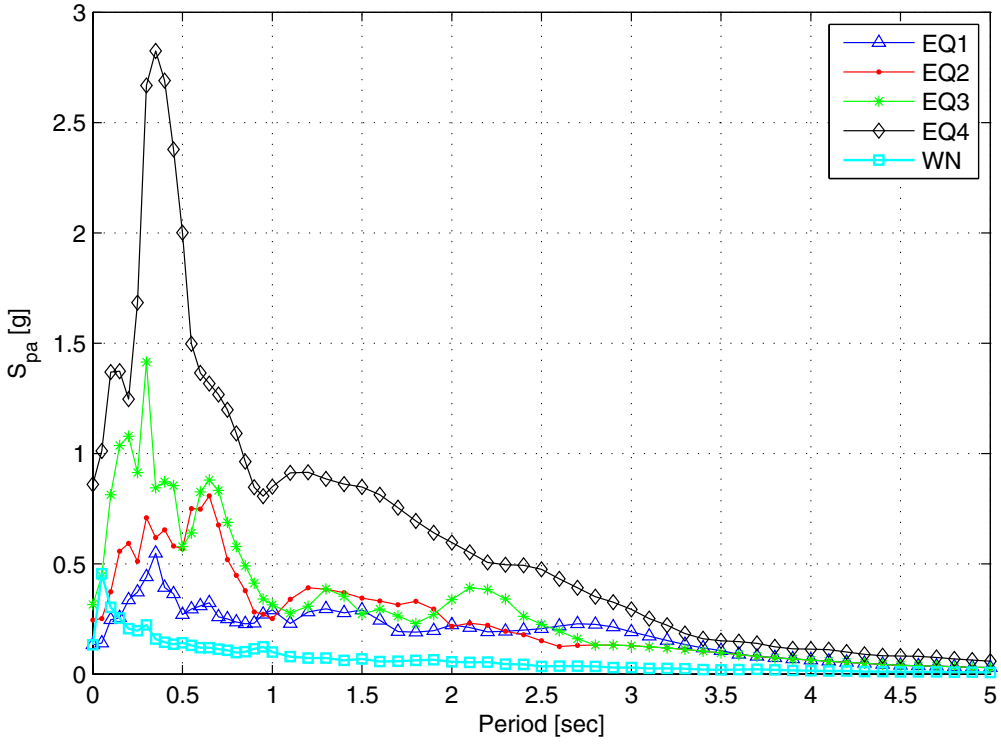

Fig. 4.10 Pseudo-acceleration response spectra (with 5% damping ratio) of the four seismic records and the white noise base excitation (0.03g RMS)

4.3.1 Output-Only System Identification Methods

The first three algorithms are based on output-only data and are applied to the measured vibration data from both ambient vibration and white noise base excitation tests.

4.3.1.1 Multiple-reference Natural Excitation Technique Combined with Eigensystem Realization Algorithm (MNExT-ERA)

The basic principle behind the NExT is that the theoretical cross-correlation function between two response measurements made along two degrees of freedom (DOF) collected from an ambient (broad-band) excited structure has the same analytical form as the free vibration response of the structure (James et al. 1993). Once an estimation of the response cross-correlation vector is obtained for a given reference channel, the ERA method (Juang and Pappa 1985) can be used to extract the modal parameters. A key issue in the application of NExT is to select the reference channel so as to avoid missing modes in the identification process due to the proximity of the reference channel to a modal node. In the MNExT, instead of using a single reference response channel as in the NExT, a vector of reference channels (three reference channels in this study) is used to obtain an output cross-correlation matrix. The response cross-correlation functions were estimated through inverse Fourier transformation of the corresponding cross-spectral density (CSD) functions. CSD function estimation was based on Welch-Bartlett's method using Hanning windows of length 116sec (27,840 samples) for white noise base excitation and 15sec (3,600 samples) for ambient vibration, with 50 percent of window overlap. The estimated cross-correlation functions were then down-sampled to 80Hz for acceleration measure-

ments and 40Hz for LVDT strain measurements in order to improve the computational efficiency and finally they were used to form Hankel matrices of size $(28 \times 150) \times 150$ (28 output channels, 150 block rows and 150 columns) for applying ERA in the second stage of the modal identification. After down-sampling, the Nyquist frequency (40Hz or 20 Hz) remains higher than the natural frequencies of vibration modes of interest which are significantly excited (25Hz for accelerometer and 6Hz for LVDT measurements, see Figures 4.5 and 4.7). The identified natural frequencies and damping ratios of the five most significant vibration modes (longitudinal, torsional and coupled longitudinal-torsional) are reported in Table 4.3 based on the ambient vibration data and in Tables 4.4 and 4.5 based on the white noise base excitation response (output) data.

4.3.1.2 Data-Driven Stochastic Subspace Identification (SSI-DATA)

The SSI-DATA method determines the system model in state-space based on the output-only measurements directly (Van Overschee and De Moor 1996). One advantage of this method compared to two-stage time-domain system identification methods such as covariance-driven stochastic subspace identification and NExT-ERA is that it does not require any pre-processing of the data to calculate correlation functions or spectra of output measurements for example. In addition, robust numerical techniques such as QR factorization, singular value decomposition (SVD) and least squares are involved in this method.

Table 4.3 Natural frequencies and damping ratios identified based on acceleration data from ambient vibration tests

State / Test No.	System ID Method	Natural Frequency [Hz]					Damping Ratio [%]				
		1st-L mode	1st-T mode	1st-L-T mode	2nd-L mode	3rd-L mode	1st-L mode	1st-T mode	1st-L-T mode	2nd-L mode	3rd-L mode
S0 / Test 39	MNExT-ERA	1.92	-	7.05	10.49	24.79	3.0	-	5.0	2.5	0.9
	SSI	1.89	-	7.07	10.53	24.58	1.9	-	4.1	2.4	0.4
	EFDD	1.90	-	7.22	10.93	24.76	1.3	-	0.2	0.2	0.2
S1 / Test 41	MNExT-ERA	1.86	-	6.62	10.27	22.98	1.2	-	3.5	3.4	2.4
	SSI	1.86	-	6.81	10.24	24.30	2.0	-	2.9	2.6	0.6
	EFDD	1.88	-	6.62	10.33	23.45	0.5	-	0.3	0.6	0.0
S2 / Test 46	MNExT-ERA	1.67	2.04	7.58	10.34	22.78	2.1	1.0	3.4	1.6	1.4
	SSI	1.67	2.05	7.58	10.16	22.60	1.3	0.9	3.0	1.4	0.9
	EFDD	1.66	2.07	7.54	10.14	22.80	2.5	1.4	0.2	0.2	0.2
S3.1 / Test 49	MNExT-ERA	1.46	-	7.21	10.06	21.89	3.4	-	2.7	1.4	1.7
	SSI	1.46	1.91	7.18	9.28	21.60	2.9	1.4	2.1	1.1	1.6
	EFDD	1.44	-	7.03	9.28	21.81	0.8	-	0.1	0.2	0.1
S3.2 / Test 61	MNExT-ERA	1.58	1.95	-	8.39	22.97	1.5	0.5	-	2.3	1.2
	SSI	1.58	1.95	-	8.52	22.83	1.4	1.1	-	2.8	1.0
	EFDD	1.58	1.95	-	8.44	22.87	2.0	1.1	-	0.3	0.1
S4 / Test 64	MNExT-ERA	1.02	-	-	5.68	15.04	1.2	-	-	2.4	0.8
	SSI	1.02	-	-	5.69	15.05	1.0	-	-	1.8	1.3
	EFDD	1.00	-	-	5.74	15.10	1.7	-	-	0.2	0.1

In the implementation of SSI-DATA, the filtered acceleration data were down-sampled to 80Hz (40Hz for LVDT strain measurements) in order to increase the computational efficiency. For each dynamic test, an output Hankel matrix was formed including 35 block rows with 28 rows in each block (28 longitudinal acceleration channels) for both white

noise and ambient vibration tests, with 24,931 columns for white noise tests and 14,331 columns for ambient vibration tests. It should be noted that the lengths of the ambient vibration tests (3min) and white noise base excitation tests (8min) are different (see Table 4.2). Therefore, different number of columns were used in their corresponding Hankel matrices. The natural frequencies and damping ratios of the first five most significant vibration modes identified using SSI-DATA are reported in Table 4.3 based on the ambient vibration data and in Tables 4.4 and 4.5 based on the white noise base excitation response (output) data.

4.3.1.3 Enhanced Frequency Domain Decomposition (EFDD)

The Frequency Domain Decomposition (FDD), a non-parametric frequency-domain approach, is an extension of the Basic Frequency Domain approach also referred to as peak picking technique. According to the FDD technique, the modal parameters are estimated through SVD of the CSD matrix performed at all discrete frequencies. Through this SVD, CSD functions are decomposed into single degree of freedom (SDOF) CSD functions, each corresponding to a single vibration mode of the dynamic system. Considering a lightly damped system, the contribution of different vibration modes at a particular frequency is limited to a small number (usually 1 or 2). In the EFDD (Brincker et al. 2001), the natural frequency and damping ratio of a vibration mode are identified from the SDOF CSD function corresponding to that mode. In doing so, the SDOF CSD function is taken back to the time domain by inverse Fourier transformation, and the frequency and damping ratio of the mode considered are estimated from the zero-crossing times and the

logarithmic decrement, respectively, of the corresponding SDOF auto-correlation function. In applying the EFDD method, the measured acceleration and strain data were down-sampled to 80Hz and 40Hz, respectively, and then the CSD functions were estimated based on Welch-Bartlett's method using Hanning windows with 50 percent overlap. After estimating the CSD functions, the (28×28) response CSD matrix was singular value decomposed at each discrete frequency. The modal parameters obtained as outlined above are given in Table 4.3 based on the ambient vibration data and in Tables 4.4 and 4.5 based on the white noise base excitation response (output) data.

4.3.2 Input-Output System Identification Methods

The three input-output system identification methods are only applied to the white noise base excitation data during which the input base excitation is measured.

4.3.2.4 Deterministic-Stochastic Subspace Identification (DSI)

The deterministic-stochastic state-space model for linear time-invariant systems can be written as

$$\begin{aligned} \mathbf{x}(k+1) &= \mathbf{A}\mathbf{x}(k) + \mathbf{B}\mathbf{u}(k) + \mathbf{w}(k) \\ \mathbf{y}(k) &= \mathbf{C}\mathbf{x}(k) + \mathbf{D}\mathbf{u}(k) + \mathbf{v}(k) \end{aligned} \tag{1}$$

where **A**, **B**, **C** and **D** refer to the state-space matrices, $\mathbf{u}(k)$ and $\mathbf{y}(k)$ denote the input and output vectors, respectively, and $\mathbf{x}(k)$ is the state vector. In the deterministic-stochastic model, the process noise $\mathbf{w}(k)$, corresponds to disturbances (small unmeasured excitations) and modeling inaccuracies, while the measurement noise $\mathbf{v}(k)$, model the sensor

inaccuracies. However, in the stochastic subspace identification (SSI) output-only methods, both noise terms (**w** and **v**) also implicitly include the input information since it is impossible to distinguish the input information from the noise terms. Considering the following two assumptions: (1) the deterministic input $\mathbf{u}(k)$ is uncorrelated with the process noise $\mathbf{w}(k)$ and measurement noise $\mathbf{v}(k)$, and (2) both noise terms are not identically zero, a robust identification algorithm was developed by Van Overschee and De Moor (1996) in order to identify the state-space matrices in the combined deterministic-stochastic system. Similar to SSI-DATA, robust numerical techniques such as QR factorization, SVD, and least squares are involved in this method. Using the DSI method, the state-space matrices **A**, **B**, **C**, **D** are determined from the measured input and output vibration data directly. Then, the modal parameters are identified based on these state-space matrices. In the application of this method, the measured input (shake table acceleration) and the relative horizontal acceleration response data were down-sampled to 80Hz. For each dynamic test, an input-output Hankel matrix was formed including 35 block rows with 29 rows in each block (1 input and 28 output channels) and 24,931 columns using the down-sampled data. The identified natural frequencies and damping ratios of the first five significant vibration modes (first three longitudinal, first torsional and first coupled longitudinal-torsional) are reported in Table 4.4.

Table 4.4 Natural frequencies and damping ratios identified based on acceleration data from white noise base excitation tests (0.03g RMS)

State / Test No.	System ID Method	Natural Frequency [Hz]					Damping Ratio [%]				
		1st-L mode	1st-T mode	1st-L-T mode	2nd-L mode	3rd-L mode	1st-L mode	1st-T mode	1st-L-T mode	2nd-L mode	3rd-L mode
S0 / Test 39	MNExT-ERA	1.71	2.35	8.64	11.49	24.67	3.1	-1.1	5.4	4.8	1.3
	SSI	1.66	-	8.67	11.65	24.61	2.2	-	3.6	4.4	0.2
	EFDD	1.72	-	8.52	11.88	24.64	2.6	-	1.3	0.5	0.4
	DSI	1.72	1.80	9.03	10.70	24.55	2.2	3.5	4.2	4.5	0.5
	OKID-ERA	1.70	-	8.95	10.78	25.06	1.7	-	0.1	1.5	1.4
	GRA	1.71	-	9.05	11.05	24.31	2.1	-	1.8	1.8	0.5
S1 / Test 41	MNExT-ERA	1.54	2.34	8.51	11.35	24.65	4.3	1.1	4.7	7.7	0.9
	SSI	1.51	1.73	8.37	11.25	24.57	2.4	4.0	4.9	3.3	0.2
	EFDD	1.49	-	8.17	11.33	24.56	3.3	-	1.0	0.4	0.2
	DSI	1.57	1.78	8.76	10.67	24.42	3.1	2.9	3.9	3.2	0.3
	OKID-ERA	1.60	-	-	10.75	24.57	3.8	-	-	0.3	1.9
	GRA	1.54	-	8.65	10.98	24.28	2.0	-	1.1	1.7	0.2
S2 / Test 46	MNExT-ERA	1.22	-	7.42	10.88	21.26	3.4	-	6.0	0.3	3.9
	SSI	1.25	-	7.26	11.10	22.82	4.5	-	4.2	4.9	2.0
	EFDD	1.29	-	7.43	10.75	21.08	5.2	-	0.9	0.3	0.2
	DSI	1.27	2.02	7.67	10.23	21.56	3.5	11.6	6.7	4.8	2.7
	OKID-ERA	1.24	-	7.86	10.93	21.08	2.8	-	-0.3	1.7	2.9
	GRA	1.24	-	7.60	11.11	21.59	3.0	-	4.0	2.9	0.5
S3.1 / Test 49	MNExT-ERA	1.11	-	7.01	10.24	19.77	3.5	-	8.6	7.0	5.6
	SSI	1.13	2.13	7.14	9.87	20.40	3.9	10.7	3.7	1.9	2.3
	EFDD	1.13	-	7.07	10.06	19.83	4.0	-	0.3	0.2	0.1
	DSI	1.14	2.20	7.20	-	20.42	3.3	13.3	4.9	-	2.7
	OKID-ERA	1.17	-	7.15	10.47	20.40	5.6	-	0.2	1.8	1.1
	GRA	1.14	-	7.32	9.77	19.68	3.9	-	4.3	1.6	0.5
S3.2 / Test 61	MNExT-ERA	1.18	2.37	-	11.00	21.32	5.0	0.0	-	6.0	5.7
	SSI	1.20	2.62	-	10.89	21.04	3.5	4.3	-	5.4	2.0
	EFDD	1.23	-	-	10.41	20.68	4.6	-	-	0.4	0.1
	DSI	1.22	-	-	-	21.47	3.6	-	-	-	2.7
	OKID-ERA	1.20	-	-	-	20.47	2.8	-	-	-	2.8
	GRA	1.20	-	-	10.45	21.11	3.5	-	-	2.0	0.3

Table 4.4 Natural frequencies and damping ratios identified based on acceleration data from white noise base excitation tests (0.03g RMS)

State / Test No.	System ID Method	Natural Frequency [Hz]					Damping Ratio [%]				
		1^{st}-L mode	1^{st}-T mode	1^{st}-L-T mode	2^{nd}-L mode	3^{rd}-L mode	1^{st}-L mode	1^{st}-T mode	1^{st}-L-T mode	2^{nd}-L mode	3^{rd}-L mode
S4 / Test 64	MNExT-ERA	0.83	-	-	4.68	13.24	3.3	-	-	7.6	0.4
	SSI	0.85	-	-	4.68	14.02	5.6	-	-	5.5	2.9
	EFDD	0.86	-	-	4.71	13.81	3.8	-	-	0.4	0.2
	DSI	0.85	-	-	4.72	13.31	3.6	-	-	6.1	4.8
	OKID-ERA	0.87	-	-	4.79	14.69	2.9	-	-	3.6	0.0
	GRA	0.88	-	-	4.81	13.29	5.5	-	-	3.8	0.9

4.3.2.5 Observer/Kalman Filter Identification Combined with ERA (OKID-ERA)

In this method, developed by Phan et al. (1992), the system input-output relationship is expressed in terms of an observer, which is made asymptotically stable by an embedded eigenvalue assignment procedure. The prescribed eigenvalues for the observer may be real, complex, mixed real and complex, or zero (i.e., deadbeat observer). In this formulation, the Markov parameters of the observer are identified from input-output data. The Markov parameters of the actual system are then recovered from those of the observer and then used to obtain a state-space model of the system by ERA. The method performs quite well for finite-dimensional systems under the following conditions: (1) the input-output data time histories are sufficiently long, (2) the noise is white and of zero-mean, and (3) the noise-to-signal ratio is small (Lus et al. 2002). This approach seems attractive, especially for single input systems as in the case of structures subjected to base excitation. In the application of OKID-ERA, the filtered and then detrended acceleration responses from white noise base excitation tests were down-sampled to 60Hz. An output matrix $\hat{\mathbf{Y}} = [\ \mathbf{y}(0)\ \ldots\ \mathbf{y}(p)\ \ldots\ \mathbf{y}(l-1)\ ]$ of size (28×1000) and an input-output matrix

$$\mathbf{V} = \begin{bmatrix} \mathbf{u}(0) & \mathbf{u}(1) & \dots & \mathbf{u}(\mathrm{p}) & \dots & \mathbf{u}(l-1) \\ \mathbf{0} & \boldsymbol{\nu}(0) & \dots & \boldsymbol{\nu}(\mathrm{p}-1) & \dots & \boldsymbol{\nu}(l-2) \\ \dots & \dots & \dots & \dots & \dots & \dots \\ \mathbf{0} & \mathbf{0} & \dots & \boldsymbol{\nu}(0) & \dots & \boldsymbol{\nu}(l-\mathrm{p}-1) \end{bmatrix}$$ of size (7251×1000) are formed based on inputs $\mathbf{u}(\mathrm{k})$, outputs $\mathbf{y}(\mathrm{k})$, and input-output vectors $\boldsymbol{\nu}(\mathrm{k}) = \begin{bmatrix} \mathbf{u}(\mathrm{k}) \\ \mathbf{x}(\mathrm{k}) \end{bmatrix}$. Once the system's Markov parameters are identified, the ERA is used for estimation of the modal parameters which are reported in Table 4.4.

Table 4.5 Natural frequencies, damping ratios, and MAC values identified based on LVDT strain data from white noise base excitation tests (0.03g RMS)

Damage State / Test No.	Vibration Mode	Natural Frequency [Hz]			Damping Ratio [%]			MAC		
		MNEx T-ERA	SSI	EFDD	MNEx T-ERA	SSI	EFDD	MNExT & SSI	MNExT & EFDD	SSI & EFDD
S0 / Test 39	1st-L mode	1.66	1.69	1.68	3.2	2.6	3.2	1.00	1.00	1.00
	2nd-T mode	3.33	3.30	3.26	3.7	2.8	0.3	1.00	1.00	1.00
S1 / Test 41	1st-L mode	1.50	1.56	1.51	2.6	4.8	2.2	1.00	1.00	1.00
	2nd-T mode	3.01	3.05	2.89	3.6	4.1	0.9	1.00	0.98	0.98
S2 / Test 46	1st-L mode	1.26	1.19	1.24	5.5	5.0	5.4	0.96	0.99	0.98
	2nd-T mode	2.45	2.45	2.44	3.3	4.8	1.5	0.97	0.95	0.99
S3.1 / Test 49	1st-L mode	1.13	1.10	1.12	4.4	4.5	1.8	1.00	1.00	1.00
	2nd-T mode	2.22	2.21	2.20	3.0	4.1	0.5	1.00	1.00	1.00
S3.2 / Test 61	1st-L mode	1.18	1.18	1.18	4.3	5.9	1.6	0.95	1.00	0.96
	2nd-T mode	2.35	2.38	2.34	3.4	5.3	0.7	0.94	1.00	0.96
S4 / Test 64	1st-L mode	0.83	0.83	0.85	4.7	3.3	5.4	0.99	0.99	1.00
	2nd-T mode	1.63	1.63	1.64	2.1	3.1	0.7	0.96	1.00	0.97

4.3.2.6 General Realization Algorithm (GRA)

GRA (De Callafon et al., 2007) is a system realization algorithm to identify modal parameters of linear dynamic systems based on general input-output data. This algorithm is an extension of ERA. While ERA is based on singular value decomposition (SVD) of a Hankel matrix constructed from impulse response or free vibration response data, GRA is based on SVD of a weighted Hankel matrix, where the weighting is defined by the loading. Using GRA, the state-space matrices are estimated in a two-step process that includes a state reconstruction followed by a least squares optimization yielding a minimum prediction error for the response. In the application of GRA, a weighted Hankel matrix of size $(28 \times 50) \times 7000$ is formed based on the input-output data. After performing an SVD of this weighted Hankel matrix, a state-space realization of the system is estimated from which the modal parameters are extracted. The natural frequencies and damping ratios identified using GRA are reported in Table 4.4.

4.4 MODAL IDENTIFICATION RESULTS

Modal parameters of the test structure were identified using the system identification methods outlined above based on output-only (for the first three methods) and input-output (for the last three methods) data measured from low amplitude dynamic tests (i.e., ambient vibration tests and white noise base excitation tests) performed at various damage states (S0, S1, S2, S3.1, S3.2, and S4). Damage state S0 is defined as the undamaged (baseline) state of the structure before its exposure to the first seismic excitation (EQ1), while damage states S1, S2, S3 and S4 correspond to the state of the structure after expo-

sure to the first (EQ1), second (EQ2), third (EQ3), and fourth (EQ4) seismic excitation, respectively (see Table 4.2). Damage state S0 does not correspond to the uncracked state of the structure, since the structure had already been subjected to low-amplitude white noise base excitations (0.02-0.03g RMS) for the purposes of checking the instrumentation and data acquisition system and tuning the shaking table controller. It should be noted that during damage state S3, the bracing system between the slabs of the test specimen and the post-tensioned column was modified (stiffened). Therefore, damage state S3 is subdivided into state S3.1 (before modification of the braces) and state S3.2 (after modification of the braces). The identified modal parameters are presented and discussed in the following three subsections based on the type of excitation (ambient or white noise base excitation) and type of measurement data (acceleration from accelerometers or strains from LVDTs) used in the identification process.

4.4.1 Modal Parameters Identified Based on Ambient Vibration Acceleration Data

The modal parameters identified based on acceleration data from ambient vibration tests are discussed in this section. Figure 4.11 shows in polar plots the complex-valued mode shapes of the five most significantly excited modes of the test structure identified using SSI-DATA based on data from Test 46 (damage state S2). The real parts of these mode shapes are displayed in Figure 4.12. The five most significant vibration modes identified at this damage state consist of the first three longitudinal (1^{st}-L, 2^{nd}-L, 3^{rd}-L), the first torsional (1^{st}-T) and the first coupled longitudinal-torsional (1^{st}-L-T) modes. The polar plot representation of a mode shape provides information on the degree

of non-classical (or non-proportional) damping characteristics of that mode. If all the components of a mode shape (each component being represented by a vector in polar plot) are collinear, that vibration mode is classically damped. The more the mode shape components are scattered in the complex plane, the more the system is non-classically (non-proportionally) damped in that mode. However, measurement noise (low signal-to-noise ratio), estimation errors, and modeling errors can also cause a truly classically damped vibration mode to be identified as non-classically damped. From Figure 4.11, it is observed that the first longitudinal and first torsional modes at damage state S2 are identified as perfectly classically damped. Some degree of non-proportional damping is identified for the other modes (2^{nd}-L, 3^{rd}-L, and 1^{st}-L-T).

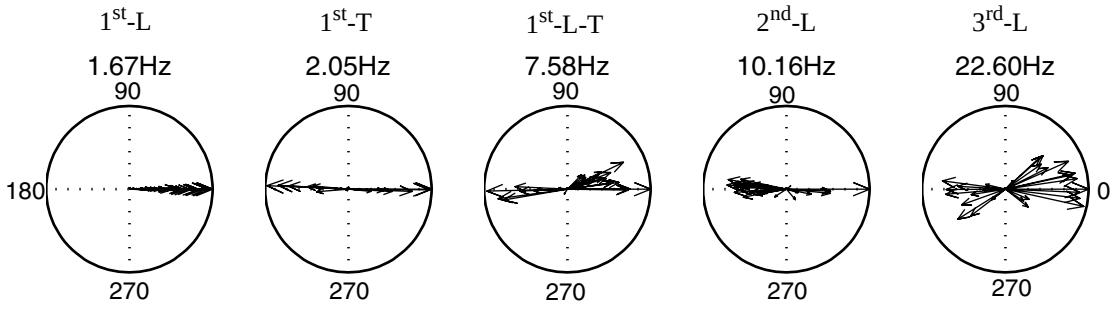

Fig. 4.11 Polar plot representation of complex-valued mode shapes of the building at damage state S2 obtained using SSI-DATA based on ambient vibration acceleration data

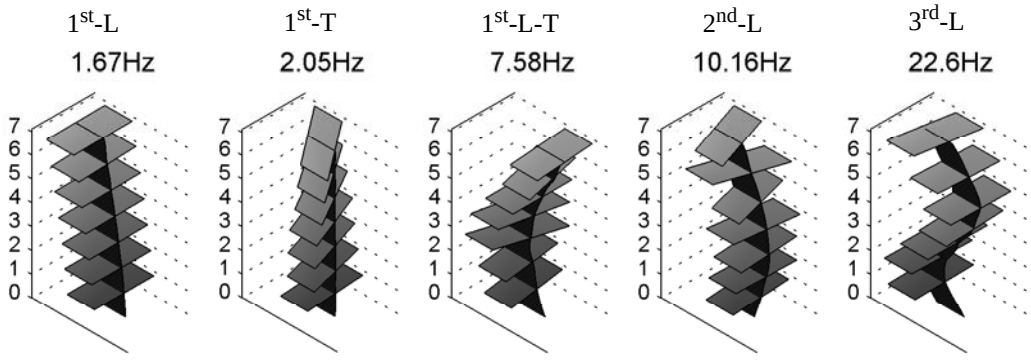

Fig. 4.12 Vibration mode shapes of the building at damage state S2 obtained using SSI-DATA based on ambient vibration acceleration data

The natural frequencies and damping ratios of the five most significantly excited modes identified based on ambient vibration acceleration data are given in Table 4.3 for all damage states considered and the three output-only system identification methods (MNExT-ERA, SSI, EFDD). The identified natural frequencies and damping ratios are also represented in bar plots in Figures 4.13 and 4.14, respectively.

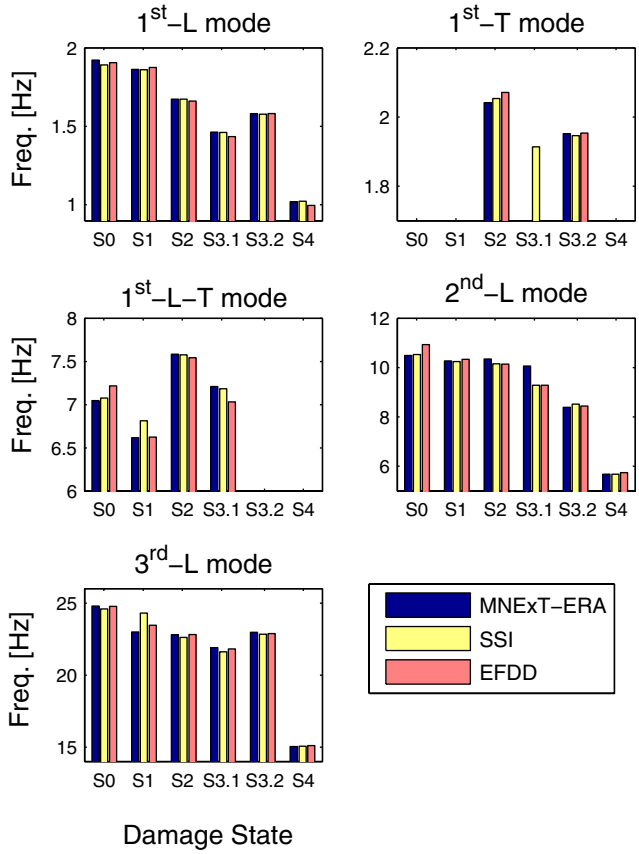

Fig. 4.13 Natural frequencies identified based on ambient vibration acceleration data using different methods

From Table 4.3 and Figures 4.13 and 4.14, it is observed that: (1) The natural frequencies identified using different methods are in good agreement at each damage state, while the identified damping ratios display larger variability across the different system identification methods. (2) The identified natural frequencies of the longitudinal modes

only (1^{st}-L, 2^{nd}-L, 3^{rd}-L) decrease with increasing level of damage, except from damage states S3.1 to S3.2, during which the steel braces (see Figure 4.3) were modified (stiffened), while the identified damping ratios do not show a clear trend as a function of increasing structural damage. The fact that the identified natural frequencies of the other two modes do not decrease with increasing damage could be explained by the fact that under low amplitude ambient vibration conditions, concrete cracks do not open as much as under forced based excitation and therefore damage does not affect the identified modal parameters of these vibration modes. (3) The first torsional vibration mode (1^{st}-T) could only be identified at damage states S2, S3.1 and S3.2. (4) The identified damping ratios are in a reasonable range (0-5%) validating the modal identification results. (5) The modal damping ratios identified using EFDD are systematically lower than their counterparts identified using the other two methods. This can be due to the fact that in the application of EFDD, a high MAC value is used to decompose the noisy CSD functions to SDOF CFD function which yields to estimation of a narrow peak (low-damped) SDOF CFD function.

Modal Assurance Criterion (MAC) values (Allemang and Brown 1982) were computed in order to compare the corresponding complex-valued mode shapes identified using the three output-only system identification methods considered and are reported in Table 4.6. The high MAC values obtained in most cases (each case being defined by a vibration mode, a pair of system identification methods and a damage state) indicate a good agreement in general between the mode shapes identified using different methods. From Table 4.6, it is also observed that the MAC values between corresponding mode

shapes identified using SSI-DATA & EFDD are in general the highest among the three combinations of system identification methods (i.e., MNExT-ERA & SSI-DATA, MNExT-ERA & EFDD, SSI-DATA & EFDD), implying that the mode shapes identified using MNExT-ERA based on ambient vibration acceleration data are the least accurate among the three output-only methods considered. This could be due to the fact that in the application of MNExT-ERA, if the selected reference channels are close to modal nodes of a vibration mode, the estimation uncertainty of that mode will be relatively large.

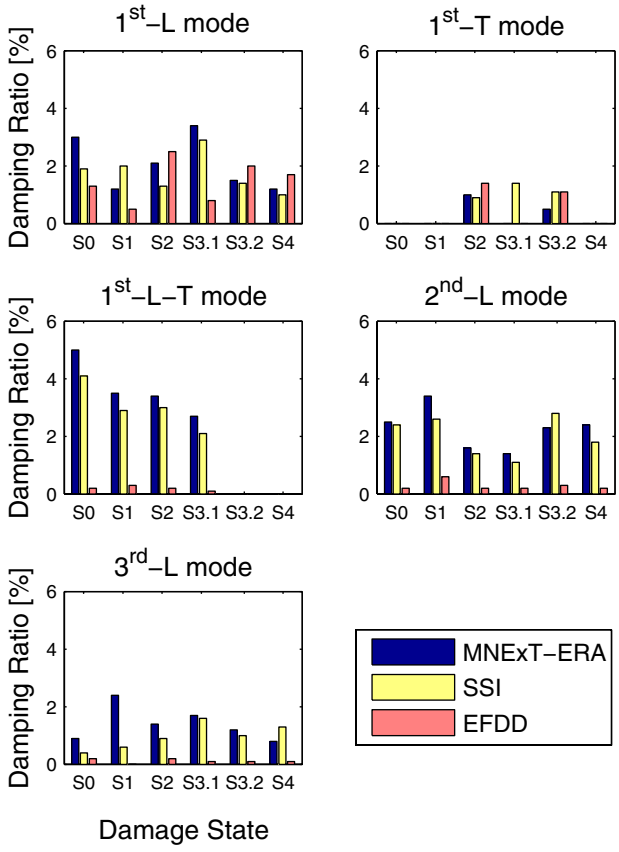

Fig. 4.14 Damping ratios identified based on ambient vibration acceleration data using different methods

Table 4.6 MAC values between corresponding mode shapes identified using different methods based on acceleration data from ambient vibration tests

Damage State / Test No.	System ID Methods	1^{st}-L mode	1^{st}-T mode	1^{st}-L-T mode	2^{nd}-L mode	3^{rd}-L mode
S0 / Test 39	MNExT & SSI	0.99	-	0.26	0.86	0.70
	MNExT & EFDD	0.99	-	0.46	0.49	0.74
	SSI & EFDD	1.00	-	0.82	0.77	0.97
S1 / Test 41	MNExT & SSI	0.91	-	0.78	0.89	0.79
	MNExT & EFDD	0.97	-	0.84	0.89	0.88
	SSI & EFDD	0.79	-	0.84	0.98	0.89
S2 / Test 46	MNExT & SSI	1.00	0.98	0.98	0.56	0.95
	MNExT & EFDD	1.00	0.98	0.96	0.43	0.96
	SSI & EFDD	1.00	1.00	0.98	0.97	0.95
S3.1 / Test 49	MNExT & SSI	0.99	-	0.92	0.39	0.93
	MNExT & EFDD	1.00	-	0.78	0.49	0.96
	SSI & EFDD	0.99	-	0.92	0.96	0.98
S3.2 / Test 61	MNExT & SSI	1.00	0.97	-	1.00	0.97
	MNExT & EFDD	1.00	0.98	-	1.00	0.98
	SSI & EFDD	1.00	0.98	-	1.00	0.99
S4 / Test 64	MNExT & SSI	1.00	-	-	0.99	0.96
	MNExT & EFDD	1.00	-	-	0.99	0.98
	SSI & EFDD	1.00	-	-	1.00	0.98

4.4.2 Modal Parameters Identified Based on Acceleration Data from Shake Table Tests

The modal parameters identified based on acceleration data from white noise base excitation tests are presented and discussed in this section. Figure 4.15 shows in polar plots the complex-valued mode shapes of the five most significant modes of the building identified using MNExT-ERA based on data from Test 39 (damage state S0). The real part of these mode shapes are displayed in Figure. 4.16. The five most significant vibration modes identified in this case consist of the first three longitudinal (1^{st}-L, 2^{nd}-L, 3^{rd}-L), the

first torsional (1^{st}-T), and the first coupled longitudinal-torsional (1^{st}-L-T) modes. From Figure 4.15, it is observed that the first longitudinal (1^{st}-L) vibration mode is identified as nearly perfectly classically damped, while the other identified modes (1^{st}-T, 1^{st}-L-T, 2^{nd}-L, 3^{rd}-L) display some non-classical damping characteristics. Figure 4.17 shows the modal decomposition of the floor acceleration response, simulated using the state-space model realized based on GRA, at floors 1, 4, and 7 during the white noise base excitation test at damage state S0 (Test 39). This figure also provides a comparison of selected acceleration responses simulated using the realized model with their counterparts measured by accelerometers from the test structure. It is observed that: (1) the simulated and measured acceleration responses are in good agreement, validating the accuracy of the realized model, and (2) the 1st-L mode has a predominant contribution to the total response of the building, while the other identified modes do not contribute significantly to its total response and are therefore characterized by a lower signal-to-noise ratio than the 1st-L mode.

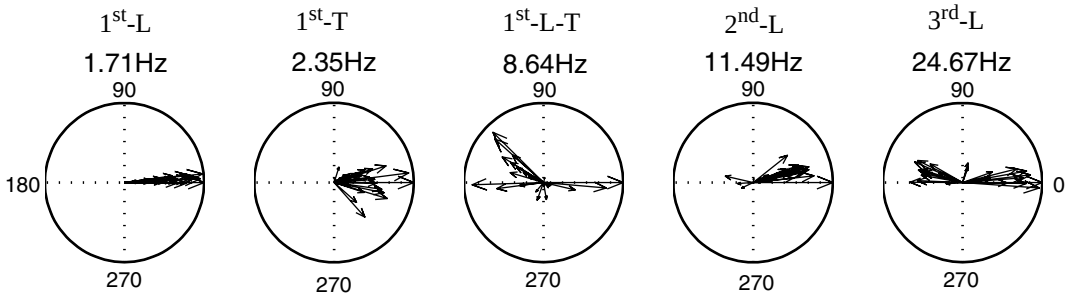

Fig. 4.15 Polar plot representation of complex-valued mode shapes of the building at damage state S0 obtained using MNExT-ERA based on white noise test acceleration data

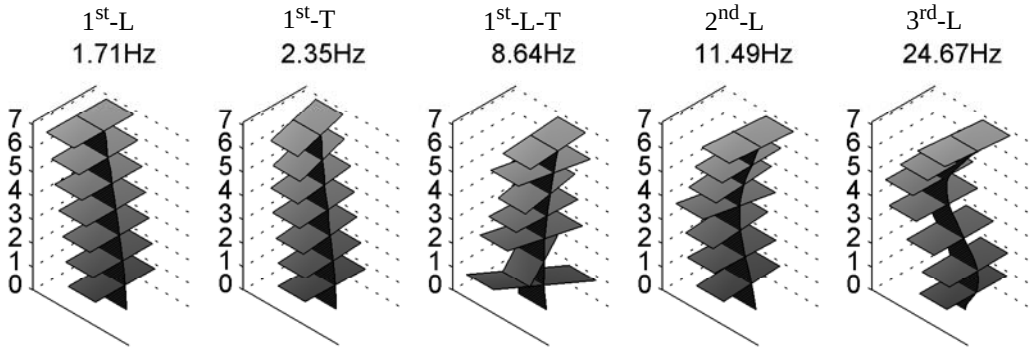

Fig. 4.16 Vibration mode shapes of the building at damage state S0 obtained using MNExT-ERA based on white noise test acceleration data

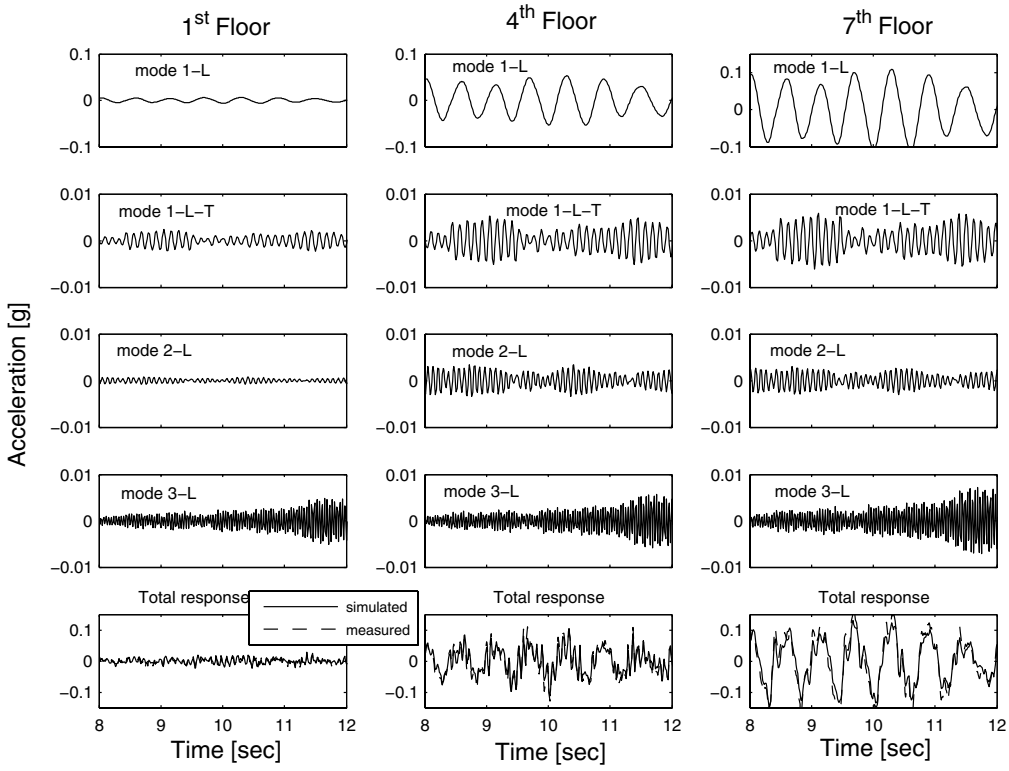

Fig. 4.17 Modal decomposition using GRA of acceleration measurements at floors 1, 4, and 7 during white noise base excitation test at damage state S0

Table 4.4 reports the natural frequencies and damping ratios of the five most significantly excited vibration modes identified based on acceleration data from white noise base excitation tests at all damage states considered. Figures 4.18 and 4.19 show in bar plots these

natural frequencies and damping ratios, respectively, identified using the six system identification methods considered. From Table 4.4 and Figures 4.18 and 4.19, it is observed that: (1) The natural frequencies identified using different methods are reasonably consistent at each damage state, while the identified damping ratios exhibit much larger variability. It appears that when a mode is not significantly excited, its modal damping estimate using EFDD is consistently very low compared to other methods. (2) Some vibration modes (especially the first torsional mode) could not be identified by each of the system identification methods. (3) The identified natural frequencies of all the identified vibration modes decrease with increasing level of structural damage, except from damage state S3.1 to S3.2, during which the steel braces (see Figure 4.3) were modified (stiffened), while the identified damping ratios do not exhibit a clear trend as a function of damage. (4) The first longitudinal modal frequencies identified based on white noise test acceleration data are systematically lower than their counterparts identified based on ambient vibration acceleration data at all damage states considered (compare Tables 4.3 & 4.4 as well as Figs 4.13 & 4.18). This is most likely due to the fact that the test structure is nonlinear (even at the relatively low levels of excitation considered in this system identification study) with effective modal parameters depending strongly on the amplitude of the excitation and therefore of the structural response. (5) At each damage state, the identified modal parameters of the first longitudinal mode (1^{st}-L) appear to be the least sensitive to the identification method used, which could be due to the predominant contribution of this mode to the total response.

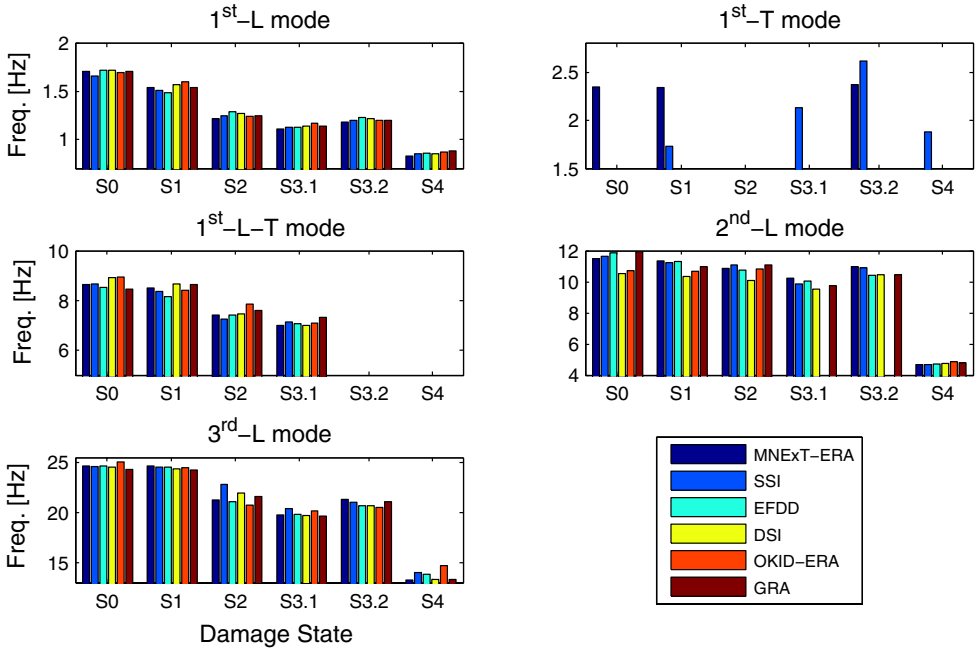

Fig. 4.18 Natural frequencies identified based on white noise test data from accelerometers using different methods

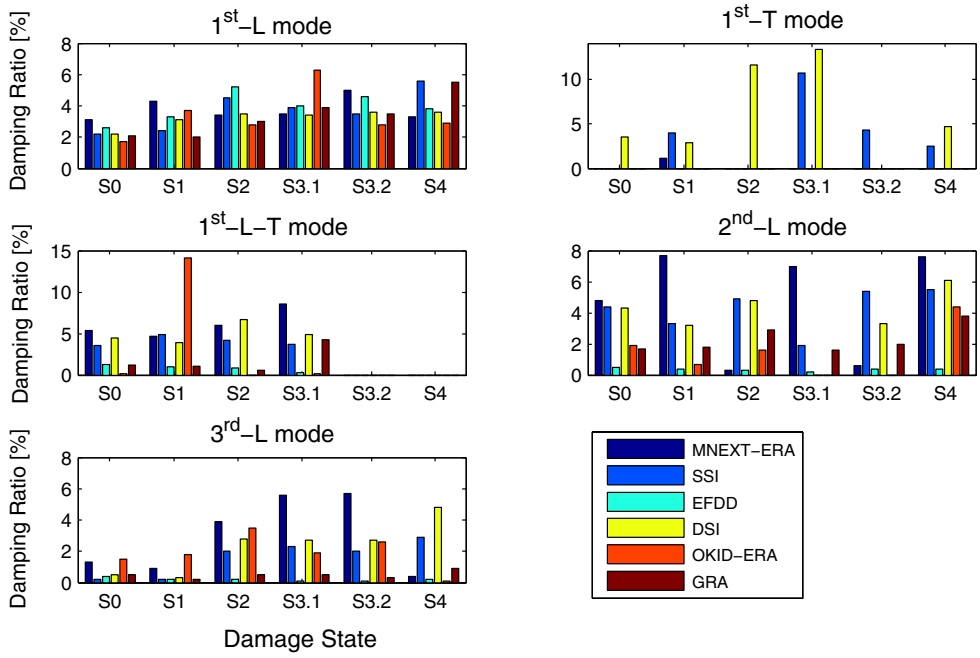

Fig. 4.19 Damping ratios identified based on white noise test data from accelerometers using different methods

Table 4.7 reports the MAC values calculated between corresponding complex-valued mode shapes identified using the three output-only system identification methods (i.e., MNExT-ERA & SSI-DATA, MNExT-ERA & EFDD, SSI-DATA & EFDD), the three input-output system identification methods (i.e., DSI & OKID-ERA, DSI & GRA, OKID-ERA & GRA), and also between corresponding mode shapes identified using an output-only and an input-output system identification method (SSI-DATA & GRA). From the results in Table 4.7, it is observed that: (1) the MAC values calculated for the 1st-L mode shape identified using different methods are very close to unity for all damage states considered, indicating the high level of accuracy (i.e., low level of estimation uncertainty) in the identification of this mode shape. (2) Lower MAC values obtained for the 1st-L-T mode shape indicates its larger estimation uncertainty. (3) In general, the MAC values calculated across output-only methods are higher than those calculated across input-output methods. It appears that the output-only methods perform very well (are very accurate) when the hypothesis based on which they are developed are satisfied (i.e., when the input excitation is a white noise sequence). (4) The MAC values between corresponding mode shapes identified using SSI-DATA (output-only method) and GRA (input-output method) are in general high indicating the corresponding mode shapes are in good agreement, especially for the three longitudinal mode shapes (i.e., 1^{st}-L, 2^{nd}-L, 3^{rd}-L).

Table 4.7 MAC values between corresponding mode shapes identified using different methods based on acceleration data from white noise base excitation tests

Damage State / Test No.	System ID Methods	1st-L mode	1st-T mode	1st-L-T mode	2nd-L mode	3rd-L mode
S0 / Test 39	MNExT & SSI	1.00	-	0.90	0.96	0.99
	MNExT & EFDD	0.99	-	0.82	0.94	0.97
	SSI & EFDD	1.00	-	0.82	0.97	0.99
	DSI & OKID	1.00	-	0.58	0.65	0.92
	DSI & GRA	1.00	-	0.66	0.24	0.80
	OKID & GRA	1.00	-	0.76	0.71	0.94
	SSI & GRA	1.00	-	0.70	0.95	0.98
S1 / Test 41	MNExT & SSI	1.00	0.96	0.51	0.99	0.99
	MNExT & EFDD	1.00	-	0.75	0.96	0.99
	SSI & EFDD	1.00	-	0.49	0.99	1.00
	DSI & OKID	1.00	-	-	0.54	0.83
	DSI & GRA	1.00	-	0.49	0.39	0.88
	OKID & GRA	1.00	-	-	0.90	0.56
	SSI & GRA	1.00	-	0.30	0.99	0.99
S2 / Test 46	MNExT & SSI	1.00	-	0.76	0.97	0.67
	MNExT & EFDD	1.00	-	0.82	0.98	0.86
	SSI & EFDD	1.00	-	0.81	0.99	0.87
	DSI & OKID	1.00	-	0.24	0.20	0.91
	DSI & GRA	1.00	-	0.59	0.22	0.64
	OKID & GRA	1.00	-	0.44	0.89	0.72
	SSI & GRA	1.00	-	0.73	0.99	0.98
S3.1 / Test 49	MNExT & SSI	1.00	-	0.54	0.97	0.73
	MNExT & EFDD	1.00	-	0.42	0.98	0.76
	SSI & EFDD	1.00	-	0.80	0.99	0.75
	DSI & OKID	1.00	-	0.48	-	0.88
	DSI & GRA	1.00	-	0.65	-	0.86
	OKID & GRA	1.00	-	0.84	0.78	0.94
	SSI & GRA	1.00	-	0.74	0.95	0.90
S3.2 / Test 61	MNExT & SSI	1.00	0.70	-	0.94	0.99
	MNExT & EFDD	1.00	-	-	0.85	0.89
	SSI & EFDD	1.00	-	-	0.84	0.90
	DSI & OKID	1.00	-	-	-	0.91
	DSI & GRA	1.00	-	-	-	0.90
	OKID & GRA	1.00	-	-	-	0.97
	SSI & GRA	1.00	-	-	0.72	0.98

Table 4.7 MAC values between corresponding mode shapes identified using different methods based on acceleration data from white noise base excitation tests

Damage State / Test No.	System ID Methods	1st-L mode	1st-T mode	1st-L-T mode	2nd-L mode	3rd-L mode
S4 / Test 64	MNExT & SSI	1.00	-	-	0.99	0.51
	MNExT & EFDD	1.00	-	-	0.96	0.58
	SSI & EFDD	1.00	-	-	0.96	0.94
	DSI & OKID	1.00	-	-	0.97	0.68
	DSI & GRA	1.00	-	-	0.94	0.91
	OKID & GRA	1.00	-	-	0.93	0.77
	SSI & GRA	1.00	-	-	0.97	0.73

4.4.3 Modal Parameters Identified Based on LVDT Data from Shake Table Tests

In this section, the modal parameters of the two most significantly excited vibration modes identified based on LVDT strain data from white noise base excitation tests are presented and discussed. Based on the identified natural frequencies of these strain mode shapes and by comparison with those of the displacement mode shapes identified based on acceleration data and those of the finite element model presented in a later section, it is found that the two LVDT-based identified modes correspond to the first longitudinal (1st-L) and second torsional (2nd-T) vibration modes of the test structure. Figure 4.20(a) shows in polar plots the complex-valued strain mode shapes of these two modes identified using MNExT-ERA based on LVDT strain data from white noise base excitation Test 39 (damage state S0). The real parts of these strain mode shapes are displayed in Figure 4.20(b). From Figure 4.20(a), it is observed that the 1st-L mode is identified as nearly perfectly classically damped, while the 2nd-T mode displays some nonclassical damping characteristics.

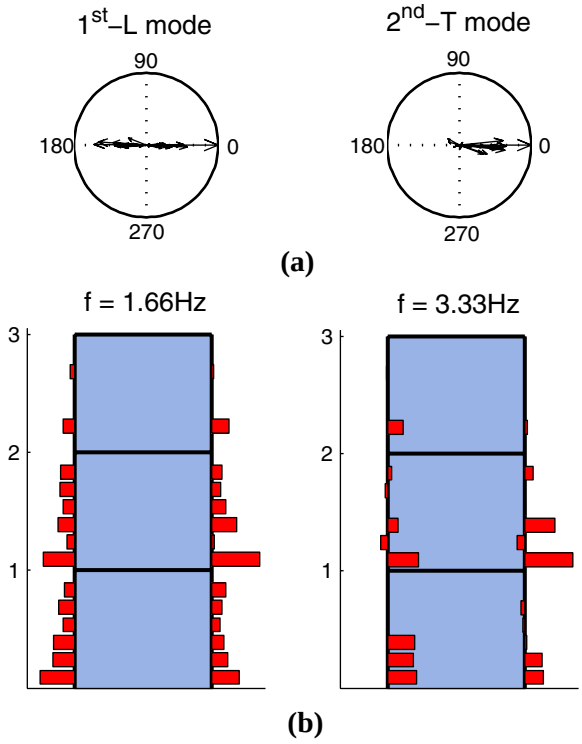

Fig. 4.20 Strain mode shapes at damage state S0 obtained using MNExT-ERA based on white noise test data from LVDTs: (a) polar plot representation, (b) bar plot representation of real-part of strain mode shapes

Table 4.5 reports the natural frequencies, damping ratios, and MAC values calculated between corresponding complex-valued mode shapes identified using the three output-only methods based on LVDT strain data from white noise base excitation tests at all damage states considered. From the results in Table 4.5, it is observed that: (1) The natural frequencies identified using different methods are in very good agreement at each damage state. (2) Considering the larger estimation variability of the damping ratios (as compared to natural frequencies), the identified damping ratios at each damage state are in relatively good agreement, except for the damping ratio of the 2nd-T mode identified using EFDD which is generally much lower than its counterparts identified using the other two meth-

ods. (3) The identified natural frequencies decrease with increasing level of structural damage except from damage state S3.1 to S3.2, while the damping ratios do not follow a clear trend as a function of damage. (4) At each damage state, the first longitudinal mode natural frequency and damping ratios identified based on white noise test data from LVDTs are in excellent and good agreement, respectively, with their counterpart identified based on white noise test data from accelerometers. (5) The MAC values calculated between corresponding complex-valued strain mode shapes obtained using different system identification methods are near unity for all damage states considered, implying that these strain mode shapes have been accurately identified.

4.5 COMPARISON BETWEEN EXPERIMENTAL AND ANALYTICAL MODAL PARAMETERS

In order to further validate and better understand the modal parameters identified from ambient vibration and white noise base excitation test data, a three-dimensional (3D) linear elastic finite element model of the shear wall test structure was developed in SAP2000 (Computers and Structures, Inc. 2004). This finite element model is composed of: (1) 126 frame elements to model the gravity columns, part of the post-tensioned column, and steel braces connecting the slabs to the post-tensioned column, (2) 1346 shell elements to model the web wall, flange wall, floor slabs, and part of the post-tensioned column. The distributed inertia properties of the structure are discretized into translational lumped masses applied at the nodes. This finite element model has 8,907 degrees-of-freedom (DOFs). It was used for designing the shake table test sequence (including the low

amplitude white noise base excitations between earthquake tests) and selecting the number, types and locations of sensors. The natural frequencies and mode shapes of the first twenty vibration modes were computed from this 3D finite element model of the test structure. Figure 4.21 shows these calculated natural frequencies and mode shapes for the first five and the eleventh vibration modes. It should be noted that in the first torsional mode (1st-T), the web wall rotates around the back wall while in the second torsional mode (2nd-T), the web wall rotates around the post-tensioned column. These analytical results show reasonable agreement with the modal parameters of the test structure in its undamaged state (damage state S0) identified based on acceleration data (for the first three longitudinal and the first torsional vibration modes) as well as LVDT strain data (for the first longitudinal and the second torsional vibration modes). The natural frequencies computed from the finite element model are in better agreement with those identified based on ambient vibration test data than with those identified based on white noise base excitation test data (see Tables 4.3-4.5). This is most likely due to the fact that uncracked section properties (with section moment of inertia taken as gross section moment of inertia) were assumed in developing the finite element model of the test structure.

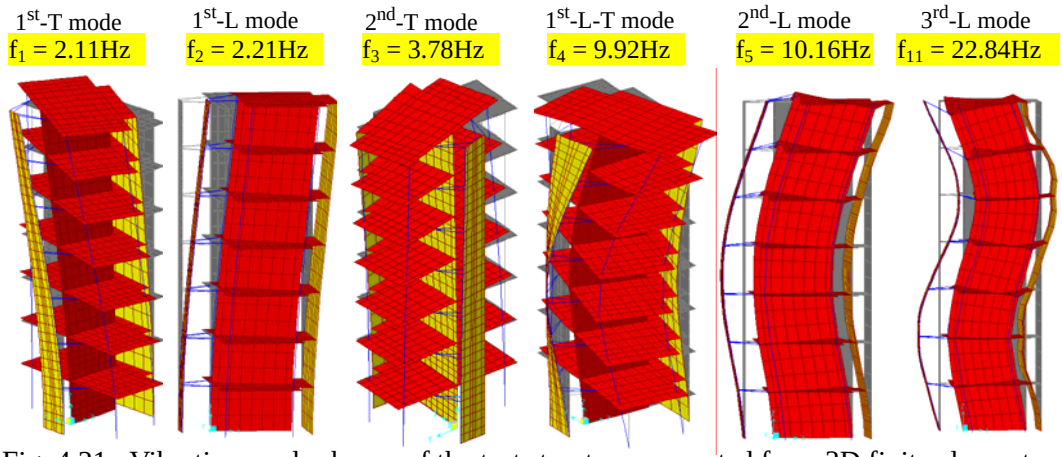

Fig. 4.21 Vibration mode shapes of the test structure computed from 3D finite element model

4.6 CONCLUSIONS

A full-scale seven-story reinforced concrete shear wall building slice was tested on the UCSD-NEES shake table in the period October 2005 - January 2006. The shake table tests were designed so as to damage the building progressively through several historical seismic motions reproduced on the shake table. At various levels of damage, several low amplitude white noise base excitations were applied through the shake table to the building which responded as a quasi-linear system with modal parameters depending on the level of structural damage. Six different state-of-the-art system identification methods including three output-only and three input-output methods were used to estimate the modal parameters (natural frequencies, damping ratios, and mode shapes) of the building in its undamaged (baseline) and various damage states based on the response of the building to ambient as well as white noise base excitation measured using both accelerometers and linear variable displacement transducers (LVDTs).

From the results of this system identification study, it is observed that: (1) The natural frequencies identified using different methods are reasonably consistent at each damage state, while the identified damping ratios exhibit much larger variability across system identification methods. (2) The natural frequencies identified based on white noise test data decrease with increasing level of damage except from damage state S3.1 to S3.2, during which the steel braces were stiffened, while only the longitudinal modal frequencies identified based on ambient vibration data decrease consistently with increasing level of structural damage. This can be explained by the fact that under low amplitude ambient vibration conditions, concrete cracks do not open as much as under forced base excitation and therefore damage does not affects the identified modal parameters of some vibration modes. (3) At each damage state, the identified modal parameters of the first longitudinal mode appear to be the least sensitive to the identification method used, which is most likely due to the predominant contribution of this mode to the total response. (4) The first longitudinal modal frequency identified based on white noise test acceleration data is systematically lower than its counterpart identified based on ambient vibration acceleration data at all damage states considered. This is most likely due to the fact that the test structure is nonlinear (even at the relatively low levels of excitation considered in this system identification study) with effective modal parameters depending on the amplitude of the excitation and therefore of structural response.

In order to further validate and better understand the modal parameters identified from ambient vibration and white noise base excitation test data, a three-dimensional linear elastic finite element model of the shear wall test structure was developed in SAP2000.

The natural frequencies and mode shapes computed from the finite element model are in reasonably good agreement with their identified counterparts (especially when modal identification is based on the ambient vibration data) for the first three longitudinal and the first two torsional vibration modes of the test structure in its undamaged state (damage state S0).

The results obtained in this study provide the input to a damage identification method making use of a sensitivity-based finite element model updating strategy, which is the subject of ongoing research by the authors.

ACKNOWLEDGEMENTS

Partial support of this research by Lawrence Livermore National Laboratory with Dr. David McCallen as Program Leader and by the Englekirk Center Industry Advisory Board are gratefully acknowledged. Any opinions, findings, and conclusions or recommendations expressed in this material are those of the authors and do not necessarily reflect those of the sponsors.

REFERENCES

Allemang, R. J., and Brown, D. L. (1982). “A correlation coefficient for modal vector analysis.” *Proc. of 1st International Modal Analysis Conference, IMAC I,* Bethel, Connecticut.

Brincker, R., Ventura, C., and Andersen, P. (2001). “Damping estimation by frequency domain decomposition.” *Proc. of International Modal Analysis Conference, IMAC XIX*, Kissimmee, USA.

Computers and Structures, Inc. (2004). *SAP 2000 linear and nonlinear, static and dynamic analysis and design of three-dimensional structures: Getting started (Version 9),* Berkeley, California, USA.

De Callafon, R. A., Moaveni, B., Conte, J. P., He, X., and Udd, E. (2007). “General realization algorithm for modal identification of linear dynamic systems.” *Journal of Engineering Mechanics,* ASCE, under review.

Doebling, S. W., Farrar, C. R., Prime, M. B., and Shevitz, D. W. (1996). *Damage identification in structures and mechanical systems based on changes in their vibration characteristics: a detailed literature survey.* Los Alamos National Laboratory Report, LA-13070-MS, Los Alamos, New Mexico, USA.

Doebling, S. W., Farrar, C. R., and Prime, M. B. (1998). “A summary review of vibration-based damage identification methods.” *The Shock and Vibration Digest*, 30(2), 99-105.

James, G. H., Carne, T. G., and Lauffer, J. P. (1993). *The natural excitation technique for modal parameters extraction from operating wind turbines*. Sandia National Laboratories Report, SAND92-1666, UC-261, Sandia, New Mexico, USA.

Juang, J. N., and Pappa, R. S. (1985). “An eigensystem realization algorithm for model parameter identification and model reduction.” *J. Guidance Control Dyn.,* 8(5), 620-627.

Lus, H., Betti, R., and Longman, R. W. (2002). “Obtaining refined first order predictive

models of linear structural systems." *Earthquake Eng. Struct. Dyn.*, 31(7), 1413–1440.

Panagiotou, M., Restrepo, J. I., and Conte, J. P. (2007). *Shake table test of a 7-story full scale reinforced concrete structural wall building slice, Phase I: Rectangular section*. Report No. SSRP-07/07, Department of Structural Engineering, University of California, San Diego.

Phan, M., Horta, L. G., Juang, J.-N., and Longman, R. W. (1992). *Identification of linear systems by an asymptotically stable observer.* NASA Tech. Paper, 3164.

Sohn, H., Farrar, C. R., Hemez, F. M., Shunk, D. D., Stinemates, D. W., and Nadler, B. R. (2003). *A review of structural health monitoring literature: 1996-2001*. Los Alamos National Laboratory Report, LA-13976-MS, Los Alamos, New Mexico, USA.

Van Overschee, P., and de Moore, B. (1996). *Subspace identification for linear systems*, Kluer Academic Publishers, Massachusetts, USA.

CHAPTER 5

DAMAGE IDENTIFICATION OF A COMPOSITE BEAM USING FINITE ELEMENT MODEL UPDATING

5.1 INTRODUCTION

In recent years, structural health monitoring has received increased attention in the civil engineering research community with the objective to identify structural damage at the earliest possible stage and evaluate the remaining useful life (damage prognosis) of structures. Vibration-based, non-destructive damage identification is based on changes in dynamic characteristics (e.g., modal parameters) of a structure as a basis for identifying structural damage. Experimental modal analysis (EMA) has been used as a technology for identifying modal parameters of a structure based on its measured vibration data. It should be emphasized that the success of damage identification based on EMA depends strongly on the accuracy and completeness of the identified structural dynamic properties. Extensive literature reviews on vibration-based damage identification were provided by Doebling et al. (1996 and 1998) and Sohn et al. (2003).

Damage identification consists of detecting the occurrence of damage, localizing the damage zones, and estimating the extent of damage. Numerous vibration-based methods have been proposed to achieve these goals. Salawu (1997) presented a review on the

use of changes in natural frequencies for damage detection only. However, it is in general impossible to localize damage (i.e., obtain spatial information on the structural damage) from changes in natural frequencies only. Pandey et al. (1991) introduced the concept of using curvature mode shapes for damage localization. In their study, by using a cantilever and a simply supported analytical beam model, they demonstrated the effectiveness of employing changes in curvature mode shapes as damage indicator for detecting and localizing damage. Bernal and Gunes (2004) have incorporated changes in modal flexibility matrices (or flexibility proportional matrices) into the damage locating vector (DLV) technique to localize damage. Recently, Adeli and Jiang (2006a) presented a novel multi-paradigm dynamic time-delay fuzzy wavelet neural network (WNN) model for non-parametric identification of structures using the nonlinear auto-regressive moving average with exogenous inputs (NARMAX) approach. Jiang and Adeli (2005, 2006b) applied this WNN model to high-rise building structures, for both nonlinear system and damage identification. Methods based on changes in identified modal parameters to detect and localize damage have also been further developed for the purpose of damage quantification. Among these methods are strain-energy based methods (Shi et al., 2002) and the direct stiffness calculation method (Maeck and De Roeck, 1999). Another class of sophisticated methods consists of applying sensitivity-based finite element (FE) model updating for damage identification (Friswell and Mottershead 1995). These methods update the physical parameter of a FE model of the structure by minimizing an objective function expressing the discrepancy between analytically predicted and experimentally identified features that are sensitive to damage such as natural frequencies and mode shapes. Optimum solutions of the problem are reached through sensitivity-based optimization algorithms. In recent

years, sensitivity-based FE model updating techniques have been applied successfully for condition assessment of structures (Teughels and De Roeck, 2004).

The study presented in this paper, which is an extension of an already published conference paper (Moaveni et al. 2006), leveraged a full-scale sub-component experiment conducted in the Charles Lee Powell Structural Research Laboratories at the University of California, San Diego (UCSD). As payload project attached to a quasi-static test of a full-scale composite beam, the authors acquired a high-quality set of low-amplitude vibration response data from the beam at various damage levels. The Eigensystem Realization Algorithm (ERA) (Juang and Pappa, 1985) was applied to identify the modal parameters (natural frequencies, damping ratios, displacement and macro-strain mode shapes) of the composite beam based on its impulse responses recorded in its undamaged and various damaged states using accelerometers and long-gage fiber Bragg grating strain sensors. These identified modal parameters are presented and compared at different levels of damage. They are then used to identify damage in the beam using a sensitivity-based finite element model updating procedure.

5.2 COMPOSITE BEAM EXPERIMENT

The designed I-5/Gilman Advanced Technology Bridge is a 137*m* (450*ft*) long cable-stayed bridge supported by a 59*m* (193*ft*) high A-frame pylon, and utilizing fiber reinforced polymer (FRP) composite materials. The bridge system is a dual plane, asymmetric cable-stayed design as shown in Figure 5.1. Before the I-5/Gilman Advanced Technology Bridge can be constructed, a Validation Test Program to evaluate the performance

of the bridge was performed. The prototype test program, which was conducted at the Charles Lee Powell Structural Research Laboratories at UCSD, evaluated the manufactured FRP components at the material level, through coupon testing and other non-destructive techniques on the members, and at the element level on full-scale sub-component, connection and system tests (Brestel et al., 2003). The test leveraged in this study was conducted on a full-scale sub-component longitudinal girder of the bridge (Test L2).

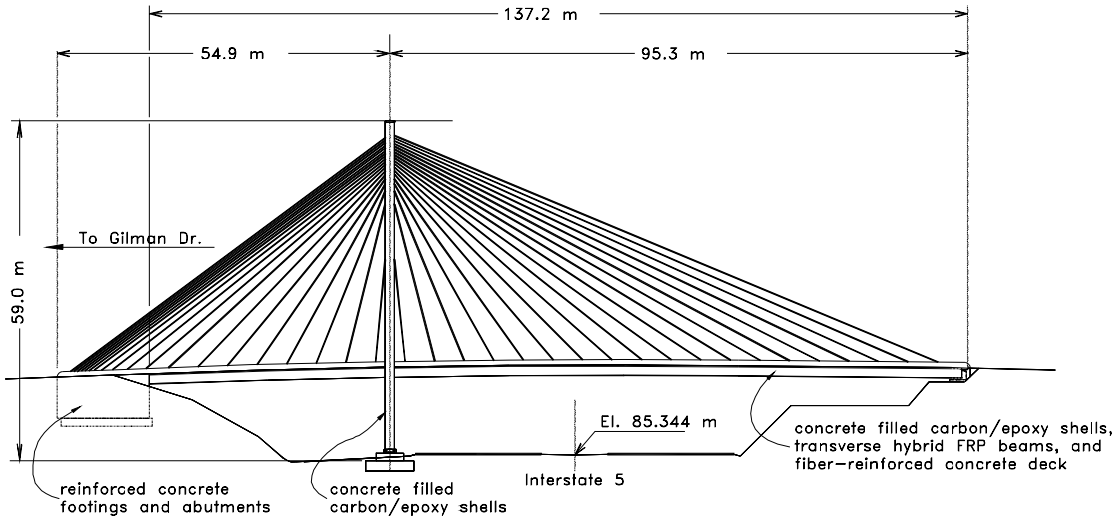

Fig. 5.1 Elevation of I-5/Gilman Advanced Technology Bridge (Brestel et al., 2003)

The objective of this experiment was to validate the design of a concrete-filled composite beam component of the planned I-5/Gilman Advanced Technology Bridge (Seible et al., 1996). For this purpose, uni-directional quasi-static cyclic load tests (i.e., load-unload cycles) of increasing amplitude were applied to the beam, gradually introducing damage. After each of several sequences of loading-unloading cycles, a set of low-amplitude dynamic tests was performed in order to investigate the changes in dynamic characteristics (extracted from the vibration response data) as a function of increasing structural damage. For this purpose, two different sources of dynamic excitation were used, namely (1) a

computer-controlled electro-dynamic shaker, and (2) an impact hammer. The vibration data obtained from the impact tests revealed to be the most informative to identify the beam modal parameters at different levels of damage. The small-strain vibration response data was measured at several damage levels using a set of four long-gage (1*m*) fiber Bragg grating (FBG) strain sensors and a set of eight single channel piezoelectric accelerometers.

5.2.1 Test Setup

The longitudinal girders for the I-5/Gilman Advanced Technology Bridge consist of prefabricated carbon/epoxy shells filled with concrete. In the second phase of the longitudinal girder test program, which is considered in this study, a girder shell specimen (L2) of diameter 0.91*m* (3*ft*) and length 9.75*m* (32*ft*) was cut into two equal halves, spliced together at mid-span with mild steel reinforcement, and filled with concrete (see Figures 5.2 and 5.3).

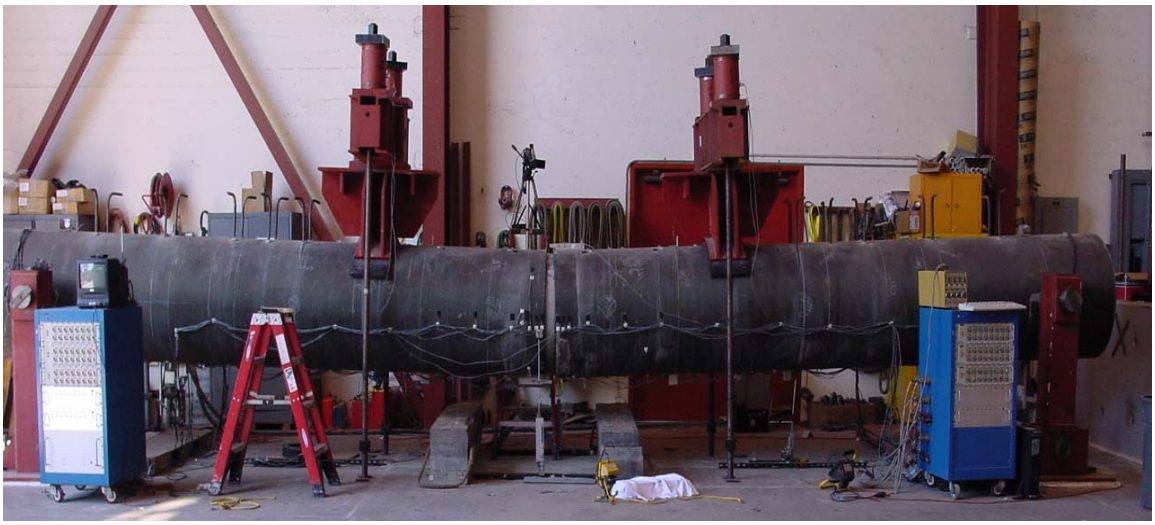

Fig. 5.2 Elevation view of the tested composite beam

The splice using longitudinal steel reinforcement allows a ductile behavior of the connection. In the FRP shell, two rows of 51*mm* (2*in*) diameter holes were drilled along the top edge of the girder and shear stirrups were embedded in the concrete core to provide interfacial shear resistance between the girder and the deck.

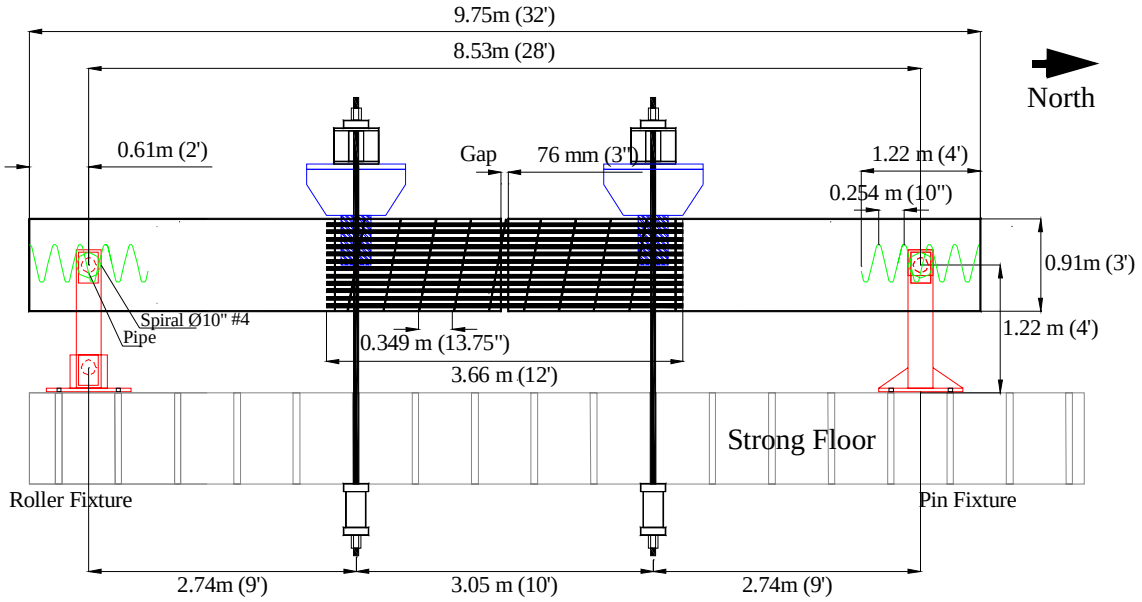

Fig. 5.3 Schematic test setup: Side elevation (Brestel et al., 2003)

A uni-directional quasi-static cyclic loading was applied to the girder using four 1335*kN* (300*kips*) displacement-controlled hydraulic actuators in a four-point bending test (see Figure 5.3). Initially, the girder was loaded to a total of 1000*kN* (225*kip*) to establish a well-lubricated pin connection at the supports of the simply supported girder. The increasing level of the cyclic load progressively introduced damage in the beam through inelastic (irreversible) deformations. The loading history for the test is summarized in Table 5.1 and the plot of the total load applied versus the girder vertical displacement at mid-span is shown in Figure 5.4. The load cycle targets for the initial yield (F_y') and the displacement

ductility levels (μ_Δ = 1.0, 1.5, 2.0, 3.0, 4.0) were determined pre-test from moment-curvature analyses. More details of the test setup are provided by Brestel et al. (2003).

Table 5.1 Loading protocol

Loading Cycle Number	Load Cycle Target	Peak Total Load (kN)
1	1000 kN	1016
2	1000 kN*	
3	F_y'	1779
4	μ_Δ = 1.0	2278
5	μ_Δ= 1.0*	
6	3000 με tensile strain	2713
7	μ_Δ = 1.5	2761
	μ_Δ = 1.5*	
8	μ_Δ = 2.0	3066
	μ_Δ = 2.0*	
9	μ_Δ = 3.0	3516
10	μ_Δ = 3.0	
11	μ_Δ = 3.0	
	μ_Δ = 4.0	3743
12	μ_Δ = 4.0*	

* At the end of these cycles, the load fixtures were removed and a set of dynamic tests were performed.

After load cycles 2, 5, 7, 8, and 12, the loading fixtures were removed to perform a sequence of dynamic tests for system and damage identification studies. This sequence of dynamic tests was performed twice before starting the quasi-static loading cycles and the corresponding undamaged states of the beam are referred to as states S0 and S1. States S2 to S6 refer to the state of the beam after loading cycles 2, 5, 7, 8 and 12, respectively, shown in Figure 5.4. The repeated sequence of dynamic tests consisted of a set of forced vibration tests using a 0.22*kN* (50*lbs)* force electro-dynamic shaker followed by a set of

impact (free vibration) tests using an impact hammer with integrated load cell recording the applied force. The forced vibration tests performed using the shaker consist of a set of sixteen (Gaussian) white noise excitations followed by three (linear) sine sweeps across the frequency ranges 12-22*Hz*, 38-48*Hz*, and 93-103*Hz*, respectively. These three frequency ranges were selected so as to excite the first three vibration modes of the beam, the frequencies of which were predicted using a finite element model of the beam. The free vibration tests conducted using the impact hammer consisted of three vertical impact tests at each of four locations along the top edge of the girder as shown in Figure 5.5. Therefore, a total of 12 vertical impact tests were performed on the beam for each of 7 different states (S0 through S6). It was found that the shaker-induced vibration data were of considerably lower amplitude than the impact response data, resulting in a much lower signal-to-noise ratio. Therefore, the modal identification results presented in this paper are based only on the data collected from the vertical impact tests.

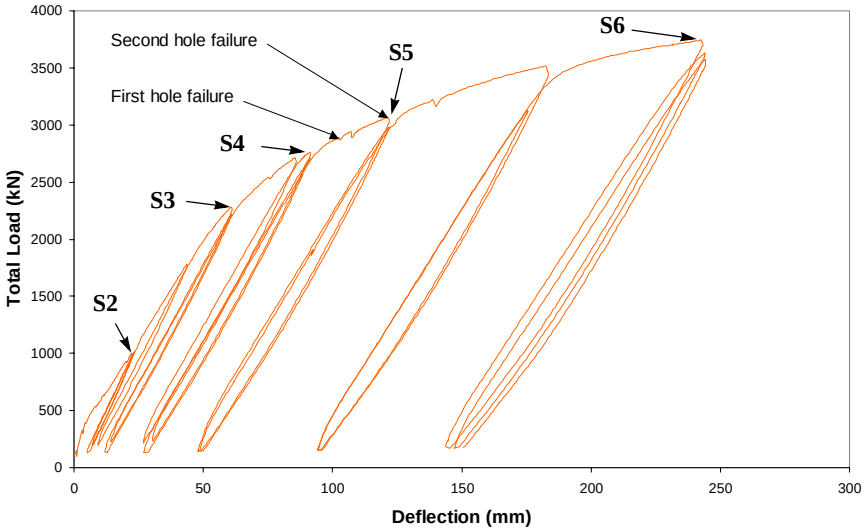

Fig. 5.4 Total load vs. girder vertical displacement at mid-span

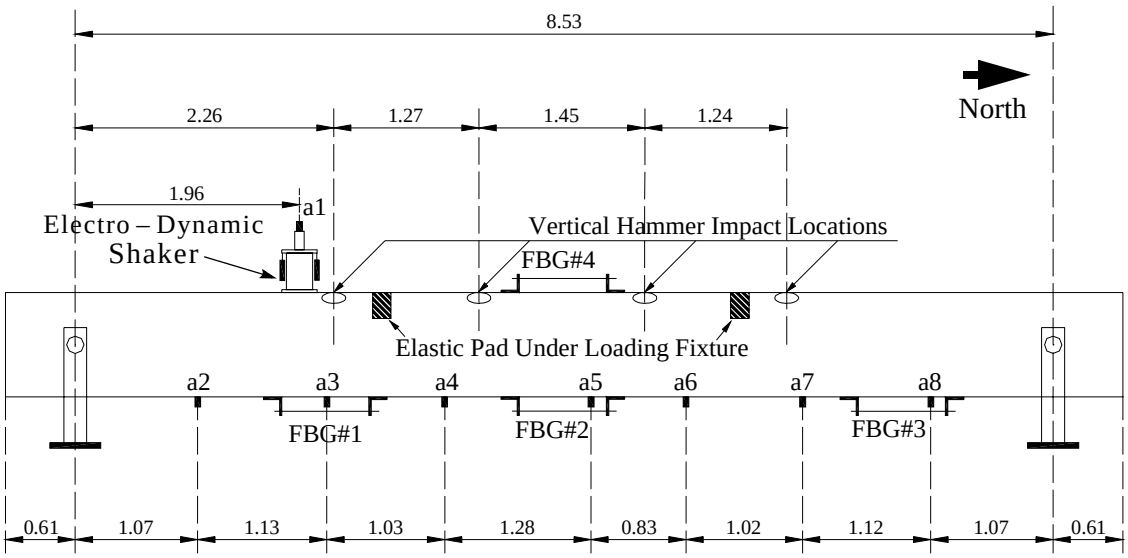

Fig. 5.5 Locations of accelerometers, FBG sensors, vertical hammer impacts and electro-dynamic shaker

5.2.2 Instrumentation

The girder was instrumented with strain gages, linear potentiometers, and inclinometers for the entire duration of the quasi-static cyclic tests. In addition, the girder was instrumented with four long-gage fiber Bragg grating (FBG) strain sensors (1m gage length) and eight accelerometers with the required sensitivity/accuracy for the purpose of the (low-amplitude) payload dynamic tests. The FBG strain sensors were surface mounted using brackets, with a pair of sensors located along the top and bottom of the beam at mid-span, and the remaining two sensors located along the bottom edge of the beam at approximately 1/3 of the beam length on either side of mid-span as shown in Figure 5.5. The FBG strain sensors were pre-strained in their long-gage packages in order to measure compression as well as tension. In addition to the FBG strain sensors, eight accelerometers were attached to the girder specimen to measure vertical acceleration. Seven of these

accelerometers were approximately equally spaced along the bottom edge of the girder and one was mounted on the moving mass of the electro-dynamic shaker to measure the dynamic force applied to the beam (see Figure 5.5). The technical characteristics of the accelerometers are: PCB model 393A03, amplitude range: 5*g* pk, frequency range (10%) 0.3-4000*Hz*, resolution $5 \times 10^{-6} g$ pk, voltage sensitivity 1000*mV/g*, excitation voltage 18 to 30*VDC*. For every dynamic test performed at each of the states S0 through S6, the vibration response of the composite girder was measured by accelerometers a2 through a8, while the four FBG strain sensors measured the vibration response for states S1 through S5 only. Figure 5.6 illustrates the acceleration (left column) and FBG strain (right column) measurements after an impact applied at location 1 (see Figure 5.5) at state S1. Figure 5.7 shows the Fourier Amplitude Spectra (FSA) of two acceleration and two FBG strain measurements for the same impact test.

5.3 IDENTIFICATION OF MODAL PARAMETERS

In this study, the Eigensystem Realization Algorithm (ERA) (Juang and Pappa, 1985) followed by a least squares optimization (De Callafon et al., 2007) was employed for identifying the modal parameters (natural frequencies, damping ratios, displacement and macro-strain mode shapes) of the composite beam in its undamaged and damaged states. The identified modal parameters using ERA are based on the impact test (free vibration) data recorded by the accelerometers or FBG strain sensors, separately. Since two separate data acquisition systems, not time-synchronized and with different sampling rates, were used to collect the acceleration and macro-strain data, it was more convenient

to apply ERA to the two types of measurements separately. A total of 12 vertical impact tests were performed on the beam at each of the 7 states S0 to S6, with states S0 and S1 representing the beam in its undamaged condition. Two different cases of modal identification are performed at each damage state, namely, (1) ERA is applied to a single test data (i.e., one test at a time), and (2) ERA is applied to all 12 impact test data in a single identification.

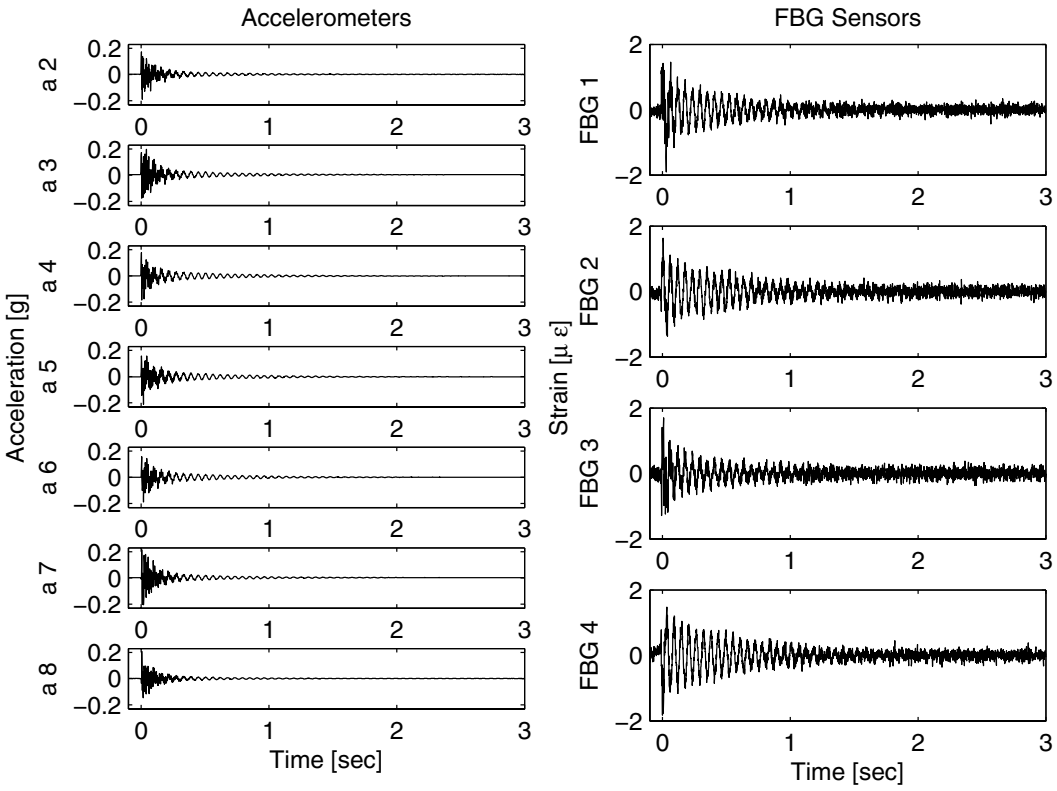

Fig. 5.6 Acceleration and FBG strain measurements during Test 1 at state S1

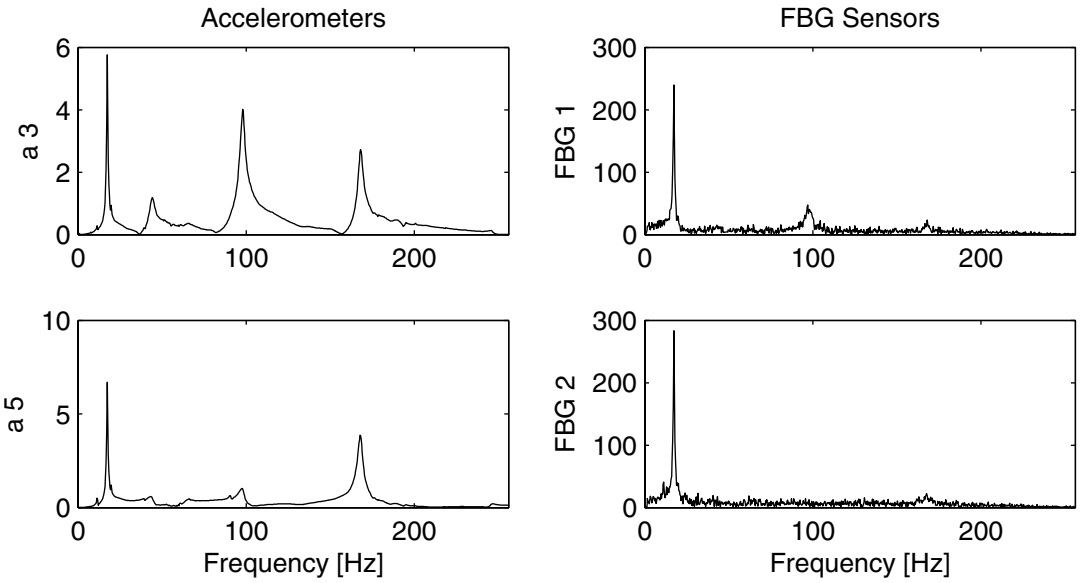

Fig. 5.7 Fourier amplitude spectra of some acceleration and FBG strain measurements during Test 1 at state S1

5.3.1 Identified Modal Parameters Based on Accelerometer Data

Figure 5.8 shows the natural frequencies of the first 5 modes identified using ERA based on accelerometer data for each of $12 \times 7 = 84$ impact tests (each circle corresponds to an identified frequency from one impact test). In each ERA realization (considering one test at a time), a Hankel matrix of size $(7 \times 250) \times 250$ was constructed based on the impulse response data sampled at 512*Hz*. Then, after performing a singular value decomposition, a system of order n = 16 was realized based on the natural frequency stabilization diagram (Peeters and De Roeck, 2001), from which a maximum of 8 physical modes of vibration could be extracted. From Figure 5.8, it is observed that: (1) At each damage state, the modal frequencies identified from each of the 12 impact tests are generally in close agreement. The few cases when an identified modal frequency is not consistent with the others could be explained by a low participation of the corresponding vibration mode

(e.g., impact applied near a modal node) resulting in a low signal-to-noise ratio. (2) As expected, the identified natural frequencies for states S0 and S1 are almost identical, since both sets of results correspond to the undamaged state of the beam. (3) With increasing level of damage in the beam, the identified modal frequencies decrease (with an exception for the 5th mode at state S2), consistent with the stiffness degradation due to damage.

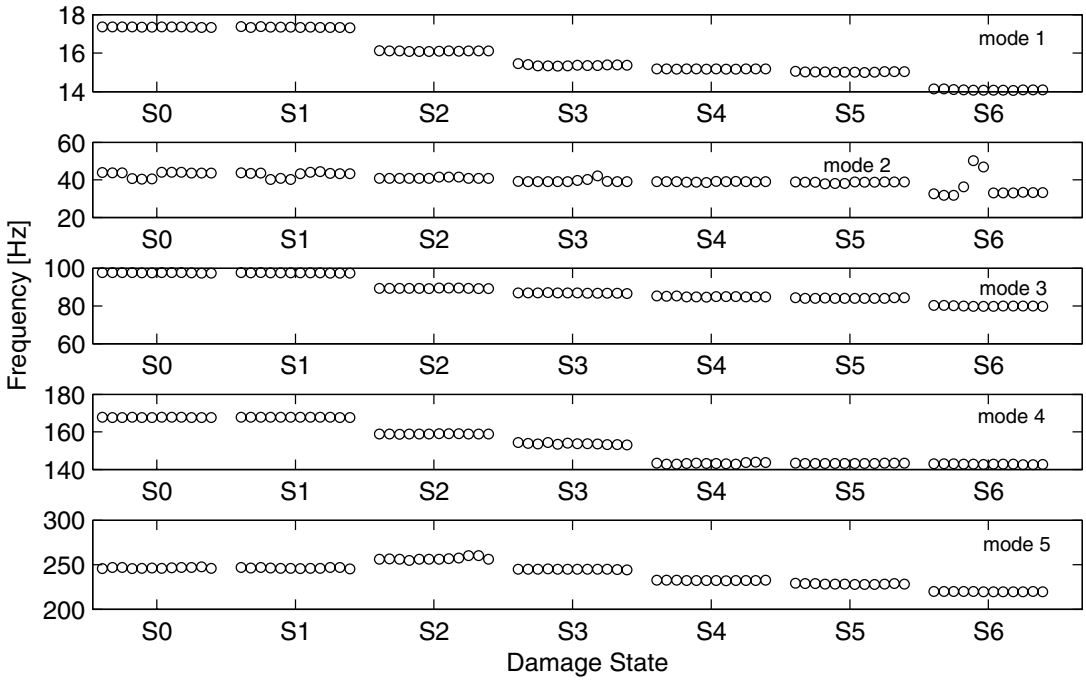

Fig. 5.8 Identified natural frequencies of the first 5 vibration modes using ERA based on acceleration data (12 separate identifications at each damage state)

It should be noted that the changes in the natural frequencies due to structural damage are much more significant than the variability (due to changes in location and amplitude of the impact force as well as the estimation uncertainty) of the identified natural frequencies within one damage state. The statistics (mean and coefficient-of-variation) of the identified modal frequencies (based on 12 identifications) are reported in Table 5.2, while Table 5.3 provides the same statistics for the identified damping ratios. The coefficient-of-varia-

tion of a random variable is defined as the ratio of its standard deviation to its (absolute) mean value.

Table 5.2 Mean [Hz] / coefficient-of-variation [%] of the natural frequencies identified using ERA based on acceleration data for states S0 to S6 (sets of 12 impact tests)

	S0	S1	S2	S3	S4	S5	S6
Mode 1	17.35/0.1	17.34/0.1	16.10/0.1	15.37/0.2	15.17/0.1	15.02/0.1	14.09/0.2
Mode 2	42.97/3.5	42.78/3.5	40.93/0.8	39.47/2.2	38.93/0.5	38.58/0.9	35.68/17.2
Mode 3	97.58/0.1	97.49/0.1	89.26/0.1	86.82/0.2	84.90/0.2	84.05/0.2	79.91/0.2
Mode 4	167.67/0.0	167.72/0.0	158.87/0.1	153.64/0.3	143.23/0.2	143.21/0.1	142.81/0.1
Mode 5	246.42/0.3	246.22/0.3	255.91/0.1	244.85/0.1	232.39/0.1	228.35/0.2	219.80/0.1

Table 5.3 Mean [%] / coefficient-of-variation [%] of the damping ratios identified using ERA based on acceleration data for states S0 to S6 (sets of 12 impact tests)

	S0	S1	S2	S3	S4	S5	S6
Mode 1	1.5/2.7	1.5/3.3	1.6/3.4	1.7/7.3	1.2/3.7	1.3/2.6	1.4/2.4
Mode 2	4.0/47.3	4.1/53.7	2.9/27.9	2.9/89.6	2.2/8.8	2.8/6.8	5.5/77.0
Mode 3	1.7/7.0	1.7/6.1	2.0/6.1	1.7/2.0	2.1/17.1	2.1/28.5	1.7/2.1
Mode 4	0.9/4.0	0.8/2.3	0.9/2.1	1.7/19.3	1.8/9.9	0.9/3.0	1.5/7.9
Mode 5	0.8/82.7	0.7/36.6	0.6/39.3	0.7/16.6	0.8/10.5	0.9/9.1	0.9/11.2

The second case of system identification was performed based on the same acceleration data, but including the data from all twelve impact tests (at each damage state) in a single identification. The basic idea behind this identification strategy is to use simultaneously the information from all impact tests to identify the modal parameters. Therefore, if a single test does not contain significant information about a vibration mode (for example due to its low modal participation), this mode can still be identified well through other

impact test data that are more informative about this mode. For this purpose, ERA is applied in its multiple input, multiple output (MIMO) formulation (Juang and Pappa, 1985), but instead of forming the Hankel matrix based on free vibration data from a truly multiple input test, the block Hankel matrix is formed by including the response measurements from (r) single input impact tests as

$$\mathbf{H} = \begin{bmatrix} \begin{bmatrix} \mathbf{g}^1(1) & \dots & \mathbf{g}^r(1) \\ \mathbf{g}^1(2) & \dots & \mathbf{g}^r(2) \\ \dots & \dots & \dots \\ \mathbf{g}^1(N) & \dots & \mathbf{g}^r(N) \end{bmatrix} & \begin{bmatrix} \mathbf{g}^1(2) & \dots & \mathbf{g}^r(2) \\ \mathbf{g}^1(3) & \dots & \mathbf{g}^r(3) \\ \dots & \dots & \dots \\ \mathbf{g}^1(N+1) & \dots & \mathbf{g}^r(N+1) \end{bmatrix} & \dots \\ \dots & \begin{bmatrix} \mathbf{g}^1(N) & \dots & \mathbf{g}^r(N) \\ \mathbf{g}^1(N+1) & \dots & \mathbf{g}^r(N+1) \\ \dots & \dots & \dots \\ \mathbf{g}^1(2N-1) & \dots & \mathbf{g}^r(2N-1) \end{bmatrix} & \end{bmatrix} \quad (5.1)$$

where $\mathbf{g}^i(k)$ denotes the impulse response vector (at time $t = k\Delta T$) from the i^{th} impact test. In this case, the block Hankel matrix was built including the data from all 12 impact tests (r = 12) at each damage state. A model of order n = 16 (from which a maximum of 8 physical vibration modes could be extracted) was realized from the data, and then the modal parameters were extracted from this state-space model. The natural frequencies and damping ratios identified using this approach are reported in Table 5.4 for all damage states considered. Figure 5.9 shows the normalized mode shapes (projection of complex mode shapes on the real axis) corresponding to state S1 (undamaged state of the beam). In Figure 5.9, the circles correspond to the identified mode shape at the sensor locations and the dashed lines represent cubic spline interpolation through the circles. It should be noted that, due to flexibility of the support structures relative to the beam, the mode shapes of the beam-support system are generally not zero at the support locations. The equivalent

stiffness of the two support structures was calculated based on their geometric and material properties and was included in the FE model of the beam-support system.

Table 5.4 Natural frequencies [Hz] and damping ratios [%] identified using ERA based on acceleration data at states S0 to S6 (all 12 impact tests considered in a single identification)

	Mode 1		Mode 2		Mode 3		Mode 4		Mode 5	
	Freq. [Hz]	Damping Ratio [%]	Freq. [Hz]	Damping Ratio [%]	Freq. [Hz]	Damping Ratio [%]	Freq. [Hz]	Damping Ratio [%]	Freq. [Hz]	Damping Ratio [%]
S0	17.35	1.5	43.48	4.3	97.57	1.7	167.70	0.8	246.63	0.4
S1	17.34	1.5	43.24	4.6	97.50	1.7	167.74	0.8	246.16	0.5
S2	16.09	1.7	40.72	2.7	89.24	2.0	158.90	0.9	254.51	1.1
S3	15.35	1.7	39.09	2.0	86.80	1.7	153.32	1.8	244.72	0.6
S4	15.17	1.3	38.91	2.2	84.82	2.2	143.24	1.3	232.25	0.8
S5	15.00	1.3	38.98	3.2	84.12	1.9	143.20	0.9	227.94	0.9
S6	14.08	1.4	33.04	2.1	79.93	1.7	142.84	1.4	219.71	0.9

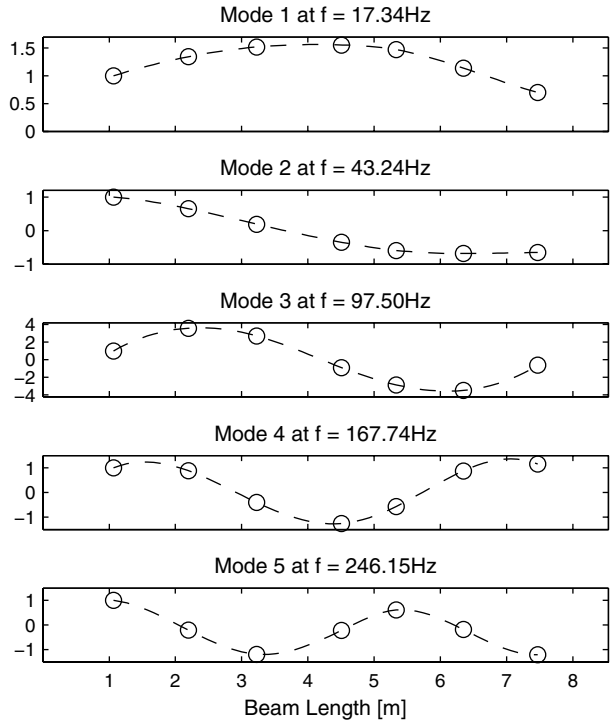

Fig. 5.9 Normalized (real) mode shapes of the composite beam at state S1

Figure 5.10 plots the identified complex-valued mode shapes in polar plots (i.e., complex plane). This representation indicates the degree of non-proportional damping of a vibration mode. If the components (each representing an observed degree of freedom) of a complex-valued mode shape are collinear (i.e., in phase or out of phase), then this mode is classically (or proportionally) damped. Scattering of the components of a mode shape in the complex plane indicates that the mode is non-classically damped. From Figure 5.10, it is observed that the first four identified modes are classically damped and the fifth identified mode is non-classically damped. It should be noted that due to low signal-to-noise ratio and/or identification or modeling errors, a truly classically-damped mode could be identified as non-classically damped.

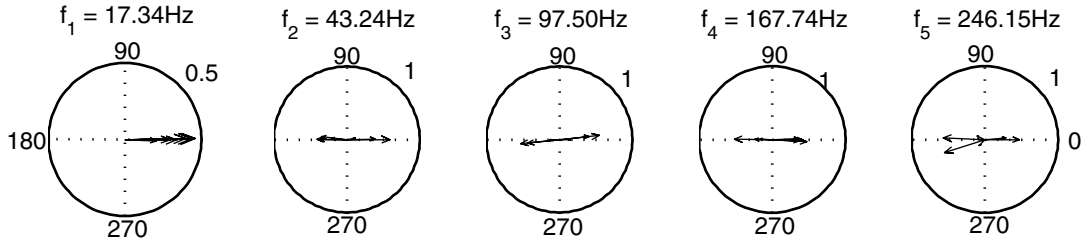

Fig. 5.10 Complex-valued (displacement) mode shapes in polar plots at state S1

Figure 5.11 provides a comparison of the impulse response (impact applied at location 1) simulated using the realized model with the corresponding response measured by accelerometers a2, a4 and a6 (see Figure 5.5) at state S1, and the modal decomposition of the simulated acceleration impulse response. This modal decomposition is obtained from the realized model of the system (De Callafon et al., 2007). This figure shows that: (1) the simulated and measured impulse responses are in excellent agreement, indicating the accuracy of the realized model, and (2) the fifth vibration mode does not contribute signif-

icantly to the total response of the system and is therefore characterized by a lower signal-to-noise ratio than the other modes. This could explain the non-classical damping characteristics identified for the fifth mode (see Figure 5.10). The first four mode shapes identified (from a single state-space model realized based on all twelve impact test data) at three increasing levels of damage (S0, S2 and S4) are shown in Figure 5.12. It is observed that the damage-induced changes in these mode shapes are small. However, as shown in the damage identification section, these small changes in some of the mode shapes are sufficient to identify (localize) damage based on finite element model updating.

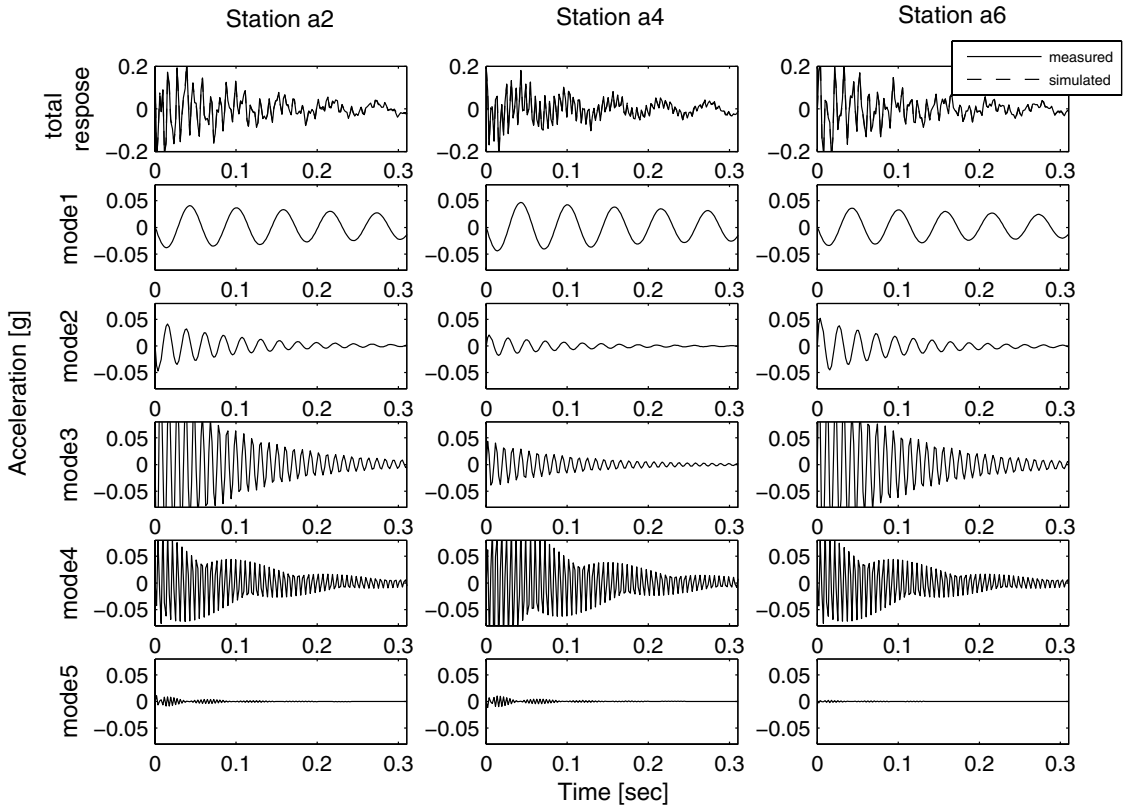

Fig. 5.11 Modal decomposition of impulse response measured by accelerometers a2, a4 and a6 at state S1

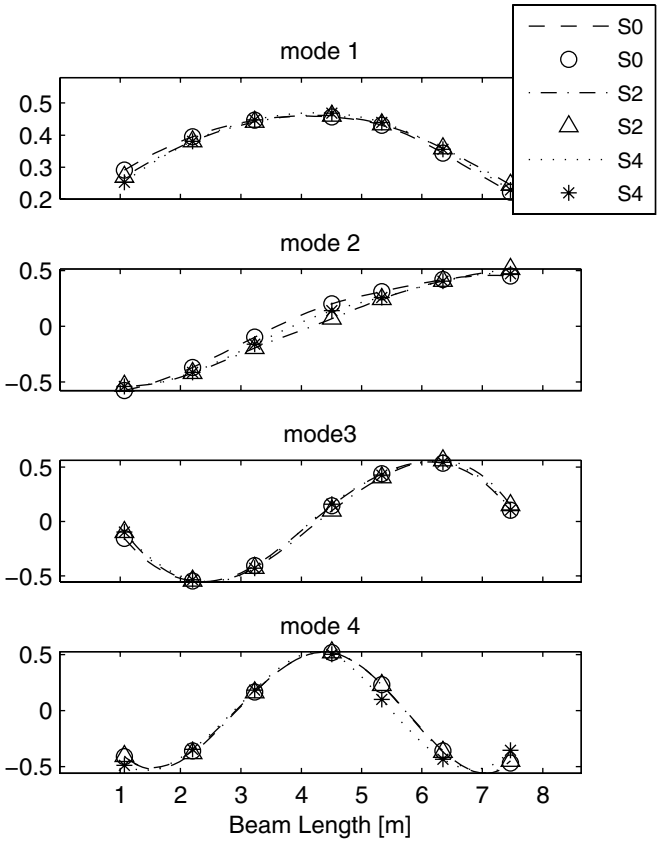

Fig. 5.12 Normalized (real) mode shapes of the composite beam at states S0, S2 and S4

5.3.2 Identified Modal Parameters Based on FBG Strain Sensor Data

The impulse response data transduced from the FBG strain sensors were also used to identify the modal parameters of the composite beam in the two identification cases defined in Section 3. Figure 5.13 shows the natural frequencies identified using ERA based on impact test data measured from the four FBG sensors at states S1 to S5. It should be recalled that the FBG strain sensors were not available during the dynamic tests performed at the first and last damage states of the beam (S0 and S6). From Figure 5.13, it is observed that some of the vibration modes cannot be identified from some impact tests. For example, at state S4, the second and fourth modal frequencies could not be identified

and also the third mode was only identified for the first three and last three of the 12 impact tests (impacts at locations one and four in Figure 5.5).

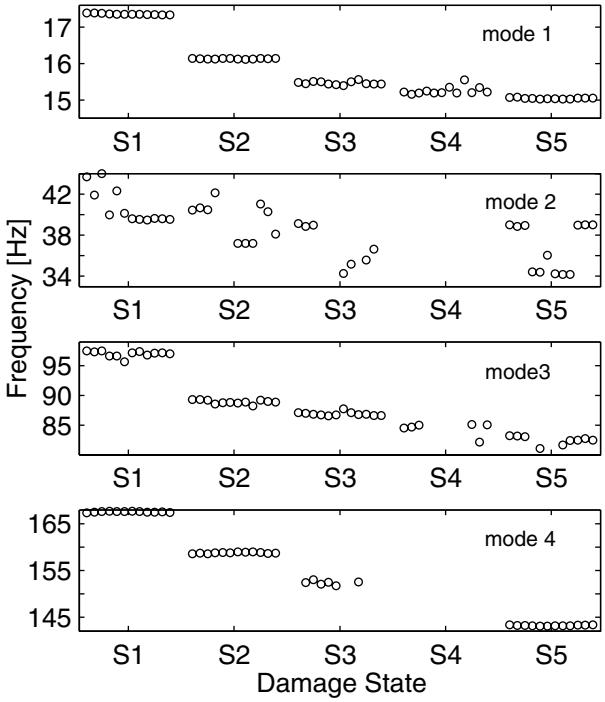

Fig. 5.13 Identified natural frequencies of the first 4 modes using ERA based on FBG sensor data at states S1-S5 (12 identifications at each damage state)

Table 5.5 provides the statistics (mean and coefficient-of-variation) of the identified modal frequencies based on sets of 12 impact tests (considered one at a time) at beam states S1 through S5. By comparing the identified modal frequencies obtained from accelerometer data with those obtained from FBG strain sensor data, it is observed that the second natural frequency is identified with less variability from acceleration data than from macro-strain data, and the fifth natural frequency can only be identified from the acceleration data. Table 5.6 reports the natural frequencies and damping ratios identified at states S1 to S5 based on all 12 impact test FBG sensor data considered at once. It is observed that

these identified natural frequencies and damping ratios are in good agreement with their counterparts obtained from acceleration data (see Table 5.4), except for the second mode.

Table 5.5 Mean [Hz] / coefficient-of-variation [%] of the natural frequencies identified using ERA based on FBG sensor macro-strain data at states S1 to S5 (sets of 12 impact tests)

	S1	S2	S3	S4	S5
Mode 1	17.35/0.1	16.13/0.1	15.46/0.3	15.25/0.7	15.04/0.1
Mode 2	40.77/4.2	39.46/4.7	36.94/5.5	NA	36.76/6.4
Mode 3	96.98/0.5	88.89/0.4	86.86/0.4	84.39/1.4	81.12/3.4
Mode 4	167.56/0.1	158.77/0.1	152.35/0.3	NA	143.19/0.1

Table 5.6 Natural frequencies [Hz] and damping ratios [%] identified using ERA based on FBG sensor macro-strain data at states S1 to S5 (all 12 impact tests considered in a single identification)

	Mode 1		Mode 2		Mode 3		Mode 4	
	Frequency [Hz]	Damping Ratio [%]	Frequency [Hz]	Damping Ratio [%]	Frequency [Hz]	Damping Ratio [%]	Frequency [Hz]	Damping Ratio [%]
S1	17.35	1.5	39.52	1.1	97.29	1.6	167.66	0.8
S2	16.12	1.6	37.13	0.6	89.06	2.0	158.86	0.9
S3	15.45	1.6	NA	NA	86.76	1.7	NA	NA
S4	15.17	1.0	NA	NA	NA	NA	NA	NA
S5	15.07	1.1	34.23	0.7	81.07	1.5	143.10	1.0

The corresponding identified macro-strain mode shapes are represented in polar plots in Figure 5.14 for state S1. The fact that vibration modes 2, 3, and 4 are identified as non-classically damped could be due to the low contribution of these modes to the total response. Figure 5.15 shows the identified macro-strain mode shapes projected on the real axis and normalized to a unit length for states S1, S2, S3 and S5. The second and fourth macro-strain modes could not be identified at state S3. From Figure 5.15, it is observed that the macro-strain mode shapes at FBG sensor #2 (see Figure 5.5) change significantly

due to damage beyond state S2. Figure 5.16 shows a comparison of the impulse response (impact applied at location 1) simulated using the realized model with the corresponding response measured by the four FBG strain sensors at state S1, and the modal decomposition of the simulated beam macro-strain impulse response. This figure indicates clearly that: (1) the simulated and measured impulse responses are in very good agreement, validating the accuracy of the realized model, and (2) the contributions of modes 2, 3 and 4 to the total impulse response are much smaller than that of the first mode.

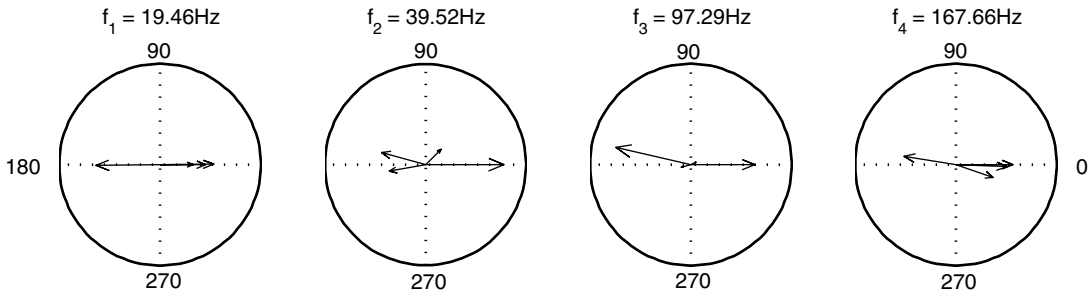

Fig. 5.14 Complex-valued macro-strain mode shapes in polar plots at state S1

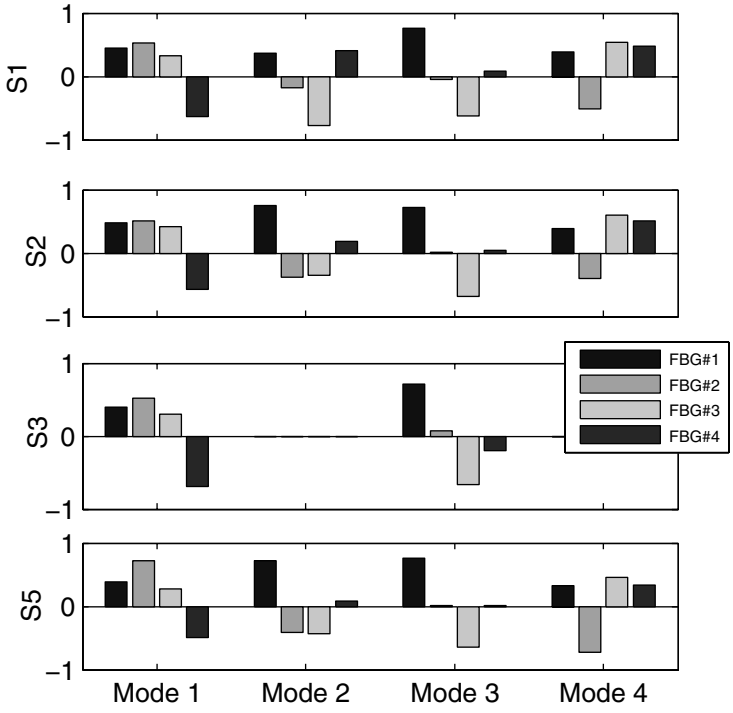

Fig. 5.15 Normalized macro-strain mode shapes for states S1, S2, S3 and S5

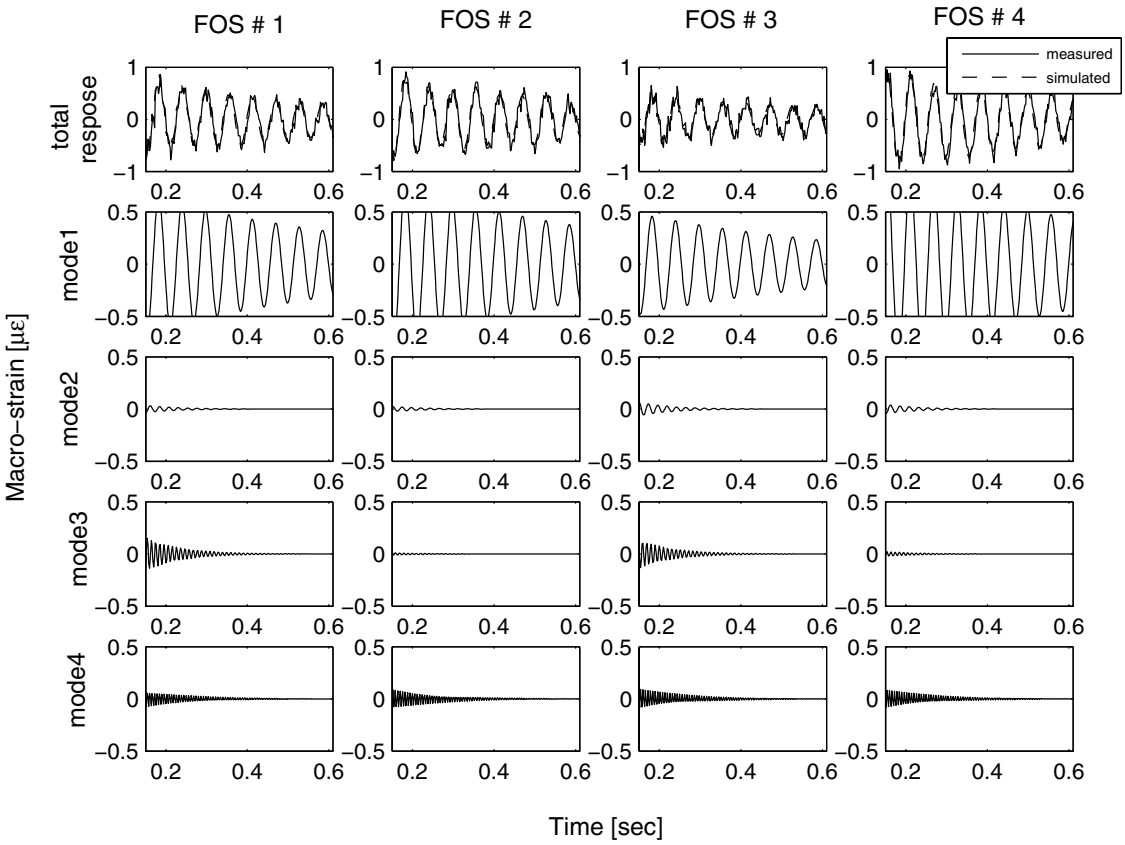

Fig. 5.16 Modal decomposition of impulse response measured by FBG strain sensors 1 to 4 at state S1

5.4 SENSITIVITY OF IDENTIFIED MODAL PARAMETERS TO DAMAGE

This section investigates the changes in identified natural frequencies and modal assurance criterion (MAC) values (between corresponding mode shapes in undamaged and damaged states) with increasing level of damage in the beam. MAC values are bounded between 0 and 1 and measure the degree of correlation between corresponding mode shapes in the undamaged and damaged states (MAC value of 1 for unchanged mode shapes). Based on the force-displacement curve for the quasi-static tests shown in Figure

5.4, the global tangent stiffness K of the beam structure is determined at several points corresponding to states S0 to S6 along the envelope curve of the hysteresis loops. The normalized changes in tangent stiffness ΔK_{Si} and normalized changes in modal frequencies Δf_{Si}^{k} are defined respectively as

$$\Delta K_{Si} = \frac{K_{S0} - K_{Si}}{K_{S0}}, \qquad \Delta f_{Si}^{k} = \frac{f_{S0}^{k} - f_{Si}^{k}}{f_{S0}^{k}} \tag{5.2}$$

in which the subscript Si denotes the damage state of the beam (e.g., S0, S1, ..., S6), K_{Si} represents the tangent stiffness at state Si, and f_{Si}^{k} denotes the identified natural frequency of the k^{th} vibration mode at state Si. The normalized changes in tangent stiffness and natural frequencies are plotted in Figure 5.17 versus the damage level (S0-S6).

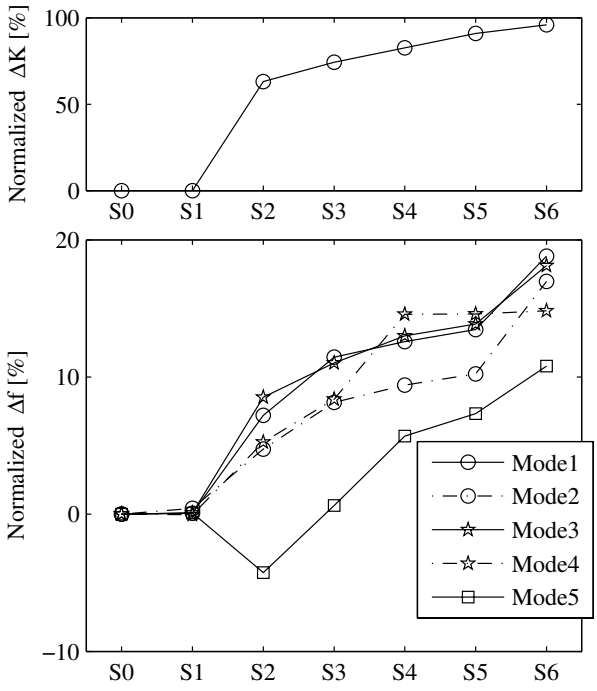

Fig. 5.17 Normalized changes in tangent stiffness (top plot) and natural frequencies (bottom plot) versus damage level

It is observed that with increasing level of damage, the tangent stiffness and natural frequencies of the first five identified modes decrease monotonically, with an exception for the 5th mode at state S2. MAC values are calculated between the identified mode shapes at each state of the beam (S0-S6) and the corresponding mode shapes at the undamaged state (S0) of the beam. Figure 5.18 displays the calculated MAC values for the first four vibration modes identified at states S0 to S6 (top plot) and the relative changes of these MAC values, $\Delta MAC = 1 - MAC_{Si}^{k}$, as a function of damage level (bottom plot).

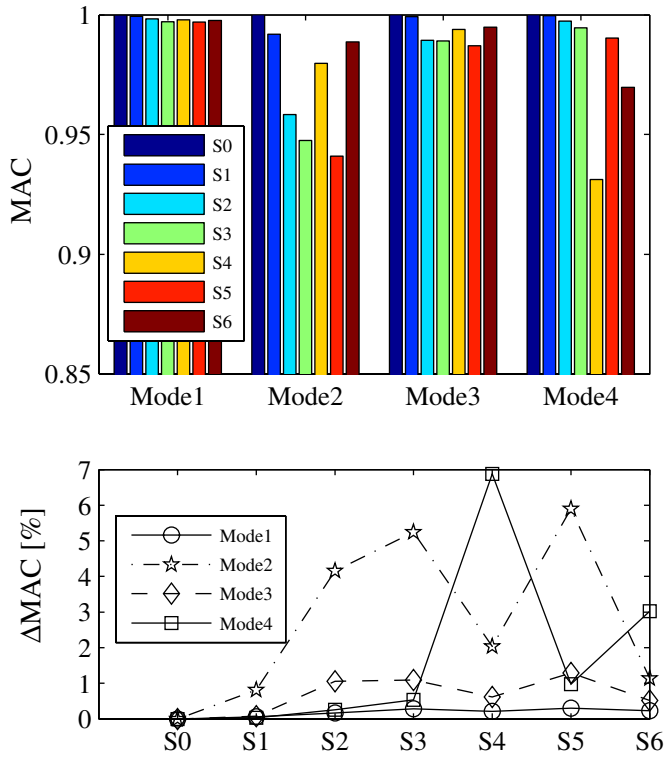

Fig. 5.18 MAC values (top plot) and their relative changes (bottom plot) at different damage levels

From this figure, it is observed that: (1) the MAC value of the first mode has the least sensitivity to damage, while the MAC value of the second mode is the most sensitive to damage, which is consistent with the observed changes in normalized displacement mode

shapes shown in Figure 5.12. (2) The MAC values obtained at states S4 and S6 are outliers of the trend between MAC value and damage level. From the changes in modal frequencies and MAC values, it is possible to detect the presence of damage, but it is very difficult (if not impossible) to determine the location and extent of damage, since both of these indicators are global in nature (i.e., aggregated quantities).

5.5 DAMAGE IDENTIFICATION BASED ON FINITE ELEMENT MODEL UPDATING

Based on the identified modal parameters of the composite beam, an element-by-element sensitivity-based finite element (FE) model updating approach (Conte and Liu, 2001; Teughels and De Roeck, 2004) was used to identify (detect, localize and quantify) the damage in the beam at various damage levels. Two separate cases of damage identification were performed using FE model updating: (1) the residuals used in the updating process are based on the natural frequencies and displacement mode shapes identified from the accelerometer data, and (2) the residuals used in the updating process are based on the natural frequencies, displacement mode shapes identified from the accelerometer data, and macro-strain mode shapes identified from the FBG strain sensor data. In both cases, damage in the beam at the various damage levels is identified as a change in stiffness (modulus of elasticity) in the finite elements. For this purpose, a linear elastic FE model of the composite beam was developed in FEDEASLab (Filippou, 2004) using 10 Bernoulli-Euler beam elements for the composite beam (elements 1 to 10) and two truss elements to model the flexible end supports (elements 11 and 12) as shown in Figure 5.19.

Both truss elements are pinned at their base (nodes 12 and 13) and the top node (node 2) of the left support (element 11) is restrained in the horizontal direction (along the beam). Nodes 3 to 9 are at the location of accelerometers a2 to a8 along the beam (see Figure 5.19). The beam elements (1-10) are assumed to have a constant mass density of 2320 Kg/ m^3, while no mass is assigned to the truss elements (11-12). The element section properties are reported in Table 5.7, where A and I denote the assigned cross-section area and moment of inertia, respectively. These two section properties are equivalent section properties accounting for the concrete (confined), composite, and steel (longitudinal reinforcement) materials. Elements 4-7 have a larger cross-section area to account for the longitudinal steel reinforcement at half-span (see Figure 5.3). The first step to identify damage in the beam is to obtain a reference (baseline) FE model based on the modal parameters identified at the undamaged state of the beam (state S1).

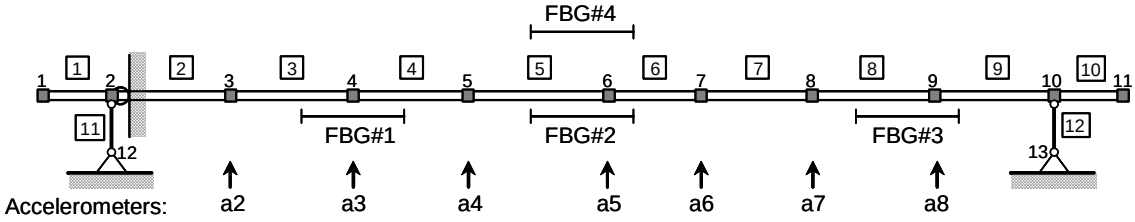

Fig. 5.19 Finite element model of the beam in FEDEASLab showing element and node numbers, locations of accelerometers, and FBG strain sensors

Table 5.7 Element section properties for all 12 elements (El.)

	El. 1	El. 2	El. 3	El. 4	El. 5	El. 6	El. 7	El. 8	El. 9	El. 10	El. 11	El. 12
E^{ref} [GPa]	2.76	51.71	59.15	38.41	42.06	32.31	50.91	38.68	51.71	2.76	57.18	132.92
A [m^2]	0.732	0.732	0.732	0.872	0.872	0.872	0.872	0.732	0.732	0.732	0.0026	0.0026
I [m^4]	0.0298	0.0298	0.0298	0.0436	0.0436	0.0436	0.0436	0.0298	0.0298	0.0298	0	0

In this study, the reference model was obtained through updating the moduli of elasticity of all 12 elements from their nominal values using residuals based on the natural frequencies and displacement mode shapes of the first five modes identified from accelerometer data. The updated values for the moduli of elasticity in the reference model (E^{ref}) for all 12 elements are also reported in Table 5.7. It should be noted that the updating parameters (moduli of elasticity) act as effective moduli of elasticity reflecting the overall stiffness of the structure, including the contributions of the structural components that are not directly (or accurately) represented in the FE model or the parameters of which are not updated. The low (unrealistic) values of the effective moduli of elasticity found for elements 1 and 10 are due to: (1) the fact that the confinement of the composite shell is much less effective at the ends of the beam than along the beam, and (2) the fact that the selected residuals are not sensitive to the updating parameters of elements 1 and 10. The lack of symmetry in the calibrated effective moduli of elasticity of the beam elements can be due to variability in the quality of concrete and concrete filling within the composite shell. After a reference/ baseline model is obtained, the effective moduli of elasticity of elements 3, 4, 5, 6, 7, 8, 11 and 12 (total of 8 elements) are updated at states S2 to S6 through minimization of an objective function. It should be noted that elements 1 and 10 are located outside of the two supports and therefore did not experience any damage during the quasi-static loading of the beam. In addition, the modal parameters used in the updating process (natural frequencies, displacement and macro-strain mode shapes) are lowly sensitive to changes in the moduli of elasticity of elements 2 and 9. Also, since there were no sensors between nodes 3 and 12 (foot of left support) as well as between nodes 9 and 13 (foot of right support),

the use of the moduli of elasticity of all four elements 2, 9, 11, 12 as updating parameters would result in compensation effects between elements 2 and 11 as well as between elements 9 and 12. Therefore, the moduli of elasticity of elements 1, 2, 9, and 10 were not used as updating parameters. However, the installation of more sensors along the beam, especially at the location of the supports, would have resulted in more refined damage identification results (in terms of the spatial distribution of damage). After completion of all the tests, the carbon shell was cut and removed in order to assess the quality of the infilled concrete and the extent of damage. No significant damage was observed at the location of elements 2 and 9.

The objective (cost) function used in this study for damage identification based on FE model updating is given by

$$f = \frac{1}{2}\,\mathbf{r}^{T}\mathbf{W}\mathbf{r} \tag{5.3}$$

where $\mathbf{r}$ denotes the residual vector, expressing the discrepancy between experimentally identified modal parameters and their analytically predicted (using the FE model) counterparts, and $\mathbf{W}$ is a diagonal weighting matrix with each diagonal component inversely proportional to the standard deviation of the natural frequency of the corresponding vibration mode based on the 12 identifications at each damage state (see Table 5.2). The residual vector can be partitioned as $\mathbf{r} = \begin{bmatrix}\mathbf{r}_f \\ \mathbf{r}_s\end{bmatrix}$ where $\mathbf{r}_f$ and $\mathbf{r}_s$ define eigen-frequency and mode shape residuals, respectively, as

$$\mathbf{r}_f = \left[\frac{\lambda_j - \tilde{\lambda}_j}{\tilde{\lambda}_j}\right], \qquad \mathbf{r}_s = \left[\frac{\phi_j^l}{\phi_j^r} - \frac{\tilde{\phi}_j^l}{\tilde{\phi}_j^r}\right] \qquad j = 1, \ldots, n_m \tag{5.4}$$

where λ_j and $\tilde{\lambda}_j$ denote the analytical and experimental eigenvalues corresponding to the j^{th} vibration mode, respectively, with $\lambda_j = \omega_j^2$ and ω_j = natural frequency; ϕ_j and $\tilde{\phi}_j$ denote the analytical and experimentally identified mode shape vectors, respectively. In Equation (5.4), the superscript *r* indicates a reference component of a mode shape vector (with respect to which the other components of the mode shape are normalized), the superscript *l* refers to the components that are used in the updating process (i.e., at the locations of the accelerometers or FBG strain sensors), and n_m denotes the number of vibration modes considered in the residual vector.

In the first case of damage identification, the natural frequencies and displacement mode shapes of the first five modes (see Figure 5.9) identified from acceleration data are used to form the residual vector which has a total of 35 residual components consisting of 5 eigen-frequency and $5 \times (7 - 1) = 30$ displacement mode shape residuals. The model parameters (effective moduli of elasticity) of the reference model are updated from state S1 (reference model) through S6. In the second case of damage identification, in addition to the natural frequencies and displacement mode shapes of the first five vibration modes identified based on acceleration data, the macro-strain mode shapes of the first four vibration modes identified based on FBG strain sensor data are considered in the residual vector for a total of 47 residual components consisting of 5 eigen-frequency, 30 displacement mode shape, and $4 \times (4 - 1) = 12$ macro-strain mode shape residuals. The reference

model (which is the same for both damage identification cases) is updated at states S2, S3, and S5. It should be mentioned that the macro-strains obtained from the FBG sensors at state S4 were significantly noisier than at the other states (due to the fact that the FBG sensors were not re-tensioned at this damage state) and therefore the FE model was not updated at this damage state. In the second case of damage identification, the mode shape residual vector consists of two parts: residuals from displacement mode shapes ($\mathbf{r}_s^{acc}$) and residuals from macro-strain mode shapes ($\mathbf{r}_s^{ms}$), as $\mathbf{r}_s = \begin{bmatrix} \mathbf{r}_s^{acc} \\ \mathbf{r}_s^{ms} \end{bmatrix}$, where both parts are defined separately as in the second part of Eq. (5.4). The analytical macro-strain mode shapes are derived from the displacement mode shapes through a transformation matrix $\mathbf{T}^{ms}$. This matrix connects the nodal degrees of freedom (DOF) of the FE model to the deformation of the FBG sensors based on linear elastic Bernoulli-Euler beam theory with exact displacement interpolation functions (Conte and Liu, 2001).

The (dimensionless) damage factor of element e is defined as

$$a^e = \frac{E^e_{undamaged} - E^e_{damaged}}{E^e_{undamaged}} \tag{5.5}$$

where E^e is the effective modulus of elasticity of element e. At each damage state, the damage factors for elements 3, 4, 5, 6, 7, 8, 11, and 12 are updated in order to minimize the objective function $\boldsymbol{f}$ defined in Eq. (5.3) based on a trust region Gauss-Newton optimization algorithm (Coleman and Li, 1996). The damage factors were constrained to be in the range $[-\infty, 1]$ for calibrating the reference model at state S1 in order to result in posi-

tive moduli of elasticity. For updating the FE model at states S2 through S6, the relative damage factor defined as $a^{e}_{rel} = (E^{e}_{previous\_state} - E^{e}_{current\_state}) / E^{e}_{previous\_state}$ was constrained to be in the range [-0.2, 0.9]. The upper-bound of 90% was selected based on the observed damage in the beam (i.e., it remained far from $a^{e}_{rel} = 0.9$ even at the end of the quasi-static tests), while the lower bound of -20% was selected considering that the identified effective moduli of elasticity are not expected to increase beyond 20% between two consecutive damage states. The optimization process was performed using the function "fmincon" in Matlab (Mathworks, 2005), with Jacobian and first-order estimate of the Hessian matrices calculated analytically based on the sensitivities of modal parameters to the updating variables (Fox and Kapoor 1968). It should be noted that the Fox and Kapoor's sensitivity formulas apply only for translational DOFs in the mode shapes. The sensitivities of rotational DOFs, which are required in the second case of damage identification for macro-strain mode shapes, were calculated based on the work of Conte and Liu (2001).

Table 5.8 reports the values of the updated effective moduli of elasticity (E^{e}) for elements 3-8, 11, 12 (see Figure 5.19) as well as the damage factors of these elements calculated relative to the reference/baseline state S1 at states S2 through S6 for the first case of damage identification. For each state S2-S6, Table 5.9 presents the experimentally identified modal frequencies together with their analytical counterparts obtained from the updated FE model as well as the MAC values between experimental and analytical mode shapes for the first case of damage identification. It should be noted that the analytical mode shapes were truncated at the locations of the accelerometers in order to match the

size of the experimental mode shapes. From Table 5.9, it is observed that: (1) the experimentally identified modal parameters match very well their analytical counterparts, especially for the first four vibration modes, (2) the discrepancies between analytical (from updated FE model) and experimental modal parameters tend to increase with increasing damage, and (3) at each damage state, the largest discrepancies between analytical and experimental modal parameters are exhibited by the fifth vibration mode. This is due to the fact that (1) this mode has the lowest modal contribution to the total measured acceleration response (see Figure 5.10), (2) the estimation variability of the identified modal parameters is relatively large for this mode compared to the other modes (see Section 3), and therefore smaller weights are assigned to the fifth mode residuals in the objective function. It should be noted that the modal parameters of the fifth vibration mode were not used in the FE model updating process at state S2.

Table 5.8 Effective moduli of elasticity E^e [GPa] / damage factors a^e [%] (relative to reference state S1) of updated elements (# 3-8, 11, 12) at states S2-S6 for first case of damage identification

	El. 3	El. 4	El. 5	El. 6	El. 7	El. 8	El. 11	El. 12
S2	46.30/ 21.7	31.35/ 18.4	34.30/ 18.5	31.41/ 2.8	49.60/ 2.6	32.15/ 16.9	61.82/ -8.1	72.78/ 45.2
S3	39.44/ 33.3	35.92/ 6.5	27.30/ 35.1	30.68/ 5.1	48.36/ 5.0	30.19/ 21.9	58.16/ 1.7	59.84/ 55.0
S4	27.52/ 53.5	35.42/ 7.8	24.36/ 42.1	33.49/ -3.6	52.48/ -3.1	28.01/ 27.6	55.52/ 2.9	70.82/ 46.7
S5	27.64/ 53.3	39.27/ -2.2	24.30/ 42.2	26.93/ 16.6	43.56/ 14.4	27.62/ 28.6	58.80/ -2.8	74.91/ 43.6
S6	33.17/ 43.9	26.72/ 30.4	24.50/ 41.8	25.81/ 20.1	32.55/ 36.1	25.39/ 34.4	36.28/ 36.5	77.91/ 41.4

Table 5.9 Comparison of experimental and analytical modal frequencies [Hz] and MAC values between experimental and analytical mode shapes at states S1 through S6 (first case of damage identification)

		Mode 1	Mode 2	Mode 3	Mode 4	Mode 5
S1	Freq. (experiment)	17.34	43.24	97.50	167.74	246.15
	Freq. (updated model)	17.31	43.28	97.80	167.74	245.02
	MAC	0.999	0.998	0.997	0.993	0.839
S2	Freq. (experiment)	16.09	40.72	89.24	158.90	-
	Freq. (updated model)	16.08	40.97	89.16	158.93	-
	MAC	1.000	0.999	0.994	0.993	-
S3	Freq. (experiment)	15.35	39.09	86.80	153.32	244.72
	Freq. (updated model)	15.37	38.75	86.91	153.18	236.03
	MAC	0.999	0.994	0.994	0.992	0.974
S4	Freq. (experiment)	15.17	38.91	84.82	143.24	232.25
	Freq. (updated model)	15.10	39.24	83.80	145.99	233.30
	MAC	1.000	0.998	0.982	0.977	0.898
S5	Freq. (experiment)	15.00	38.98	84.12	143.20	227.94
	Freq. (updated model)	14.91	40.29	83.13	144.46	229.84
	MAC	1.000	0.993	0.981	0.986	0.916
S6	Freq. (experiment)	14.08	33.04	79.93	142.84	219.71
	Freq. (updated model)	13.94	34.60	80.05	144.19	224.47
	MAC	0.999	0.996	0.991	0.967	0.935

Figure 5.20 shows a bar plot of the updated values of E^e for beam elements 1-10 (as explained above) at states S1 to S6 for the first case of damage identification. It is recalled that the effective moduli of elasticity of elements 1, 2, 9, 10 are not updated beyond state S1. From the results presented in Table 5.8 and Figure 5.20, it is observed that the effective moduli of elasticity display an overall decreasing trend with increasing level of damage. There are some exceptions to this decreasing trend in some beam elements, which can be due to: (1) measurement errors and estimation variability of the identified modal parameters, (2) low sensitivity of the residuals to some of the updating parameters (E^e),

(3) modeling errors and uncertainties, and (4) optimization errors in the FE model updating process (i.e., local but not global minimum).

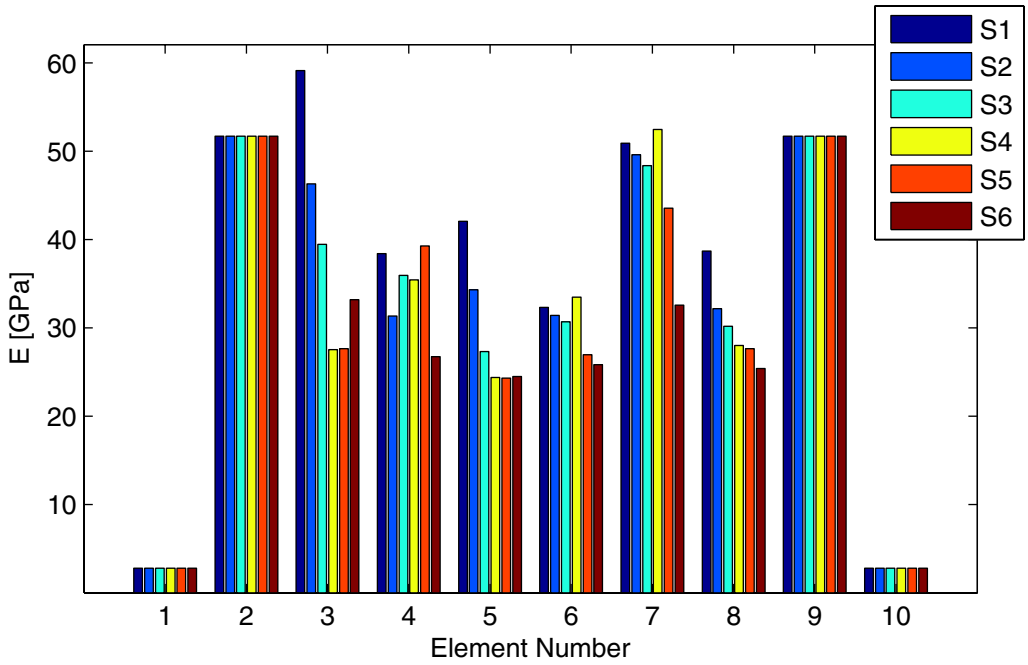

Fig. 5.20 Updated effective moduli of elasticity of 10 beam elements at different damage states (S1 to S6) for first case of damage identification

For the second case of damage identification, Table 5.10 gives the updated E^e for the updating elements (# 3-8, 11, 12) and the corresponding damage factors (relative to the reference state S1) at states S2, S3 and S5, while Figure 5.21 shows in a bar plot the updated E^e for all beam elements at states S1, S2, S3 and S5. Table 5.11 presents the experimentally identified modal frequencies together with their analytical counterparts obtained from the updated FE model as well as the MAC values between experimental and analytical mode shapes (for both displacement and macro-strain mode shapes considered separately) at states S2, S3 and S5.

Table 5.10 Effective moduli of elasticity E^e [GPa] / damage factors a^e [%] (relative to reference state S1) of updated elements (# 3-8, 11, 12) at states S2, S3, and S5 for the second case of damage identification

	El. 3	El. 4	El. 5	El. 6	El. 7	El. 8	El. 11	El. 12
S2	39.06/ 34.0	38.23/ 0.5	38.01/ 9.6	32.09/ 0.7	42.85/ 15.8	36.78/ 4.9	57.18/ 0	58.61/ 55.9
S3	44.07/ 24.4	38.41/ 0	27.43/ 34.8	28.16/ 12.8	31.37/ 38.4	35.70 7.7	57.18/ 0	64.60/ 51.4
S5	32.28/ 45.4	38.36/ 0.1	20.97/ 50.1	32.01/ 0.9	29.96/ 41.2	37.67/ 2.6	57.18/ 0	66.16/ 50.2

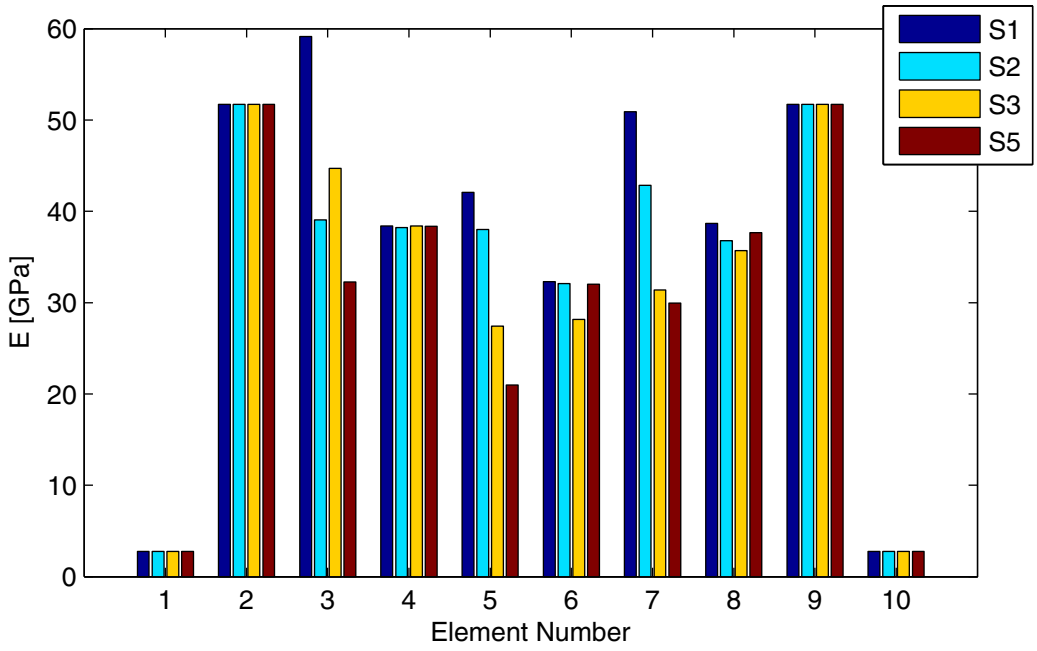

Fig. 5.21 Updated effective moduli of elasticity of 10 beam elements at different damage states (S1, S2, S3 and S5) for second case of damage identification

Figure 5.22 compares the damage factors of all updating elements (3-8, 11, 12) obtained from the two considered cases of damage identification at states S2, S3, and S5. From this figure, it is observed that the damage factors computed from these two cases are in relatively good agreement for elements 3, 5, 6, 11 and 12. Damage is identified along element 4 in the first case and not in the second case. Since FBG sensor # 1 is covering part of ele-

ment 4 (see Figure 5.5), it is expected that the results from the second case of damage identification for element 4 are more accurate than those from the first case. In the first case, damage is identified along element 8 with almost no damage along element 7, while in the second case, damage is identified along element 7 with very small damage along element 8. Again, the results from the second case of damage identification are expected to be more accurate for elements 7 and 8, since most of FBG sensor #3 is contained in element 8 (see Figure 5.5). This will be confirmed below by the observed damage in the beam at the end of the experiments. The differences in the identified damage obtained from the two different cases can be due to: (1) different type of residuals were used in two cases (addition of macro-strain mode shapes in the second case), and (2) different weights were assigned to residuals in the two cases.

Table 5.11 Comparison of experimental and analytical modal frequencies [Hz] and MAC values between experimental and analytical mode shapes at states S2, S3 and S5 (second case of damage identification)

		Mode 1	Mode 2	Mode 3	Mode 4	Mode 5
S2	Freq. (experiment)	16.09	40.72	89.24	158.90	254.51
	Freq. (updated model)	16.01	38.59	89.19	160.40	-
	MAC (acc. mode shapes)	1.000	0.999	0.988	0.988	-
	MAC (strain mode shapes)	0.997	0.765	0.998	0.987	-
S3	Freq. (experiment)	15.35	39.09	86.80	153.32	244.72
	Freq. (updated model)	15.26	39.20	87.70	156.56	234.31
	MAC (acc. mode shapes)	0.999	0.993	0.995	0.994	0.980
	MAC (strain mode shapes)	0.982	-	0.974	-	-
S5	Freq. (experiment)	15.00	38.98	84.12	143.20	227.94
	Freq. (updated model)	14.71	39.20	84.74	150.14	230.17
	MAC (acc. mode shapes)	1.000	0.995	0.980	0.983	0.933
	MAC (strain mode shapes)	0.972	0.823	0.996	0.937	-

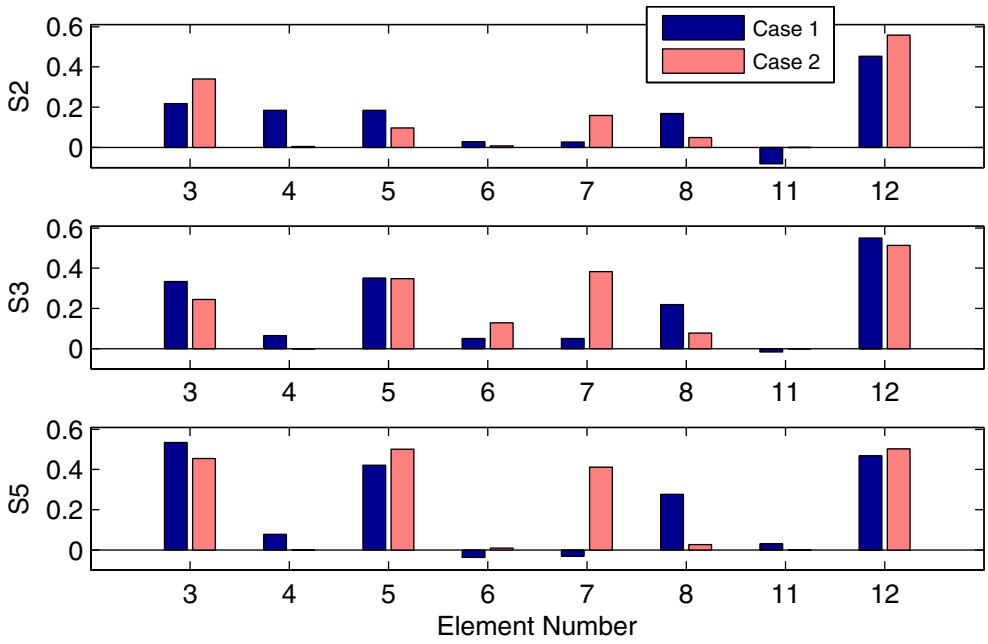

Fig. 5.22 Comparison of damage factors obtained from the two cases of damage identification at states S2, S3 and S5

At the end of the experiments, the carbon shell was cut and removed from the concrete core to assess the quality of the infilled concrete and the extent of damage in the concrete, especially in the splice region. Figure 5.23 shows a picture of the damaged concrete core at the splice location (i.e., mid-span of the girder). Significant flexural cracks can be observed at the top and bottom of the gap region. This gap is located inside element 5 of the FE model (see Figures 5.5 and 5.19), and therefore the high damage factors identified at element 5 in both damage identification cases (see Figure 5.22) are in good agreement with the observed damage. Figure 5.24 shows local failures in the composite shell at the location of stirrups both near accelerometer a3 (next to the electro-dynamic shaker) inside element 3 (close to element 4) and near accelerometer a7 at the limit between elements 7 and 8. Thus, the damage identification results at elements 3, 7, and 8 (see Figure 5.22) are consistent with the observed damage in the composite shell.

Fig. 5.23 Damage in the concrete core at the splice location

(a) (b)

Fig. 5.24 Composite shell failure at location of stirrup holes: (a) near accelerometer a3, and (b) near accelerometer a7

Furthermore, pitted and shrinkage-cracked concrete can be observed in the picture of Figure 5.25, corresponding to locations of elements 7 and 8, further validating the damage identification results. Finally, it is worth noting that the large damage factor identified in

element 12 (representing the north support) is likely due to the initial friction in the support pin, i.e., the pin was not well lubricated initially and broke free during the first set of quasi-static tests leading to state S2.

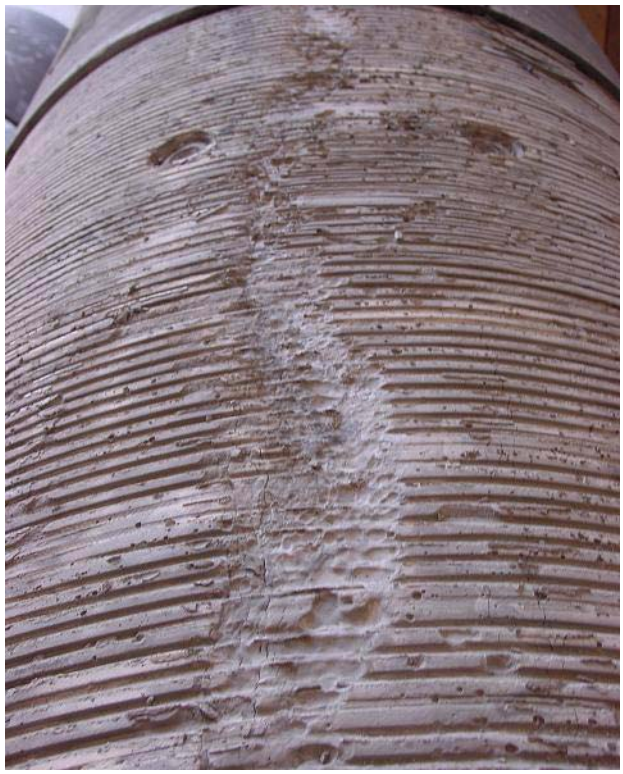

Fig. 5.25 Concrete core at north side of the splice (see Figures 2 and 4)

5.6 CONCLUSIONS

This paper presents the application of a state-of-the-art two-stage damage identification method to a full-scale composite beam (sub-component) based on its measured vibration response. In the first stage, modal parameters (modal frequencies, damping ratios, displacement and macro-strain mode shapes) of the test structure are identified based on its impulse response data measured using accelerometers and long-gage fiber

Bragg grating (FBG) strain sensors. In the second stage, changes (from damage state to damage state) in the modal parameters identified in the first stage are used to identify (detect, localize and quantify) damage in the girder using an element-by-element sensitivity based finite element model updating algorithm. This damage identification study leveraged a full-scale sub-component experiment conducted in the Charles Lee Powell Structural Research Laboratories at the University of California, San Diego, and consisting of uni-directional quasi-static cyclic load tests. After each of several sequences of loading-unloading cycles, a high-quality set of low-amplitude vibration response data was acquired from the beam at various damage levels. Based on impulse (free vibration) response data measured using accelerometers and FBG strain sensors from different impact tests, the Eigensystem Realization Algorithm followed by a least squares optimization was employed for modal parameter identification of the composite beam in its undamaged (baseline) and various damaged states. The modal identification results from different tests at a given damage state using different types of data (acceleration or macro-strain) show very good agreement, thus validating the system identification results used in the first stage of the damage identification procedure.

The identified modal parameters are then used to identify the damage in the structure using a finite element model updating strategy. Two separate cases of damage identification were performed: (1) the residuals in the objective function used in the FE model updating procedure are based on the natural frequencies and displacement mode shapes identified from accelerometer data, and (2) the residuals are based on the natural frequencies, displacement mode shapes identified from accelerometer data, and macro-strain

mode shapes identified from FBG strain sensor data. From the obtained damage identification results, it is observed that the effective moduli of elasticity (used as updating parameters) display an overall decreasing trend with increasing level of damage, which is consistent with the damage-induced stiffness degradation. The updated effective moduli of elasticity obtained from the two different damage identification cases are found to be in relatively good agreement and consistent with the damage observed in the composite beam during and at the end of the experiments. This provides an important validation example for vibration based damage identification using finite element model updating, performed on a full-scale structural component tested in laboratory conditions. However, similar studies are still needed to further evaluate the feasibility of vibration based structural health monitoring for large and complex structures in field conditions.

ACKNOWLEDGEMENTS

Chapter 5, in full, is a reprint of the material as it is accepted for publication in Journal of Computer-Aided Civil and Infrastructure Engineering (2008), Moaveni, B., He, X., Conte, J.P., and De Callafon, R.A. The dissertation author was the first author and primary investigator of this paper.

This work was partially funded by the National Science Foundation, Grant No. DMI-0131967 under a Blue Road Research STTR Project in which UCSD was the principal subcontractor, and a grant from Lawrence Livermore National Laboratory with Dr. David McCallen as Program Leader. These sources of support are gratefully acknowledged. The authors wish to thank Professor Vistasp Karbhari at UCSD, and Dr. Charles

Sikorsky at Caltrans for allowing them to perform the dynamic tests used in this research, as a payload project to their full-scale sub-component experiment. The authors are also grateful to Dr. Michael Fraser for his significant help in acquiring the acceleration data.

REFERENCES

Adeli, H., and Jiang, X. (2006). “Dynamic fuzzy wavelet neural network model for structural system identification.” *Journal of Structural Engineering*, ASCE, 132(1), 102-111.

Bernal, D., and Gunes, B. (2004). “Flexibility based approach for damage characterization: benchmark application.” *Journal of Engineering Mechanics*, ASCE, 130(1), 61-70.

Brestel, D., Van Den Einde, Y., Karbhari, V. M., and Seible, F. (2003). “Characterization of concrete filled structural formwork.” *Proceeding of the 48th International SAMPE Symposium*, Long Beach, CA, Book 2, 2115-2128, May 11-15.

Catbas, F. N., Brown, D. L., and Aktan, A. E. (2004). “Parameter estimation for multiple-input multiple-output modal analysis of large structures.” *Journal of Engineering Mechanics*, ASCE, 130 (8), 121-130.

Coleman, T. F., and Li, Y. (1996). “An interior, Trust Region approach for nonlinear minimization subject to bounds.” *SIAM Journal on Optimization*, 6, 418-445.

Computers and Structures, Inc. (2004). *SAP2000 linear and nonlinear, static and dynamic analysis and design of three-dimensional structures: getting started, version 9*. Berkeley, California, USA.

Conte, J. P., and Liu, M. (2001). *Use of long-gage fiber optic sensors for earthquake response monitoring and non-destructive evaluation of structures*. *CUREE Report*, Publication No. CKIII-04, CUREE-Kajima Joint Research Program - Phase III.

De Callafon, R. A., Moaveni, B., Conte, J. P., He, X., and Udd, E. (2007). “General Realization Algorithm for modal identification of linear dynamic systems.” *Journal of Engineering Mechanics*, ASCE, Under Review.

Doebling, S. W., Farrar, C. R., Prime, M. B., and Shevitz, D. W. (1996). *Damage identification in structures and mechanical systems based on changes in their vibration characteristics: a detailed literature survey.* Los Alamos National Laboratory Rep.

No. LA-13070-MS, Los Alamos, N.M.

Doebling, S. W., Farrar, C. R., and Prime, M. B. (1998). "A summary review of vibration-based damage identification methods." *The Shock and Vibration Digest,* 30(2), 99-105.

Filippou, F. C., and Constantinides, M., (2004). *FEDEASLab getting started guide and simulation examples*. Technical Report NEESgrid-2004-22, http://fedeaslab.berkeley.edu.

Fox, R. L., and Kapoor, M. P. (1968). "Rates of change of eigenvalues and eigenvectors." *AIAAJ,* 6(12), 2426-2429.

Friswell, M. I., and Mottershead, J. E. (1995). *Finite element model updating in structural dynamics*. Kluwer Academic Publishers, Boston, USA.

Jiang, X., and Adeli, H. (2005). "Dynamic wavelet neural network for nonlinear identification of highrise buildings." *Computer-Aided Civil and Infrastructure Engineering*, 20(5), 316-330.

Jiang, X. and Adeli, H. (2006). "Pseudospectra, MUSIC, and dynamic wavelet neural network for damage detection of highrise buildings." *International Journal for Numerical Methods in Engineering*, in press.

Juang, J. N. and Pappa, R. S. (1985). "An eigensystem realization algorithm for model parameter identification and model reduction." *Journal of Guidance, Control, and Dynamics,* 8(5), 620-627.

Maeck, J., and De Roeck, G. (1999). "Dynamic bending and torsion stiffness derivation from modal curvatures and torsion rates." *Journal of Sound and Vibration*, 225(1), 153-170.

MathWorks Inc. (2005). *Matlab - high performance numeric computation and visualization software, user's Guide*. The MathWorks Inc., Natick, MA.

Moaveni, B., He, X., Conte, J. P., and Udd, E. (2006). "Effect of damage on modal parameters using full-scale test data." *Proc. of International Conference on Modal Analysis (IMAC-XXIV)*, St. Louis, USA.

Pandey, A. K., Biswas, M., and Samman, M. M. (1991). "Damage detection from changes in curvature mode shapes." *Journal of Sound and Vibration*, 145(2), 321-332.

Peeters, B., and De Roeck, G. (2001). "Stochastic system identification for operational modal analysis: A review." *Journal of Dynamic Systems, Measurement, and Control*, 123, 1-9.

Salawu, O.S. (1997). "Detection of structural damage through changes in frequency: A review." *Engineering Structures*, 19(9), 718-723.

Seible, F., Hegemier, G. A., Karbhari, V. M., Davol, A., Burgueño, R., Wernli, M., and Zhao, L. (1996). *The I-5/Gilman advanced composite cable stayed bridge study.* Department Resport, University of California, San Diego, SSRP-96/05.

Shi, Z. Y., Law, S. S., and Zhang, L. M. (2002), Improved damage quantification from elemental modal strain energy change, *Journal of Engineering Mechanics*, ASCE, 128(5), 521-529.

Smyth, A. W., Pei, J. S., and Masri, S. F. (2003). "System identification of the Vincent Thomas suspension bridge using earthquake records." *Earthquake Engineering and Structural Dynamics*, 32, 339-367.

Sohn, H., Farrar, C. R., Hemez, F. M., Shunk, D. D., Stinemates, D. W., and Nadler, B. R. (2003). *A review of structural health monitoring literature: 1996-2001*. Los Alamos National Laboratory Report LA-13976-MS.

Teughels, A., and De Roeck, G. (2004). "Structural damage identification of the highway bridge Z24 by finite element model updating." *Journal of Sound and Vibration*, 278(3), 589–610.

Zhu H. P., and Xu, Y. L. (2005). "Damage detection of mono-coupled periodic structures based on sensitivity analysis of modal parameters." *Journal of Sound and Vibra-*

tion, 285, 365–390.

CHAPTER 6

Damage Identification of Seven-Story Reinforced Concrete Building Slice Tested on the UCSD-NEES Shake Table

6.1 INTRODUCTION

In recent years, structural health monitoring has received increasing attention in the civil engineering research community with the objective to develop methods through which structural damage can be identified at the earliest possible stage and the remaining useful life of structures evaluated (damage prognosis). Vibration-based, non-destructive damage identification makes use of changes in dynamic characteristics (e.g., modal parameters) to identify structural damage. Experimental modal analysis (EMA) has been used as a technology for identifying modal parameters of a structure based on low amplitude vibration data. It should be emphasized that the success of damage identification based on EMA depends strongly on the accuracy and completeness of the identified structural dynamic properties. Extensive literature reviews on vibration-based damage identification were provided by Doebling et al. (1996 and 1998) and Sohn et al. (2003).

Damage identification consists of: (1) detecting the occurrence of damage, (2) localizing the damage zones, and (3) estimating the extent of damage in the various damage zones. Numerous vibration-based methods have been proposed to achieve these goals.

Salawu (1997) presented a review on the use of changes in natural frequencies for damage detection only. However, it is in general impossible to localize damage (i.e., obtain spatial information on the detected structural damage) from changes in natural frequencies only. Pandey et al. (1991) introduced the concept of using curvature mode shapes for damage localization. In their study, by using a cantilever and a simply supported analytical beam model, they demonstrated the effectiveness of employing changes in curvature mode shapes as damage indicator for detecting and localizing damage. Bernal and Gunes (2004) have incorporated changes in modal flexibility matrices (or flexibility proportional matrices) into the damage locating vector (DLV) technique to localize damage. Recently, Adeli and Jiang (2006) presented a novel multi-paradigm dynamic time-delay fuzzy wavelet neural network (WNN) model for non-parametric identification of structures using the nonlinear auto-regressive moving average with exogenous inputs (NARMAX) approach. Methods based on changes in identified modal parameters to detect and localize damage have also been further developed for the purpose of damage quantification. Among these methods are strain-energy based methods (Shi et al., 2002) and the direct stiffness calculation method (Maeck and De Roeck, 1999). Another class of sophisticated methods consists of applying sensitivity-based finite element (FE) model updating for damage identification (Friswell and Mottershead 1995). These methods update the physical parameters of a FE model of the structure by minimizing an objective function expressing the discrepancy between FE predicted and experimentally identified structural dynamic properties that are sensitive to damage such as natural frequencies and mode shapes. Optimum solutions of the problem are reached through sensitivity-based constrained optimization algorithms. In recent years, sensitivity-based FE model updating methods have been

applied successfully for condition assessment of structures (Teughels and De Roeck, 2004).

The UCSD-NEES shake table is located at the Englekirk Structural Engineering Center, 15km east of the main campus of University of California, San Diego (UCSD). This unique facility, commissioned in October 2004, allows to perform landmark seismic experiments on large- or full-scale structural and soil-foundation-structure interaction systems. A full-scale seven-story reinforced concrete shear wall building slice was tested on the UCSD-NEES shake table in the period October 2005 - January 2006. The objective of this test program was to verify the seismic performance of a mid-rise reinforced concrete shear wall building designed for lateral forces obtained from a displacement-based design methodology, which are significantly smaller than those dictated by current force-based seismic design provisions in United States (Panagiotou et al. 2007). The shake table tests were designed so as to damage the building progressively through several historical seismic motions reproduced on the shake table. At various levels of damage, several low amplitude white noise base excitations were applied through the shake table to the building which responded as a quasi-linear system with dynamic parameters depending on the level of structural damage. In addition to white noise base excitation tests, ambient vibration tests were also performed on the building specimen at different damage levels. Different state-of-the-art system identification methods were applied to acceleration response measurements in order to estimate modal parameters (natural frequencies, damping ratios and mode shapes) of the building in its undamaged (baseline) and various damage states.

In this study, a FE model updating strategy is applied for damage identification of the structure in various damage states. The objective function for damage identification is defined as a combination of natural frequency and mode shape residuals measuring the discrepancy between the analytically predicted (using a FE model) and experimentally identified modal parameters. Two cases of damage identifications are considered in this study, namely (1) residuals are constructed from the modal parameters identified based on ambient vibration data, and (2) residuals are formed using the modal parameters identified based on white noise base excitation test data. The identified damage from both cases is then compared to the damage observed in the test structure.

6.2 TEST SPECIMEN, TEST SETUP AND DYNAMIC EXPERIMENTS

6.2.1 Seven-Story Reinforced Concrete Shear Wall Building Slice

The test structure which represents a slice of a full-scale reinforced concrete shear wall building consists of a main shear wall (web wall), a back wall perpendicular to the main wall (flange wall) for transversal stability, a concrete slab at each floor level, an auxiliary post-tensioned column to provide torsional stability, and four gravity columns to transfer the weight of the slabs to the shake table. Pin-pin slotted slab connections capable of transferring in-plane diaphragm forces are placed between the web and flange walls at floor levels in order to minimize the moment transfer and coupling between the two walls. Figures 6.1 and 6.2 show the test structure mounted on the shake table and an elevation view with its general dimensions, respectively. Figure 6.3 displays a plan view of the

structure with walls and slab dimensions at different levels. Details about construction drawings and material test data are available in Panagiotou et al. (2007).

Fig. 6.1 Test structure

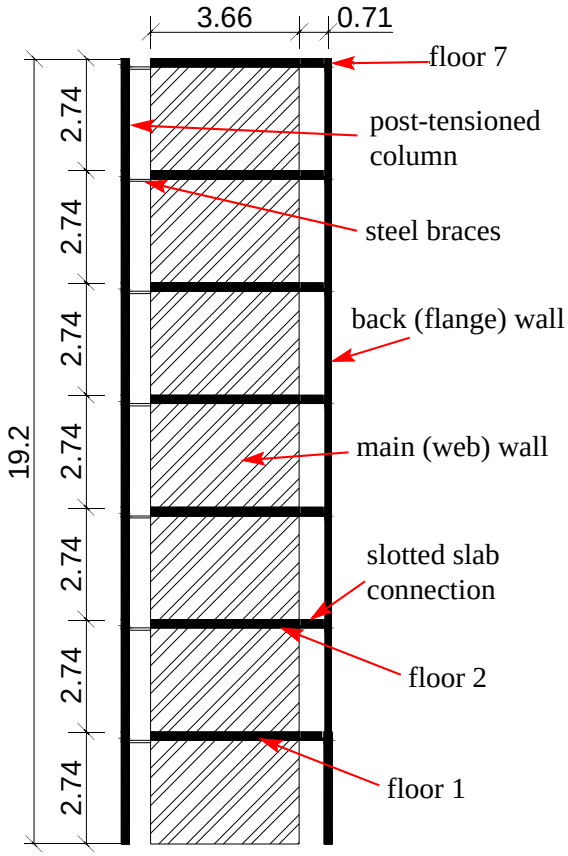

Fig. 6.2 Elevation of test structure (units: m)

6.2.2 Instrumentation Layout

The test structure was instrumented with an extensive array of accelerometers, strain gages, potentiometers, and Linear Variable Displacement Transducers (LVDTs), all sampling data simultaneously using a nine node distributed data acquisition system. The accelerometer array consisted of 14 uni-axial accelerometers on the foundation/pedestal of the test structure, 106 uni-axial accelerometers on the floor slabs and the web wall, 8 uni-axial accelerometers on the platen of the shake table, 9 uni-axial accelerometers on the

reaction block of the shake table and 1 tri-axial accelerometer on the surrounding ground (free field), resulting in a total of 140 channels of acceleration measurements. The 54 LVDTs were installed along both edges (east and west) of the web wall, while the 8 potentiometers were installed diagonally along only the first two stories of the web wall. A total of 231 strain gages were deployed on the test specimen consisting of 143 on the longitudinal and horizontal steel reinforcement of the web wall, 64 on the longitudinal and horizontal steel reinforcement of the flange wall, 16 on the gravity columns and 8 on the steel braces connecting the slabs to the post-tensioned column.

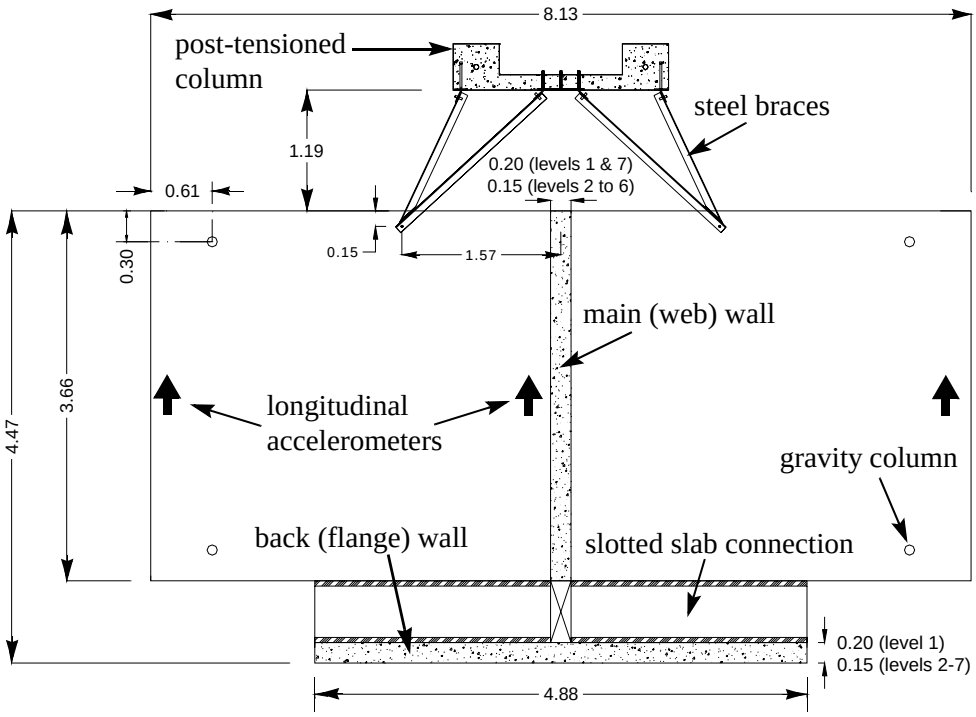

Fig. 6.3 Plan view of test structure (units: m)

In addition, the displacement response of selected points on the structure were measured in three dimensions using 6 global positioning system (GPS) sensors, 3 of them on the top floor slab, 2 on the flange wall and 1 on the platen of the shake table. Table 6.1 provides a

summary of the heterogeneous sensor array installed on the test structure. The technical characteristics of the accelerometers are: MEMS-Piezoresistive MSI model 3140, amplitude range: +/-5g, frequency range (min): 0-300Hz, voltage sensitivity: 400mV/g. The data acquisition system used had 16 bits of resolution.

Table 6.1 Summary of instrumentation deployed on the test structure

Sensor Type	Location	Quantity
Accelerometer (138)	Foundation/pedestal	14
	Slabs and walls	106
	Shake table platen	8
	Reaction block	9
	Free field	1 (tri-axial)
LVDT (54)	Web wall (levels 1-2)	34
	Web wall (levels 3-7)	20
Potentiometer (8)	Web wall (levels 1-2)	8
GPS (6)	Top floor	3
	Flange wall	2
	Platen	1
Strain Gage (231)	Web wall	143
	Flange wall	64
	Gravity columns	16
	Braces connecting slabs to post-tensioned column	8

In this study, measured response data from 14 longitudinal accelerometers on the web wall (at each floor level as shown in Figure 6.3 and at mid-height of each story) were used to identify the modal parameters of the test structure. The measured acceleration responses were sampled at a rate of 240Hz resulting in a Nyquist frequency of 120Hz,

which is much higher than the modal frequencies of interest in this study (< 25Hz). Before applying the system identification methods, all the measured data were band-pass filtered between 0.5Hz and 25Hz using a high order (1024) FIR filter. Figure 6.4 shows six filtered absolute acceleration time histories recorded on the web wall at floor levels 1, 4 and 7 during white noise base excitation (left column) and ambient vibration (right column) tests performed on the test structure in its undamaged state.

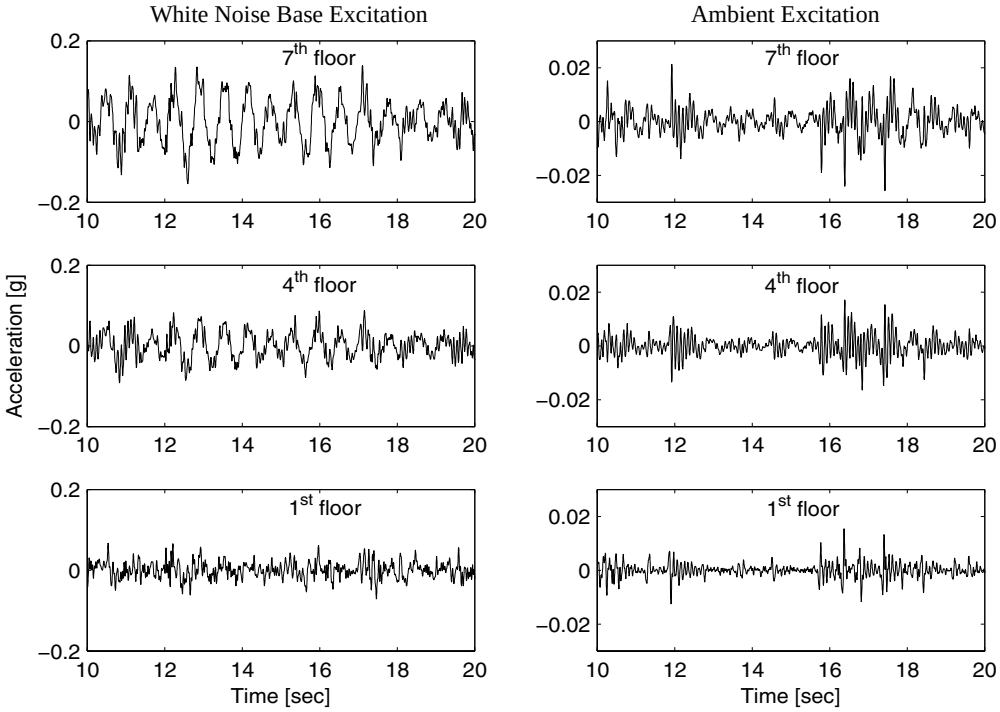

Fig. 6.4 Absolute acceleration time histories at floors 1, 4, and 7 due to white noise base excitation (left) and ambient excitation (right)

The corresponding Fourier Amplitude Spectra (FAS) are given in Figure 6.5. From Figure 6.5, it is observed that: (1) the FAS plots are very jagged/noisy which can be due to some rattling behavior caused by loose connections, especially at both ends of the steel braces connecting the slabs to the post-tensioned column; (2) the first longitudinal vibration mode has a predominant contribution to the total response, especially at the higher

floors, which renders the identification of higher (than the first longitudinal) vibration modes more difficult; and (3) the FAS of the acceleration response histories at the first floor have a drop in their amplitude around 11.5 Hz which is due to the application of a notch filter in the control loop of the shake table to reduce the effects of the oil column resonance.

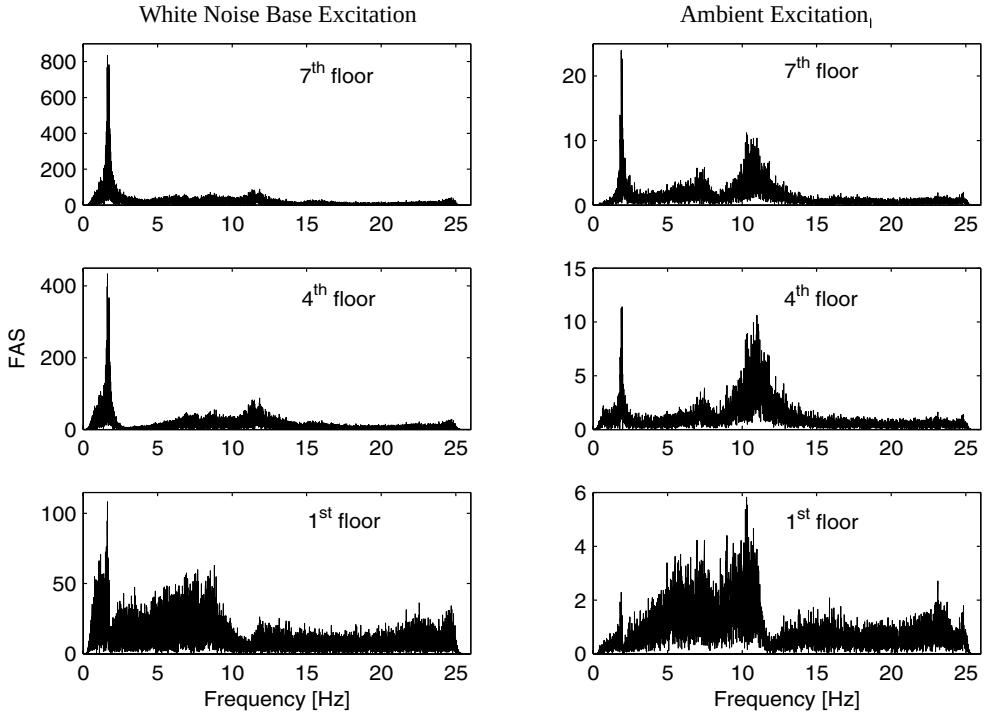

Fig. 6.5 Fourier Amplitude Spectra of filtered absolute acceleration time histories at floors 1, 4, and 7 due to white noise base excitation (left) and ambient excitation (right)

6.2.3 Dynamic Tests Performed

A sequence of dynamic tests (68 tests in total) was applied to the test structure during the period October 2005 - January 2006 including ambient vibration, free vibration, and forced vibration tests (white noise and seismic base excitations) using the UCSD-NEES shake table. The shear wall structure was damaged progressively through a

sequence of four historical ground motion records used as table input motions and the modal parameters of the test structure were identified at different damage states using six different system identification methods based on various dynamic test data. The four earthquake records applied to the test structure consist of (http://peer.berkeley.edu/smcat): (1) longitudinal component of the 1971 San Fernando earthquake (M = 6.6) recorded at the Van Nuys station (EQ1), (2) transversal component of the 1971 San Fernando earthquake recorded at the Van Nuys station (EQ2), (3) longitudinal component of the 1994 Northridge earthquake (M = 6.7) recorded at the Oxnard Boulevard station in Woodland Hill (EQ3), and (4) 360 degree component of the 1994 Northridge earthquake recorded at the Sylmar station (EQ4). The input white noise base excitation consisted of a realization of a banded white noise (0.25-25Hz) process with a root-mean-square (RMS) amplitude of 0.03g. Table 6.2 describes the dynamic tests used in this study on system identification of the shear wall building at different damage states.

Table 6.2 Dynamic tests used in this study
(WN: white noise base excitation test and AV: ambient vibration test)

Test No.	Date	Test Description	Damage State
37	11/18/05	8min WN (0.03*g*)	S0
39	11/21/05	8min WN (0.03*g*) + 3min AV	S0
40	“	EQ1	
41	“	8min WN (0.03*g*) + 3min AV	S1
43	“	EQ2	
45	11/22/05	2min WN (0.03*g*)	S2
46	“	8min WN (0.03*g*) + 3min AV	S2
48	“	EQ3	
49	“	8min WN (0.03*g*) + 3min AV	S3.1

Table 6.2 Dynamic tests used in this study
(WN: white noise base excitation test and AV: ambient vibration test)

56	12/5/05	8min WN (0.03*g*)	S3.1
61	1/14/06	8min WN (0.03*g*) + 3min AV	S3.2
62	"	EQ4	
64	1/14/06	8min WN (0.03*g*) + 3min AV	S4
67	"	8min WN (0.03*g*)	S4

6.3 SYSTEM IDENTIFICATION RESULTS

Modal parameters of the test structure were identified using state-of-the-art system identification methods based on measured data from low amplitude dynamic tests (i.e., ambient vibration tests and white noise base excitation tests) performed at various damage states S0, S1, S2, S3.1, S3.2, and S4 (Moaveni et al. 2007). Damage state S0 is defined as the undamaged (baseline) state of the structure before its exposure to the first seismic excitation (EQ1), while damage states S1, S2, S3 and S4 correspond to the state of the structure after exposure to the first (EQ1), second (EQ2), third (EQ3), and fourth (EQ4) seismic excitations, respectively (see Table 6.2). Damage state S0 does not correspond to the uncracked state of the test structure, since the latter had already been subjected to low-amplitude white noise base excitations (0.02-0.03g RMS) for the purposes of checking the instrumentation and data acquisition system and tuning the shaking table controller. It should be noted that during damage state S3, the bracing system between the slabs of the test specimen and the post-tensioned column was stiffened. Therefore, damage state S3 is subdivided into S3.1 (before modification of the braces) and S3.2 (after modification of the braces). In this study, the natural frequencies and mode shapes of the first three longi-

tudinal vibration modes are used for damage identification of the test structure at damage states S1, S2, S3.1, and S4. Figure 6.6 shows in polar plots the complex-valued mode shapes of the first three longitudinal vibration modes (1^{st}-L, 2^{nd}-L, 3^{rd}-L) of the test structure identified using the Multiple-reference Natural Excitation Technique combined with Eigensystem Realization Algorithm (MNExT-ERA) based on ambient vibration data from Test 39 at damage state S0. The real part of each of these identified mode shapes is displayed in Figure 6.7. The polar plot representation of a mode shape provides information on the degree of non-classical (or non-proportional) damping characteristics of that mode. If all the components of a mode shape (each component being represented by a vector in polar plot) are collinear, that vibration mode is classically damped. The more the mode shape components are scattered in the complex plane, the more the system is non-classically (non-proportionally) damped in that mode. However, measurement noise (low signal-to-noise ratio), estimation errors, and modeling errors can also cause a truly classically damped vibration mode to be identified as non-classically damped. From Figure 6.6, it is observed that the first longitudinal mode at damage state S0 is identified as perfectly classically damped. Some degree of non-proportional damping is identified for the 3^{rd}-L mode, while the 2^{nd}-L mode is identified with high level of non-proportional damping, which is probably caused at least in part by the high estimation uncertainty characterizing this vibration mode.

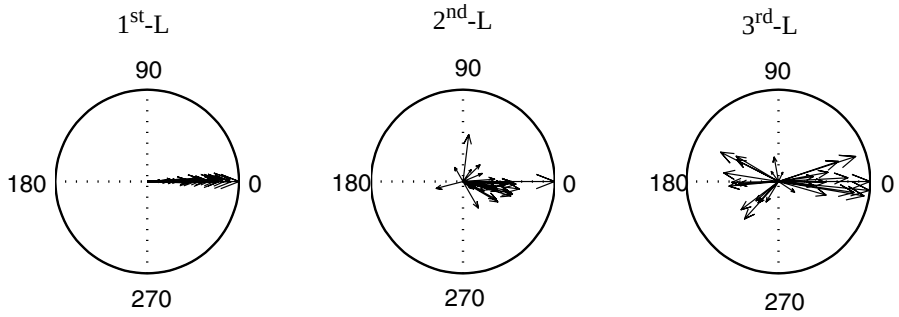

Fig. 6.6 Polar plot representation of complex-valued mode shapes of the building at damage state S0 obtained using MNExT-ERA method based on ambient vibration data

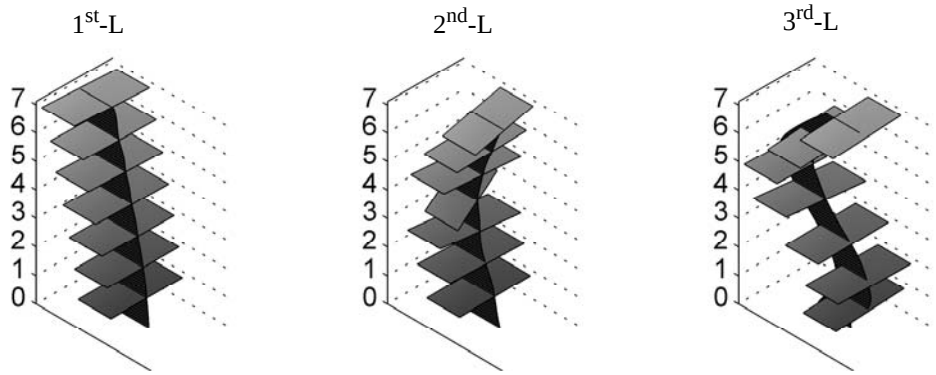

Fig. 6.7 Vibration mode shapes of the building at damage state S0 obtained using MNExT-ERA method based on ambient vibration data

Tables 6.3 and 6.4 report the natural frequencies, damping ratios, and modal assurance criterion (MAC) values of these three longitudinal vibration modes (1st-L, 2nd-L, 3rd-L) identified based on acceleration data from ambient vibration and white noise base excitation tests, respectively, at all damage states considered. The MAC values are calculated between normalized mode shapes identified at various damage states with their counterparts identified at the undamaged state of the building. Normalization was performed by projecting all mode shape components onto their major principal axis (in the complex plane) and then scaling this projected mode shape vector for a unit value of its largest component. This normalization results in real valued mode shapes which are more suitable

to be used in FE model updating. From Tables 6.3 and 6.4, it is observed that: (1) The identified natural frequencies decrease with increasing level of damage, except from damage states S3.1 to S3.2, during which the steel braces (see Figure 6.3) were modified (stiffened and strengthened), while the identified damping ratios do not show a clear trend as a function of increasing structural damage. (2) The calculated MAC values exhibit a general decreasing trend with increasing level of damage. This trend is less consistent than that of the identified natural frequencies.

Table 6.3 Natural frequencies, damping ratios and MAC values identified based on acceleration data from ambient vibration tests

Damage State	Natural Frequency [Hz]			Damping Ratio [%]			MAC		
	1^{st}-L mode	2^{nd}-L mode	3^{rd}-L mode	1^{st}-L mode	2^{nd}-L mode	3^{rd}-L mode	1^{st}-L mode	2^{nd}-L mode	3^{rd}-L mode
S0	1.91	10.51	24.51	2.3	2.4	0.5	1.00	1.00	1.00
S1	1.88	10.21	24.31	2.9	2.7	0.6	1.00	1.00	1.00
S2	1.67	10.16	22.60	1.3	1.4	0.9	1.00	0.97	0.96
S3.1	1.44	9.23	21.82	2.7	1.3	1.4	1.00	0.96	0.92
S3.2	1.58	8.48	22.72	1.3	1.9	1.2	1.00	0.99	0.99
S4	1.02	5.67	15.09	1.0	1.7	1.0	0.99	0.87	0.81

6.4 FINITE ELEMENT MODEL UPDATING FOR DAMAGE IDENTIFICATION

In this study, a sensitivity-based FE model updating strategy is used to identify (detect, localize and quantify) the damage in the test structure. The residuals used in the updating procedure are based on the identified natural frequencies and mode shapes for the first thee longitudinal modes of the shear wall building slice. Damage in the structure

is identified as a change in material stiffness (effective modulus of elasticity) of the finite elements in the different substructures of the FE model used for damage identification. For the purpose of damage identification, the effective moduli of elasticity of elements in various substructures (each assumed to have a uniform value of the effective modulus of elasticity) are updated at each damage state. Each time, the effective moduli of elasticity of the various substructures are updated from the reference/baseline model through constrained minimization of an objective function.

Table 6.4 Natural frequencies, damping ratios, and MAC values identified based on acceleration data from white noise base excitation tests (0.03g RMS)

Damage State	Natural Frequency [Hz]			Damping Ratio [%]			MAC		
	1^{st}-L mode	2^{nd}-L mode	3^{rd}-L mode	1^{st}-L mode	2^{nd}-L mode	3^{rd}-L mode	1^{st}-L mode	2^{nd}-L mode	3^{rd}-L mode
S0	1.71	11.05	24.31	2.1	1.8	0.5	1.00	1.00	1.00
S1	1.54	10.98	24.28	2.0	1.7	0.2	1.00	0.98	0.96
S2	1.24	11.11	21.59	3.0	2.9	0.5	1.00	0.87	0.77
S3.1	1.14	9.77	19.68	3.9	1.6	0.5	1.00	0.85	0.92
S3.2	1.20	10.45	21.11	3.5	2.0	0.3	1.00	0.69	0.79
S4	0.88	4.81	13.29	5.5	3.8	0.9	0.98	0.37	0.62

6.4.1 Objective Function

The objective function for damage identification is defined as

$$\begin{aligned} \min_{\boldsymbol{\theta}} f(\boldsymbol{\theta}) &= \mathbf{r}(\boldsymbol{\theta})^{\mathrm{T}}\mathbf{W}\mathbf{r}(\boldsymbol{\theta}) + (\mathbf{a}(\boldsymbol{\theta}) - \mathbf{a}^{0})^{\mathrm{T}}\mathbf{W}^{\mathrm{a}}(\mathbf{a}(\boldsymbol{\theta}) - \mathbf{a}^{0}) \\ &= \sum_{i}[w_i r_i(\boldsymbol{\theta})^2] + \sum_{k}[w_k^{\mathrm{a}}(a_k(\boldsymbol{\theta}) - a_k^{0})^2] \end{aligned} \tag{6.1}$$

where $\boldsymbol{\theta}$ = set of physical parameters (effective moduli of elasticity) which must be adjusted in order to minimize the objective function; $\mathbf{r}(\boldsymbol{\theta})$ = residual vector containing the differences between analytically computed (FE predicted) and experimentally identified modal parameters; $\mathbf{a}(\boldsymbol{\theta})$ = vector of dimensionless damage factors representing the level of damage in each of the substructures of the FE model used for damage identification (see next section); $\mathbf{a}^0$ = vector of initial damage factors used as starting point in the optimization process. At each damage state, $\mathbf{a}^0$ is selected as the identified damage factors for the previous damage state and $\mathbf{a}^0 = \mathbf{0}$ for damage state S1. In Equation 6.1, $\mathbf{W}$ is a weighting matrix for modal residuals, a diagonal weighting matrix with each component assigned based on the estimation uncertainty (coefficient-of-variation) of the corresponding mode natural frequency as well as the modal contribution of considered mode. The first vibration mode has a predominant contribution to the total response of the structure at all damage states, and therefore its corresponding residuals are assigned the largest weights among the three vibration modes. Still in Equation 6.1, $\mathbf{W}^a$ is a weighting matrix for damage factors, a diagonal weighting matrix with each diagonal component defining the relative cost (or penalty) of changing/updating the corresponding damage factor. The weights for damage factors reduce the estimation error of the damage factors in the presence of estimation uncertainty in the modal parameters, especially for the substructures with updating parameters to which the used residuals are less sensitive. In this study, these weight are set to $w_k^a = 0.01 \times w_1$ with $k = 1, \ldots, n_{sub}$ where n_{sub} denotes the number of substructures considered in FE model updating and w_1 is the weight assigned to the

modal residual associated to the natural frequency of the first mode. A combination of residuals in natural frequencies, and mode shape components is used in the objective function as

$$\mathbf{r}(\boldsymbol{\theta}) = \begin{bmatrix} \mathbf{r}_{\mathrm{f}}(\boldsymbol{\theta}) \\ \mathbf{r}_{\mathrm{s}}(\boldsymbol{\theta}) \end{bmatrix} \tag{6.2}$$

in which $\mathbf{r}_{\mathrm{f}}(\boldsymbol{\theta})$ and $\mathbf{r}_{\mathrm{s}}(\boldsymbol{\theta})$ represent the eigen-frequency and mode shape residuals, respectively, as

$$\mathbf{r}_{\mathrm{f}}(\boldsymbol{\theta}) = \left[\frac{\lambda_j(\boldsymbol{\theta}) - \tilde{\lambda}_j}{\tilde{\lambda}_j}\right], \qquad \mathbf{r}_{\mathrm{s}} = \left[\frac{\phi_j^{l}(\boldsymbol{\theta})}{\phi_j^{r}(\boldsymbol{\theta})} - \frac{\tilde{\phi}_j^{l}}{\tilde{\phi}_j^{r}}\right], \qquad l \neq r, \qquad j = 1, \ldots, \mathrm{n_m} \tag{6.3}$$

where $\lambda_j(\boldsymbol{\theta})$ and $\tilde{\lambda}_j$ denote the analytical (FE predicted) and experimental eigenvalues, respectively, corresponding to the $\mathrm{j^{th}}$ vibration mode with $\lambda_j(\boldsymbol{\theta}) = \omega_j^2$ and ω_j = natural circular frequency; $\boldsymbol{\phi}_j(\boldsymbol{\theta})$ and $\tilde{\boldsymbol{\phi}}_j$ denote the analytical (FE predicted) and experimentally identified mode shape vectors, respectively. It should be noted that for each vibration mode, the mode shapes $\boldsymbol{\phi}_j(\boldsymbol{\theta})$ and $\tilde{\boldsymbol{\phi}}_j$ are normalized in the same way, i.e., scaled to a reference component. In Equation 6.3, the superscript *r* indicates the reference component of a mode shape vector (with respect to which the other components of the mode shape are normalized), the superscript *l* refers to the mode shape components that are used in the FE model updating process (i.e., at the locations and in the directions of the sensors), and $\mathrm{n_m}$ denotes the number of vibration modes considered in the damage identification process. In this study, the natural frequencies and mode shapes of the first three longitudinal vibration

modes of the structure (see Figure 6.7) are used to form the residual vector $\mathbf{r}(\boldsymbol{\theta})$ which has a total of 42 residual components (when using 14 sensors) consisting of 3 eigen-frequency and $3 \times (14 - 1) = 39$ mode shape component residuals, respectively.

6.4.2 Damage Factors and Modal Residual Sensitivities

In the process of FE model updating, the material stiffness (effective modulus of elasticity) of each of the damage substructures are used as updating parameters in the FE model of the structure. Instead of the absolute value of each updating parameter, a dimensionless damage factor is defined as

$$\alpha_k = \frac{E^k_{\text{undamaged}} - E^k_{\text{damaged}}}{E^k_{\text{undamaged}}} \tag{6.4}$$

where E^k is the effective modulus of elasticity of all finite elements in substructure k ($k = 1, \ldots, n_{\text{sub}}$). Thus, the damage factor α_k indicates directly the level of damage (relative change in effective modulus of elasticity) in substructure k when FE model updating is used for the purpose of structural damage identification. The sensitivity of the modal residuals with respect to the damage factor α_k can be obtained from Equation 6.3 using the modal parameter sensitivities as

$$\frac{\partial \mathbf{r}_f}{\partial \alpha_k} = \left[\frac{1}{\tilde{\lambda}_j} \frac{\partial \lambda_j}{\partial \alpha_k} \right] \quad \text{and} \quad \frac{\partial \mathbf{r}_s}{\partial \alpha_k} = \left[\frac{1}{\phi_j^r} \frac{\partial \phi_j^l}{\partial \alpha_k} - \frac{\phi_j^l}{(\phi_j^r)^2} \frac{\partial \phi_j^r}{\partial \alpha_k} \right] \qquad (l \neq r) \tag{6.5}$$

where the modal sensitivities $\frac{\partial \lambda_j}{\partial a_k}$ and $\frac{\partial \boldsymbol{\Phi}_j}{\partial a_k}$ are available in Fox and Kapoor (1968). Notice that according to Equation 6.5, the sensitivity of the reference mode shape component with respect to a_k equals zero as it should be.

6.4.3 Optimization Algorithm

The optimization algorithm used to minimize the objective function defined in Equation 6.1 is a standard Trust Region Newton method (Coleman and Li, 1996), which is a sensitivity-based iterative method available in the MATLAB optimization Toolbox (Mathworks, 2005). The damage factors were constrained to be in a selected range (see Section 6.5) at each damage state. The optimization process was performed using the "fmincon" function in Matlab, with the Jacobian matrix and a first-order estimate of the Hessian matrix calculated analytically based on the sensitivities of modal parameters to the updating variables as given in Equation 6.5. The use of the analytical Jacobian, rather than the Jacobian estimated through finite difference calculations, increases significantly the efficiency of the minimization of the objective function.

6.4.4 Finite Element Modeling of Test Structure in FEDEASLab

A three dimensional linear elastic FE model of the test structure was developed using a general-purpose FE structural analysis program, FEDEASLab (Filippou and Constantinides, 2004) as shown in Figure 6.8. This model is defined by 340 nodes and 322 linear elastic shell and truss elements. A four-node linear elastic flat shell element (with four

Gauss integration points) borrowed from the FE literature was implemented in FEDEA-SLab in order to model the web wall, flange wall, concrete slabs, and the post-tensioned column (He et al., 2006). This shell element is based on the mixed discrete variational principle proposed by Hughes and Brezzi (1989) in conjunction with Allman type interpolation (Allman, 1988) for the membrane part and the discrete Kirchhoff plate element derived by Batoz and Tahar (1982) for the plate part. The resulting finite element has six degrees of freedom (DOFs) per node, including a true drilling DOF. In this FE model, the web wall at each of the first three stories is modeled using 16 shell elements, while the higher stories (5 to 7) are modeled using 4 shell elements each. The 4^{th} story of the web wall is modeled using 8 shell elements. The floor slabs are modeled using 24 shell elements for each of the first three floors and 12 shell elements for each of the higher floors (4 to 7). The flange wall and the post-tensioned column are modeled using 8 and 10 shell elements per story, respectively. The gravity columns and braces connecting the post-tensioned column to the building slabs are modeled using truss elements. The inertia properties of the test structure are discretized into lumped translational masses at each node of the FE model. This initial FE model of the shear wall building slice is based on the measured material properties and blue prints of the test structure (i.e., average material properties over 2 samples per story). Table 6.5 reports the measured moduli of elasticity (through concrete cylinder tests) at various heights (stories) of the test structure, which are used in the initial FE model of the test structure.

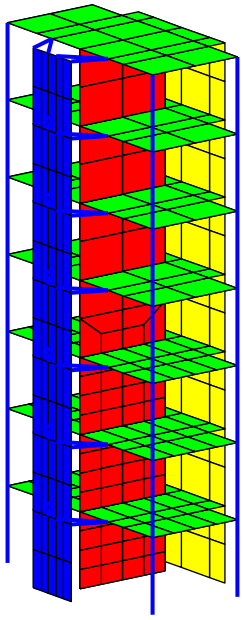

Fig. 6.8 Finite element model of the shear wall building slice in FEDEASLab

6.5 DAMAGE IDENTIFICATION

In this study, two different cases of damage identification are performed using the FE model updating algorithm described above based on two different sets of identified modal parameters of the test structure, namely (1) the modal parameters identified based on ambient vibration data, and (2) the modal parameters identified based on white noise base excitation test data. In each of these cases, the first step to identify damage in the test structure consists of obtaining a reference/baseline FE model based on the modal parameters identified at the undamaged (or baseline) state of the building (S0). In this step, the initial FE model is updated to match the identified modal parameters at the undamaged state of the test structure by updating the stiffness (effective moduli of elasticity) of seventeen (in the first case of damage identification) or twenty four (in the second case of dam-

age identification) substructures. The effective modulus of elasticity is assumed to be uniform/constant over each substructure. Therefore all finite elements of a substructure share the same value of the effective modulus of elasticity.

The seventeen substructures considered in the first damage identification case consist of: 10 substructures along the web wall (6 along the first three stories, every half story each, and 4 along higher stories, every story each) as shown in Figure 6.9, and 7 substructures consisting each of a floor slab. The twenty four substructures considered in the second damage identification case consist of the same seventeen substructures as those considered in the first damage identification case and 7 additional substructures containing each the braces (4 components) connecting one of the seven slabs to the post-tensioned column. It should be noted that the steel braces appeared to play an important role in the response of the test structure during the white noise base excitation tests due to the partial slackness (stick-slip behavior) of their connections to the slabs and post-tensioned column. The partial slackness of these connections was not fully exercised during the low-amplitude ambient vibration tests which did not cause any rattling behavior of the brace connections (i.e., the brace connections remained in the stick phase of their stick-slip behavior).

The effective moduli of elasticity of the various substructures obtained based on the modal parameters identified at the undamaged state S0 of the test structure, referred to herein as reference values, are reported in Table 6.5 for both cases of damage identifications together with the corresponding measured values of the concrete modulus of elasticity (on the day of the test) used in the initial FE model. For both cases of damage

identification, the “damage factors” are constrained in the range $[-\infty, 1]$ for updating the initial FE model to the reference FE model in order to result in positive effective moduli of elasticity. From the results obtained in Table 6.5, the following observations can be made: (1) The reference (calibrated) effective moduli of elasticity of the web wall differ from the corresponding measured (initial) values, especially in the second case which is based on white noise base excitation test data. This is due to the facts that (1) the updating parameters (moduli of elasticity) act as effective moduli of elasticity reflecting the overall stiffness of the test structure, including the contributions of other structural components such as flange wall, post-tensioned column and gravity columns for which the parameters are not calibrated/updated, and (2) the structure under white noise base excitation behaves as a cracked structure as opposed to the mainly uncracked behavior of the test structure under ambient excitation.

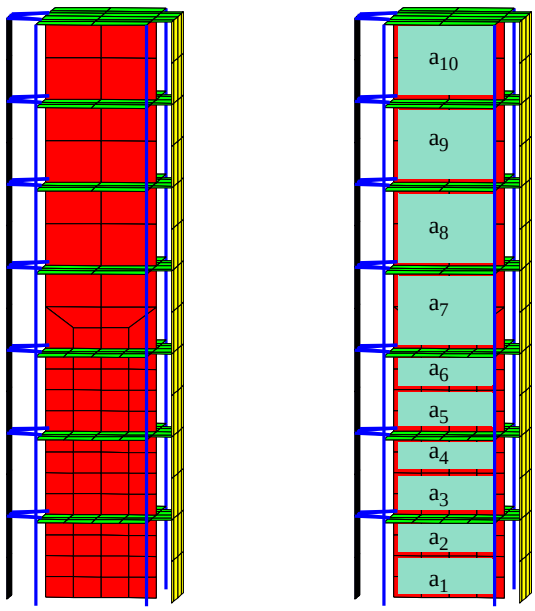

Fig. 6.9 Substructures along the web wall considered for damage identification

Table 6.5 Measured and effective moduli of elasticity of structural components at different substructures of initial and reference FE models

Substructure	Moduli of Elasticity [GPa]		
	Initial FE model	Reference FE model based on ambient vibration data	Reference FE model based on white noise test data
Web wall, 1st story (bot.)	24.5	17.1	31.9
Web wall, 1st story (top)	24.5	21.6	18.6
Web wall, 2nd story (bot.)	26.0	27.4	7.8
Web wall, 2nd story (top)	26.0	25.9	22.4
Web wall, 3rd story (bot.)	34.8	35.3	45.0
Web wall, 3rd story (top)	34.8	37.5	49.1
Web wall, 4th story	30.2	33.9	49.7
Web wall, 5th story	28.9	28.4	44.3
Web wall, 6th story	32.1	34.4	50.4
Web wall, 7th story	33.5	34.6	43.3
Slab, 1st floor	24.5	22.9	29.1
Slab, 2nd floor	26.0	24.6	23.6
Slab, 3rd floor	34.8	35.6	27.0
Slab, 4th floor	30.2	26.2	30.6
Slab, 5th floor	28.9	25.5	32.8
Slab, 6th floor	32.1	28.0	37.3
Slab, 7th floor	33.5	28.9	39.2
Steel braces, 1st floor	200	200[a]	252
Steel braces, 2nd floor	200	200[a]	18
Steel braces, 3rd floor	200	200[a]	42
Steel braces, 4th floor	200	200[a]	215
Steel braces, 5th floor	200	200[a]	306
Steel braces, 6th floor	200	200[a]	10
Steel braces, 7th floor	200	200[a]	2

a. These parameters were not updated for the reference FE model based on ambient vibration data.

6.5.1 Case I: Damage Identification Based on Ambient Vibration Data

In this case of damage identification, once the reference model is determined, 10 updating parameters (corresponding to 10 substructures) are updated from the reference FE model to damage states S1, S2, S3.1, and S4. These 10 substructures are selected along the web wall 6 along the first three stories (every half story each), and 4 along higher stories (every story each) as shown in Figure 6.9(b). The value of the other updating parameters (moduli of elasticity of other substructures considered in Table 6.5) are fixed as in the reference FE model. In each of the considered damage states, the natural frequencies and mode shapes of the first three longitudinal vibration modes are used in the objective function for damage identification, resulting in a residual vector with 42 components (i.e., 3 natural frequencies and 3 vibration mode shapes of $14 - 1 = 13$ components each).

For updating the FE model to states S1 through S4, the dimensionless damage factors were constrained to be in the range [0, 0.95]. The upper-bound of 95% was selected based on the observed damage in the test structure, while the lower bound of 0% was selected considering that the identified effective moduli of elasticity are not expected to increase with increasing damage. As already mentioned in Section 6.4.1, at each damage state the initial damage factors used as starting point in the optimization process are selected as the identified damage factors for the previous damage state or zero for damage state S1. The damage factors (relative to the reference FE model or reference state) obtained at different damage states are presented in a bar plot in Figure 6.10. These results

indicate that: (1) the severity of structural damage increases as the structure is exposed to stronger earthquake excitations; and (2) the extent of damage decreases rapidly along the height of the structure (damage concentrated in the two bottom stories), except for a false alarm in the fourth story at damage state S4. The large identified damage factor in the fourth story may be due to the facts that: (i) the identified modal parameters at damage state S4 are characterized by a higher level of estimation uncertainty than at the previous damage states; and (ii) the optimization algorithm used is not a global optimization algorithm and the probability to converge to a local minimum (which is not the global minimum) increases with increasing difference between the identified modal parameters at two consecutive damage states.

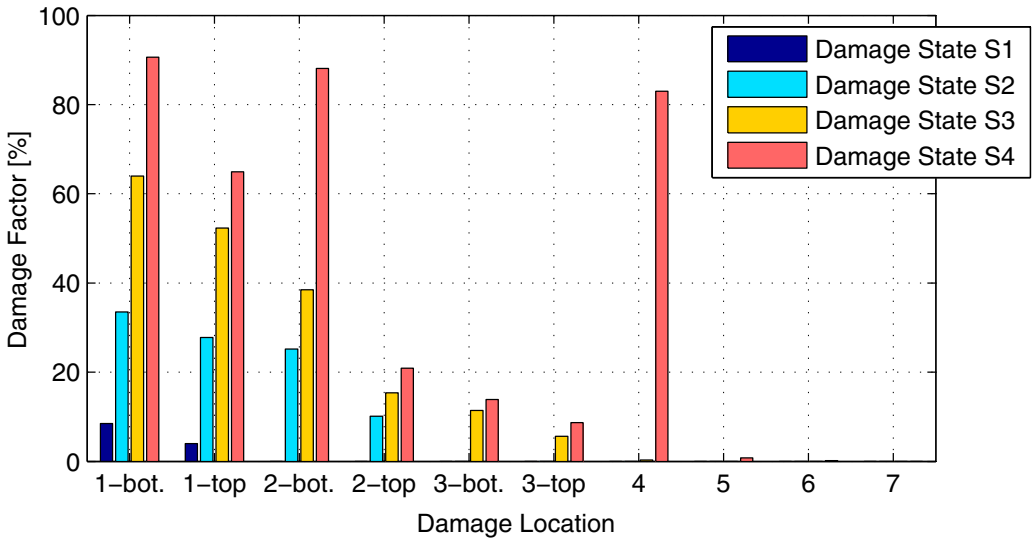

Fig. 6.10 Identified damage factors at various substructures for damage identification case I (based on ambient vibration data)

Table 6.6 presents the natural frequencies computed from the updated FE model at each damage state together with their counterparts identified from ambient vibration data as well as the MAC values between analytical (FE computed) and experimental mode

shapes. It should be noted that the analytical (FE computed) mode shapes were truncated at the locations of the accelerometers in order to match the size of the experimental mode shapes. Figure 6.11 shows the comparison between analytical and experimental natural frequencies in bar plots. From Table 6.6 and Figure 6.11, it is observed that: (1) in general, the discrepancies between analytical and identified natural frequencies are larger (in both absolute and relative terms) for the second and third modes than for the first mode. This is due to the fact that the identified modal parameters of the second and third modes are not as accurate as (i.e., have a larger estimation uncertainty than) those of the first mode, resulting in smaller weight factors being assigned to their corresponding residuals. (2) The MAC values between analytical and identified mode shapes are very close to unity at all damage states except damage state S4 at which the MAC values for the second and third modes are lower. This will result in a lower level of confidence for the identified damage at damage state S4. Pictures of the actual damage at the bottom two stories of the web wall at damage state S4 are shown in Figures 6.12 to 6.15. Figures 6.12 and 6.13 show that horizontal flexural cracks as well as inclined/diagonal cracks are developed at the first two stories of the web wall. During the seismic test EQ4, a lap-splice failure (i.e., debonding between longitudinal steel reinforcement bars and the surrounding concrete) occurred in the web wall at the bottom of the second story on the west side as shown in Figure 6.15. Figure 6.16 shows the envelope of concrete tensile strains along the shear wall height for the first two stories measured from LVDTs during the four seismic tests. Figure 6.17 shows the envelope of steel tensile strains along the vertical steel reinforcement bars measured from strain gages during the four seismic tests. Figures 6.14 and 6.15 together with the envelope of the tensile strains along the concrete of the web wall and in the longitudi-

nal steel reinforcement bars in Figures 6.16 and 6.17 provide a physical observation/measure of the damage in the wall. The damage identification results (see Figure 6.10) obtained in this study are consistent with the actual damage observed in the test structure. They capture correctly the concentration of damage in the first two stories of the web wall and the fact that in each of these two stories there is more damage in the bottom half than in the top half.

Table 6.6 Comparison of FE computed and experimentally identified modal parameters

Damage State	Experimentally Identified Natural Frequencies [Hz]			FE Computed Natural Frequencies [Hz]			MAC		
	1^{st}-L mode	2^{nd}-L mode	3^{rd}-L mode	1^{st}-L mode	2^{nd}-L mode	3^{rd}-L mode	1^{st}-L mode	2^{nd}-L mode	3^{rd}-L mode
S0	1.91	10.51	24.51	1.89	10.37	25.03	1.00	0.99	0.96
S1	1.88	10.21	24.31	1.86	10.25	24.91	1.00	0.99	0.97
S2	1.67	10.16	22.60	1.69	9.82	22.43	1.00	0.98	0.98
S3.1	1.44	9.28	21.82	1.46	9.06	21.36	1.00	0.97	0.96
S4	1.02	5.67	15.09	1.01	5.82	15.59	1.00	0.90	0.88

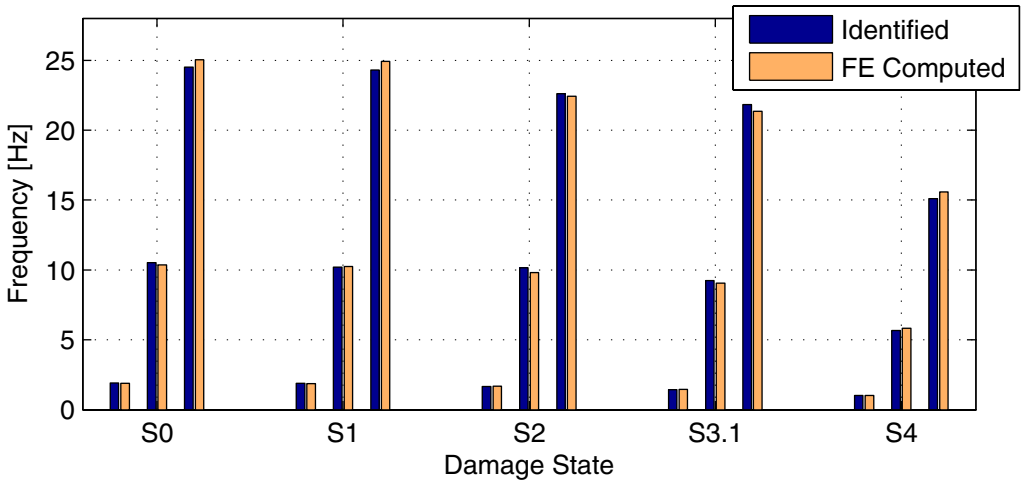

Fig. 6.11 Natural frequencies computed from the updated FE model at each damage state together with their counterparts identified from ambient vibration data

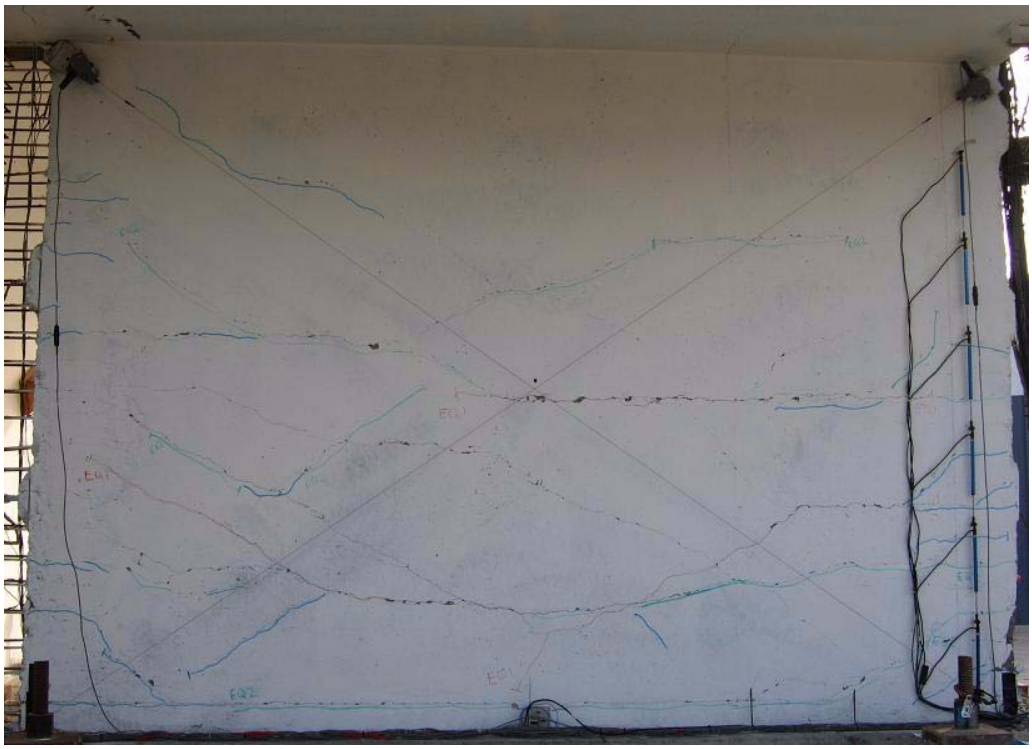

Fig. 6.12 Observed cracks at the first story of the web wall at damage state S4

Fig. 6.13 Observed cracks at the second story of the web wall at damage state S4

Fig. 6.14 Observed damage at the bottom of the first story of the web wall on the west side at damage state S4

(a) (b)

Fig. 6.15 Splitting crack due to lap-splice failure at the bottom of the second story of the web wall on the west side at damage state S4

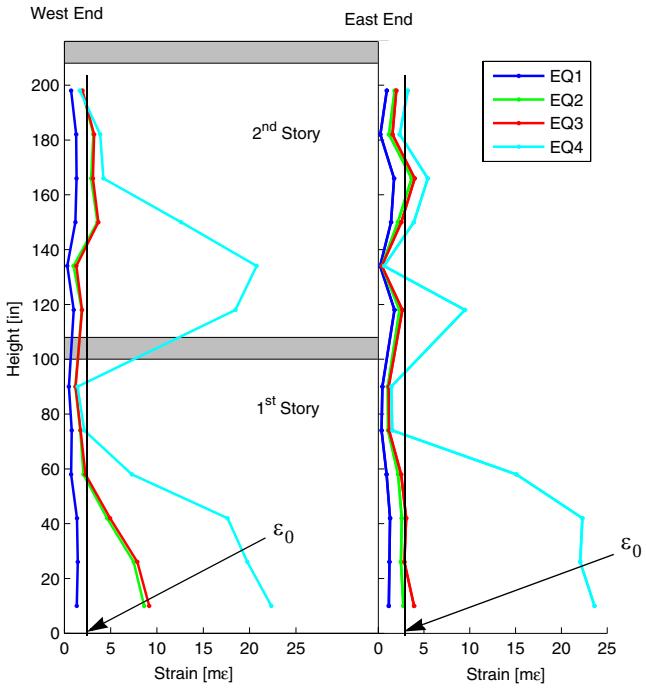

Fig. 6.16 Envelope of concrete tensile strains along the shear wall height for the first two stories measured from LVDTs during the four seismic tests (ε_0 = strain corresponding to maximum compressive stress of concrete)

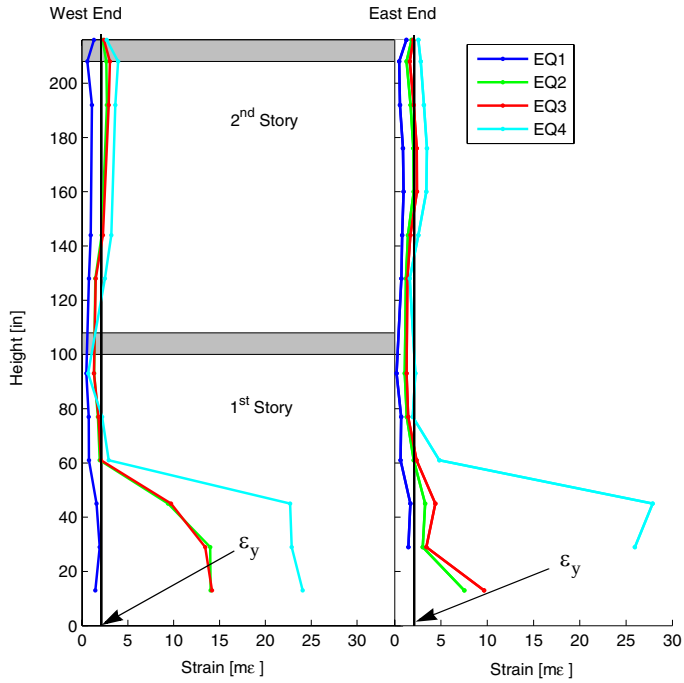

Fig. 6.17 Envelope of steel tensile strains along the vertical steel reinforcement bars measured from strain gages during the four seismic tests (ε_y = yield strain of reinforcement steel)

6.5.2 Case II: Damage Identification Based on White Noise Base Excitation Data

In the second case of damage identification, 24 updating parameters (corresponding to 24 substructures) are updated to damage states S1, S2, S3.1, and S4. These 24 substructures are the same as those used for updating the initial FE model to the reference FE model. The twenty four substructures consist of 10 substructures along the web wall (6 along the first three stories, every half story each, and 4 along the higher stories, every story each), 7 substructures consisting each of a floor slab, and 7 substructures each containing the set of four steel braces connecting one of the seven slabs to the post-tensioned column. As already mentioned, the steel braces appeared to play an important role in the response of the test structure for the case of white noise base excitation due to the partial slackness (stick-slip behavior) of their connections to the slabs and post-tensioned column. This phenomenon was not significant in the ambient vibration tests which were of too low amplitude to exercise the stick-slip (rattling) behavior of the brace connections. At each damage state, the initial damage factors used as starting point in the optimization process are selected as the identified damage factors for the previous damage state or zero for damage state S1. In updating the reference FE model to states S1 through S4, the dimensionless damage factors for the first seventeen substructures (web wall and floor slabs) were constrained to be in the range [0, 0.95]. The damage factors for the seven substructures each consisting of a set of steel braces connecting a floor slab to the post-tensioned column were constrained to be in the range [-2.00, 0.95]. The lower bound of -2.00 was selected since after some of the seismic tests, the braces were modified to remove the partial slackness of their connections, with the most significant modification (retrofit) made

after EQ3. The identified damage factors (relative to the reference state) obtained for the web wall and floor slabs at various damage states are presented in bar plot in Figure 6.18. These results indicate that: (1) the severity of structural damage increases as the structure is exposed to stronger earthquake excitations; (2) in general, the level of damage identified in the floor slabs is smaller than that identified in the web wall; and (3) at each damage state, the most severe damage is identified at the first story (top and bottom) and second story (bottom) of the web wall. However, at damage state S4, severe damage is spuriously identified at the top of the third and the fifth stories. The large identified damage factors at these two locations can be due to the following facts: (1) the estimation uncertainty in the identified modal parameters at damage state S4 (especially for the third mode) is higher than at lower damage states; (2) the optimization algorithm used to update the FE model parameters is not a global optimization algorithm and becomes less robust for larger changes in identified modal parameters between two consecutive damage states; and (3) with increasing level of damage, the level of nonlinearity in the structural response (even to the relatively low amplitude 0.03g RMS white noise base excitation) increases. Therefore, the assumption that the structure behaves as a linear dynamic system is violated and a linear dynamic model (modal model) is not strictly able to represent well the structure (modal parameters become effective modal parameters).

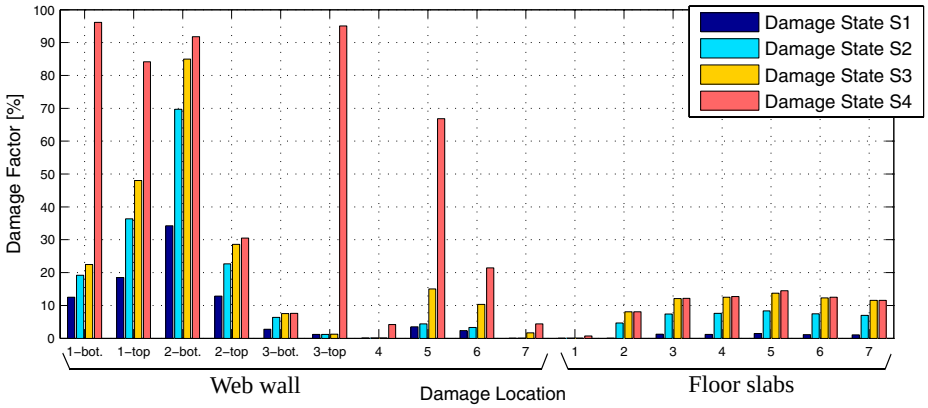

Fig. 6.18 Identified damage factors at 17 substructures for damage identification case II (based on white noise base excitation data)

Table 6.7 presents the natural frequencies computed from the updated FE model at each damage state together with their counterparts identified from white noise base excitation test data as well as the MAC values between analytical (FE computed) and experimental mode shapes. The analytical (FE computed) mode shapes were truncated at the locations and directions of the accelerometers in order to match the size of the experimental mode shapes. Figure 6.19 represents the identified and FE computed natural frequencies in bar plots. From Table 6.7 and Figure 6.19, it is observed that: (1) the discrepancies between analytical and identified natural frequencies are larger (in both absolute and relative terms) for the second and third modes than for the first mode. This is due to the fact that the identified modal parameters of the second and third modes are not as accurate as (i.e., have a larger estimation uncertainty than) those of the first mode and therefore smaller weight factors are assigned to their corresponding residuals in the objective function. (2) The MAC values between analytical and identified mode shapes of the first and third longitudinal modes are close to unity for all damage states, indicating the high correlation obtained between analytical and identified mode shapes for these vibration modes.

However the low MAC value obtained for the second vibration mode can be due to the fact that the estimation uncertainty for this mode was relatively large (maybe due to the proximity of the natural frequency of this vibration mode to the oil-column frequency of the shake table). By comparing these results (on the match between analytical and identified modal parameters at all damage states considered) to their counterparts from damage identification case one, it is observed that the analytical and experimental modal parameters in case one are in better agreement than in case two. This could be due to larger modeling error in case two in which the assumption of linear dynamic behavior was not as well satisfied as in case 1 even for the relatively low amplitude of dynamic excitation (0.03g RMS acceleration). Therefore, the results from the first case of damage identification are expected to be more accurate.

Table 6.7 Comparison of FE computed and experimentally identified modal parameters

Damage State	Experimentally Identified Natural Frequencies [Hz]			FE Computed Natural Frequencies [Hz]			MAC		
	1^{st}-L mode	2^{nd}-L mode	3^{rd}-L mode	1^{st}-L mode	2^{nd}-L mode	3^{rd}-L mode	1^{st}-L mode	2^{nd}-L mode	3^{rd}-L mode
S0	1.71	11.05	24.31	1.73	10.48	23.87	1.00	0.99	0.99
S1	1.54	10.98	24.28	1.55	9.93	24.06	1.00	0.97	0.99
S2	1.24	11.11	21.59	1.28	9.34	19.43	1.00	0.81	0.91
S3.1	1.14	9.77	19.68	1.10	8.54	19.42	1.00	0.58	0.93
S4	0.88	4.81	13.29	0.84	4.90	13.64	0.99	0.85	0.93

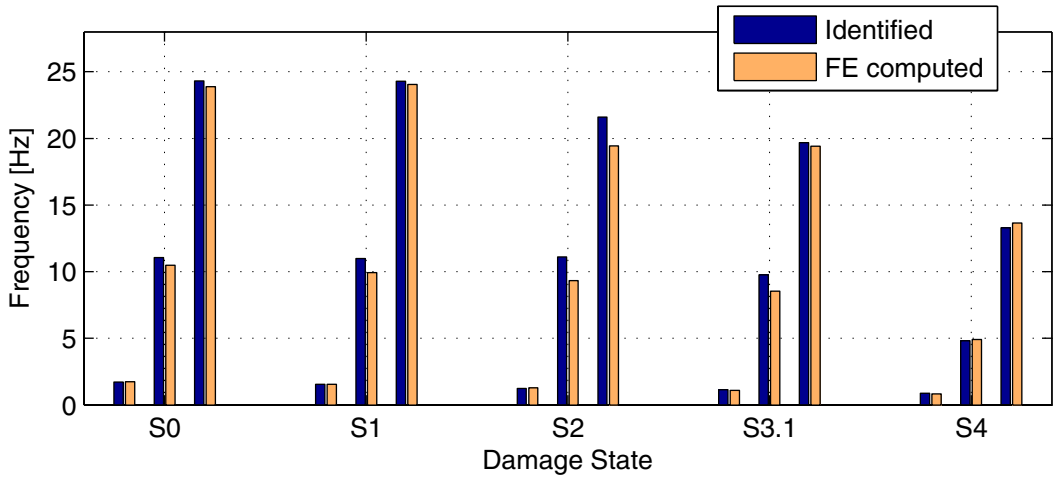

Fig. 6.19 Natural frequencies computed from the updated FE model at each damage state together with their counterparts identified from white noise test data

The differences in the identified damage results obtained from the two different cases can be due to a number of reasons: (1) different identified modal parameters are used in the two cases, each with different level of estimation uncertainty (the ambient vibration data satisfy better the assumption of system linearity and therefore are more appropriate as inputs for linear FE model updating inputs), (2) different reference/baseline models are considered for the two identification cases, (3) different weights were assigned to the modal residuals in the two cases (due to different estimation uncertainties), and (4) different numbers of updating parameters are used in the two cases.

6.6 CONCLUSIONS

A full-scale seven-story reinforced concrete shear wall building slice was tested on the UCSD-NEES shake table in the period October 2005 - January 2006. The shake table tests were designed so as to damage the building progressively through several historical seismic motions reproduced on the shake table. At various levels of damage, low ampli-

tude white noise base excitations were applied through the shake table to the building which was assumed to respond as a quasi-linear system with modal parameters depending on the level of structural damage. In addition to white noise base excitation tests, ambient vibration tests were performed on the building specimen at various damage levels. Based on the modal parameters identified at different damage states, a sensitivity-based finite element model updating strategy is applied for damage identification of the test structure. Accordingly, damage in the test structure is identified as a change in stiffness (effective modulus of elasticity) of finite elements in the different substructures the structural model is subdivided into. In the FE model updating procedure, the objective function is defined as a weighted sum of modal residuals in natural frequencies and mode shape components of the first three longitudinal vibration modes of the test structure. The optimization algorithm used to minimize the objective function is a standard Trust Region Newton method, which is a sensitivity-based iterative method available in the MATLAB optimization Toolbox. Analytical sensitivities of the objective function to the updating parameters are used in the optimization algorithm.

Two different cases of damage identification are performed using the FE model updating algorithm based on two different sets of identified modal parameters of the test structure, namely (1) the modal parameters identified based on ambient vibration data, and (2) the modal parameters identified based on white noise base excitation test data. From the damage identification results obtained the following observations can be made. (1) In both damage identification cases as expected, the severity of structural damage increases as the structure is exposed to stronger earthquake excitations. (2) At each damage state,

the most severe damage is identified at the first story (top and bottom) and second story (bottom) of the web wall. The damage identification results obtained in this study are consistent with the actual damage directly observed in the test structure or inferred from strain gages and LVDT measurement data. They capture correctly the concentration of damage in the bottom two stories of the web wall. However, at damage state S4, severe damage is spuriously identified at some higher stories of the web wall (fourth story in case I, third and fifth stories in case II). The large identified damage factors at these locations can be due to the following facts: (i) the estimation uncertainty in the identified modal parameters at damage state S4 (especially for the third mode) is higher than at lower damage states; (ii) the optimization algorithm used to update the FE model parameters is not a global optimization algorithm and becomes less robust for larger changes in identified modal parameters between two consecutive damage states; and (iii) with increasing level of damage, the level of nonlinearity in the structural response (even to the relatively low amplitude 0.03g RMS white noise base excitation) increases. Therefore, a linear dynamic model (modal model) is not strictly able to represent well the actual test structure.

The differences in the identified damage results obtained from the two different cases can be due to a number of reasons: (1) different identified modal parameters are used in the two cases, each with different level of estimation uncertainty (the ambient vibration data are more representative of a linear system and are therefore more appropriate for linear FE model updating), (2) different reference/baseline models are considered for the two identification cases, (3) different weights were assigned to the modal residuals in the two cases, and (4) different numbers of updating parameters are used in the two cases.

The analytical modal parameters obtained from the updated FE models are in better agreement with their experimentally identified counterparts in case I than in case II. This could be due to a larger modeling error in case II in which the assumption of linear dynamic behavior was not as satisfied as in case I, even for the relatively low amplitude of dynamic excitation (0.03g RMS acceleration). Therefore, the results from case I of damage identification are expected to be more accurate. Finally, it should be noted that the success of vibration-based damage identification depends significantly on the accuracy and completeness of the available identified modal parameters. Clearly, if estimation uncertainty in the modal parameters is larger than their changes due to damage, it is impossible to resolve/identify the actual damage in the structure.

ACKNOWLEDGEMENTS

Partial support of this research by Lawrence Livermore National Laboratory with Dr. David McCallen as Program Leader and by the Englekirk Center Industry Advisory Board are gratefully acknowledged. Any opinions, findings, and conclusions or recommendations expressed in this material are those of the authors and do not necessarily reflect those of the sponsors.

REFERENCES

Allman, D. J. (1988). “A quadrilateral finite element including vertex rotations for plane elasticity analysis.” *International Journal for Numerical Methods in Engineering*, Vol. 26, No. 3, 717-730.

Batoz, J. L., and Tahar, M. B. (1982). “Evaluation of a new quadrilateral thin plate bending element.” *International Journal for Numerical Methods in Engineering*, Vol. 18, No. 11, 1655-1677.

Adeli, H., and Jiang, X. (2006). “Dynamic fuzzy wavelet neural network model for structural system identification.” *Journal of Structural Engineering,* ASCE, 132(1), 102-111.

Bernal, D., and Gunes, B. (2004). “Flexibility based approach for damage characterization: benchmark application.” *Journal of Engineering Mechanics*, ASCE, 130(1), 61-70.

Coleman, T. F., and Li, Y. (1996). “An interior, Trust Region approach for nonlinear minimization subject to bounds.” *SIAM Journal on Optimization*, 6(2), 418-445.

Doebling, S. W., Farrar, C. R., Prime, M. B., and Shevitz, D. W. (1996). *Damage identification in structures and mechanical systems based on changes in their vibration characteristics: a detailed literature survey.* Los Alamos National Laboratory Report, LA-13070-MS, Los Alamos, New Mexico, USA.

Doebling, S. W., Farrar, C. R., and Prime, M. B. (1998). “A summary review of vibration-based damage identification methods.” *The Shock and Vibration Digest*, 30(2), 99-105.

Filippou, F. C., and Constantinides, M., (2004). *FEDEASLab getting started guide and simulation examples*. Technical Report NEESgrid-2004-22, http://fedeaslab.berkeley.edu.

Fox, R. L., and Kapoor, M. P. (1968). “Rates of change of eigenvalues and eigenvectors.” *AIAAJ,* 6(12), 2426-2429.

Friswell, M. I., and Mottershead, J. E. (1995). *Finite element model updating in structural dynamics.* Kluwer Academic Publishers, Boston, USA.

He, X., Moaveni, B., Conte, J. P., Restrepo, J. I., and Elgamal, A. (2006). "Damage identification of a seven-Story reinforced concrete shear wall building tested on UCSD-NEES shake table" *Proc. of 4th World Conference on Structural Control and Monitoring,* San Diego, USA.

Hughes, T. J. R., and Brezzi, F., (1989). "On drilling degrees of freedom." *Computer Methods in Applied Mechanics and Engineering*, Vol. 72, 105-121.

Maeck, J., and De Roeck, G. (1999). "Dynamic bending and torsion stiffness derivation from modal curvatures and torsion rates." *Journal of Sound and Vibration*, 225(1), 153-170.

MathWorks Inc. (2005). *Matlab - High performance numeric computation and visualization software, User's Guide.* The MathWorks Inc., Natick, MA.

Moaveni, B., He, X., and Conte, J. P., (2008). "System identification of a seven-Story reinforced concrete shear wall building tested on the UCSD-NEES shake table", *Journal of Structural Engineering,* ASCE, under review.

Panagiotou, M., Restrepo, J. I., and Conte, J. P. (2007). *Shake table test of a 7-story full scale reinforced concrete structural wall building slice, Phase I: Rectangular section*. Department of Structural Engineering, University of California, San Diego, Report No. SSRP-07/07.

Pandey, A. K., Biswas, M., and Samman, M. M. (1991). "Damage detection from changes in curvature mode shapes." *Journal of Sound and Vibration*, 145(2), 321-332.

Salawu, O.S. (1997). "Detection of structural damage through changes in frequency: A review." *Engineering Structures*, 19(9), 718-723.

Shi, Z. Y., Law, S. S., and Zhang, L. M. (2002). "Improved damage quantification from elemental modal strain energy change." *Journal of Engineering Mechanics*, ASCE, 128(5), 521-529.

Sohn, H., Farrar, C. R., Hemez, F. M., Shunk, D. D., Stinemates, D. W., and Nadler, B. R. (2003). *A review of structural health monitoring literature: 1996-2001*. Los Alamos National Laboratory Report, LA-13976-MS, Los Alamos, New Mexico, USA.

Teughels, A., and De Roeck, G. (2004). "Structural damage identification of the highway bridge Z24 by finite element model updating." *Journal of Sound and Vibration*, 278(3), 589–610.

CHAPTER 7

UNCERTAINTY ANALYSIS OF MODAL PARAMETERS OBTAINED FROM THREE SYSTEM IDENTIFICATION METHODS

7.1 INTRODUCTION

In recent years, structural health monitoring has received increased attention from the civil engineering research community as a potential tool to identify damage at the earliest possible stage and evaluate the remaining useful life of structures (damage prognosis). Standard damage identification procedures involve conducting repeated vibration surveys on the structure during its lifetime. Experimental modal analysis (EMA) has been explored as a technology for identifying dynamic characteristics as well as identifying damage in structures. Extensive literature reviews on damage identification methods based on changes in dynamic properties are provided by Doebling et al. (1998) and Sohn et al. (2003). It should be indicated that the success of damage identification based on EMA depends strongly on the accuracy and completeness of the identified structural dynamic properties. This study investigates that the level of confidence which can be placed in the identified structural dynamic properties for structural health monitoring purposes is a function of, not only the magnitude of damage, but also choices made to design the experimental procedure, collect and process the measurements.

A full-scale seven-story reinforced concrete (R/C) shear wall building slice was tested on the UCSD-NEES shake table in the period October 2005 - January 2006. The shake table tests were designed so as to damage the building progressively through several historical seismic motions reproduced on the shake table. At various levels of damage, several low amplitude white noise base excitations were applied, through the shake table, to the building that responded as a quasi-linear system with design parameters evolving as a function of damage. Three state-of-the-art system identification algorithms based on output-only data were used to estimate the modal parameters (natural frequencies, damping ratios and mode shapes) of the building at its undamaged (baseline) and various damage states (Moaveni et al., 2006). In this study, the performance of these system identification algorithms is systematically investigated as a function of uncertainty/variability in the following input factors: (1) amplitude of input excitation (considered at 3 levels), (2) spatial density of measurements (considered at 3 levels), (3) measurement noise (considered at 4 levels), and (4) length of response data used in the identification process (considered at 4 levels). This uncertainty analysis is performed based on the response of the structure simulated with a three-dimensional nonlinear finite element model generated in the analysis framework OpenSees (Mazzoni et al., 2006). A full factorial design of experiments is used that considers $3 \times 3 \times 4 \times 4 = 144$ combinations of the aforementioned four factors. Due to the random characteristics of the added noise vector processes, at each combination of the four factors studied, 100 independent noise vector processes are generated and added to the simulated response which results in a total of 14,400 identification runs for each method considered or 43,200 overall identification runs for the three methods. The mean and standard deviation values of the identified modal parameters over these 100 identifi-

cation runs with independent noise vector processes are considered in this study. The overall 43,200 system identification runs are performed in Matlab using a fast server computer with Intel Xeon processor (3.0GHz) and the total computation time is approximately 108 hours. Two methods are employed to quantify the variability of the identified modal parameters due to variation of the four input factors: (1) effect screening through analysis-of-variance (ANOVA) (Saltelli et al., 2000), and (2) meta-modeling (Wu et al., 2000).

7.2 NUMERICAL SIMULATION OF BUILDING SLICE RESPONSE DATA

The full-scale seven-story R/C building slice tested on the UCSD-NEES shake table consists of a main wall (web wall), a back wall perpendicular to the main wall (flange wall) for lateral stability, concrete slabs at each floor level, an auxiliary post-tensioned column to provide torsional stability, and four gravity columns to transfer the weight of the slabs to the shake table. Figure 7.1 shows a picture of the test structure, a drawing of its elevation, and a rendering of its finite element (FE) model. Also, a plan view of the structure is presented in Figure 7.2. Details about construction drawings, material test data, and other information on the experimental set-up is available at the UCSD-NEES web site (http://nees.ucsd.edu/7Story.html). A three dimensional nonlinear finite element model of the building is developed using the object-oriented software framework OpenSees for advanced modeling and response simulations of structural and/or geotechnical systems with applications in earthquake engineering (Mazzoni et al., 2006).

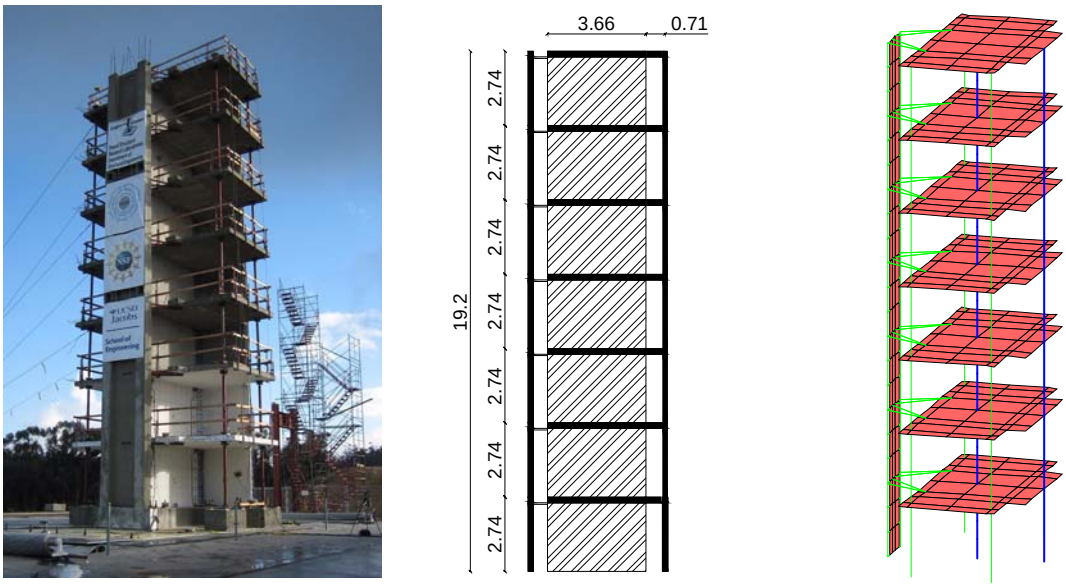

(a) Test structure (b) Elevation dimensions (unit: m) (c) Finite element model

Fig. 7.1 R/C shear wall building slice

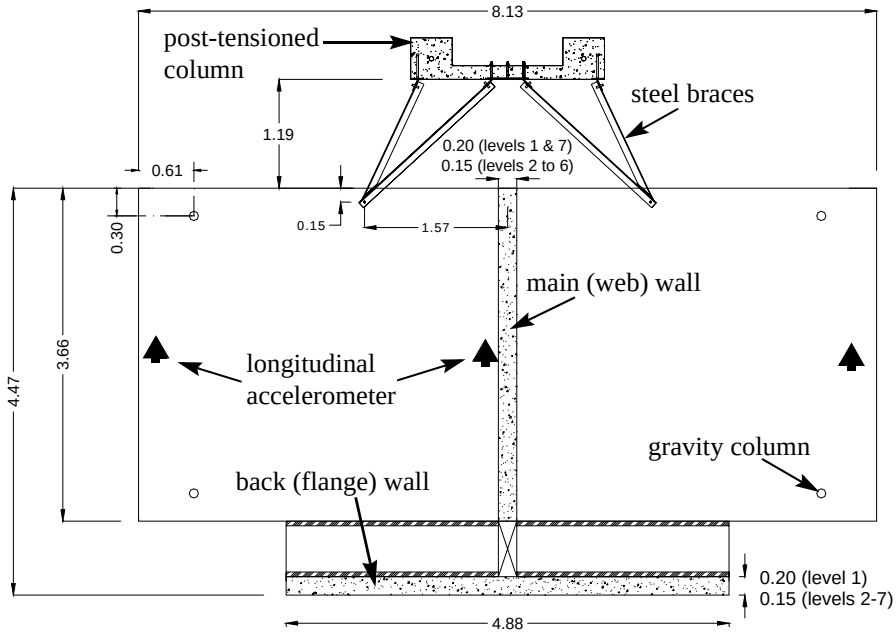

Fig. 7.2 Plan view of the test structure (unit: m)

The FE model shown in Figure 7.1(c) is composed of 509 nodes, 233 beam-column elements and 315 linear elastic shell elements. Both the web and flange walls are

modeled as force-based nonlinear beam-column elements with fiber cross-sections. These elements consider the spread of plasticity along the height of the walls. The fiber cross-sections are defined from the cross-sectional geometry, longitudinal reinforcement bars, and material properties of the walls. As illustration, one of the fiber elements and its components are shown in Figure 7.3. For each story, the web wall is discretized into four elements, and along the length of each element four Gauss-Lobatto integration points are used. From the foundation to the first level, the fiber cross-section of the web wall contains the following sub-regions: two regions near the ends of the wall containing confined concrete; one region near one of the ends also containing confined concrete but with a different level of confinement; and the cover and central regions containing unconfined concrete. From the second to the last story, the entire cross-sections of both the web and flange walls are modeled with unconfined concrete material. All the longitudinal reinforcing steel bars are discretized at the locations specified on the construction drawings. The material type Concrete04 is used to model both the unconfined (cover) and confined concrete regions. This new OpenSees uni-axial material constitutive model is based on the modified Kent-Park model to represent the concrete compressive stress-strain curve enhanced by using the pre- and post-peak curves proposed by Popovics in 1973 (Mazzoni et al., 2006). The unloading and reloading stress-strain characteristics are based on the work by Karsan and Jirsa (1969). Tension capacity and softening are also specified for the concrete material models used in the FE model. The properties of the confined concrete fibers are determined according to Mander's model (Mazzoni et al., 2006). The deformed mild steel reinforcement is modeled using the Steel02 material model, which corresponds to the Menegotto-Pinto model that is able to reproduce the Bauschinger effect (Paulay and

Priestley, 1992). The fiber section accounts properly for the nonlinear material coupling between the axial and bending behaviors, and the linear-elastic shear force-deformation behavior is aggregated in an uncoupled way at the section level. Shear behavior is coupled to the bending behavior only at the element level through equilibrium. For more details about the models used and the underlying theory, the interested reader is referred to the OpenSees User's Manual (Mazzoni et al., 2006).

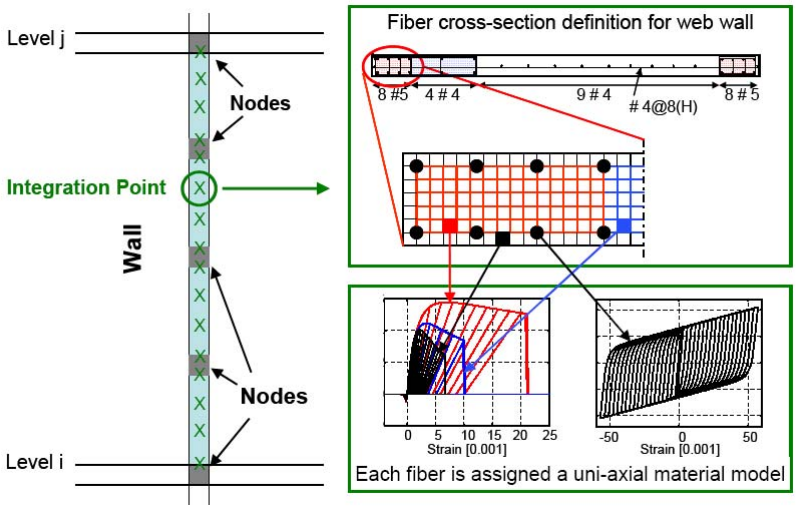

Fig. 7.3 Force-based nonlinear beam-column element

The gravity columns, braces and post-tensioned column are assumed to remain linear elastic during the analyses, so they are modeled as linear elastic elements. For the same reason, the slabs are also modeled as linear elastic shell elements. The slotted connection between the slab and flange wall is modeled using shell elements with reduced thickness. All tributary masses and corresponding gravity loads are applied to the slab nodes. Rayleigh damping is assigned to the model by matching a damping ratio of 2.5% at 2Hz and 10Hz, which is based on the results from previous system identification studies on this structure (Moaveni et al., 2006). During the analysis, the gravity loads are first

applied to the model quasi-statically followed by the rigid-base excitation, which is applied dynamically. As base acceleration records, three records are generated as Gaussian banded white noise processes (between 0.25Hz and 30Hz) with a root mean square acceleration of 0.03g, 0.06g or 0.09g, respectively, where g denotes the acceleration of gravity. The implicit Newmark integration procedure with a time-step of 1/120sec is used as time-stepping scheme. The longitudinal acceleration response histories are recorded at 28 different locations that correspond to the sensor locations on the test structure. They include three accelerometers at each floor level (Figure 7.2) and one at the mid-height of each story. The first three longitudinal mode shapes together with their corresponding natural frequencies and damping ratios are shown in Figure 7.4.

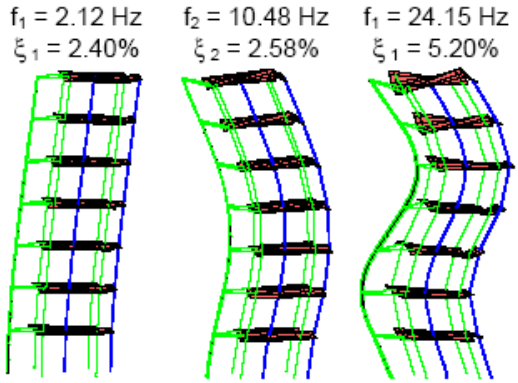

Fig. 7.4 First three longitudinal mode shapes of FE model of test structure

These mode shapes and natural frequencies were computed based on the initial tangent stiffness matrix (after application of gravity loads) and are in good agreement with their experimentally identified counterparts for the undamaged structure (Moaveni et al., 2006). The FE model is validated by comparing the simulated response histories with their experimental counterparts when subject to the same input excitations. The maximum roof

displacements closely match their experimentally measured counterparts for the same amplitudes of excitations considered in this study.

7.3 DESCRIPTION OF INPUT FACTORS STUDIED AND DESIGN OF EXPERIMENTS

As already mentioned, the objective of this study is to analyze and quantify the variability of the modal parameters obtained using three system identification methods due to the variability of four input factors: (1) excitation amplitude (level of nonlinearity in the structural response), (2) spatial density of the sensors, (3) level of measurement noise, and (4) length of structural response records used for system identification. Selection of these four factors is based on expert judgment and previous experience (Moaveni et al., 2006).

7.3.1 Excitation Amplitude

The three above-mentioned system identification methods produce estimates of the modal parameters of a linear structure. In reality, with increasing level of input excitation, most structures start to behave nonlinearly. To study the performance of these system identification methods as applied to nonlinear structural data, the nonlinear response of the test structure is simulated for three levels of banded white noise input excitation (0.25-30Hz) with root mean square (RMS) of 0.03, 0.06, and 0.09g, respectively. Figure 7.5 plots the coherence function between the base input excitation and the roof acceleration response for the three different levels of excitation. From this figure, it can be seen that the

response nonlinearity increases significantly as the input RMS exceeds 0.03g. This is consistent with the moment-curvature hysteretic plots at the bottom of the web wall, in which the plastic curvature increases significantly as the input RMS exceeds 0.03g.

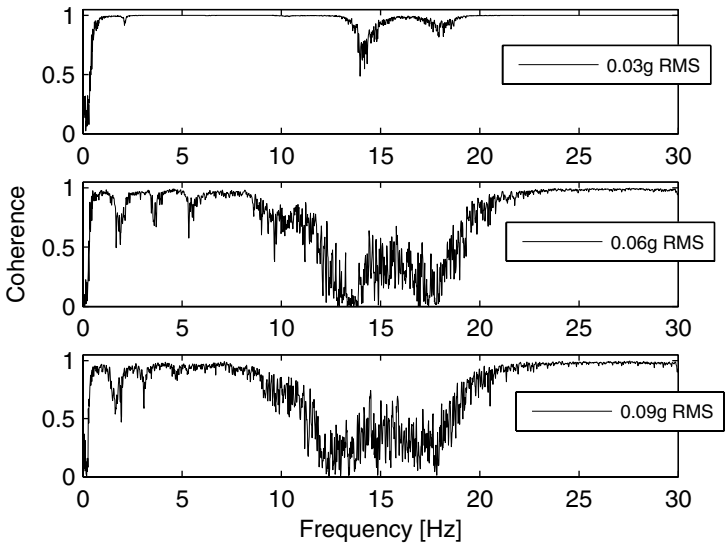

Fig. 7.5 Coherence functions of the base input and roof acceleration response for 0.03, 0.06, and 0.09g RMS white noise base excitation

7.3.2 Spatial Density of Sensors

An instrumentation array of 28 acceleration channels is simulated for each of the three base excitation levels using the nonlinear FE model of the structure in OpenSees. This array of 28 acceleration channels consists of three channels on each floor slab as shown in Figure 7.2 and one channel on the web wall at mid-height of each story. To study the performance of the system identification methods as a function of the spatial density of the sensor array (i.e., number of sensors), three different subsets of the 28 sensor array are considered. The three configurations of accelerometers consist of: (1) 7 accelerometers on

the web wall at floor levels (i.e., top of each story wall), (2) 14 accelerometers on the web wall at floor levels and mid-height of each story, and (3) full array of 28 accelerometers.

7.3.3 Measurement Noise

In this study, the measurement/sensor noise is modeled as a zero-mean Gaussian white noise process that is added to all channels of simulated acceleration response. This type of measurement noise is commonly used in research to approximate modeling errors (e.g., missing high frequency dynamics). Four levels of measurement noise, namely 0%, 20%, 40% and 60%, are considered here to study the effect of measurement noise on the variability of the identified modal parameters. The noise level is defined as the ratio of the RMS of the noise process to the RMS of the acceleration response process at each channel. This ratio is kept constant for all channels for a given noise level. The noise process added to each acceleration channel is statistically independent from the noise processes added to the other channels. Due to the random characteristics of the added noise vector processes, for each combination of the four factors studied (excitation amplitude, spatial density of the sensors, measurement noise, and length of output records), a set of 100 identification runs is performed using independent Gaussian white noise vector processes. Variability of the mean and standard deviation statistics of the identified modal parameters for these 100 identification trials is studied as a function of the input factors. As an illustration, Figure 7.6 shows the roof acceleration response with four different levels of noise added.

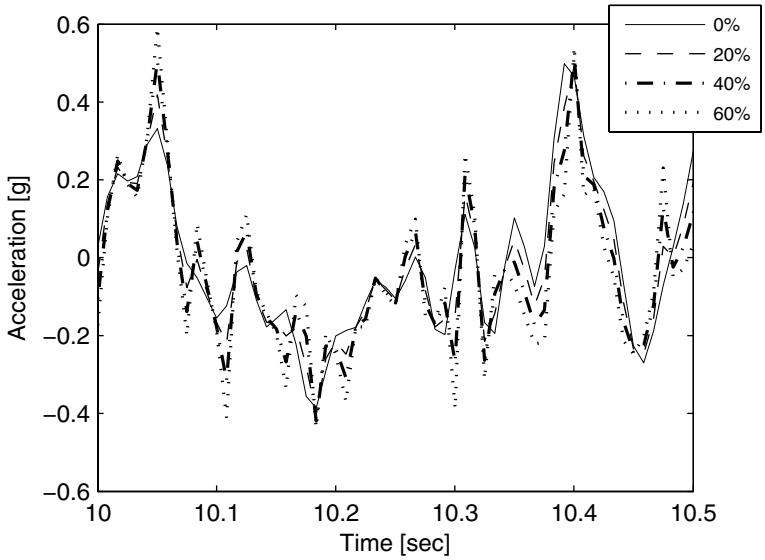

Fig. 7.6 Roof acceleration time histories for four different levels of added measurement noise

7.3.4 Length of Response Measurement Data

Four different lengths of output data are used in this uncertainty study: (1) 600 data points (5sec), (2) 2,400 data points (20sec), (3) 9,600 data points (80sec), and (4) 38,400 data points (320sec). From previous experience, this factor is expected to play an important role in the variability of the identified modal parameters.

Table 7.1 summarizes the input factors and their levels considered in this study. A design of experiments (DOE) provides an organized approach for setting up experiments (physical or numerical). A common experimental design with all possible combinations of the input factors set at all levels is called a full factorial design. A full factorial design is used in this study, therefore a total of $3 \times 3 \times 4 \times 4 \times 100 = 14400$ identification runs are performed for each of the three identification methods (i.e., 43,200 runs in total). These

43,200 system identification runs were performed using a fast server computer with Intel Xeon processor (3.0GHz) with a total computation time of about 108 hours.

Table 7.1 Description of factors studied and their levels considered

Factor	Description	Levels
M	System identification method	3 levels (NExT, SSI, EFDD)
A	Excitation amplitude	3 levels (0.03, 0.06, 0.09g)
S	Spatial density of sensors	3 levels (7, 14, 28)
N	Noise level	4 levels (0, 20, 40, 60%)
L	Length of measured data	4 levels (5, 20, 80, 320sec)
T	Measurement noise trial	100 seed numbers

7.4 BRIEF REVIEW OF SYSTEM IDENTIFICATION METHODS APPLIED

Three different state-of-the-art output-only system identification methods are applied to estimate the modal parameters of the FE structural model used to generate the response/output data. The system identification methods used consist of: (1) Natural Excitation Technique combined with the Eigensystem Realization Algorithm (NExT-ERA), (2) Data-driven Stochastic Subspace Identification (SSI-DATA), and (3) Enhanced Frequency Domain Decomposition (EFDD). These three methods are briefly reviewed in this section. The acceleration responses are simulated at a rate of 120Hz resulting in a Nyquist frequency of 60Hz, which is higher than the modal frequencies of interest in this study (< 25Hz). Before applying the aforementioned system identification methods to the simu-

lated data, all acceleration response time histories are low-pass filtered below 30Hz using a high order (1,024) FIR filter with a sharp corner frequency.

7.4.1 Natural Excitation Technique Combined with Eigensystem Realization Algorithm (NExT-ERA)

The basic principle behind the NExT is that the theoretical cross-correlation function between two response/output channels from an ambient (broad-band) excited structure has the same analytical form as the free vibration response of the structure (James et al., 1993). Once an estimation of the response cross-correlation vector is obtained for a given reference channel, the ERA method (Juang and Pappa, 1985) can be used to extract the modal parameters. A key issue in the application of NExT-ERA is to select the reference channel so as to avoid missing modes in the identification process due to the proximity of the reference channel to a modal node. In this study, the reference channel selected depends on the configuration of the sensor array considered in the identification. In the case of 7 or 14 channels, the sensor at the second floor on the web wall is selected as reference channel. In the case of 28 acceleration channels, one of the two channels on the second slabs is selected as reference channel. The response cross-correlation functions are estimated through inverse Fourier transformation of the corresponding cross-spectral density (CSD) functions. Estimation of the CSD functions is based on Welch-Bartlett's method using three Hanning windows of equal length with 50 percent of window overlap. Cross-correlation functions are then used to form Hankel matrices for applying ERA in the second stage of the modal identification.

7.4.2 Data-Driven Stochastic Subspace Identification (SSI-DATA)

The SSI-DATA method determines the system model in state-space based on the output-only measurements directly (Van Overshee and De Moore, 1996). One advantage of this method compared to two-stage time-domain system identification methods such as covariance-driven stochastic subspace identification and NExT-ERA is that it does not require any pre-processing of the data to calculate correlation functions or spectra of output measurements. In addition, robust numerical techniques such as QR factorization, singular value decomposition (SVD) and least squares are involved in this method. In the implementation of SSI-DATA, the filtered acceleration response data are used to form an output Hankel matrix including 20 block rows (10 block rows when using a signal length of 5sec) with either 7, 14 or 28 rows in each block (equal to the number of acceleration channels considered).

7.4.3 Enhanced Frequency Domain Decomposition (EFDD)

The Frequency Domain Decomposition (FDD), a non-parametric frequency-domain approach, is an extension of the Basic Frequency Domain approach also referred to as the peak picking technique. The FDD technique estimates the vibration modes using a SVD of the power spectral density (PSD) matrices at all discrete frequencies. Based on this SVD, single-degree-of-freedom (SDOF) systems are estimated, each corresponding to a single vibration mode of the dynamic system. Considering a lightly damped system, the contribution of different vibration modes at a particular frequency is limited to a small number (usually 1 or 2). In the EFDD (Brincker et al., 2001), the natural frequency and

damping ratio of a vibration mode are identified from the PSD function estimate of the SDOF system corresponding to that mode. In this approach, the estimated PSD function corresponding to a vibration mode is taken back to the time domain by inverse Fourier transformation, and the frequency and damping ratio are estimated from the zero-crossing times and the logarithmic decrement of the corresponding SDOF auto-correlation function (i.e., free vibration response), respectively. In the application of the EFDD method, the PSD functions are estimated based on Welch-Bartlett's method using Hanning windows of length 300, 600, 1,200, and 2,400 samples, respectively, for the 4 levels of measurement length, with 50 percent of window overlap. After estimating the auto/cross spectral density functions, the response PSD matrices at all discrete frequencies are subjected to singular value decomposition. The modal parameters are then estimated as explained above.

7.5 UNCERTAINTY QUANTIFICATION

In this section, two methods are employed to quantify the variability of the modal parameters identified using NExT-ERA, SSI, or EFDD due to variation of the four input factors (i.e., excitation amplitude, spatial density of the sensors, measurement noise, and length of measured response). These two methods are: (1) effect screening which is achieved using analysis-of-variance (ANOVA) (Saltelli et al., 2000), and (2) meta-modeling (Wu et al., 2000). Figure 7.7 shows the spread of mean values of the identified modal parameters (natural frequencies, damping ratios, and MAC values between the identified mode shapes and their nominal counterparts computed from the FE model) over 100 identification trials with statistically independent added measurement noise for the three iden-

tification methods used and the first three longitudinal modes. The spread of the sample mean of the identified modal parameters comes from varying the four input factors A, S, N, and L resulting in $3 \times 3 \times 4 \times 4 = 144$ combinations. It should be noted that for each combination of these four factors, 100 system identifications are performed based on 100 statistically independent measurement noise trials resulting in a total of 14,400 runs for each method (i.e., each of the 144 points in this figure corresponds to the mean over 100 identification trials with independent noise processes). This analysis can be viewed as a crude variance reduction technique that reduces the variability of the output features (modal parameters) due to selection of the noise vector process (i.e., seed number of the noise process). Figure 7.7, however, does not quantify the contribution of each input or combination of inputs to the total variability of the identified modal parameters.

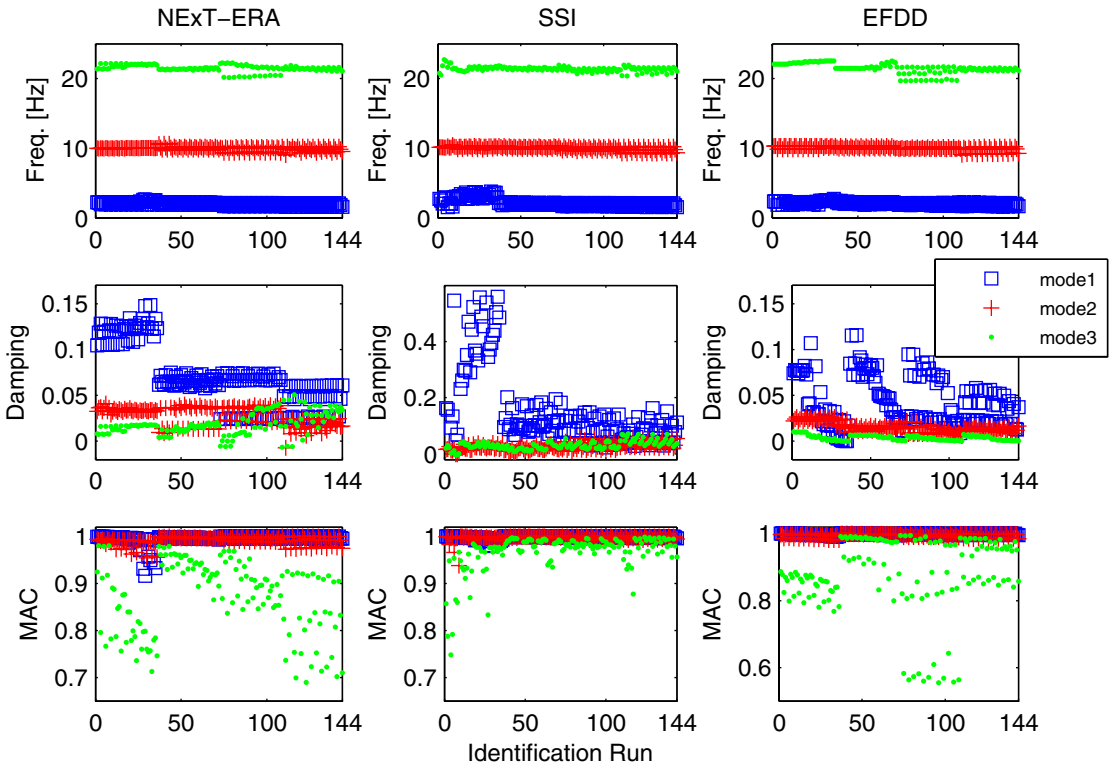

Fig. 7.7 Variability of the identified modal parameters from varying the four input factors

Table 7.2 reports the mean and coefficient of variation (COV) of the 14,400 sets of identified modal parameters for each of the three system identification methods. It should be noted that the large bias and variance in the modal identification results can be expected, since these methods are used for some extreme identification cases such as 60% measurement noise level, or the use of only 5sec long data records.

Table 7.2 Mean and coefficient of variation (COV) of the 14,400 sets of identified modal parameter

Method		Natural Frequency [Hz]			Damping Ratio [%]			MAC		
		Mode1	Mode2	Mode3	Mode1	Mode2	Mode3	Mode1	Mode2	Mode3
Nominal (FE Model)		2.12	10.48	24.15	2.4	2.6	5.2	1	1	1
NExT-ERA	Mean	2.00	9.94	21.51	7.2	2.7	1.8	0.995	0.991	0.869
	COV [%]	18.0	3.0	2.5	55.9	42.5	92.8	4.2	1.2	10.3
SSI	Mean	2.20	9.99	21.38	16.6	2.6	3.1	0.998	0.997	0.967
	COV [%]	31.7	2.9	2.0	120.9	52.2	57.3	0.8	0.6	5.0
EFDD	Mean	2.07	10.01	21.52	4.4	1.5	0.4	0.998	0.995	0.881
	COV [%]	13.3	3.0	3.5	68.0	40.8	82.5	0.2	0.6	13.5

7.5.1 Effect Screening through ANOVA

To investigate where the observed variability of the identified modal parameters comes from, ANOVA is performed and its results are discussed in this section. The theoretical foundation of ANOVA is that the total variance of the output features can be decomposed into a sum of partial variances or correlation coefficients, each representing the effect of varying an individual factor independently from the others. The correlation coefficients are estimated by the R-square values. The input factor with the largest value of R-square for an output feature has the most contribution to the variability of that output

feature. In this study, ANOVA is applied to 144 data sets of output features (mean and standard deviation of the identified modal parameters over the set of 100 identification trials with independent measurement noise processes) using a full-factorial design where the four factors A, S, N, and L (see Table 7.1) are varied in the design space for each of the three system identification methods. The full-factorial design requires a set of 100 identification trials for each combination of factors (M, A, S, N, and L), but it offers the advantage of minimizing aliasing during the ANOVA. Figure 7.8 shows the R-square values of the mean of the identified modal parameters for the first three longitudinal vibration modes using NExT-ERA, SSI, and EFDD due to variation of the four input factors A, S, N, and L. The R-square values are scaled such that their sum over all factors equates 100%. From Figure 7.8, it can be observed that: (1) the variability in the spatial density of the sensors (number of sensors) produces the least amount of variability in the modal parameters identified using all three methods considered, (2) variability of the mean value of the identified natural frequencies is most sensitive to factors L and A (i.e., signal length and amplitude of input excitation) for all three methods, and (3) the mean values of the identified damping ratios and mode shapes (MAC value between identified mode shapes and their nominal counterparts from the FE model) are sensitive to three factors A, N, and L, but the relative contributions of these factors to the total variance change for different methods and vibration modes. Similarly, Figure 7.9 shows the corresponding R-square values of the standard deviation (over 100 identification trials) of the output features. By comparing Figures 7.8 and 7.9, it can be concluded that the level of measurement noise contributes significantly to varying the standard deviation of the identified modal parameters, which is not the case for the mean values of the identified modal parameters.

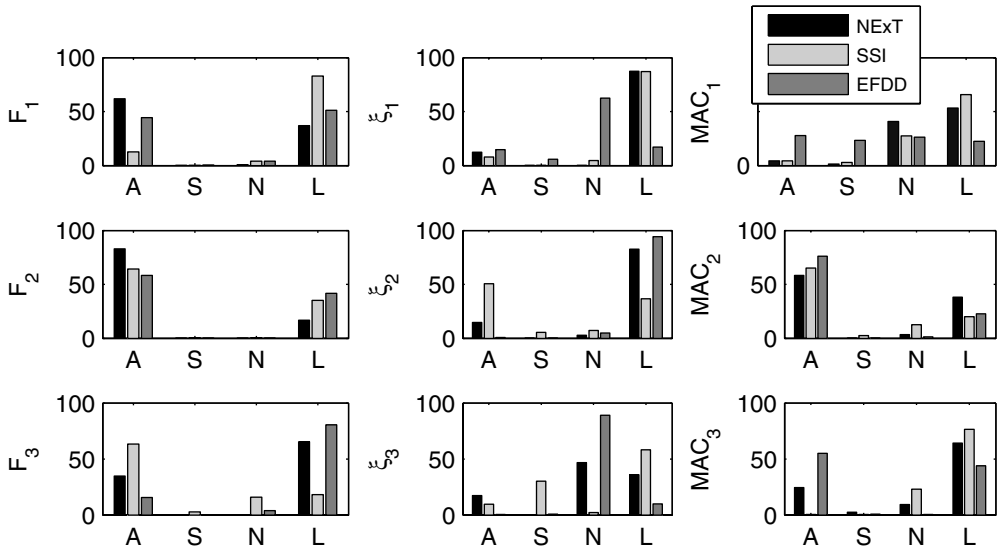

Fig. 7.8 R-square of the mean value (over 100 measurement noise trials) of the modal parameters identified using the three system identification methods due to variability of factors A, S, N, and L

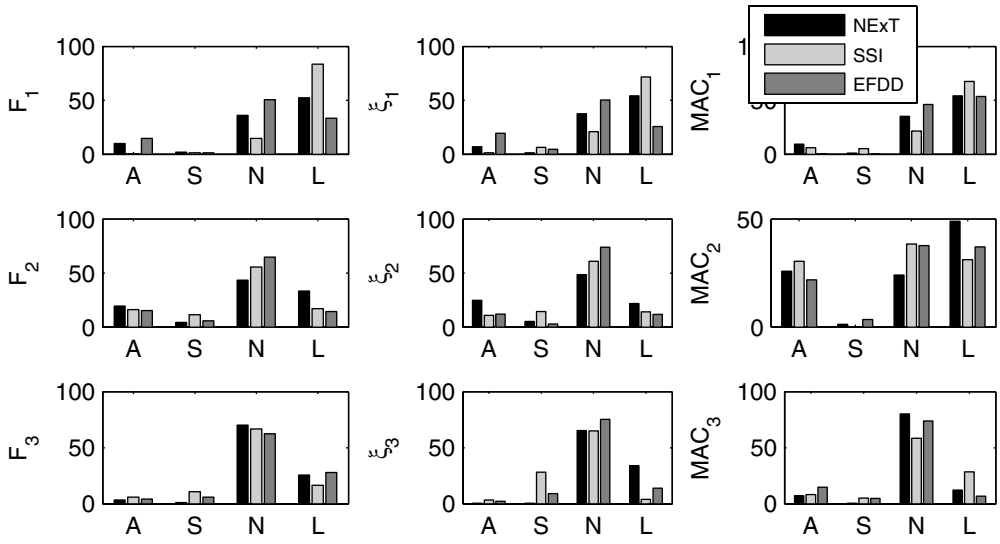

Fig. 7.9 R-square of the standard deviation (over 100 measurement noise trials) of the modal parameters identified using the three system identification methods due to variability of factors A, S, N, and L

A linear interaction ANOVA (Saltelli et al., 2000) is also performed to investigate the influence of coupling effects such as AS, AN, AL, SN, SL, and NL to the observed total variance of the output features. Linear interaction ANOVA is based on the same prin-

ciple as the main effect ANOVA, except that the factors are varied in pairs. The R-square statistics for the linear interaction ANOVA for the mean of the identified natural frequencies are shown in Figure 7.10. From this figure, it can be observed that different pairs of input factors have almost equal influence on the mean value of the identified natural frequencies. The analysis of variability based on ANOVA explains how the modal parameters vary over the entire design space of input factors (A, S, N, and L). It is emphasized that these statistical techniques are more powerful than local sensitivity analysis. Local sensitivity refers to the estimation of derivatives, such as the derivative of a resonant frequency with respect to the excitation amplitude A, using analytical equations or finite differences. Derivatives only provide local information that does not explain the overall variability of modal parameters.

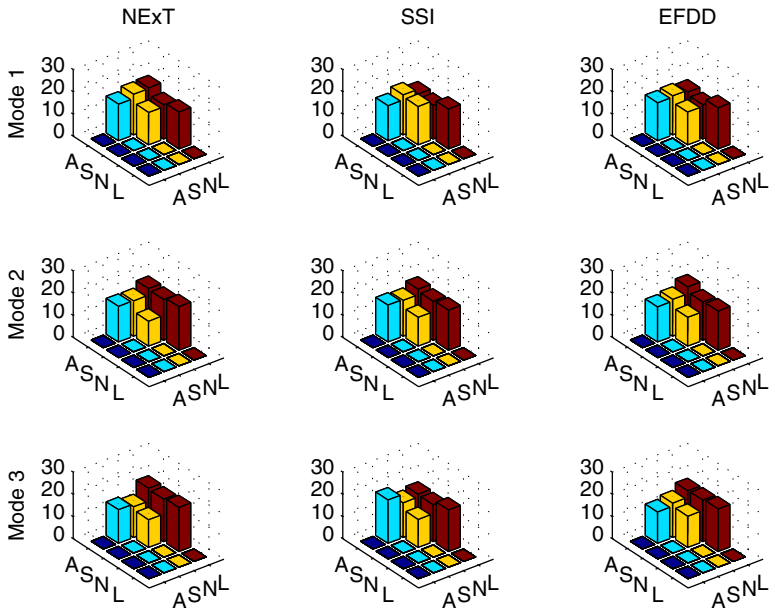

Fig. 7.10 R-square of the mean value (over 100 noise trials) of identified natural frequencies due to linear interaction of input factors AS, AN, AL, SN, SL, and NL

7.5.2 Global Sensitivity Analysis

In addition to ANOVA, sensitivities of the identified modal parameters are investigated as a function of data length, as well as measurement noise. Statistical properties (bias, variance and consistency) of the modal parameters identified via NExT-ERA, SSI and EFDD are investigated for seven different lengths of data (750, 1500, 3000, 6000, 12000, 24000, and 48000 data points), while the other input factors remain fixed. Values of the other fixed factors are: 0.03g excitation RMS amplitude; 20% measurement noise; and 28 acceleration records in the array of sensors. For this purpose, a set of 100 identifications is performed for each of the seven different lengths of data used. The added noise vector processes for the 100 identification trials are simulated as statistically independent.

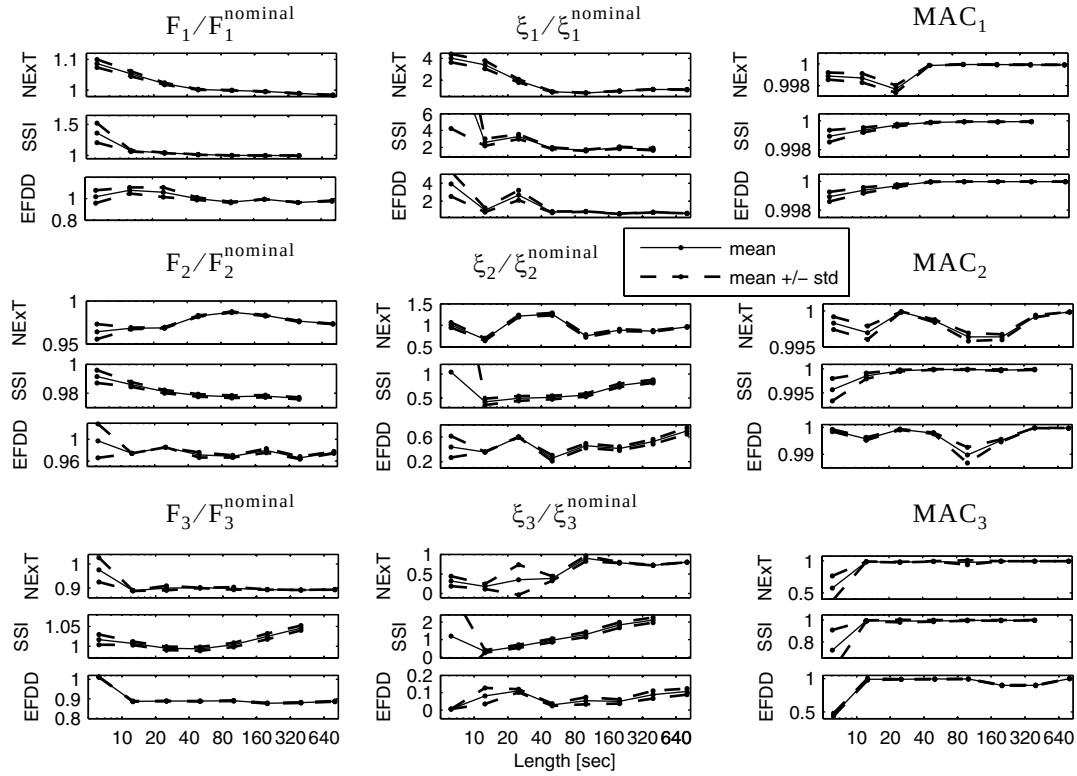

Fig. 7.11 Statistics (mean, mean +/- standard deviation) of the identified modal parameters with increasing length of data for the first three longitudinal modes

Figure 7.11 shows mean and mean +/- one standard deviation of the identified-to-nominal natural frequencies, damping ratios and MAC values as a function of data length and for the first three longitudinal vibration modes. This figure shows that: (1) variances of the identified modal parameters decrease with increasing length of data used, and (2) identified modal parameters of the 1st mode converge to their nominal counterparts with increasing length of data, which is not the case for the identified modal parameters of the 2nd and 3rd modes.

Changes in the statistical properties of the identified modal parameters are also studied as functions of measurement noise for nine different noise levels (0, 10, 20, 30, 40, 50, 60, 70, and 80% in the RMS sense) while the other input factors remain fixed. Values of the other fixed factors are: 0.03g excitation RMS amplitude; data length of 9,600 points (80sec); and 28 acceleration records in the array of sensors. A set of 100 identification trials is performed at each of the nine different levels of measurement noise and the statistics of the identified modal parameters are computed over these 100 identification trials. Figure 7.12 plots the mean and mean +/- one standard deviation of the identified-to-nominal natural frequencies, damping ratios and MAC values as a function of measurement noise and for the first three longitudinal vibration modes. From these results, it is observed that: (1) variances of the identified modal frequencies and MAC values are very small even at high levels of measurement noise, (2) variances of the identified modal parameters increase with increasing level of added measurement noise, and (3) bias of the identified natural frequencies (also damping ratios identified using NExT-ERA and SSI) are rather

insensitive to the level of noise which is not the case for the MAC values and damping ratios identified using EFDD.

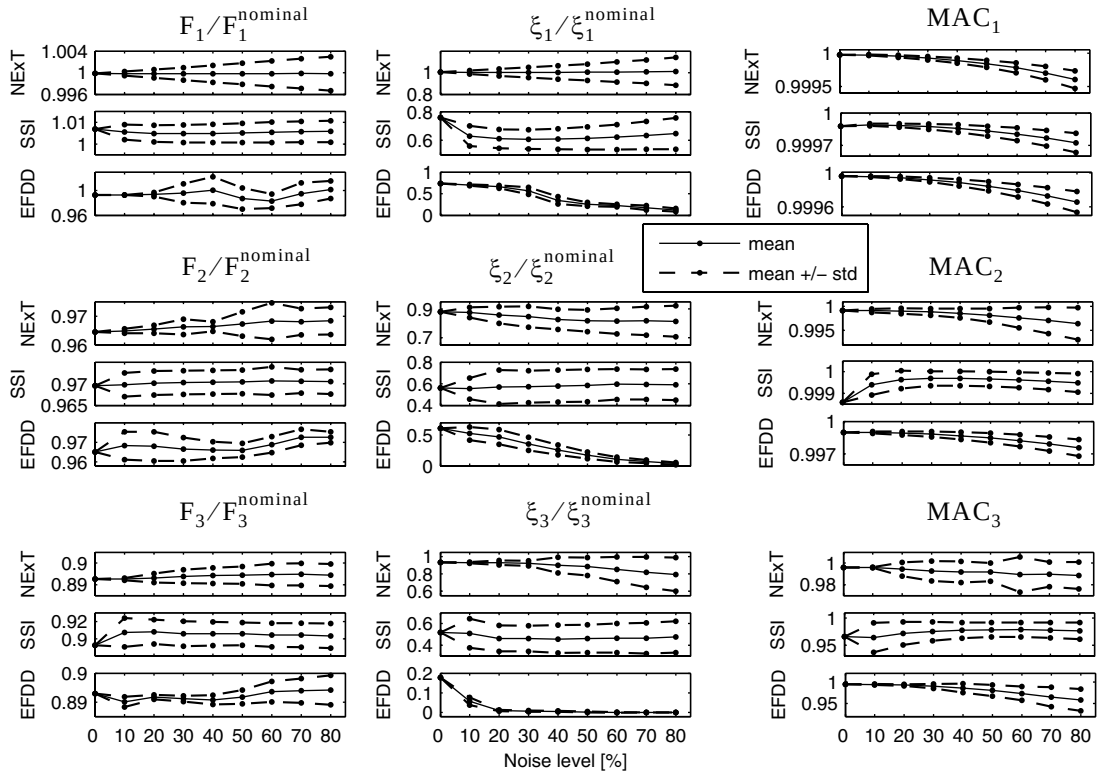

Fig. 7.12 Statistics (mean, mean +/- standard deviation) of the identified modal parameters with increasing level of measurement noise for the first three longitudinal modes

7.5.3 Meta Modeling

Meta-models (also known as surrogate models) represent the relationship between input factors and output features without including any physical characteristics of the system (i.e., black-box models). The advantage of surrogate models is that they can be analyzed at a fraction of the cost it would take to perform the physics-based simulations. Meta-models must be trained, which refers to the identification of their unknown functional forms and coefficients. Their quality can be evaluated independently of the training

step. In this section, a polynomial model is fitted to the identified modal parameters by including all main effects and linear interactions as expressed by

$$Y = \beta_0 + \beta_A A + \beta_S S + \beta_N N + \beta_L L + \beta_{AS} AS + \beta_{AN} AN + \beta_{AL} AL + \beta_{SN} SN + \beta_{SL} SL + \beta_{NL} NL \quad (7.1)$$

It should be noted that: (1) the values of the input factors are scaled between -1 and 1, and (2) the identified natural frequencies and damping ratios are normalized by their nominal counterparts so that the estimated β coefficients all have dimensionless units and the same order of magnitude for different features, and (3) the value of β_0 corresponds to the mean value of the output feature. Figure 7.13 shows the absolute values of regression coefficients obtained by best-fitting polynomials (based on least-squares) for the mean values (over a set of 100 identification trials) of modal parameters identified with the three identification methods.

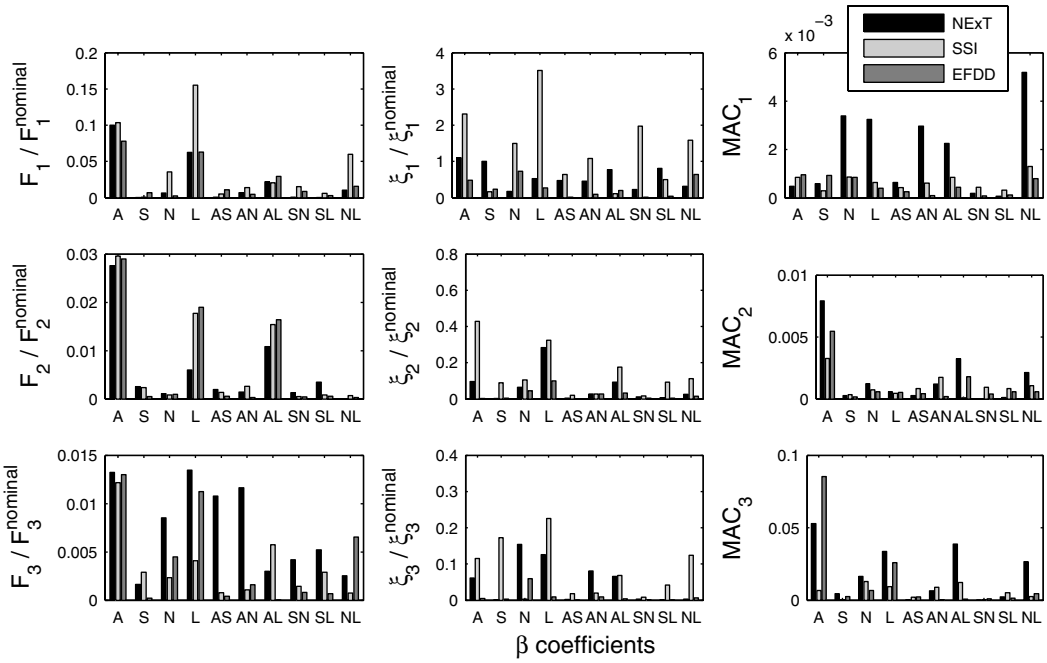

Fig. 7.13 Absolute values of coefficients of the best-fitted polynomial to the modal parameters

From Figure 7.13, it can be observed that: (1) the identified natural frequencies are more sensitive to factors A, L (as already indicated by ANOVA), and the linear interaction AL, (2) the dependency of the damping ratios and mode shapes (MAC values) on the input factors are not as consistent across the three identification methods as for the natural frequencies. Overall, the modal damping ratios and MAC values are more sensitive to the noise level than the natural frequencies.

7.6 CONCLUSIONS

A full-scale seven-story reinforced concrete (R/C) shear wall building slice was tested on the UCSD-NEES shake table in the period October 2005 to January 2006. Three output-only system identification methods, namely (1) Natural Excitation Technique combined with the Eigensystem Realization Algorithm (NExT-ERA), (2) Data-driven Stochastic Subspace Identification (SSI-DATA), and (3) Enhanced Frequency Domain Decomposition (EFDD) were used to extract the modal parameters (natural frequencies, damping ratios, and mode shapes) of the building at different damage states. In this study, the performance of these system identification methods is systematically investigated based on the response of the structure simulated using a three-dimensional nonlinear finite element model developed in OpenSees. The variability of the identified modal parameters due to the variability of four input factors is analyzed and quantified through effect screening and meta-modeling. The four input factors are: (1) amplitude of input excitation (level of nonlinearity in the structural response), (2) spatial density of measurements (number of

sensors), (3) measurement noise, and (4) length of response data used in the identification process. A full-factorial design of experiments is considered for these four input factors.

From the results of effect screening, it is observed that: (1) the variability in spatial density of the sensors (number of sensors) introduces the least amount of variability in the modal parameters identified using all three methods considered, (2) the mean value of the identified natural frequencies is most sensitive to factors L and A (i.e., record length and amplitude of input excitation) for all three methods, (3) the mean value of the identified damping ratios and mode shapes (MAC value between identified mode shapes and their nominal counterparts from the FE model) are sensitive to the three factors A, N, and L, but the relative contributions of these three factors to the total variance of these identified modal parameters changes for different methods and vibration modes, and (4) different combinations of input factor interactions have almost equal influence on the mean values of the identified natural frequencies. In addition to ANOVA, polynomial meta-models are best-fitted (using least-squares method) to the identified modal parameters by including all main effects and linear interactions. From the estimates of the meta-model coefficients it is observed that: (1) the identified natural frequencies are most sensitive to the main input factors A, L (as already indicated by ANOVA), and also the linear interaction AL, (2) the sensitivities of the identified damping ratios and mode shapes (MAC values) to input factors are not as consistent across different identification methods as that of the identified modal frequencies, but overall these identified modal parameters are more sensitive to the measurement noise level than the identified frequencies. In addition to ANOVA, sensitivities of the identified modal parameters are investigated as a function of

data length as well as measurement noise, while the other input factors remain fixed. From this analysis, it is seen that: (1) the variances of the identified modal parameters decrease with increasing record length and increase with increasing level of added measurement noise, (2) the identified modal parameters of the first mode converge to their nominal counterparts with increasing record length, which is not the case for the identified modal parameters of the second and third modes, and (3) the variances of the identified modal frequencies and MAC values are very small even at high levels of measurement noise. This systematic investigation demonstrates that the level of confidence which can be placed in structural health monitoring is a function of, not only the magnitude of damage, but also choices made to design the experimental procedure, collect and process the measurements.

ACKNOWLEDGEMENTS

Chapter 7, in full, is a reprint of the material as it appears in the Proceeding of International Conference on Modal Analysis (IMAC-XXV) (2007), Moaveni, B., Barbosa, A.R., Conte, J.P., and Hemez, F.M. The dissertation author was the first author and primary investigator of this paper.

Partial supports of this research by the Englekirk Center Industry Advisory Board and Lawrence Livermore National Laboratory with Dr. David McCallen as Nuclear Systems Science and Engineering Program Leader are gratefully acknowledged. The second author would also like to acknowledge the support provided by the Department of Civil Engineering of the Universidade Nova de Lisboa and the Portuguese Foundation for Sci-

ence and Technology (BD/17266/2004). The last author acknowledges the support of the Engineering Institute, a joint educational and research program of the University of California San Diego Jacobs School of Engineering and Los Alamos National Laboratory. Any opinions, findings, and conclusions or recommendations expressed in this material are those of the authors and do not necessarily reflect those of the sponsors.

REFERENCES

Brincker, R., Ventura, C. and Andersen, P., (2001). “Damping estimation by frequency domain decomposition.” *Proc. of International Modal Analysis Conference*, IMAC XIX, Kissimmee, USA.

Doebling, S.W., Farrar, C.R., and Prime, M.B., (1998). “A summary review of vibration-based damage identification methods.” *The Shock and Vibration Digest*, Vol. 30, No. 2, 99-105.

James, G.H., Carne, T.G., and Lauffer, J.P., (1993). *The Natural Excitation Technique for modal parameters extraction from operating wind turbines*. SAND92-1666, UC-261, Sandia National Laboratories, Sandia, New Mexico, USA.

Juang, J.N., and Pappa, R.S., (1985). “An Eigensystem Realization Algorithm for modal parameter identification and model reduction.” *J. Guidance Control Dyn.*, 8 (5), 620-627.

Karsan, I.D., and Jirsa, J.O., (1969). “Behavior of concrete under compressive loading.” *Journal of Structural Division*, ASCE, 95 (12).

Mazzoni, S., Scott, M.H., McKenna, F., and Fenves, G.L., (2006). *Open system for earthquake engineering simulation - User manual (Version 1.7.3)*. Pacific Earthquake Engineering Research Center, University of California, Berkeley, California, http://opensees.berkeley.edu/OpenSees/manuals/usermanual.

Moaveni, B., He, X., Conte, J.P., and Restrepo, J.I., (2006). “System identification of a seven-Story reinforced concrete shear wall building tested on UCSD-NEES shake table.” *Proc. of the 4th World Conference on Structural Control and Monitoring*, San Diego, USA.

Paulay, T., and Priestley, M.J.N., (1992). *Seismic design of reinforced concrete and masonry buildings.* John Wiley & Sons, New York.

Saltelli, A., Chan, K., and Scott, E.M., (2000). *Sensitivity analysis.* John Wiley & Sons, New York.

Sohn, H., Farrar, C.R., Hemez, F.M., Shunk, D.D., Stinemates, D.W., and Nadler, B.R., (2003). *A review of structural health monitoring literature: 1996-2001*. Los Alamos National Laboratory, Report No. LA-13976-MS, Los Alamos, New Mexico.

Van Overschee, P., and de Moore, B., (1996). *Subspace identification for linear systems*. Kluwer Academic Publishers, Massachusetts, USA.

Wu, C.F.J., and Hamada, M., (2000). *Experiments: planning, analysis, and parameter design optimization.* John Wiley & Sons, New York.

CHAPTER 8

UNCERTAINTY ANALYSIS OF DAMAGE IDENTIFICATION RESULTS OBTAINED USING FINITE ELEMENT MODEL UPDATING

8.1 INTRODUCTION

In recent years, structural health monitoring has received increasing attention in the civil engineering research community with the objective to identify structural damage at the earliest possible stage and evaluate the remaining useful life (damage prognosis) of structures. Vibration-based, non-destructive damage identification is based on changes in dynamic characteristics (e.g., modal parameters) of a structure. Experimental modal analysis (EMA) has been used as a technology for identifying modal parameters of a structure based on its measured vibration data. It should be emphasized that the success of damage identification based on EMA depends strongly on the accuracy and completeness of the identified structural dynamic properties. Extensive literature reviews on vibration-based damage identification are provided by Doebling et al. (1996, 1998) and Sohn et al. (2003).

Damage identification consists of (1) detecting the occurrence of damage, (2) localizing the damage zones, and (3) estimating the extent of damage. Numerous vibration-based methods have been proposed to achieve these goals. Salawu (1997) presented a

review on the use of changes in natural frequencies for damage detection only. However, it is in general impossible to localize damage (i.e., obtain spatial information on the structural damage) from changes in natural frequencies only. Pandey et al. (1991) introduced the concept of using curvature mode shapes for damage localization. In their study, by using a cantilever and a simply supported analytical beam model, they demonstrated the effectiveness of employing changes in curvature mode shapes as damage indicator for detecting and localizing damage. Other methods for damage localizations include strain-energy based methods (Shi et al., 2002) and the direct stiffness calculation method (Maeck and De Roeck, 2004). A class of sophisticated methods consists of applying sensitivity-based finite element (FE) model updating for damage identification (Friswell and Mottershead, 1995). These methods update the physical parameters of a FE model of the structure by minimizing an objective function expressing the discrepancy between numerically predicted and experimentally identified features that are sensitive to damage such as natural frequencies and mode shapes. Optimum solutions of the problem are reached through sensitivity-based optimization algorithms. Recently, sensitivity-based FE model updating techniques have been applied successfully for condition assessment of structures (Teughels and De Roeck, 2004).

A full-scale seven-story reinforced concrete (R/C) shear wall building slice was tested on the UCSD-NEES shake table in the period October 2005 - January 2006. The shake table tests were designed so as to damage the building progressively through several historical seismic motions reproduced on the shake table. A sensitivity-based FE model updating approach was used to identify damage at each of several damage states of the

building based on its identified modal parameters. The estimation uncertainty in both the system identification and damage identification results was observed to be significant (Moaveni et al., 2006, 2008a, 2008b; He et al., 2006). This motivated the authors to perform (through numerical simulation) an uncertainty analysis on these system and damage identification results. In an earlier study (Moaveni et al., 2007), the authors investigated the performance of three different output-only system identification methods, used for experimental modal analysis of the shear wall building, as a function of the uncertainty/ variability in the following input factors: (1) amplitude of input excitation, (2) spatial density of measurements, (3) measurement noise, and (4) length of response data used in the identification process. This paper, which is an extension of the above mentioned study, investigates the performance of damage identification using FE model updating based on the identified modal parameters of the first three longitudinal vibration modes. In this study, the identified modal parameters of the damaged structure are generated numerically using a three-dimensional FE model of the test structure with different levels of damage simulated (numerically) along the height of the structure. The uncertainty of the identified damage (location and extent) is quantified through analysis-of-variance (ANOVA) and meta-modeling due to variability of the following input factors: (1-3) level of uncertainty in the (identified) modal parameters of the first three longitudinal modes (M1, M2, M3), (4) spatial density of measurements (number of sensors) (S), and (5) mesh size in the FE model used for damage identification (modeling error) (E). A full factorial design of experiments is considered for these five input factors. In addition to ANOVA and meta-modeling for effect screening, this study investigates the sensitivity of the identified damage to the level of uncertainty in the identified modal parameters for the first three longitu-

dinal modes. This global sensitivity analysis is performed through one-at-a-time (OAT) perturbation of individual input factors M1, M2 and M3.

8.2 FINITE ELEMENT MODEL OF TEST STRUCTURE

The full-scale seven-story R/C building slice tested on the UCSD-NEES shake table consists of a main wall (web wall), a back wall perpendicular to the main wall (flange wall) for lateral stability, concrete slabs at each floor level, an auxiliary post-tensioned column to provide torsional stability, and four gravity columns to transfer the weight of the slabs to the shake table. Figure 8.1 shows a picture of the test structure, a drawing of its elevation, and a rendering of its FE model with fine mesh (one of the two FE models used in this study). Also, a plan view of the structure is presented in Figure 8.2. Details about construction drawings, material test data, and other information on the set-up and conducting of the experiments are available in (Panagiotou et al., 2007).

A three dimensional linear elastic FE model of the test structure was developed using a general-purpose FE structural analysis program, FEDEASLab (Filippou and Constantinides, 2004). A four-node linear flat shell element (with four Gauss integration points) borrowed from the FE literature was implemented in FEDEASLab in order to model the web wall, back wall, and concrete slabs (He et al., 2006). This shell element is based on the mixed discrete variational principle proposed by Hughes and Brezzi (1989) in conjunction with Allman type interpolation (Allman, 1988) for the membrane part and the discrete Kirchhoff plate element derived by Batoz and Tahar (1982) for the plate part. The resulting finite element has six degrees of freedom (DOFs) per node, including a true

drilling DOF. In the FE model of the test building, the gravity columns and braces connecting the post-tensioned column to the building slabs are modeled using truss elements. The inertia properties of the test structure are discretized into lumped translational masses at each node of the FE model. In this study, two FE models of the building with different mesh sizes (i.e., numbers of elements) are used in the FE model updating process in order to investigate the effects of mesh size (modeling error) on the damage identification results. The FE model with fine mesh is also used for generating the modal parameters of the damaged structure with damage simulated as change in material stiffness (effective moduli of elasticity) distributed over the finite elements of the web wall. Table 8.1 reports the measured moduli of elasticity (through concrete cylinder tests) at various heights (stories) of the test structure, which are used in both FE models representing the test structure in its undamaged/baseline state.

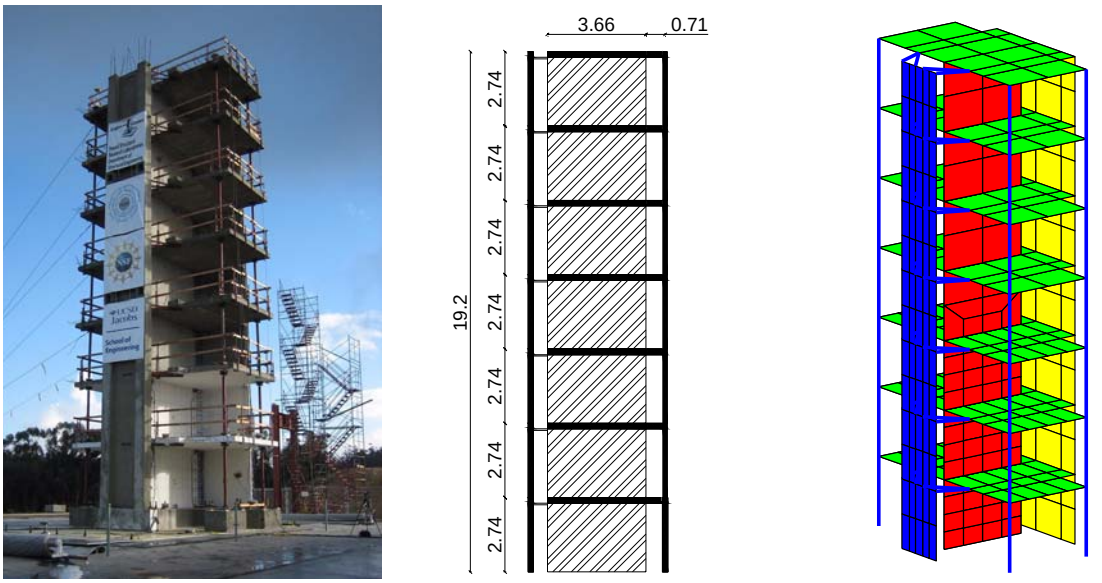

(a) Test structure (b) Elevation dimensions (unit: m) (c) Finite element model with fine mesh

Fig. 8.1 R/C shear wall building slice

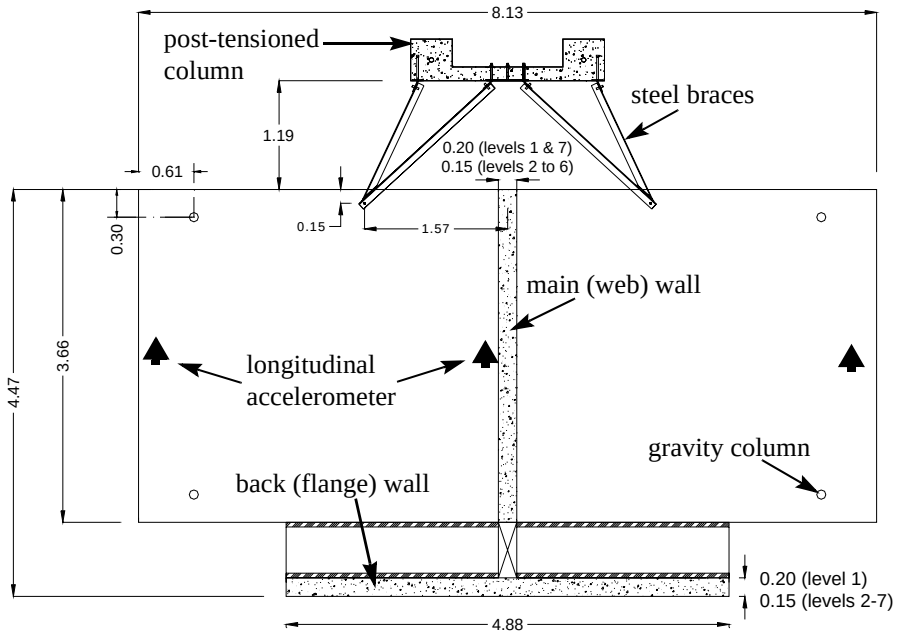

Fig. 8.2 Plan view of the test structure (unit: m)

Table 8.1 Measured moduli of elasticity at different heights of the test structure

Concrete Components	Measured Modulus of Elasticity (GPa)
First story	24.47
Second story	26.00
Third story	34.84
Fourth story	30.20
Fifth story	28.90
Sixth story	32.14
Seventh story	33.54

The natural frequencies and mode shapes of the first three longitudinal modes are used in the damage identification process. Figure 8.3 shows the modal parameters of the first three longitudinal modes computed from the fine mesh FE model representing the

building in its undamaged state. These mode shapes and natural frequencies are in relatively good agreement with their counterparts identified experimentally based on ambient measurement data recorded on the undamaged test structure (Moaveni et al., 2006, 2008a).

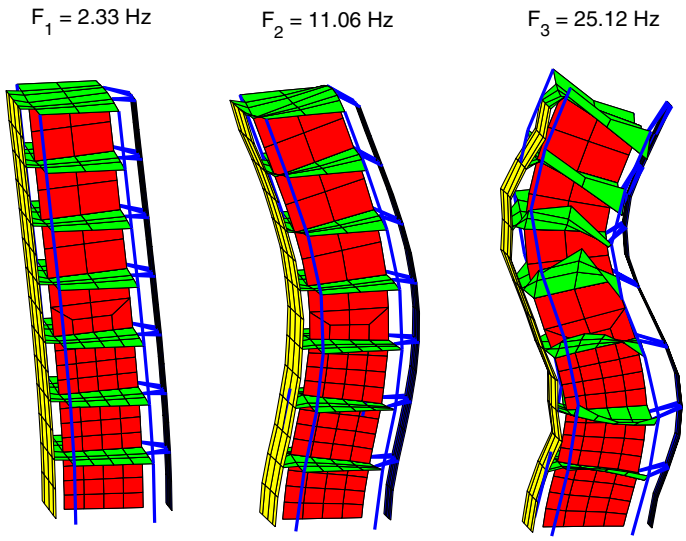

Fig. 8.3 Mode shapes of first three longitudinal modes of fine mesh FE model representing undamaged structure

8.3 DESCRIPTION OF INPUT FACTORS STUDIED AND DESIGN OF EXPERIMENTS

As already mentioned, the objective of this study is to analyze and quantify the uncertainty of the identified damage obtained using a FE model updating strategy due to the variability of five input factors: (1-3) level of uncertainty in the (identified) modal parameters of each of the first three longitudinal modes (M1, M2, M3), (4) spatial density of measurements (number of sensors) (S), and (5) mesh size in the FE model used for damage identification (a type of modeling error) (E). A number of other factors could be

considered such as modeling assumptions (e.g., type of finite elements), number of updating parameters (number of sub-structures), type and number of residuals and their weights used in the objective function. This study is restricted to the above mentioned 5 factors which are selected based on previous experience and expert opinion (Moaveni et al., 2006, 2008a, 2008b; He et al., 2006). This section briefly describes each of the input factors considered in this study and the design of experiments considered.

8.3.1 Uncertainty in Modal Parameters

In practice, the main source of uncertainty in damage identification results arises from the uncertainty in the estimates of modal parameters that are used in the damage identification process. In a previous study by the authors (Moaveni et al., 2007), it was observed that the estimation uncertainty of the modal parameters identified using three state-of-the-art output-only system identification methods (i.e., Natural Excitation Technique combined with Eigensystem Realization Algorithm, Data-driven Stochastic Subspace identification, and Enhanced Frequency Domain Decomposition) depend significantly on the variability of various input factors such as amplitude of excitation (i.e., level of nonlinearity in the response), level of measurement noise, and length of measured data used for system identification. In this study, the modal parameters of the first three longitudinal vibration modes are used in the damage identification process. Two levels of uncertainty, namely 0.5% and 1.0% coefficient-of-variation (COV), are considered for the natural frequencies and mode shape components of these three modes. These considered levels of uncertainty in modal parameters are selected based on previous experi-

ence with this test structure (Moaveni et al., 2006, 2008a). In this study, the modal parameter estimators are assumed to be unbiased (i.e., mean value of parameter estimates coincides with the “exact” parameter value). For each natural frequency and mode shape component of a vibration mode at a considered level of uncertainty, 20 noise realizations are generated from zero-mean Gaussian distributions with standard deviations scaled to result in the considered COV. The random estimation errors added to the natural frequencies and mode shape components are statistically independent (across the realizations and across natural frequencies and mode shape components). Statistics in terms of mean and standard deviation (over the 20 identification runs for each combination of input factors) of the identified damage extent at each location (i.e., substructure) are studied as a function of the variability/uncertainty of the input factors.

8.3.2 Spatial Density of Sensors

During the dynamic testing of the shear wall building, the web wall of the test structure was instrumented with 14 longitudinal accelerometers. The measured data were used later for modal identification of the test structure. To study the performance of FE model updating for damage identification as a function of the spatial density of the sensor array (i.e., number of sensors), two different subsets of the 14 sensor array are considered, namely (1) 10 accelerometers on the web wall at all floor levels (i.e., top of floor slabs) and at mid-height of the first three stories, and (2) 14 accelerometers on the web wall at all floor levels and at mid-height of each story.

8.3.3 Mesh Size of FE Model Used for Damage Identification

The last input factor considered in this study is the modeling error due to the mesh size of the FE model (i.e., spatial discretization of the test structure) used for damage identification. This input factor is considered at two levels, i.e., two FE models of the building are used in the FE model updating process. The first model is defined by 340 nodes and 322 shell and truss elements. The web wall at each story is modeled using 4 shell elements and the floor slabs are discretized into 12 shell elements each. The second model, which has a more refined mesh, is defined by 423 nodes and 398 elements. In this model, the web wall at each of the first three stories is modeled using 16 shell elements, while the higher stories (5 to 7) are modeled using 4 shell elements each. The 4th story of the web wall is modeled using 8 shell elements. The floor slabs are modeled using 24 shell elements for each of the first three floors and 12 shell elements for each of the higher floors (4 to 7). The back wall, post-tensioned column, gravity columns and steel braces are modeled in the same way in both FE models. It should be noted that these two FE models with different mesh size have different modal parameters (especially for the 3 modes considered in this study), even though the same material properties are used in the two models. The modal frequencies computed using the first model (coarse mesh) are

$$f_{\text{Coarse Mesh}} = \begin{bmatrix} 2.35 & 11.19 & 25.34 \end{bmatrix} \text{ Hz} \tag{8.1}$$

which are slightly higher than their counterparts obtained using the second model (fine mesh) (see Figure 8.3). The “true” modal parameters of the damaged structure are computed using the second model (fine mesh) with damage represented as change of material stiffness (i.e., effective modulus of elasticity) distributed spatially and intensity-wise over

the FE model according to the observed damage in the actual test structure (Moaveni et al., 2008b).

Table 8.2 summarizes the input factors and their levels considered in this study. A design of experiments (DOE) provides an organized approach for setting up experiments (physical or numerical). A common DOE with all possible combinations of the input factors set at all levels is called a full factorial design. A full factorial design is used in this study and therefore a total of $2 \times 2 \times 2 \times 2 \times 2 \times 20 = 640$ identification runs are performed for the damaged case considered. These 640 damage identification runs were performed using two fast server computers with dual-core Intel Xeon processors (3.0GHz) and also parallel computation on the "On Demand Cluster" of the San Diego Supercomputer Center (SDSC). Each of these identifications takes approximately an hour of CPU time on the fast server computers (for the fine mesh FE model).

Table 8.2 Description of factors studied and their levels considered

Factor	Description	Levels
M1	Uncertainty in modal parameters of mode 1	2 levels (0.5, 1.0% COV)
M2	Uncertainty in modal parameters of mode 1	2 levels (0.5, 1.0% COV)
M3	Uncertainty in modal parameters of mode 1	2 levels (0.5, 1.0% COV)
S	Spatial density of sensors	2 levels (10, 14 sensors)
E	FE mesh size	2 levels (322, 398 finite elements)

8.4 SENSITIVITY BASED FINITE ELEMENT MODEL UPDATING FOR DAMAGE IDENTIFICATION

In this study, a sensitivity-based FE model updating strategy (Friswell and Mottershead, 1995; Teughels and De Roeck, 2004) is used to identify (detect, localize and quantify) the numerically simulated damage in the structure. The residuals in the objective function used for the FE model updating process are based on the natural frequency and mode shape estimates of each of the first three longitudinal modes of the test structure. It should be recalled that the modal parameter estimates are based on the exact modal parameters computed from the FE model of the damaged structure and then polluted with random noise added at the level of estimation uncertainty considered. As already mentioned, damage in the structure is introduced as changes (reduction) in material stiffness (effective modulus of elasticity) distributed over the finite element mesh of the web wall in the (fine mesh) FE model. For the purpose of damage identification, the web wall is subdivided into ten sub-structures (each assumed to have a uniform value of the effective modulus of elasticity), 6 along the first three stories (every half story each) and 4 along the 4th to 7th stories (every story each). The level of damage simulated in these sub-structures is selected based on the profile of the observed damage in the real test structure as

$$\mathbf{a}_{\text{exact}} = \left[45\%\ 25\%\ 66\%\ 20\%\ 10\%\ 7\%\ 4\%\ 4\%\ 2\%\ 1\%\right]^{T} \tag{8.2}$$

from bottom to top of the web wall, where the damage factors $\mathbf{a}_{\text{exact}}$ in percent represent the reduction in effective material modulus relative to the undamaged state. The bottom of the second story was observed to be the most damaged location in the building due to a

lap-splice failure of the longitudinal steel reinforcement at this location. In order to identify damage in the structure, the effective moduli of elasticity of the sub-structures in the FE models are updated through minimization of an objective function. It should be noted that the sub-structures used in the updating process are the same as those used in simulating the damaged structure, which makes it possible to identify the exact damage in the absence of estimation uncertainty in the modal parameters. The natural frequencies of the first three longitudinal modes computed using the fine mesh FE model of the structure with simulated damage given in Equation 2 are

$$f_{\text{Damaged Structure}} = \begin{bmatrix} 1.97 & 9.97 & 22.96 \end{bmatrix} \text{ Hz} \tag{8.3}$$

8.4.1 Objective Function

The objective function used for damage identification is defined as

$$\min_{\boldsymbol{\theta}} f(\boldsymbol{\theta}) = \mathbf{r}(\boldsymbol{\theta})^{\mathrm{T}} \mathbf{W} \mathbf{r}(\boldsymbol{\theta}) = \sum_{j} [w_j r_j(\boldsymbol{\theta})^2] \tag{8.4}$$

where $\mathbf{r}(\boldsymbol{\theta})$ = residual vector containing the differences between FE computed and experimentally estimated modal parameters; $\boldsymbol{\theta}$ = a set of physical parameters (effective moduli of elasticity), which must be adjusted in order to minimize the objective function; $\mathbf{W}$ = a diagonal weighting matrix with each diagonal component inversely proportional to the square of the COV of the natural frequency of the corresponding vibration mode (Christodoulou and Papadimitriou, 2007). A combination of residuals in natural frequencies and mode shape components is used to define the objective function as

$$\mathbf{r}(\boldsymbol{\theta}) = \begin{bmatrix} \mathbf{r}_f(\boldsymbol{\theta}) \\ \mathbf{r}_s(\boldsymbol{\theta}) \end{bmatrix} \tag{8.5}$$

in which $\mathbf{r}_f(\boldsymbol{\theta})$ and $\mathbf{r}_s(\boldsymbol{\theta})$ = natural frequency and mode shape residual vectors, respectively. The two types of residuals are expressed, respectively, as

$$\mathbf{r}_f(\boldsymbol{\theta}) = \left[\frac{\lambda_j(\boldsymbol{\theta}) - \tilde{\lambda}_j}{\tilde{\lambda}_j}\right], \qquad \mathbf{r}_s = \left[\frac{\phi_j^l(\boldsymbol{\theta})}{\phi_j^r(\boldsymbol{\theta})} - \frac{\tilde{\phi}_j^l}{\tilde{\phi}_j^r}\right] \qquad j = 1, \ldots, n_m \tag{8.6}$$

where $\lambda_j(\boldsymbol{\theta})$, $\tilde{\lambda}_j$ = FE computed and experimentally identified eigenvalues (i.e., $\lambda_j(\boldsymbol{\theta}) = (2\pi \cdot f_j)^2$), respectively; $\boldsymbol{\phi}_j(\boldsymbol{\theta})$ and $\tilde{\boldsymbol{\phi}}_j$ = FE computed and experimentally identified mode shape vectors. In Equation 6, the superscript *r* indicates a reference component of a mode shape vector (with respect to which the other components of the mode shape are normalized), the superscript *l* refers to the components that are used in the updating process (i.e., at the sensor locations), and n_m denotes the number of vibration modes considered in the residual vector. In this study, the natural frequencies and mode shapes of the first three longitudinal modes (see Figure 8.3) of the structure are used to form the residual vector that has a total of 42 (when using 14 sensors) or 30 (when using 10 sensors) residual components consisting of 3 eigen-frequencies and $3 \times (14 - 1) = 39$ or $3 \times (10 - 1) = 27$ mode shape residuals, respectively.

8.4.2 Damage Factors and Residual Sensitivities

In the process of FE model updating, the effective moduli of elasticity of the ten sub-structures are used as updating parameters. These ten sub-structures are distributed along the height of the web wall, with 6 of them along the first three stories (one per half story) and 4 from the fourth to the seventh story (one per story). Instead of the absolute value of each updating parameter, a dimensionless damage factor a^j is defined as

$$a^j = \frac{E^j_{\text{undamaged}} - E^j_{\text{damaged}}}{E^j_{\text{undamaged}}} \tag{8.7}$$

where E^j is the effective modulus of elasticity of the elements in sub-structure j ($(j = 1, 2, \ldots, 10)$). The damage factor a^j indicates directly the level of damage in sub-structure j (relative reduction in effective modulus of elasticity). The sensitivity of the residuals with respect to the damage factors a^j can be obtained through the modal parameter sensitivities as

$$\frac{\partial \mathbf{r}_f}{\partial a^j} = \left[\frac{1}{\tilde{\lambda}_i}\frac{\partial \lambda_i}{\partial a^j}\right] \quad \text{and} \quad \frac{\partial \mathbf{r}_s}{\partial a^j} = \left[\frac{1}{\phi_i^r}\frac{\partial \phi_i^l}{\partial a^j} - \frac{\phi_i^l}{(\phi_i^r)^2}\frac{\partial \phi_i^r}{\partial a^j}\right] \tag{8.8}$$

where the modal sensitivities $\frac{\partial \lambda_i}{\partial a^j}$ and $\frac{\partial \boldsymbol{\phi}_i}{\partial a^j}$ are available in Fox and Kapoor (1968).

8.4.3 Optimization Algorithm

The optimization algorithm used to minimize the objective function defined in Equation 3 is a standard Trust Region Newton method (Coleman and Li, 1996), which is a sensitivity-based iterative method available in the MATLAB optimization Toolbox (Mathworks Inc., 2005). The damage factors were constrained to be in the range [0 0.90] for updating the undamaged FE model. The upper-bound of 90% was selected because no sub-structure of the building is expected to be damaged even close to 90% (largest simulated damage factor is 66%), while the lower bound of zero was selected considering that the identified effective moduli of elasticity cannot increase due to damage. The optimization process was performed using the “fmincon” function in Matlab, with Jacobian and first-order estimate of the Hessian matrices calculated analytically based on the sensitivities of the modal parameters to the updating variables, as given in Equation 8. It is important to mention that the proposed method was verified to be able to identify the exact simulated damage (given in Equation 2) in the absence of estimation uncertainty in the modal parameters used.

8.5 UNCERTAINTY QUANTIFICATION

In this section, two methods are employed to quantify the uncertainty of the identified damage factor at each sub-structure due to variation of the five input factors considered. These two methods are: (1) effect screening which is achieved using analysis-of-variance (ANOVA) (Saltelli et al., 2000), and (2) meta-modeling (Wu and Hamada, 2000). Figure 8.4 shows the spread of the identified damage factors at the different sub-structures

along the web wall height for all 640 damage identification runs. The horizontal solid line in each subplot indicates the value of the exact simulated damage for the corresponding substructure. The ensemble of identified damage factors is obtained by varying the five input factors M1, M2, M3, S and E, resulting in $2 \times 2 \times 2 \times 2 \times 2 = 32$ combinations. For each combination of these five factors, 20 damage identification runs are performed based on modal parameters polluted with statistically independent realizations of the estimation errors, resulting in a total of $32 \times 20 = 640$ identification runs.

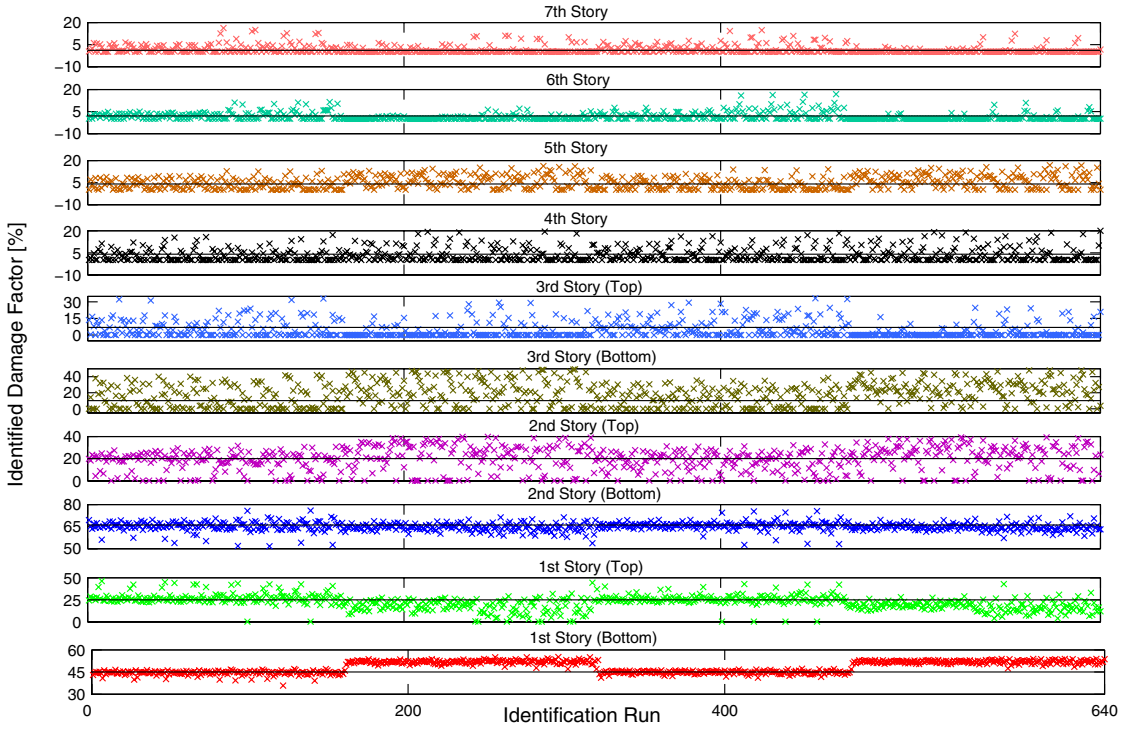

Fig. 8.4 Spread of the identified damage factors at different sub-structures along the wall height (640 realizations)

Figure 8.5 shows in box plots the distributions of the identified damage factors together with their exact value (red solid line) at the different sub-structures. In such plots, the endpoints of the boxes are formed by lower and upper quartiles of the data, namely

$a^j_{0.25}$ and $a^j_{0.75}$. The vertical line within the box represents the median $a^j_{0.5}$, and the mean is displayed by the large dot. The bar on the right of the box extends to the minimum of $a^j_{0.75} + 1.5 \times (a^j_{0.75} - a^j_{0.25})$ and a^j_{max}. In a similar manner, the bar on the left of the box extends to the maximum of $a^j_{0.25} - 1.5 \times (a^j_{0.75} - a^j_{0.25})$ and a^j_{min}. The observations falling outside of these bars are shown with crosses. Table 8.3 reports the mean and standard deviation of the 640 sets of identified damage factors at the different sub-structures. The large bias and standard deviation in the identified damage factors in some sub-structures are due to the fact that the residuals used in the objective function are less sensitive to the updating parameters representing in these sub-structures.

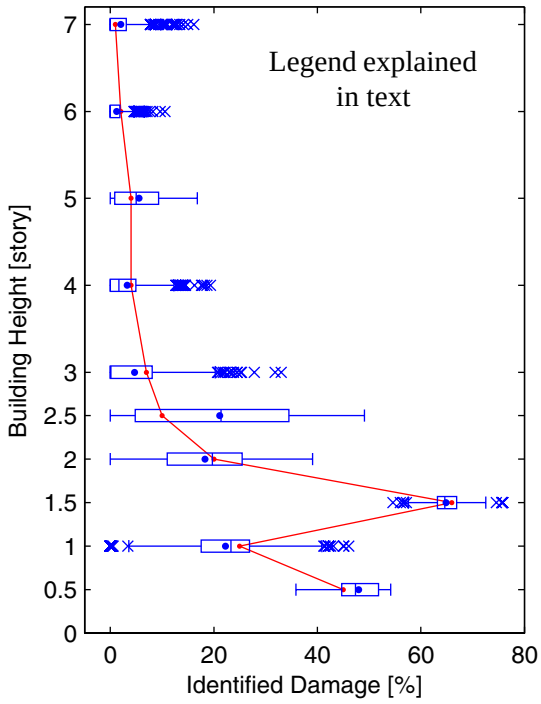

Fig. 8.5 Distributions of identified damage factors in box plots together with their exact values

The uncertainty quantification is performed on the mean and standard deviation of the identified damage factors (over the sets of 20 damage identification runs each). This analysis can be viewed as a crude variance reduction technique that reduces the variability of the output features (identified damage factors) arising from the 20 seed numbers corresponding to the 20 realizations of the random modal estimation errors. Figures 8.6 and 8.7 show the spread of the mean and standard deviation of the identified damage factors, respectively, at the different sub-structures for all 32 combinations of the input factors. From Figures 8.6 and 8.7, it is not possible to quantify the contribution of each input factor or combination of input factors to the total uncertainty of the mean or standard deviation of the identified damage factors. Therefore ANOVA and meta-modeling are used for the uncertainty quantification of the mean and standard deviation.

Table 8.3 Mean and standard deviation (STD) of identified damage factors at different substructures

Substructures Location	Exact [%]	Mean [%]	STD
Seventh story	1	1.6	2.8
Sixth story	2	1.6	2.6
Fifth story	4	5.0	4.4
Fourth story	4	3.7	4.9
Third story (top)	7	5.4	8.3
Third story (bottom)	10	18.3	14.5
Second story (top)	20	19.7	10.9
Second story (bottom)	66	64.9	3.1
First story (top)	25	22.1	7.9
First story (bottom)	45	48.2	3.9

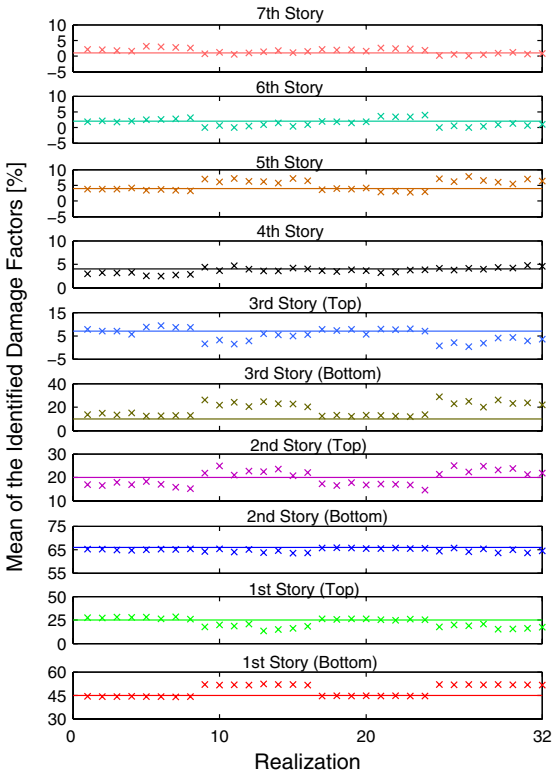

Fig. 8.6 Spread of the mean of identified damage factors at different sub-structures (32 combinations of input factors)

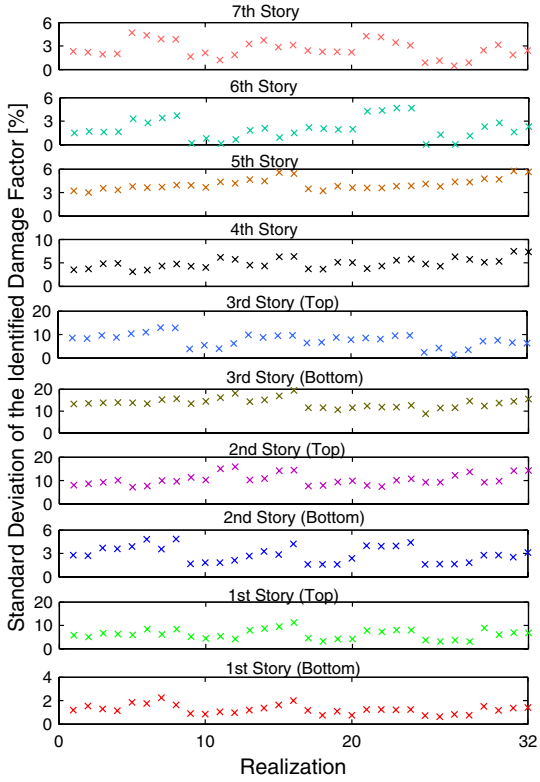

Fig. 8.7 Spread of the standard deviation of identified damage factors at different sub-structures (32 combinations of input factors)

8.5.1 Effect Screening through ANOVA

To investigate the source of the observed uncertainty of the mean and standard deviation of identified damage factors shown in Figures 8.6 and 8.7, ANOVA is performed and the results are presented and discussed in this section. The theoretical foundation of ANOVA is that the total variance of the output features can be decomposed into a sum of partial variances, each representing the effect of varying an individual factor independently from the others. These partial variances are estimated by the so-called R-square values. The input factor with the largest R-square value for an output feature has the most contribution to the uncertainty of that output feature. In this study, ANOVA is applied to

32 data sets of output features (i.e., mean and standard deviation of the identified damage factors over the set of 20 identification runs with independent realizations of the modal estimation errors, see Figures 8.6 and 8.7). A full-factorial design of experiments is used, where the five factors M1, M2, M3, S, and E (see Table 8.2) are varied in the design space. The full-factorial design requires a total of 640 damage identification runs (a set of 20 identification runs for each combination of factors), but it offers the advantage of minimizing aliasing during the ANOVA (Saltelli et al., 2000). Figure 8.8 shows the R-square values of the mean and standard deviation of the identified damage factors for the 10 substructures considered. These R-square values are scaled such that their sum over all factors equates 100%. From Figure 8.8, the following observations can be made. (1) Mesh size (E) is the most significant input factor in introducing uncertainty in the mean value (i.e., estimation bias) of the identified damage. (2) Variability in the spatial density of the sensors (S) produces the least amount of uncertainty in the mean value of the identified damage factors at the different locations. However, this input factor has more relative contribution on the standard deviation of the identified damage. (3) In general, the level of uncertainty in the modal parameters (as measured by COV of estimated modal parameters) of the second and third longitudinal modes (M2 and M3) introduces more uncertainty on both mean and standard deviation of the identified damage than the uncertainty in the modal parameters of the first longitudinal mode (M1). This can be due to the fact that mode shape curvatures are well known to be one of the most sensitive features to local damage and higher modes have higher curvatures. (4) Mesh size (E) also introduces considerable amount of uncertainty to the standard deviation of the identified damage. How-

ever, this factor contributes less to the total uncertainty of the standard deviations than to that of the mean values of the identified damage.

8.5.2 Meta Modeling

Meta-models (also known as surrogate models) represent the relationship between input factors and output features without including any physical characteristics of the system (i.e., black-box models) (Wu and Hamada, 2000). The advantage of surrogate models is that they can be analyzed at a fraction of the cost it would take to perform the physics-based simulations. Meta-models must be trained, which refers to the identification of their unknown functional forms and coefficients. Their quality can be evaluated independently of the training step. In this section, a linear polynomial model is fitted to the identified damage factors by including all input factors considered here and is expressed as

$$Y^j = \beta_0^j + \beta_{M1}^j M1 + \beta_{M3}^j M3 + \beta_S^j S + \beta_E^j E \tag{8.9}$$

where Y^j denotes the j^{th} output feature (i.e., mean identified damage factor at j^{th} sub-structure), and β^j's are the meta-model coefficients to be determined. In the above equation: (1) the values of the input factors are scaled between -1 and +1; (2) the identified damage factors are normalized by their corresponding exact values so that the estimated β coefficients all have dimensionless units and the same order of magnitude for different output features (damage factors); and (3) the value of β_0 corresponds to the mean value of the output feature (over all 640 damage identification runs). Figure 8.9 shows the absolute values of the regression coefficients obtained by least-square fitting the polynomial in

Equation 9 to the mean values (over sets of 20 identification runs) of identified damage factors at different sub-structures. Notice the different scales on the vertical axes of the subplots in Figure 8.9. From Figure 8.9, the following observations can be made. (1) For each sub-structure, the regression coefficient corresponding to the mesh size (β_{E}^{j}) has the largest value indicating that E is the most significant input factor in introducing uncertainty in the mean value of the identified damage, which is consistent with the ANOVA results. (2) The regression coefficients for the first two stories are in general smaller than their counterparts for the higher stories, indicating less uncertainty in the mean value of the identified damage factors (i.e., less damage identification bias) at lower stories. (3) Uncertainty of the identified damage due to the first four input factors (M1, M2, M3, S) is not consistent across the different sub-structures.

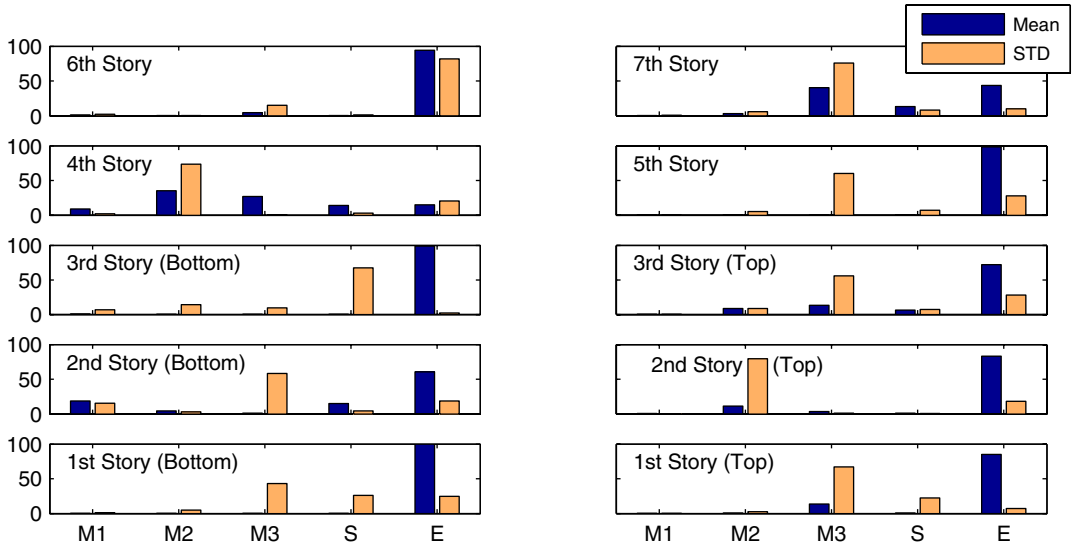

Fig. 8.8 R-square of the mean and standard deviation (STD) of identified damage factors at different sub-structures due to variability of factors M1, M2, M3, S, and E

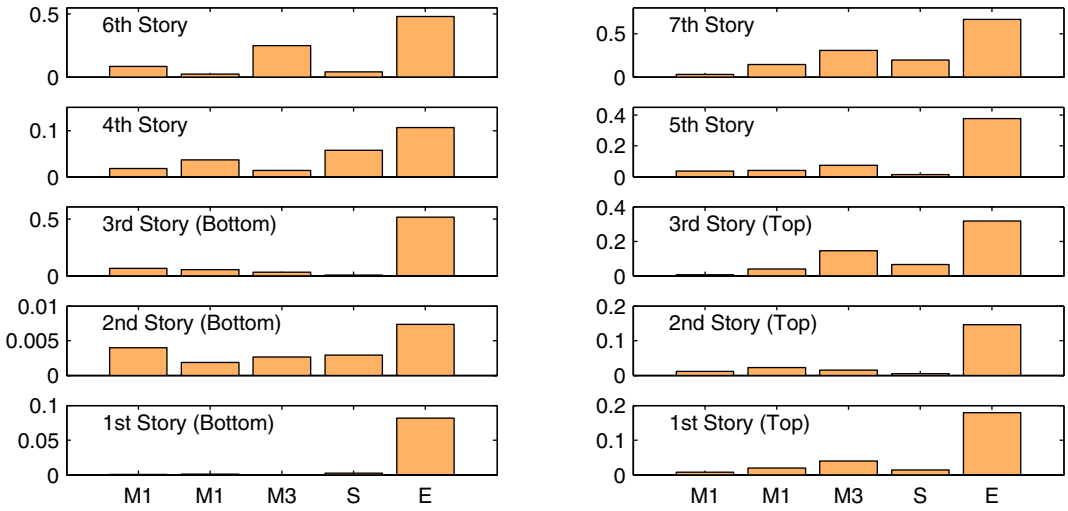

Fig. 8.9 Absolute values of coefficients of the best-fitted polynomials to mean damage factors

8.5.3 One-at-a-Time (OAT) Sensitivity Analysis

In addition to ANOVA and meta-modeling, this study investigates the sensitivity of the identified damage to the level of uncertainty in the identified modal parameters of the first three longitudinal modes. This global sensitivity analysis is performed through one-at-a-time (OAT) perturbation of the individual input factors M1, M2 and M3. Statistical properties (mean/bias and standard deviation) of the identified damage are investigated for six different levels of uncertainty (0.5, 1.0, 1.5, 2.0, 2.5 and 3.0% COV) in the modal parameters of the mode considered, while the other input factors remain fixed. Values of the other fixed factors are: uncertainty of 0.5% in COV for the modal parameters of the other two longitudinal modes, spatial density of 14 sensors along the web wall, and fine mesh FE model (i.e., 398 elements). A set of 10 identifications is performed for each of the six different levels of uncertainty. The random estimation errors added to the natural

frequencies and mode shape components are statistically independent. This global sensitivity analysis of M1, M2 and M3 results in an additional identification runs. Figure 10 shows the mean and mean +/- one standard deviation of the identified damage factors at the 10 sub-structures as a function of the OAT perturbation in the uncertainty level of the modal parameters of the three longitudinal modes considered. Each column of subplots corresponds to the perturbation in the uncertainty level of the modal parameters of one vibration mode, while the other input factors remain fixed.

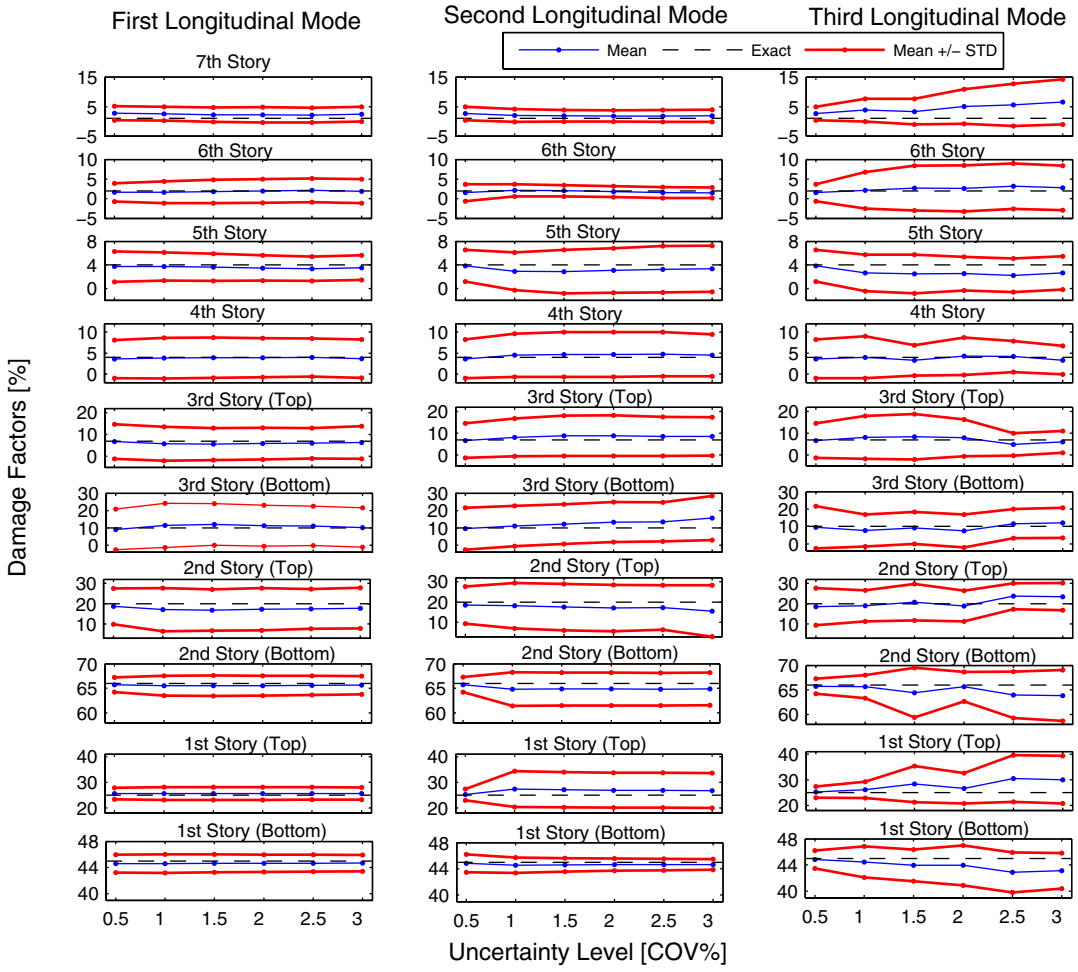

Fig. 8.10 Statistics (mean, mean +/- standard deviation) of the identified damage with increasing level of uncertainty in modal parameters

From this figure the following conclusions can be made. (1) The mean/bias and standard deviation of the identified damage factors are very little sensitive to the level of uncertainty in the modal parameters of the first longitudinal mode for the range of uncertainty level considered in this study (0.5-3% COV). (2) The mean/bias and standard deviation of the identified damage factors at the first (top) and second (bottom and top) stories increase when the level of uncertainty in the modal parameters of the second mode increases from 0.5% to 1% COV, and remain almost constant for higher levels of uncertainty (1-3% COV). (3) The mean/bias and standard deviation of the identified damage factors at the first (bottom and top), second (bottom), sixth and seventh stories tend to increase monotonically with increasing level of uncertainty in the modal parameters of the third longitudinal mode. In general, the uncertainty level in the modal parameters of the third longitudinal mode has the most significant influence (among the three modes) on the estimation uncertainty (mean and standard deviation) of the damage identification results.

8.6 CONCLUSIONS

A full-scale seven-story reinforced concrete (R/C) shear wall building slice was tested on the UCSD-NEES shake table in the period October 2005 - January 2006. The shake table tests were designed so as to damage the building progressively through several historical seismic motions reproduced on the shake table. A sensitivity-based finite element (FE) model updating strategy was used to identify damage at each of several damage states of the building based on changes in its identified modal parameters. The estimation uncertainty in both the system identification and damage identification results was

observed to be significant. This motivated the authors to perform (through numerical simulation) an uncertainty analysis on these system and damage identification results. In this study, the performance of FE model updating for damage identification is systematically investigated. The damaged structure is simulated numerically through a change in stiffness in selected regions of a FE model of the shear wall test structure. The uncertainty of the identified damage (location and extent) is quantified through analysis-of-variance (ANOVA) and meta-modeling due to variability/uncertainty of the following input factors: (1-3) level of uncertainty in the (identified) modal parameters of the first three longitudinal modes (M1, M2, M3), (4) spatial density of measurements (number of sensors) (S), and (5) mesh size in the FE model used for damage identification (modeling error). A full factorial design of experiments is used in this study, resulting in $2 \times 2 \times 2 \times 2 \times 2 = 32$ combination of the input factors. For each combination of these five factors, 20 damage identification runs are performed based on modal parameters polluted with statistically independent realizations of the estimation errors, resulting in a total of $32 \times 20 = 640$ identification runs.

From the results of ANOVA, the following observations can be made. (1) Mesh size (E) is the most significant input factor affecting the uncertainty in the mean value (i.e., estimation bias) of the identified damage. (2) Variability in the spatial density of the sensors (S) produces the least amount of uncertainty in the mean value of the identified damage factors. However, the relative contribution of this input factor (S) is stronger for the standard deviation of the identified damage. (3) In general, uncertainty in the modal parameters of the second and third longitudinal modes (M2 and M3) affects more signifi-

cantly both the mean and standard deviation of the identified damage than the uncertainty in the modal parameters of the first longitudinal mode (M1). This is most likely due to the fact that mode shape curvature is well known to be one of the most sensitive features to local damage and higher modes have higher curvatures. In addition to ANOVA, polynomial meta-models are best-fitted (using least-squares method) to the mean identified damage factors by including all the main factors. From the regression coefficients of the best-fitted polynomials, the following observations can be made. (1) For each sub-structure, the regression coefficient corresponding to the mesh size has the largest value indicating that E is the most significant input factor affecting the mean value of the identified damage, which is consistent with the ANOVA results. (2) The regression coefficients for the first two stories are in general smaller than those for the higher stories, indicating less uncertainty in the mean value of the identified damage factors (i.e., less damage identification bias) at lower stories, where the damage is largest.

Finally, sensitivities of the identified damage factors are investigated as a function of the level of uncertainty in the modal parameters of the first three longitudinal modes. This global sensitivity analysis is performed through one-at-a-time (OAT) perturbation of the individual input factors M1, M2 and M3. Statistical properties (mean/bias and standard deviation) of the identified damage factors are investigated for six different levels of uncertainty in the modal parameters of the considered mode, while the other input factors remain fixed. From this global OAT sensitivity analysis, the following observations can be made. (1) In general, the uncertainty level in the modal parameters of the third longitudinal mode has the most significant influence (among the three modes) on the estimation

uncertainty (mean and standard deviation) of the damage identification results. (2) The mean/bias and standard deviation of the identified damage factors at the first (top) and second (bottom and top) stories increase when the level of uncertainty in the modal parameters of the second mode increases from 0.5% to 1% COV, and remain almost constant for higher levels of uncertainty (1-3% COV).

This systematic investigation demonstrates that the level of confidence in the damage identification results obtained through FE model updating is a function of not only the level of uncertainty in the identified modal parameters, but also choices made in the design of experiments (e.g., spatial density of measurements) and modeling errors (e.g., mesh size).

ACKNOWLEDGEMENTS

Chapter 8, in full, is a reprint of the material submitted for possible publication in the Journal of Computer Aided Civil and Infrastructure Engineering (2007), Moaveni, B., Conte, J.P., and Hemez, F.M. The dissertation author was the first author and primary investigator of this paper.

Partial supports of this research by Lawrence Livermore National Laboratory with Dr. David McCallen as Program Leader and by the Englekirk Center Industry Advisory Board are gratefully acknowledged. Any opinions, findings, and conclusions or recom¬mendations expressed in this material are those of the authors and do not necessarily reflect those of the sponsors. The first author also wants to acknowledge Mr. Dong Ju Choi of San Diego Supercomputer Center (SDSC) and Dr. Ronnie Hoogerwerf and Mr.

Patrick Boyle of Interactive Supercomputing Corporation for their help in performing parallel computations using StarP on the “On Demand Cluster” of SDSC.

REFERENCES

Allman, D.J., (1988). “A quadrilateral finite element including vertex rotations for plane elasticity analysis.” *International Journal for Numerical Methods in Engineering,* Vol. 26, No. 3, 717-730.

Batoz, J.L., and Tahar, M.B., (1982). “Evaluation of a new quadrilateral thin plate bending element.” *International Journal for Numerical Methods in Engineering,* Vol. 18, No. 11, 1655-1677.

Christodoulou, K., and Papadimitriou, C., (2007). “Structural identification based on optimally weighted modal residuals.” *Mechanical Systems and Signal Processing,* Vol. 21, No. 1, 4-23.

Coleman, T.F., and Li, Y., (1996). “An interior, Trust Region approach for nonlinear minimization subject to bounds.” *SIAM Journal on Optimization,* Vol. 6, No. 2, 418-445.

Doebling, S.W., Farrar, C.R., Prime, M.B., and Shevitz, D.W., (1996). *Damage identification in structures and mechanical systems based on changes in their vibration characteristics: A detailed literature survey.* Los Alamos National Laboratory, Rep. No. LA-13070-MS, Los Alamos, New Mexico, USA.

Doebling, S.W., Farrar, C.R., and Prime, M.B., (1998). “A summary review of vibration-based damage identification methods.” *The Shock and Vibration Digest,* Vol. 30, No. 2, 99-105.

Filippou, F.C., and Constantinides, M., (2004). *FEDEASLab getting started guide and simulation examples.* Technical Report NEESgrid-2004-22, http://fedeaslab.berkeley.edu.

Fox, R.L., and Kapoor, M.P., (1968). “Rates of change of eigenvalues and eigenvectors.” *AIAAJ,* Vol. 6, No. 12, 2426-2429.

Friswell, M.I., and Mottershead, J.E., (1995). *Finite element model updating in structural dynamics.* Kluwer Academic Publishers, Boston, USA.

He, X., Moaveni, B., Conte, J.P., Restrepo, J.I. and Elgamal, A., (2006). “Damage identification of a seven-story reinforced concrete shear wall building tested on UCSD-NEES shake table.” *Proc. of 4th World Conference on Structural Control and Monitoring*, San Diego, USA.

Hughes, T.J.R., and Brezzi, F., (1989). “On drilling degree of freedom.” *Computer Methods in Applied Mechanics and Engineering*, Vol. 72, 105-121.

Maeck, J., and De Roeck, G., (1999). “Dynamic bending and torsion stiffness derivation from modal curvatures and torsion rates.” *Journal of Sound and Vibration*, Vol. 225, No. 1, 153-170.

MathWorks Inc., (2005). *Matlab - High performance numeric computation and visualization software, user’s guide.* The MathWorks Inc., Natick, MA.

Moaveni, B., Barbosa, A.R., Conte, J.P., and Hemez, F.M., (2007). “Uncertainty analysis of modal parameters obtained from three system identification methods.” *Proc. of International Conference on Modal Analysis (IMAC-XXV)*, Orlando, USA.

Moaveni, B., He, X., and Conte, J.P., (2008a). “System identification of a seven-story reinforced concrete shear wall building slice tested on the UCSD-NEES shake table.” *Journal of Structural Engineering, ASCE*, under review.

Moaveni, B., He, X., and Conte, J.P., (2008b). “Damage identification of seven-story reinforced concrete shear wall building slice tested on the UCSD-NEES shake table.” *Journal of Structural Engineering*, ASCE, under preparation.

Moaveni, B., He, X., Conte, J.P., and Restrepo, J.I. “System identification of a seven-story reinforced concrete shear wall building tested on UCSD-NEES shake table.” *Proc. of the 4th World Conference on Structural Control and Monitoring*, San Diego, USA, (2006).

Panagiotou, M., Restrepo, J.I., and Conte, J.P., (2007). *Shake table test of a 7-story full scale reinforced concrete structural wall building slice, Phase I: Rectangular section.* Report No. SSRP-07/07, Department of Structural Engineering, University of California, San Diego.

Pandey, A.K., Biswas, M., and Samman, M.M., (1991). “Damage detection from changes in curvature mode shapes.” *Journal of Sound and Vibration,* Vol. 145, No. 2, 321-332.

Salawu, O.S., (1997) “Detection of structural damage through changes in frequency: A review.” *Engineering Structures*, Vol. 19, No. 9, 718-723.

Saltelli, A., Chan, K., and Scott, E.M., (2000). *Sensitivity analysis.* John Wiley & Sons, New York.

Shi, Z.Y., Law, S.S., and Zhang, L.M., (2002) “Improved damage quantification from elemental modal strain energy change.” *Journal of Engineering Mechanics,* ASCE, Vol. 128, No. 5, 521-529.

Sohn, H., Farrar, C.R., Hemez, F.M., Shunk, D.D., Stinemates, D.W., and Nadler, B.R., (2003). *A review of structural health monitoring literature: 1996-2001*. Los Alamos National Laboratory, Report No. LA-13976-MS, Los Alamos, New Mexico, USA.

Teughels, A., and De Roeck, G., (2004). “Structural damage identification of the highway bridge Z24 by finite element model updating.” *Journal of Sound and Vibration,* Vol. 278, No. 3, 589-610.

Wu, C.F.J., and Hamada, M., (2000). *Experiments: planning, analysis, and parameter design optimization.* John Wiley & Sons, New York.

CHAPTER 9

CONCLUSIONS

9.1 SUMMARY OF CONTRIBUTIONS AND HIGHLIGHT OF FINDINGS

The research work presented in this thesis contributes to three different research areas: (1) system identification of structures considered as linear dynamic systems, (2) damage identification of structures, and (3) uncertainty analysis of system and damage identification results.

The principal contributions and major findings of this research work are summarized below:

(1) The General Realization Algorithm (GRA) is developed to identify modal parameters of linear multi-degree-of-freedom dynamic systems subjected to measured (known) arbitrary dynamic loading from known initial conditions. The GRA is a generalization of the Eigensystem Realization Algorithm (ERA), which is based on singular value decomposition (SVD) of a Hankel matrix constructed from impulse (or free vibration) response data. This generalization is obtained through SVD of a weighted Hankel matrix of input-output data, where the weighting is determined by the loading. Using GRA, the state-space matrices are estimated in a two-step process that includes

a state reconstruction followed by a least squares optimization yielding a minimum prediction error for the response.

An application example consisting of an eight-story shear building model subjected to earthquake base excitation is used for the multiple purposes of validating the new algorithm, evaluating its performance, and investigating the statistical properties (i.e., bias/unbias, variance, and robustness to added output noise introduced to model measurement noise and modeling errors) of the GRA modal parameter estimates. Based on the extensive simulation study performed, it is found that the proposed new algorithm yields very accurate estimates of the modal parameters (natural frequencies, damping ratios, and mode shapes) in the case of noise free input-output data or low output noise. The bias and variance of the modal parameter estimates increase with the level of output noise and with the vibration mode order (due to the lower participation of higher modes to the total response and weak signal-to-noise ratio in the application example considered).

(2) As payload project leveraging a quasi-static test of a full-scale sub-component composite beam, a high-quality set of low-amplitude vibration response data was acquired from the beam at various damage levels. The Eigensystem Realization Algorithm was applied to identify the modal parameters (natural frequencies, damping ratios, displacement and macro-strain mode shapes) of the composite beam based on its impulse responses recorded in its undamaged and various damaged states using accelerometers and long-gage fiber Bragg grating strain sensors. The modal identification results from different tests at a given damage state using different types of data (acceleration or macro-strain) show very good agreement, thus validating the system identi-

fication results used in the first stage of the damage identification procedure. This study also investigates the sensitivity of the identified modal parameters to actual structural damage.

The identified modal parameters are then used to identify the damage in the beam through a finite element model updating strategy. Two separate cases of damage identification are performed. In case I, the modal residuals in the objective function used in the FE model updating procedure are based on the natural frequencies and displacement mode shapes identified from accelerometer data. In case II, the modal residuals are based on the natural frequencies, displacement mode shapes identified from accelerometer data, and macro-strain mode shapes identified from FBG strain sensor data. From the damage identification results obtained, it is observed that the effective moduli of elasticity (used as updating parameters) display an overall decreasing trend with increasing level of damage, which is consistent with the damage-induced stiffness degradation. The updated effective moduli of elasticity obtained from the two different damage identification cases are found to be in relatively good agreement and consistent with the damage observed in the composite beam during and at the end of the experiments. This provides an important validation example for vibration based damage identification using finite element model updating based on a heterogeneous sensor array, performed on a full-scale structural component tested in laboratory conditions.

(3) A comprehensive comparative study of six state-of-the-art system identification methods is performed. These system identification methods including three output-only and three input-output methods were used to estimate the modal parameters (natural fre-

quencies, damping ratios, and mode shapes) of a seven-story reinforced concrete shear wall building slice tested on the UCSD-NEES shake table in its undamaged (baseline) and various damage states. These methods were applied to the response of the building to ambient as well as white noise base excitation measured using both accelerometers and linear variable displacement transducers (LVDTs).

From the results of this system identification study, it is observed that: (1) The natural frequencies identified using different methods are reasonably consistent at each damage state, while the identified damping ratios exhibit much larger variability across system identification methods. (2) The natural frequencies identified based on white noise test data decrease with increasing level of damage except from damage state S3.1 to S3.2, during which the steel braces were stiffened, while only the longitudinal modal frequencies identified based on ambient vibration data decrease consistently with increasing level of structural damage. This can be explained by the fact that under low amplitude ambient vibration conditions, concrete cracks do not open as much as under forced base excitation and therefore damage does not affects the identified modal parameters of some vibration modes. (3) At each damage state, the identified modal parameters of the first longitudinal mode appear to be the least sensitive to the identification method used, which is most likely due to the predominant contribution of this mode to the total response. (4) The first longitudinal modal frequency identified based on white noise test acceleration data is systematically lower than its counterpart identified based on ambient vibration acceleration data at all damage states considered. This is most likely due to the fact that the test structure is nonlinear (even at the relatively low levels of excitation considered in this system identification

study) with effective modal parameters depending on the amplitude of the excitation and therefore of the structural response.

In order to further validate and better understand the modal parameters identified from ambient vibration and white noise base excitation test data, a three-dimensional linear elastic finite element model of the shear wall test structure was developed in SAP2000. The natural frequencies and mode shapes computed from the finite element model are in reasonably good agreement with their identified counterparts (especially when modal identification is based on the ambient vibration data) for the first three longitudinal and the first two torsional vibration modes of the test structure in its undamaged state (damage state S0).

(4) A finite element model updating strategy is applied for damage identification of the full-scale seven-story reinforced concrete building slice tested on the UCSD-NEES shake table. The shake table tests were designed so as to damage the building progressively through a sequence of historical earthquake records reproduced on the shake table. Two different cases of damage identifications are performed based on two different sets of identified modal parameters of the test structure, namely (1) the modal parameters identified based on ambient vibration data, and (2) the modal parameters identified based on white noise base excitation test data.

From the damage identification results obtained, the following observations can be made. (1) In both damage identification cases, as expected the severity of structural damage increases as the structure is exposed to stronger earthquake excitations. (2) At each damage state, the most severe damage is identified at the first story (top and bottom) and second story (bottom) of the web wall. The damage identification results

obtained in this study are consistent with the actual damage observed directly in the test structure and inferred from strain gauge and LVDT measurement data recorded during the damaging seismic tests. They capture correctly the concentration of damage at the bottom two stories of the web wall. However, at damage state S4, severe damage is spuriously identified at some higher stories of the web wall (fourth story in case I, third and fifth stories in case II). The large identified damage factors at these locations can be due to the following facts: (i) the estimation uncertainty of the identified modal parameters at damage state S4 (especially for the third mode) is higher than at lower damage states; (ii) the optimization algorithm used to update the FE model parameters is not a global optimization algorithm and becomes less robust for larger changes in identified modal parameters between two consecutive damage states; and (iii) with increasing level of damage, the level of nonlinearity in the structural response (even to the relatively low amplitude 0.03g RMS white noise base excitation) increases. Therefore, the assumption that the structure behaves as a linear dynamic system is violated and a linear dynamic model (modal model) is not strictly able to represent well the structure (modal parameters become effective modal parameters).

The analytical modal parameters obtained from the updated FE models are in better agreement with their experimentally identified counterparts in case I than in case II. This could be due to a larger modeling error in case II in which the assumption of linear dynamic behavior is not as well satisfied as in case I even for the relatively low amplitude of dynamic excitation (0.03g RMS acceleration). Therefore, the results from case I of damage identification are expected to be more accurate. Finally, it

should be noted that the success of damage identification depends significantly on the accuracy and completeness of the available identified modal parameters. Clearly, if estimation uncertainty in the modal parameters is larger than their change due to damage, it is impossible to resolve/identify the actual damage in the structure.

(5) Performance of three state-of-the-art output-only system identification methods is investigated based on the response of the seven-story building structure simulated using a three-dimensional nonlinear finite element model thereof. Analysis-of-variance (ANOVA) and meta-modeling are used to quantify the variability of the identified modal parameters due to variability of the following input factors: (1) amplitude of input excitation (level of nonlinearity in the response) (A), (2) spatial density of measurements (number of sensors) (S), (3) measurement noise (N), and (4) length of response data used in the identification process (L).

From the results of effect screening through ANOVA and meta-modeling, it is observed that: (1) the variability in spatial density of the sensors (number of sensors) introduces the least amount of variability in the modal parameters identified using the three methods considered, (2) the mean value of the identified natural frequencies is most sensitive to factors L and A (i.e., record length and amplitude of input excitation) for the three methods, (3) the mean value of the identified damping ratios and mode shapes (MAC value between identified mode shapes and their nominal counterparts from the FE model) are sensitive to the three factors A, N, and L, but the relative contributions of these three factors to the total variance of these identified modal parameters depend on the system identification used and the vibration mode, and (4)

pairwise interactions of input factors have almost equal influence on the mean values of the identified natural frequencies.

In addition to ANOVA and meta-modeling, sensitivities of the identified modal parameters are investigated as a function of data length and measurement noise, respectively, while the other factors remain fixed. From this analysis, it is seen that: (1) the variances of the identified modal parameters decrease with increasing record length and increase with increasing level of added measurement noise, (2) the identified modal parameters of the first mode converge to their nominal (FE computed) counterparts with increasing record length, which is not the case for the identified modal parameters of the second and third modes, and (3) the variances of the identified modal frequencies and MAC values are very small even at high levels of measurement noise.

(6) The performance of FE model updating for damage identification is systematically investigated. The damaged structure was simulated numerically through a change in stiffness in selected regions of a FE model of the shear wall test structure. The uncertainty of the identified damage (location and extent) due to variability of five input factors is quantified through analysis-of-variance (ANOVA) and meta-modeling. These five input factors are: (1-3) level of uncertainty in the (identified) modal parameters of each of the first three longitudinal modes (M1, M2, M3), (4) spatial density of measurements (number of sensors) (S), and (5) mesh size in the FE model used in the FE model updating procedure (modeling error) (E). A full factorial design of experiments is considered for these five input factors.

From the results of effect screening through ANOVA and meta-modeling, the following observations can be made. (1) Mesh size (E) is the most significant input factor affecting the uncertainty in the mean value (i.e., estimation bias) of the identified damage. (2) Variability in the spatial density of the sensors (S) produces the least amount of uncertainty in the mean value of the identified damage factors. However, the relative contribution of this input factor (S) to the variability of the standard deviation of the identified damage is stronger. (3) In general, uncertainty in the modal parameters of the second and third longitudinal modes (M2 and M3) affects more significantly both the mean and standard deviation of the identified damage than the uncertainty in the modal parameters of the first longitudinal mode (M1). This is most likely due to the fact that mode shape curvature is one of the most sensitive features to local damage and higher modes have higher curvatures.

Finally, sensitivities of the identified damage factors are investigated as a function of the level of uncertainty in the modal parameters of the first three longitudinal modes. This global sensitivity analysis is performed through one-at-a-time (OAT) perturbation of the individual input factors M1, M2 and M3. From this global OAT sensitivity analysis, the following observations can be made. (1) In general, the uncertainty level in the modal parameters of the third longitudinal mode has the most significant influence (among the three modes) on the estimation uncertainty (mean and standard deviation) of the damage identification results. (2) The mean/bias and standard deviation of the identified damage factors at the first (top half) and second (bottom and top halves) stories increase when the level of uncertainty in the modal parameters of the

second mode increases from 0.5% to 1% COV, and remain almost constant for higher levels of uncertainty (1-3% COV).

This systematic investigation demonstrates that the level of confidence in the damage identification results obtained through FE model updating is a function of not only the level of uncertainty in the identified modal parameters, but also choices made in the design of experiments (e.g., spatial density of measurements) and modeling errors (e.g., mesh size).

9.2 RECOMMENDATIONS FOR FUTURE WORK

Based on the research work performed and presented herein, several research areas have been identified as open to and in need of future work.

(1) An important issue not addressed in this study is the effect of environmental conditions on system and damage identification results. An interesting topic of future research is to study the variability in system and damage identification results due to variability of environmental conditions such as temperature and humidity.

(2) Separation of changes in modal parameters due to structural damage from those due to other sources such as changes in environmental conditions is another important subject of future research in vibration based structural health monitoring.

(3) Based on the results obtained and experience gained through the research presented herein, it is concluded that probabilistic damage identification methods are preferable. Such methods must allow to account for all pertinent sources of uncertainty and must express the damage identification results in probabilistic terms. The development of

probabilistic damage identification methods (e.g., Bayesian FE model updating) is therefore an area in need of future research. Such methods should be applied to laboratory and/or field measurement data and validated against observed damage in real structural components and structures.

(4) Further investigation of the effects of modeling errors on model based damage identification methods is needed.

(5) Application of FE model updating for damage identification of the seven-story shear wall building slice based on a denser and heterogeneous array of sensors (including accelerometers, LVDTs, and strain gages) is a worthy area of future work.

(6) The development of analytical or semi-analytical methods to propagate uncertainties through system identification and damage identification algorithms is an important area of future research. It will allow system identification and damage identification results to be expressed in probabilistic terms.